Aus dem Institut für Immunologie im Biomedizinischen Centrum
der Ludwig-Maximilians-Universität München
Vorstand: Prof. Dr. rer. nat. Thomas Brocker

Role of post-transcriptional gene regulation by Roquin proteins in the prevention of autoinflammation and pancreatic cancer

Dissertation
zum Erwerb des Doktorgrades der Naturwissenschaften
an der Medizinischen Fakultät der
Ludwig-Maximilians-Universität München

vorgelegt von
Timsse Raj

aus
Kabul

2021

Mit Genehmigung der Medizinischen Fakultät
der Universität München

Betreuer:	Prof. Dr. rer. nat. Vigo Heissmeyer
Zweitgutachter:	PD Dr. Naoto Kawakami, Ph.D.
Dekan:	Prof. Dr. med. Thomas Gudermann
Tag der mündlichen Prüfung:	22. Juni 2022

Für meine Familie.

Eidesstattliche Versicherung

Ich erkläre hiermit an Eides statt, dass ich die vorliegende Dissertation mit dem Titel

Role of post-transcriptional gene regulation by Roquin proteins in the prevention of autoinflammation and pancreatic cancer

Selbstständig verfasst, mich außer der angegebenen keiner weiteren Hilfsmittel bedient und alle Erkenntnisse, die aus dem Schrifttum ganz oder annähernd übernommen sind, als solche kenntlich gemacht habe und nach ihrer Herkunft unter Bezeichnung der Fundstelle einzeln nachgewiesen habe.

Ich erkläre des Weiteren, dass die hier vorgelegte Dissertation nicht in gleicher oder in ähnlicher Form bei einer anderen Stelle zur Erlangung eines akademischen Grades eingereicht wurde.

München, den 27. Juli 2022	Timsse Raj
……	……..
Ort und Datum	Unterschrift

Summary

Post-transcriptional gene regulation by the RNA-binding-proteins Roquin-1/2 and Regnase-1 is important for the maintenance of immune homeostasis and controls T helper cell fate decisions. Deficiencies in one or all of these proteins lead to aberrant activation of the immune system and the development of autoimmunity and autoinflammation. To date investigations have mainly focused on T cell intrinsic consequences of Roquin-1/2 and/or Regnase-1 loss-of-function. In my research project, I demonstrated that Roquin-1/2 loss-of-function has T cell intrinsic and extrinsic effect, whereas Regnase-1 acted predominantly in a T cell intrinsic manner.

In adoptive transfer experiments, I showed that DKO^{T} T cells cause bystander activation of WT $CD8^{+}$ T cells, bystander T_{FH} differentiation of WT $CD4^{+}$ T cells and concomitant accumulation of GC B cells. T_{FH} cell differentiation did not require IFNγ, IL-6 or ICOS signaling in recipient cells. This effect was independent of SAP signaling but did require interactions with B cells. Furthermore, DKO^{T} cells were able to replace co-stimulatory signals that potently activated bystander T cells, which lacked normal B7-mediated CD28 stimulation. Several molecules that could be responsible for the observed *trans*-effect were identified in an mRNASeq experiment and CD86 and CD40L were further investigated.

The second and third parts of the thesis focused on extrinsic functions of DKO^{T} T cells that caused a spontaneous, inflammation-mediated cancer development in the pancreas. Specifically, I showed that mice with conditional Roquin-1/2 deletion in T cells spontaneously developed pancreas pathology and pre-neoplastic low grade panIN lesions. In these mice, inflammatory $CD11b^{+}$ $Gr1^{+}$, $T_{H}17$ and T_{FH} cells accumulated, both systemically as well as locally in the pancreas draining lymph nodes and $Ly6G^{+}$ neutrophils infiltrated into pancreas tissue. In the context of acinar cell-specific oncogenic $Kras^{G12D}$ signaling DKO^{T} T cell-mediated local accumulation of inflammatory cells in the pancreas microenvironment accelerated cancer development and progression. I described a role of Roquin proteins in the prevention of tissue inappropriate expression of G-CSF in $CD4^{+}$ T cells by direct repression of the G-CSF encoding mRNA through its 3'UTR. In conclusion, in this work I described a mouse model of spontaneous pancreas cancer development that is driven by DKO^{T} $T_{H}17$ cells via the IL-17A/G-CSF/neutrophil axis and provided evidence of a T cell extrinsic role of post-transcriptional gene regulation in the prevention of pathology.

Zusammenfassung

Post-transkriptionelle Genregulation durch die RNS-bindenden Proteine Roquin-1/2 und Regnase-1 spielt bei der Aufrechterhaltung von Immunhomöostase und der Kontrolle der T Zell Differenzierung eine entscheidende Rolle. Eine Defizienz in einem oder mehreren dieser Proteine führt zu einer aberranten Aktivierung des Immunsystems und der Entwicklung von Autoimmun- und autoinflammatorischen Erkrankungen. Bisherige Studien fokussierten sich auf die Untersuchung von T Zell-intrinsischen Konsequenzen, die durch einen Funktionsverlust von Roquin-1/2 und/oder Regnase-1 ausgelöst werden. In dieser Arbeit konnte ich zeigen, dass ein Funktionsverlust von Roquin-1/2 sowohl T Zell-intrinsische als auch extrinsische Effekte hatte, wohingegen Regnase-1 hauptsächlich T Zell-intrinsische Funktionen hatte.

In adoptiven T Zelltransferexperimenten habe ich gezeigt, dass Roquin-defiziente T Zellen sowohl eine Aktivierung von unbeteiligten, *bystander* Wildtyp $CD8^+$ T Zellen, als auch eine T_{FH} Differenzierung von WT $CD4^+$ T Zellen und eine damit verbundene Akkumulation von follikulären B Zellen verursachen. Für die aberrante T_{FH} Differenzierung war keine Signaltransduktion durch IFNγ, IL-6 or ICOS in den Wildtyp Rezipienten notwendig. Die Differenzierung war außerdem unabhängig von einer Signalübertragung durch SAP Proteine, während eine Interaktion mit B Zellen jedoch notwendig war. Des Weiteren waren Roquin-defiziente T Zellen in der Lage unbeteiligte T Zellen, die bisher keine Stimulation über eine Interaktion von B7 mit CD28 erhalten hatten, mit co-stimulierenden Signalen zu versorgen. Durch RNS Sequenzierung wurden mehrere potenzielle Kandidaten identifiziert, die den beobachteten *Trans*-Effekt verursachen könnten und zwei der vielversprechendsten Kandidaten wurden in weiteren Experimenten untersucht.

Im zweiten und dritten Teil dieser Dissertation habe ich mich auf Zell-extrinsiche Konsequenzen von Roquin-defizienten T Zellen fokussiert, die eine spontane, durch eine Entzündungsreaktion vermittelte Entstehung von Pankreaskrebs verursachen. Ich habe gezeigt, dass Mäuse mit einer T Zellspezifischen konditionellen Deletion von Roquin-1/2 pathologische Veränderungen des Pankreas bis hin zu gering-gradigen präneoplastischen Läsionen entwickeln. In diesen Mäusen akkumulierten entzündungsfördernde $CD11b^+$ $Gr1^+$, T_H17 und T_{FH} Zellen sowohl systemisch, als auch lokal in pankreatischen Lymphknoten und $Ly6G^+$ Neutrophile infiltrierten ins

Pankreasgewebe. Im Zusammenhang mit krebserregenden $Kras^{G12D}$ Signalen in Azinuszellen führten Roquin-defiziente T Zellen zur lokalen Ausbildung einer entzündungsfördernden Umgebung im Pankreas und der damit verbundenen beschleunigten Krebsentstehung und Progression. Darüber hinaus konnte ich eine Funktion von Roquin Proteinen in der Verhinderung einer unzweckmäßigen Expression von G-CSF durch T Zellen beschreiben. Roquin interagierte direkt mit der 3‘ UTR der mRNS, die für G-CSF kodiert. Zusammengefasst beschreibt diese Arbeit ein Mausmodel der spontanen Karzinogenese des Pankreas, die durch Roquin-defiziente T_H17 Zellen über die IL-17A/G-CSF/Neutrophile Achse getrieben wird und eine T Zell-extrinsiche Rolle von post-transkriptioneller Genregulation bei der Verhinderung von Pathologie.

Table of Contents

List of Figures

List of Tables

Abbreviations

-/-	knock out
aa	amino acid
ADE	alternative decay element
ADM	acinar-to-ductal metaplasia
ANA	anti-nuclear antibodies
ANOVA	analysis of variance
APC	antigen-presenting cell
ARE	AU rich element
ASK1	apoptosis-signaling kinase 1
BCR	B cell receptor
bp	base pairs
C-terminal	carboxy terminal
CAF	cancer-associated fibroblasts
CD	cluster of Differentiation
CDE	constitutive decay element
CDS	coding sequence
CGC	cancer genome consortium
CLIP	UV cross-linking and immunoprecipitation
CM	central memory
CNA	copy number alteration
CTV	cell trace violet
CXCR	chemokine receptor
d	day
DC	dendritic cell
DF	dilution Factor
DKO	double knock out
DMSO	dimethylsulfoxide
DTT	dithiothreitol
ECM	extracellular matrix
EDTA	ethylendiamintetraacetat
EGFP	enhanced green fluorescent protein
ELISA	enzym-linked immunosorbent assay
EM	effector memory
EMT	epithelial-to-mesenchymal transition
ENU	N-ethyl-N-nitrosourea
FC	flow cytometry
FCS	fetal calf serum
FW	forward
G-CSF	granulocyte colony-stimulating factor
GC	germinal center
gDNA	genomic DNA
GO	Gene Ontology
h	human
HEK	human embryonic kidney cells
$HEPN_C$	higher eukaryotes and procaryotes nucleotide – binding C-terminal
$HEPN_N$	higher eukaryotes and procaryotes nucleotide – binding N-terminal
HRP	horseradish peroxidase
i	inducible
i.p.	intra peritoneal
i.v.	intra venous
ICOS	Inducible T-Cell Co-Stimulator
ICOSL	Inducible T-Cell Co-Stimulator Ligand
IFN	Interferon
Ig	Immunoglobulin
IL-	Interleukin

ILC	innate lymphoid cells
IRES	internal ribosomal entry site
KEGG	Kyoto Encyclopedia of Genes and Genomes
KO	knock out
KSRP	K-homology splicing regulatory protein
LBE	linear binding element
LN	lymph node
LOH	loss of heterozygosity
LPS	lipopolysaccharide
LTR	long terminal repeat
MDSC	myeloid-derived suppressor cells
MEF	mouse embryonic fibroblasts
MHC	major histocompatibillity complex
miRNA	microRNA
MNAB	membrane-associated nucleic acid binding protein
mRNA	messanger RNA
N-terminal	amino terminal
N.d.	not detectable
NK	natural killer cells
NKT	natural killer T cells
O/N	over-night
P-bodies	processing bodies
p:MHC	peptide:MHC
PAMP	pathogen associated molecular pattern
PanIN	pancreatic intraepithelial neoplasia
panLN	pancreatic lymph nodes
PBS	phosphate buffered saline
PCA	principal component analysis
PCR	polymerase chain reaction
PD-1	programmed cell death 1
PDAC	pancreatic ductal adenocarcinoma
Pen-Strep	Penicillin-Streptomycin
PFA	Paraformaldehyde
PRR	proline-rich regions
QC	QuickChange
qPCR	quantitive polymerase chain reaction
RBP	RNA-binding protein
rh	recombinant human
RING	really interesting new gene
rm	recombinant mouse
RNA	ribonucleic acid
RNASeq	RNA sequencing
ROS	reactive oxygen species
RT	room temperature
rv	reverse
san/san	sanroque
SAP	SLAM-associated protein
SDS-PAGE	sodium dodecylsulfate polyacrylamide gel electrophoresis
SELEX	Systematic Evolution of Ligands by Exponential Enrichment
SEM	standard error of mean
SL	stem-loop
SLAM	signaling lymphocyte activation molecule
SLDE	stem-loop destabilizing element
SLE	systemic lupus erythematosus
SNV	single nucleotide variations
SPF	specific pathogen-free
STAT	signal transducer and activator of transcription
TAC	tris-ammonium-chloride

TAM	tissue-associated macrophages
TCR	T cell receptor
TCS	tissue culture supernatants
TF	Transcription factor
T_{FH}	T follicular helper cell
T_{FR}	T follicular regulatory cell
TGFβ	transforming growth factor β
T_H	Helper T cell
TKO	tripple knock out
TME	tumor microenvironment
TNF	Tumor necrosis factor
T_{reg}	regulatory T cell
TTP	tristetraproline
tT_{reg}	thymic regulatory T cells
U	Units
UPL	Universal Probe Library
UTR	untranslated regions
WB	Western blot
WES	whole exome sequencing
WT	wild type
ZFP36L1	Butyrate response factor1

1. Introduction

1.1 General aspects of the immune system

Our bodies are exposed to a plethora of pathogens every day. To be able to combat these pathogens and other foreign substances our bodies have developed an intricate system made up of cells, proteins, small molecules and barriers, which protects us from disease.

1.1.1 Innate and adaptive immunity

Broadly, the immune system can be subdivided into innate and adaptive immune responses, which are both dependent on the activity of leukocytes, most of which develop and mature in the bone marrow. Mature immune cells can be found in peripheral tissues, in the blood stream as well as in the lymphatic system, and can be subdivided in cells derived from the lymphoid or myeloid lineage. T and B cells, as well as innate lymphoid cells (ILCs) and natural killer (NK) cells arise from the common lymphoid progenitor. T and B cells express antigen receptors and differentiate in the thymus and bone marrow, respectively. The rest of the leukocytes, including granulocytes, neutrophils, dendritic cells, erythrocytes and megakaryocytes develop from the common myeloid progenitor (Murphy, 2017).

The innate immune system

The innate immune system is activated immediately after infection and serves as the first line of defense by controlling pathogenic infections. This is achieved by phagocytosis, activation of the complement system or by the production of antimicrobial peptides. Cells of the innate immune system express pattern recognition receptors that bind pathogen associated molecular patterns (PAMPs). PAMPs are highly conserved structures that are exclusively found in microorganisms (e.g. lipopolysaccharide (LPS)), are crucial for their survival and are shared by large groups of pathogens (Medzhitov and Janeway, 2000). Engagement of pattern recognition receptors on professional antigen-presenting cells (APCs) triggers an immediate but unspecific immune response which does not protect from re-infection by the same pathogen. Recognition of PAMPs by the innate immune system does not only prompt

a pro-inflammatory response but also leads to the maturation of dendritic cells (DCs), i.e. DCs process antigens, migrate to the lymph nodes where they can prime naïve antigen-specific T cells and provide co-stimulatory signals, thus linking the innate and the adaptive immune system (Charles A. Janeway and Medzhitov, 2002; Iwasaki and Medzhitov, 2004; Medzhitov and Janeway, 2000).

The adaptive immune system

The adaptive immune system is the antigen specific part of the immune response and confers immunological memory. The two major cell types of the adaptive immune system are T and B cells, each of which is equipped with a highly specific antigen receptor. Naïve lymphocytes, i.e. lymphocytes that have not encountered their antigen, are very inactive and acquire effector function upon interaction with an antigen (Murphy, 2017).

B cells express the B cell receptor (BCR) which belongs to the class of immunoglobulins (Fröland et al., 1971), develop in bone marrow where they acquire their highly specific BCRs via ordered rearrangement of the heavy and light chain loci (Alt et al., 1986). Following antigen recognition B cells mature and differentiate into plasma cells that secrete antibodies of the same specificity as the BCR of the original B cell. This process occurs during the germinal center (GC) reaction, whereby B cells undergo class switch recombination, somatic hypermutation and clonal expansion (Jacob et al., 1991; LeBien and Tedder, 2008).

T cells express the T cell receptor (TCR) and develop in the thymus. In contrast to the BCR that can recognize almost any type of structure, the TCR only recognizes its cognate antigen when it is presented on MHC-molecules (major histocompatibility complex). MHC-molecules are expressed on APCs and are loaded with short peptide sequences after the initial pathogenic agent has been processed (Hennecke and Wiley, 2001). T cells require a second not antigen-specific co-stimulatory signal for differentiation and clonal expansion. Without the co-stimulatory signal T cells that were only stimulated via their TCR become anergic or die (Janeway and Bottomly, 1994; Jenkins et al., 1988; Webb et al., 1990). Similar to BCRs, TCRs also undergo somatic rearrangement processes, commonly known as V(D)J-recombination. Through this process cells of the adaptive immunity can generate 10^{14} and 10^{18} different BCRs and TCRs, respectively (Medzhitov and Janeway, 2000).

1.1.2 T cell activation and differentiation

On a broad scale, peripheral T cells can be subdivided into two major categories. Cytotoxic T cells express the CD8 co-receptor and recognize cognate antigens presented on the MHCI molecules. Helper T cells (T_H) express the CD4 co-receptor and recognize antigen presented on MHCII. CD4 T cells can be further subdivided into five main subsets based on their function and effector cytokine production (Cantrell, 2015; Murphy, 2017).

Before T cells can exert their designated function, they need to be activated. This activation occurs in secondary lymphoid organs (spleen, lymph nodes), where T cells encounter professional APCs, which present cognate p:MHC (peptide:MHC) ligands. Binding of TCR to p:MHC as well as engagement of the CD4 or CD8 co-receptors is the first of three signals required for T cell activation and differentiation (Artyomov et al., 2010; Chen and Flies, 2013). The second signal is provided through the engagement of co-stimulatory or co-inhibitory receptors, such as CD28, Ox40, ICOS or CTLA4 on the surface of T cells by their respective ligands (Bour-Jordan et al., 2011; Walker and Sansom, 2011). The third signal stems from cytokines present in the environment which drive cell fate decisions (O'Shea and Paul, 2010). Integration of all inputs received from these three signals leads to T cell activation, differentiation and expansion (Mescher et al., 2006; Murphy, 2017; Ruterbusch et al., 2020). Following activation T cells migrate to the site of infection where they can exert their function.

The main functions of cytotoxic $CD8^+$ T cells are the protection against intracellular pathogens and the eradication of cancerous cells. Upon recognition of antigen on the surface of an infected cell perforin is released and forms pores in the membrane of the target cell. Through these pores cytotoxic T cells can deliver granzymes into the cytoplasm of the target cells which triggers apoptosis (Barber et al., 2003; Murphy, 2017). Activation of $CD8^+$ T cells requires stronger co-stimulation compared to $CD4^+$ T cells, due to the destructive nature of their effector function.

Distinct from $CD8^+$ T cells, $CD4^+$ cells can differentiate into several different subsets of effector cells depending on their cytokine milieu, and they mainly function by providing help to other immune and non-immune cell in the clearance of pathogens. The main subsets are T_H1, T_H2, T_H17, T_{FH} and T_{reg} cells, each of which is characterized by the expression of a master transcription factor as well as a hallmark cytokine (O'Shea and Paul, 2010) **(Fig. 1).**

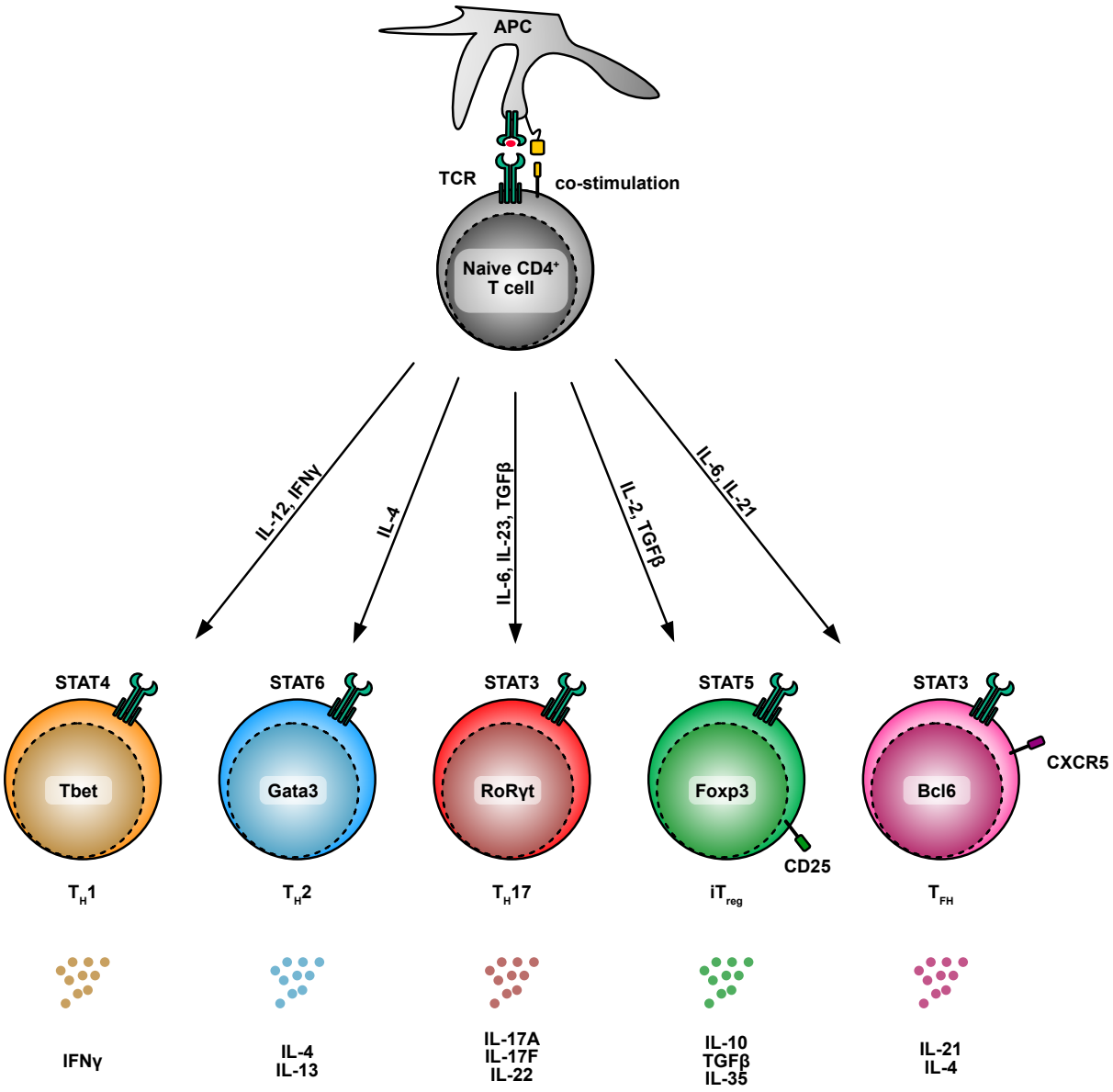

Fig. 1: Schematic overview over CD4⁺ T cell subsets.

CD4⁺ T cells differentiate into five major subsets: T_H1, T_H2, T_H17, T_{FH} and iT_{regs}. Differentiation is initiated by interaction of the TCR with the cognate peptide-loaded MHCII on APCs and co-stimulation. The cytokine milieu drives cell-fate decisions by phosphorylation of STAT proteins, which translocate into the nucleus and induce expression of lineage-defining transcription factors. Upon terminal differentiation each subset secrets a specific set of cytokines and expresses specific surface molecules. Based on (Murphy and Reiner, 2002; Murphy, 2017; O'Shea and Paul, 2010).

The T_H1 and T_H2 cell subsets were the first two CD4⁺ T cell subsets discovered and produce the effector cytokines IFNγ and IL-4, respectively (Murphy and Reiner, 2002). T_H1 cells are required for the defense against intracellular pathogens and differentiate in response to IL-12 followed by IFNγ signaling, which lead to phosphorylation of

STAT4 (signal transducer and activator of transcription) and STAT1, respectively, and subsequent expression of Tbet (Mullen et al., 2001; Murphy and Reiner, 2002; Szabo et al., 2000). T_H2 cells are necessary for the control of infections with extracellular parasites. This subset develops in response to IL-4 signaling, which causes phosphorylation of STAT6 and subsequent expression of the T_H2 lineage defining transcription factor GATA3 (Kaplan et al., 1996; Swain et al., 1990; Takeda et al., 1996).

T_H17 cells, which are necessary to combat extracellular bacteria and fungi, are the third major subset of $CD4^+$ effector cells and were discovered several decades after the first two T helper subsets (Acosta-Rodriguez et al., 2007b; Park et al., 2005). T_H17 cells differentiate in response to IL-6 and transforming growth factor β (TGFβ), signaling through which leads to the phosphorylation of STAT3. This induces expression of the master regulator RoRγt and the subsequent production of the hallmark cytokine IL-17 (Acosta-Rodriguez et al., 2007a; Ivanov et al., 2006; Park *et al.*, 2005; Yang et al., 2007). Furthermore, IL-23 has been shown to be important for the expansion of T_H17 cells (Aggarwal et al., 2003).

Interestingly, since the discovery of T_H17 cells in 2005 more and more studies have found that these cells not only play protective roles, but can also become pathogenic and promote inflammation, autoimmunity and cancer (Bettelli et al., 2006; Ghoreschi et al., 2010; Hofstetter et al., 2005; Langowski et al., 2006; Weaver et al., 2007). These findings suggest that imbalances in $CD4^+$ T cell subsets can cause disease.

The main function of all the T cell subsets described above is the activation or removal of their respective target cell, allowing to clear pathogens and abnormal cells quickly and efficiently. However, if left uncontrolled effector T cells can cause pathogenicity themselves. Thus, another subset of $CD4^+$ T cells exists whose main function it is to suppress T cell responses and prevent autoimmunity and inflammation (Dominguez-Villar and Hafler, 2018; Sakaguchi et al., 1995). These cells are known as induced regulatory T cells (iT_{regs}) and develop from naïve $CD4^+$ cells following TCR engagement and co-stimulation with TGFβ and IL-2 (Chen et al., 2003; Fontenot et al., 2005; Sakaguchi et al., 2008). iT_{regs} are characterized by the expression of CD25 and of their master transcription factor Foxp3 (Fontenot et al., 2003). They exert their suppressive function via IL-10 production (Saraiva and O'Garra, 2010). Furthermore, iT_{regs} constitutively express the co-inhibitory molecule CTLA4 on their surface, which allows them to compete with naïve $CD4^+$ and $CD8^+$ T cells for co-stimulatory signals

via CD80/CD86 interaction and have also been shown to actively remove these ligands from the surface of APCs by trans-endocytosis, thus reducing the potential for co-stimulation (Qureshi et al., 2011; Yamaguchi et al., 2013). Off note, besides iT_{regs} there is another subset of regulatory T cells, the thymic T_{regs} (tT_{regs}), which arise in the thymus during T cell development and are required to dampen immune responses and prevent self-reactivity (Murphy, 2017; Sakaguchi *et al.*, 2008).

1.1.3 T follicular helper cells and the germinal center response

T follicular helper cells (T_{FH}) are the last major subset of $CD4^+$ T cells, which different from the other subsets, remain in lymph nodes (LN) and in the spleen. Their primary function is to provide help to B cells, which then produce high-affinity antibodies during the germinal center (GC) reaction. These cells are characterized by the expression of the lineage-defining transcription factor Bcl6 as well as the homing surface receptor CXCR5 and the co-inhibitory receptor PD-1 (programmed cell death 1). They produce IL-4 and IL-21 as their main effector cytokines (Crotty, 2011; Haynes et al., 2007; Johnston et al., 2009; Nurieva et al., 2008; Yu et al., 2009).

In contrast to the other $CD4^+$ T cell subsets, differentiation of T_{FH} cells cannot be reduced to one single event that will define their differentiation, but is rather a multistep process that is dependent on a multitude of different signals (Crotty, 2014). The canonical T_{FH} differentiation process is induced after priming of naïve $CD4^+$ T cells by DCs in the T cell zones, followed by interaction with B cells (Crotty, 2014). The decision between a T_{FH} and non-T_{FH} cell fate is made within the first two rounds of division and is regulated by IL-6, ICOS, IL-2 and TCR signal strength during the priming phase (Choi et al., 2013b; DiToro et al., 2018; Fazilleau et al., 2009; Goenka et al., 2011). T cells with higher TCR affinity have a preference to differentiate into T_{FH} cells. This may be due to the fact that higher affinity TCRs leads to extended T cell:DC interaction and thus also increase exposure to co-stimulatory and cytokine signaling (Celli et al., 2007; Crotty, 2011; Fazilleau *et al.*, 2009).

The earliest signal in T_{FH} differentiation other than the TCR stimulus is provided by IL-6 which leads to a transient expression of Bcl6 *in vivo*. This transcription factor (TF) is necessary for the induction of CXCR5 expression and migration of early T_{FH} cells to the border of B cell follicles, where they interact with B cells via ICOS:ICOSL as well as p:MHC driving the formation of GCs (Choi et al., 2011; Choi *et al.*, 2013b; Crotty, 2019; Nurieva et al., 2009; Vinuesa et al., 2016). Interestingly, even though Bcl6 is

necessary for T_{FH} development, constitutive expression of Bcl6 *in vitro* is not sufficient for the induction of CXCR5 (Liu et al., 2014). IL-6 signaling also leads to the activation of STAT3 which has also been shown to be essential for T_{FH} differentiation, since mice deficient in STAT3 do not develop T_{FH} cells (Nurieva *et al.*, 2008) . However, IL-6 signaling by itself is not sufficient for T_{FH} differentiation, but an additional signal provided by IL-21 is required, suggesting a redundant role for these cytokines (Eto et al., 2011). ICOS expression on $CD4^+$ T cells during the priming stage is also necessary for efficient Bcl6 expression (Crotty, 2011). Contrary to the described effects of ICOS, IL-6 and IL-21, IL-2 signaling has been shown to suppress T_{FH} differentiation (Ballesteros-Tato et al., 2012; Johnston et al., 2012).

Expression of CXCR5 on $CD4^+$ T cells is critical for T_{FH} differentiation and is required for their migration to the T:B border, where the second stage of T_{FH} differentiation is executed (Arnold et al., 2007; Crotty, 2011; Garside et al., 1998; Hardtke et al., 2005). Here, the T cells can interact with activated, antigen-specific B cells via ICOS:ICOSL. This interaction is required for efficient T_{FH} differentiation and absence or blockade of ICOS signaling leads to an impaired T_{FH} development (Akiba et al., 2005; Bossaller et al., 2006; Pedros et al., 2016; Xu et al., 2013). ICOS signaling is additionally important for antibody class switch, however CD40 stimulation in the absence of ICOS can restore defective class switching (McAdam et al., 2001). T cell interaction with cognate B cells after the initial priming step is crucial for T_{FH} cell fate commitment, which is supported by the findings that in the absence of B cells T_{FH} cell phenotypes are lost (Crotty, 2011; Johnston *et al.*, 2009). On the other hand, T cell:B cell interactions are also necessary for the survival of B cells, since they have been shown to die shortly after antigen recognition if no T cell help can be provided (Akkaya et al., 2018).

Germinal centers are the location of the third and last stage of full T_{FH} cell polarization. At this stage GC T_{FH} express high levels of Bcl6, CXCR5, PD1 and ICOS, whereas T_{FH} cells with lower expression of these markers are usually located close to or in the follicle (Crotty, 2011; Haynes *et al.*, 2007). Adhesion molecules, like SLAMF6, CD84 or SLAM (signaling lymphocyte activation molecule) are important for the regulation of interaction between GC T_{FH} and GC B cells. The cytoplasmic SLAM-associated protein (SAP) is essential at this stage of differentiation for the maintenance of GC T_{FH} and B cell adhesion which is necessary for sufficient B cell help. In the absence of SAP or in conditions where SAP is defective due to genetic mutations both, T_{FH} and GC B cells cannot develop (Hu et al., 2013; Qi et al., 2008), presumably due to defective T cell:

B cell interactions so that T_{FH} cells can no longer receive sufficient signals from B cells for the final differentiation step into GC T_{FH} cells (Crotty, 2011).

The main function of fully differentiated T_{FH} cells is to provide help to B cells via IL-21 and CD40L, which promote B cell survival and differentiation into GC B cells. IL-4 produced by T_{FH} also plays important roles during the GC response (Lee et al., 2011; Weinstein et al., 2016; Yusuf et al., 2010). At the T:B border B cells compete for early T_{FH} cell help, so that only B cells with high affinity BCRs, i.e. B cells with high levels of p:MHCII expression, can enter germinal centers. B cells that have received T_{FH} cell help then undergo several rounds of division, somatic hypermutations and antibody affinity maturation, ultimately leading to the production of high affinity antibodies (Crotty, 2019; Gitlin et al., 2014; Schwickert et al., 2011).
Although the field of T_{FH} cell research has exploded since their discovery, their development is very complex and many open questions still remain concerning T_{FH} cell differentiation and function. Furthermore, although T_{FH} cells function to protect us from infections, aberrant induction of T_{FH} cells is associated with a magnitude of diseases, including autoimmune diseases, cancer and allergies (Crotty, 2019). Thus, it is important to further investigate the molecular requirements for the differentiation of these cells in more detail to fully understand their function in health and disease.

1.2 Post-transcriptional gene regulation by RNA-binding proteins

Translation of mRNA into protein is a highly regulated process and this regulation has been shown to be crucial for controlling appropriate immune responses and immune cell differentiation (Anderson, 2010; Hao and Baltimore, 2009). Post-transcriptional gene regulation mainly targets the untranslated regions (UTR) of mRNAs through binding of stabilizing or de-stabilizing *trans*-acting factors. These factors can be RNA-binding-proteins (RBPs), microRNAs (miRNAs) or long non-coding RNAs, that recognize and bind specific secondary structures or linear motifs within the UTRs, the *cis*-elements (Anderson, 2010). *Cis*-elements in the 3'UTR affect both mRNA stability and translation, whereas *cis*-elements in the 5'UTRs are more important for the regulation of translation efficiency (Rissland, 2017).

1.2.1 Mechanisms of deadenylation-dependent mRNA decay

Degradation of most mRNAs in eukaryotes is initiated by shortening of the poly(A)-tail, followed by one of two irreversible, mutually exclusive degradation processes. Decapping, i.e. removal of the 5' cap, initiates degradation from the 5' end by the exoribonuclease XRN1, whereas degradation from the 3' end is achieved by the exonuclease complex known as the exosome (Garneau et al., 2007).

The 5' – 3' decay pathway is vital for quality control of mRNAs as well as immune responses (Abernathy and Glaunsinger, 2015; Li et al., 2012), and can occur both co-transcriptionally and co-translationally (Brannan et al., 2012; Hu et al., 2009). It is initiated by shortening of the poly(A)-tail by the PAN2-PAN3 complex followed by further deadenylation via the CCR4-NOT complex (Collart, 2016; Mugridge et al., 2018; Webster et al., 2018; Wolf and Passmore, 2014).

Deadenylation is initiated when PABP or poly(A) RNAs are recognized by PAN3, which then recruits PAN2 and stimulates its deadenylase activity. PAN3 also plays a role in miRNA-mediated decay, by recruiting the deadenylase machinery to miRNA targets (Braun et al., 2011; Jonas et al., 2014; Schäfer et al., 2014). Following initial shortening of the 3' poly(A)-tail the multiprotein CCR4-NOT complex, containing the exonucleases Ccr4 and Caf1 (Ukleja et al., 2016), is needed to carry out further deadenylation. This complex can be recruited to mRNA by various adapter proteins, among others tristetraproline (TTP) (Fabian et al., 2013) and the Roquin family proteins (Leppek et al., 2013). Recent evidence suggests, that PAN2-PAN3 and CCR4-NOT mediated deadenylation not only occurs sequentially, but that at least in yeast, both complexes appear to have different preferences for RNA populations and can cause deadenylation independent from each other (Mugridge *et al.*, 2018; Sun et al., 2013). A schematic overview of the deadenylation dependent mRNA degradation mechanism is shown in **Fig. 2**.

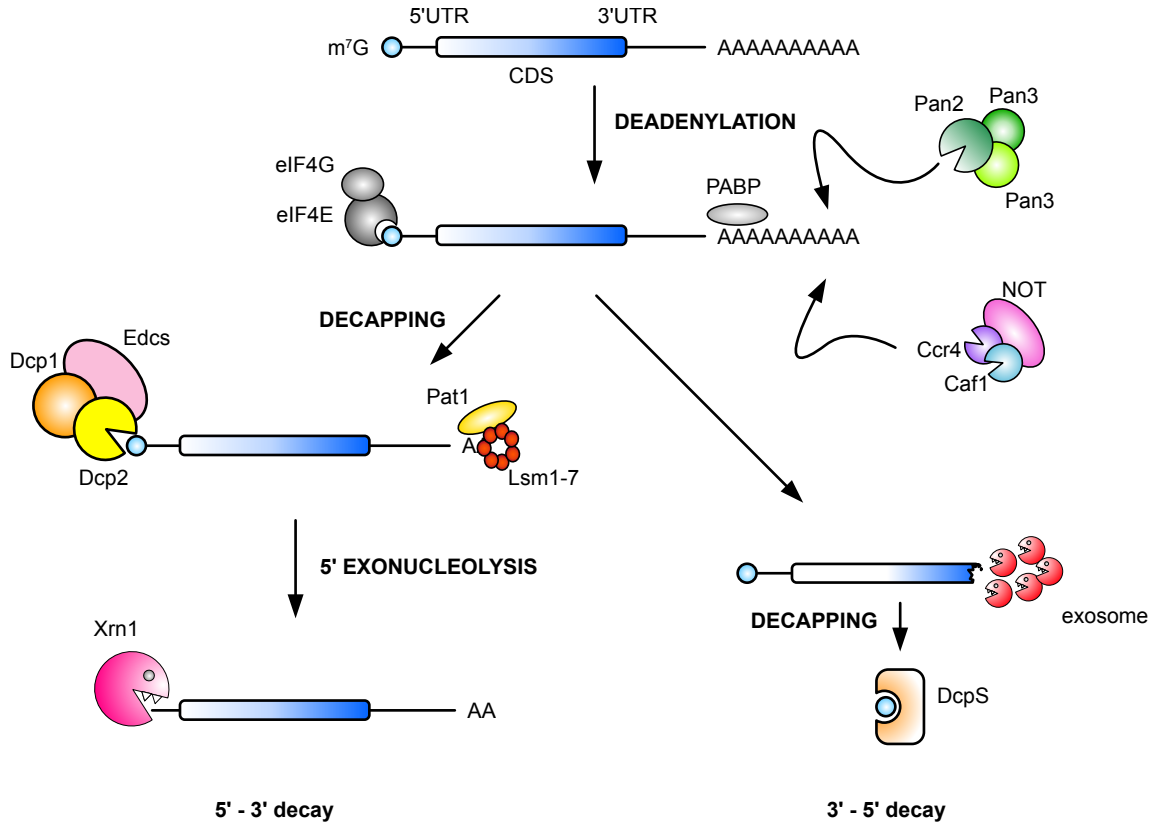

Fig. 2: Mechanisms of deadenylation-dependent mRNA decay.
Schematic representation of deadenylation-dependent mRNA decay. Mature mRNAs contain a 5'UTR (untranslated region) with an m^7G cap structure, followed by the coding sequence (CDS), a 3'UTR and a poly(A)-tail. Degradation is initiated by the removal of PABP by the Pan2-Pan3 complex and initial poly(A)-tail shortening. Further deadenylation is carried out by the CCR4-Caf1-NOT complex. 5'-3' decay entails the removal of the m^7G cap by the enzymes Dcp1, Dcp2 and Edcs, and binding of the Lsm1-7 ring structure to the shortened oligo(A)-tail. Following decapping mRNAs are degraded by the exonuclease Xrn1. 3'-5' decay is achieved through the exosome complex, followed by the digestion of the remaining m^7G cap by DcpS. Adapted from (Garneau *et al.*, 2007; Mugridge *et al.*, 2018).

The next step in deadenylation induced mRNA decay is the removal of the 5' m^7G cap by the decapping complex, made up of Dcp1 and Dcp2. Decapping is mediated by the Pat1-Lsm1-7 complex. The Lsm1-7 ring binds to the shortened oligo(A)-tail and Pat1 interacts with the disordered C-terminal tail of Dcp2 (Charenton et al., 2017; Chowdhury et al., 2007; Wu et al., 2014). The CCR4-NOT complex can also directly interact with the decapping complexes by binding to DDX6 or by binding to short linear motifs found in the decapping co-activators Edc3, Pat1 and Scd6 (Fromm et al., 2012; Mugridge *et al.*, 2018; Sharif et al., 2013). Once the 5' cap is removed, the mRNA can

be quickly degraded by binding of the exonuclease Xrn1 to the exposed 5' monophosphate of the RNA (Nagarajan et al., 2013).
3'-5' decay is achieved by a large protein complex called the exosome (Mitchell et al., 1997). It is constituted of several proteins with phosphorolytic exoribonuclease and RNA helicase activities (Garneau *et al.*, 2007; Houseley et al., 2006) . Once the mRNA is degraded by the exosome the left over 5'cap is removed by DcpS, a scavenger decapping enzyme (Liu et al., 2002).

1.2.2 Sites of mRNA decay

To be able to rapidly respond to environmental changes a strict equilibrium of mRNA translation and decay is maintained both temporally and spatially. Processing bodies (P-bodies) are membrane-less, cytoplasmic structures that are one crucial component regulating 5'-3' mRNA decay and translational repression. These structures contain core mRNA decay proteins like Dcp1 and Dcp2, Edc3 and Lsm1-7, as well as Xrn1 and the Ccr4-Not complex proteins (Decker and Parker, 2012). They are present in unstressed cells, and their abundance is adjusted dependent on the abundance of non-translating mRNAs (Teixeira and Parker, 2007). Stress granules are another structure that are important for the control of mRNA turnover. These structures form in response to stress, contain translation initiation factors and have been suggested to have a triage function, targeting certain transcripts for degradation in P-bodies (Buchan et al., 2008; Buchan et al., 2011; Kedersha et al., 2005).

1.2.3 *Cis*-regulatory elements

40-50% of changes in gene expression occur at the level of mRNA stability, which in turn is predominantly regulated via secondary structures and linear motifs within 3'UTRs (Cheadle et al., 2005; Fan et al., 2002; Garneau *et al.*, 2007).
AU-rich elements (ARE) are probably the most extensively studied stability elements and can be found in the 3'UTRs of many genes encoding for cytokines, proto-oncogenes and transcription factors (Beisang and Bohjanen, 2012; Khabar, 2005). They are made up of the pentameric sequence, AUUUA (Caput et al., 1986) and can be subdivided into three classes, according to their sequence context (Bolognani and Perrone-Bizzozero, 2008). AREs can be targeted by miRNAs and by RBPs leading to mRNA decay (Jing et al., 2005; Lai et al., 1999). One prominent example is TTP, a

zink finger protein that has been shown to bind to AREs contained in the *Tnfa* 3'UTR and to promote mRNA deadenylation by recruiting the CCR4-NOT complex (Carballo et al., 2000; Lai *et al.*, 1999; Lai et al., 2000; Lykke-Andersen and Wagner, 2005). However, AREs are not the only *cis*-regulatory elements present in the *Tnfa* 3'UTR. It has also been shown to contain a highly conserved secondary stem-loop structure topped by a pyrimidine-purine-pyrimidine (py-pu-py) tri-loop, which is necessary for efficient decay of the *Tnfa* 3'UTR. This stem loop structure is now known as the constitutive decay element (CDE) (Leppek *et al.*, 2013; Stoecklin et al., 2003) and in pull down experiment another class of RBPs with a preference for CDE binding was identified, namely the Roquin family proteins (*Rc3h1* and *Rc3h2)*. Later these proteins were also shown to be involved in CDE-mediated mRNA decay and play a major role in the control of immune cell homeostasis, which will be discussed in the following section.

1.2.4 Roquin family proteins

Roquin-1 was identified in 2005 by a N-ethyl-N-nitrosourea (ENU) mutagenesis screen for autoimmune regulators. A single homozygous mutation in Roquin-1, an exchange of methionine to arginine at position 199 (M199R), leads to the development of severe T_{FH}-driven systemic lupus erythematosus (SLE)-like autoimmune disease in the *sanroque* mouse (Vinuesa et al., 2005). Later, Roquin-1 was identified as an RBP belonging to the Roquin protein family, which is made up of two paralogues Roquin-1, encoded by *Rc3h1*, and Roquin-2, encoded by *Rc3h2.* These paralogues are important regulators of immune responses that act via mRNA degradation and post-transcriptional repression of key immune targets, thus preventing autoimmunity. In T cells, the two Roquin paralogues have redundant functions (Heissmeyer and Vogel, 2013; Pratama et al., 2013; Vinuesa *et al.*, 2005; Vogel et al., 2013).

1.2.4.1 Roquin mouse models

<u>The *sanroque* mouse</u>

Mice with a homozygous *sanroque* mutation (*Rc3h1*$^{san/san}$) developed a strong, lupus-like autoimmune phenotype at the age of 6-7 weeks or 8-16 weeks in female and male mice, respectively. It was characterized by profound splenomegaly and

lymphadenopathy, increased portions of activated CD44^{hi} CD4^{+} and CD8^{+} T cells, spontaneous accumulation of T_{FH} as well as GC B cells in the absence of immunization, and the appearance of anti-nuclear antibodies (ANAs) (Vinuesa *et al.*, 2005). Furthermore, these mice exhibited hypergammaglobulinemia, necrotizing hepatitis, anemia and proliferative glomerulonephritis with depositions of IgG-containing immune complexes, as well as autoimmune thrombocytopenia. All these pathological changes developed despite an expansion of the T_{reg} compartment and have been proposed to be due to T cell-intrinsic functions of Roquin (Athanasopoulos et al., 2010; Linterman et al., 2009a; Linterman et al., 2009b; Vinuesa *et al.*, 2005).
CD4^{+} and CD8^{+} T cells in the *sanroque* mouse showed strongly elevated ICOS expression with concomitant increases in T_{FH} cell associated markers, CXCR5, Ccl5 and IL-21. Aberrant ICOS expression is, at least in parts, responsible for the development of the *sanroque* phenotype, since mice harboring a *sanroque* mutation with a heterozygous ICOS deletion (*Rc3h1$^{san/san}$; Icos$^{+/-}$)* showed a reduction in T_{FH} and GC B cells, underlining the importance of ICOS regulation by Roquin in the prevention of T- and B- cell accumulation (Yu et al., 2007). However, complete ablation of ICOS in the *sanroque* mice did not rescue splenomegaly, but on the contrary exacerbated splenic hypercellularity, led to a production of ANAs, and a decrease in T_{reg} cells (Lee et al., 2012), suggesting that the *sanroque* phenotype was not only a consequence of ICOS overexpression. Interestingly, the M199R mutation in Roquin-1 did not interfere with RNA binding (Athanasopoulos *et al.*, 2010).

Roquin-1 loss-of-function

To dissect the mechanism of disease development in *sanroque* mice and to assess whether this single amino acid mutations caused a Roquin-1 loss-of-function several other mouse models with Roquin deletions were generated. Mice with a systemic deletion of Roquin-1 (*Rc3h1$^{-/-}$*) died within 6h of birth, displayed severe malformation of the caudal spinal column and retarded development of lung alveoli (Bertossi et al., 2011), whereas mice with a heterozygous Roquin deletion (*Rc3h1$^{+/-}$*) or *sanroque* mutations (*Rc3h1$^{san/+}$*) appeared to be healthy (Bertossi *et al.*, 2011; Vinuesa *et al.*, 2005).
To allow investigation of cell-type specific functions of Roquin-1 mice were generated that contained loxP sites flanking exons 4-6 of the *Rc3h1* gene (*Rc3h1$^{fl/fl}$*). These mice were subsequently crossed with various cre-recombinases to allow for conditional

deletions in T cells (*Cd4*-cre), B cells (*Cd19*-cre) or in all hematopoietic cells (*vav*-cre). Ablation of Roquin-1 in the T cell lineage caused elevated ICOS levels and an increase in the $CD8^+$ T cell effector-memory compartment. Ablation of Roquin-1 in B cells led to an expansion in B and effector-like T cells, and to a general deregulation of immune homeostasis. Roquin-1 deficiency in the entire hematopoietic system was characterized by increased ICOS expression, activation of $CD4^+$ and $CD8^+$ T cells, and accumulation of T_{FH} as well as GC B cells. However, all these effects were mild compared to the *sanroque* mouse and did not lead to the development of autoimmunity, suggesting that the *sanroque* mutation caused perturbations in Roquin-1 function which cannot be explained by a loss-of-function, and that other proteins may compensate for the absence of Roquin-1 (Bertossi *et al.*, 2011).

Roquin-2 loss-of-function

In higher vertebrates the Roquin protein family is made up of two paralogues, Roquin-1 (*Rc3h1*) and Roquin-2 (*Rc3h2)*, also known as MNAB (membrane-associated nucleic acid binding protein) (Heissmeyer and Vogel, 2013; Siess et al., 2000). Systemic ablation of Roquin-2, by inserting a neomycin resistance cassette ($Rc3h2^{neo/neo}$) led to decreased viability of pups and postnatal death. Similar to the systemic Roquin-1 knock out these mice showed an immature lung phenotype, albeit not as severe. Interestingly, conditional Roquin-2 ablation in T cells did not lead increased T cell activation, ICOS expression or accumulation of T_{FH} or GC B cells (Vogel *et al.*, 2013), suggesting that Roquin-1 and Roquin-2 may have redundant functions.

Roquin-1/2 conditional knock-outs

Indeed, mice with combined conditional Roquin-1 and Roquin-2 knock-out in T cells ($Rc3h1^{fl/fl}$; $Rc3h2^{fl/fl}$; *Cd4*cre or DKO^T) developed splenomegaly, lymphadenopathy, and showed strong spontaneous activation of $CD4^+$ and $CD8^+$ T cells. Furthermore, these mice exhibited elevated ICOS levels on T cells as well as increased T_{FH} and GC B cell frequencies, partially phenocopying the *sanroque* phenotype and confirming functional redundancy of Roquin proteins (Pratama *et al.*, 2013; Vogel *et al.*, 2013). Conditional Roquin-1/2 ablation in T cells resulted in severe lung inflammation with a consequent reduction in alveolar space and decreased average survival of the mice. These mice additionally developed gastritis, showed thickening of arterial walls and

sera taken from these mice were reactive against pancreatic antigens. In contrast to the *sanroque* mouse, DKO^T mice did not develop anti-nuclear antibodies. Severe lung inflammation in DKO^T mice developed due to a bias of these T cells to differentiate towards T_H17 which was mediated by elevated IκBNS expression (Jeltsch et al., 2014), unravelling a role of Roquin proteins in the control of T cell differentiation besides T_{FH} cells. Further evidence for Roquin function in T cell differentiation emerged from the analysis of natural killer T (NKT) cells in DKO^T mice, where Roquin-1/2 ablation led to an increase in hyporesponsive NKT17 cells (Drees et al., 2017). In T_{reg} cells Roquin deficiency caused a loss of suppressive capacity and aberrant development of T follicular regulatory (T_{FR}) cells (Essig et al., 2017).

Taken together, these data show that Roquin-1 and Roquin-2 play redundant roles in T cells and deficiency of these paralogues can partially phenocopy the autoimmunity observed in *sanroque* mice. Interestingly, although Roquin-2 can compensate for the absence of Roquin-1 in T cells, it cannot rescue autoimmunity in *sanroque* mice. Recently, we were able to unravel the molecular basis for this difference, by showing that the M199R mutation prevents interactions of Roquin-1 with Regnase-1, another RNA-binding protein, that shares an overlapping target set with the Roquin proteins (Behrens et al., 2021; Mino et al., 2015).
So far, work analyzing functions of Roquin proteins has mainly focused on cell intrinsic consequences of mRNA deregulation in the absence of these proteins. However, as described above Roquin-deficient T cells may also act in *trans* on bystander immune and non-immune cells. The mechanisms leading to these changes have been poorly described and require more detailed investigations.

1.2.4.2 Domain organization and function

Roquin proteins are enriched in P-bodies in the cytoplasm and re-localize to stress granules in response to stress (Athanasopoulos *et al.*, 2010; Glasmacher et al., 2010; Srivastava et al., 2015; Vinuesa *et al.*, 2005). In the absence of Roquin-1 Roquin-2, even though expressed at significantly lower levels, can compensate for the loss-of-function, demonstrating redundant functions of these paralogues (Jeltsch *et al.*, 2014; Pratama *et al.*, 2013).
The N-terminal regions which is important for RNA-binding (Sakurai et al., 2015; Schlundt et al., 2014; Schuetz et al., 2014) is highly conserved between Roquin-1 and

Roquin-2, and contains the RING (really interesting new gene)-domain, the ROQ-domain flanked by $HEPN_N$ and $HEPN_C$ (higher eukaryotes and procaryotes nucleotide-binding, N-terminal and C-terminal, respectively) stretches, and a CCCH-type zink finger. The C-terminus, which is intrinsically disordered, is important for the recruitment of the deadenylation machinery (Leppek *et al.*, 2013; Murakawa et al., 2015) and contains proline-rich regions (PRR) as well as a coiled-coil domain (Roquin-1) or hydrophobic stretches (Roquin-2) **(Fig. 3).**

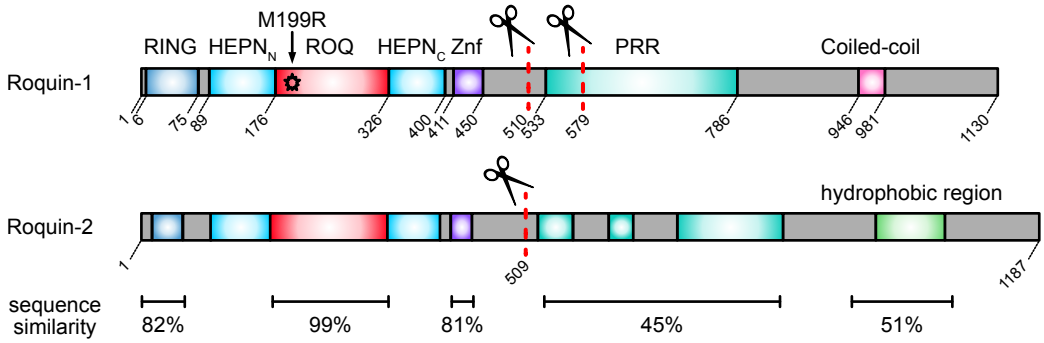

Fig. 3: Domain organization of Roquin proteins.

Schematic representation of the domain organization of Roquin-1 and Roquin-2. Both proteins contain a RING (really interesting new gene), the RNA-binding ROQ-domain embedded in a $HEPN_N$ and $HEPN_C$ domain (higher eukaryotes and procaryotes nucleotide – binding, N – terminal and C – terminal, respectively), a CCCH-type ring finger (ZnF) domain, and a proline-rich region (PRR). Roquin-1 contains a coiled-coil domain at the C-terminus, and Roquin-2 harbors a hydrophobic region. Numbers indicate the amino acid (aa) positions of the individual domains. MALT-1 cleavage sites are indicated by scissors. Position of the M199R mutation is indicated in Roquin-1. Structure and similarity information is based on and adapted from (Jeltsch and Heissmeyer, 2016; Pratama *et al.*, 2013; Schlundt *et al.*, 2014; Srivastava *et al.*, 2015).

The function of the RING domain is not completely understood to date. In RLE-1, the Roquin homolog in *C. elegans*, it has been suggested to have E3 ligase activity and to induce proteasomal degradation of apoptosis-signaling kinase 1 (ASK1) upon ROS (reactive oxygen species) induced stress (Li et al., 2007; Maruyama et al., 2014). In T cells, the RING domain was found to be necessary for the correct localization of Roquin to stress granules and was furthermore able to auto-ubiquitinate Roquin-1 thereby resulting in aberrant mTOR signaling and accumulation of T_{FH} cells (Athanasopoulos *et al.*, 2010; Ramiscal et al., 2015).

The ROQ domain is highly conserved between Roquin-1 and Roquin-2 and high-resolution structures are available, identifying the ROQ domain as the RNA-binding

domain of both Roquin paralogues (Sakurai *et al.*, 2015; Schlundt *et al.*, 2014; Schuetz *et al.*, 2014; Tan et al., 2014). It is flanked by the $HEPN_N$ and the $HEPN_C$ domains, which can bind to double-stranded RNA independently from the ROQ domain (Srivastava *et al.*, 2015).

The ROQ domain binds to specific 5-7 nucleotides (nt) long secondary structures in the 3'UTR of mRNAs called constitutive decay elements (CDE) **(Fig. 4).** These structures are topped by a pyrimidine-purine-pyrimidine (py-pu-py) tri-loop sequence and were first shown to strongly suppress mRNA expression in the *Tnfa* 3'UTR (Leppek *et al.*, 2013; Stoecklin *et al.*, 2003). Over the years, CDE and CDE-like elements have been identified in the 3'UTRs of a number of additional mRNAs, including important immune regulators and effector molecules like *Icos, Ox40, Ctla4, Nfkbid* and *Nfkbiz* (Braun et al., 2018; Codutti et al., 2015; Janowski et al., 2016; Jeltsch *et al.*, 2014; Leppek *et al.*, 2013; Schlundt *et al.*, 2014; Yu *et al.*, 2007). Roquin-RNA binding and efficient post-transcriptional regulation of its target mRNAs was strongly dependent on three amino acids within the ROQ domain (Lys220, Lys239 and Arg260). Mutations of one or several of these amino acids led to an impairment or abrogation of Roquin mediated regulation, respectively (Schlundt *et al.*, 2014).

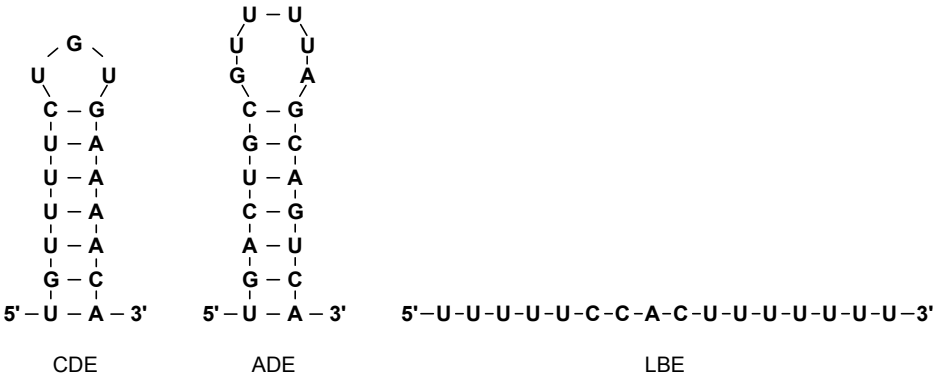

Fig. 4: Known Roquin binding structures and motifs.

Schematic of structures and sequences in Roquin target mRNAs. CDE (constitutive decay element) as found in the *Tnfa* 3'UTR. The ADE (alternative decay element) was identified in a SELEX screen (Systematic Evolution of Ligands by Exponential Enrichment) and the LBE (linear binding element) in a PARClip screen. Adapted from (Braun *et al.*, 2018; Essig et al., 2018; Janowski *et al.*, 2016; Schlundt *et al.*, 2014).

Besides the CDE Roquin has been shown to bind to U-rich hexaloop structures topping a 5-8nt stem. This element was termed the alternative decay element (ADE) **(Fig. 4)** and an ADE-like structure was identified in the *Ox40* 3'UTR. Both, ADE-like

and CDE-like structures in the *Ox40* 3'UTR were bound by Roquin and had additive effects on the regulation (Janowski *et al.*, 2016).
Recently, our group showed that Roquin is also able to bind to an additional linear binding element (LBE) via its ROQ domain. This 15nt long sequence consists of a CAC trinucleotide embedded in a linear U-rich sequence and was present in a large number of Roquin-bound mRNAs in PAR-CLIP experiments (Essig *et al.*, 2018).

Roquin proteins themselves are not able to degrade mRNAs. Instead, Roquin post-transcriptionally represses bound targets by recruiting the Ccr4-Caf1-NOT deadenylase complex via its C-terminal domain. Thus, Roquin proteins were suggested to play a role as adaptor proteins during mRNA decay (Leppek *et al.*, 2013). Furthermore, Roquin was shown to co-immunoprecipitate with Edc4 and Rck, which are involved in mRNA decapping and degradation from the 5' end. A function of Roquin proteins in mRNA decay is further supported by their localization to P-bodies (Glasmacher *et al.*, 2010). Repression of *Icos* and *Ox40* mRNA is enhanced by Roquin interaction with its co-factor NUFIP2 (Rehage et al., 2018).

1.2.4.3 Regulation of Roquin proteins in T cells

Under homeostatic conditions Roquin proteins are bound to their target mRNAs and lead to post-transcriptional repression and mRNA decay. As described before a number of important immune-related genes like *Icos, Ctla4* and *Ox40* are among the best known Roquin targets, suggesting that Roquin abundance and target release need to be tightly regulated. This is achieved through proteolytic cleavage of Roquin proteins by the paracaspase MALT1. Both, Roquin-1 and Roquin-2 contain two or one MALT1 cleavage sites, respectively. Upon T cell activation via the TCR in combination with co-stimulation through CD28, MALT1 is activated which leads to Roquin cleavage and subsequent release of the repressed mRNAs **(Fig. 5)**. Interference with or inhibition of MALT1 activity in T cells prevented cleavage of Roquin proteins (Gewies et al., 2014; Jeltsch *et al.*, 2014).

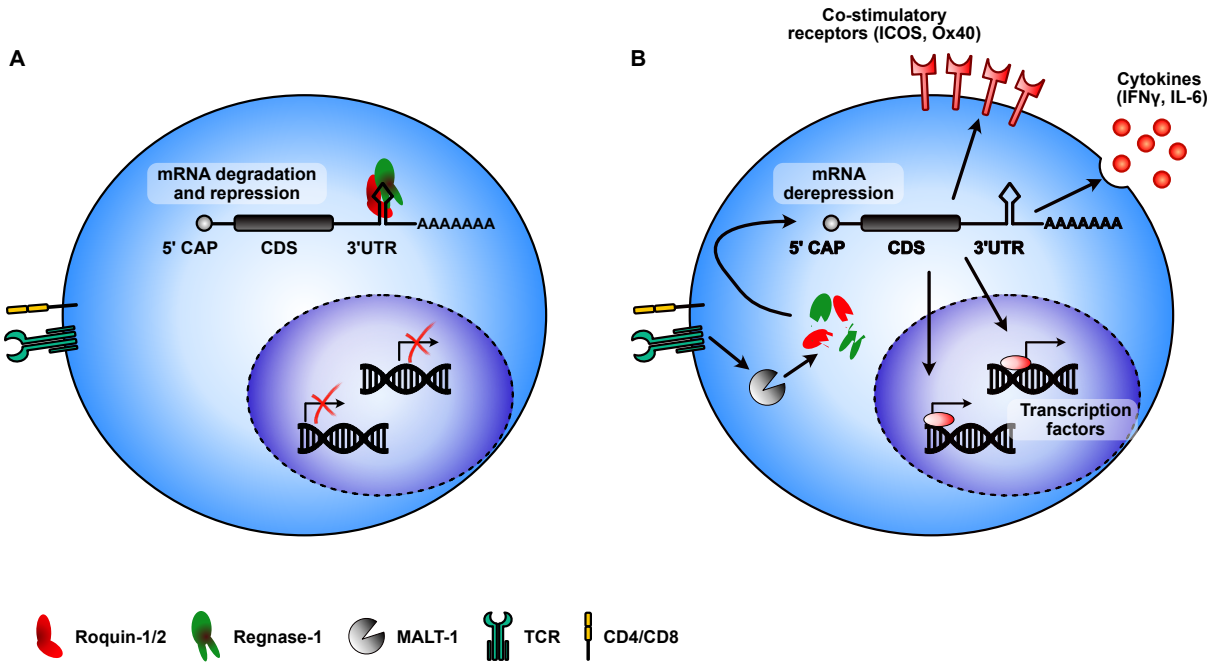

Fig. 5: Regulation of Roquin proteins in T cells.

(A) Under steady state conditions Roquin and Regnase proteins are bound to the 3'UTR of their target mRNAs and lead to post-transcriptional repression and mRNA decay. **(B)** TCR stimulation leads to an activation of the paracaspase MALT1 which cleaves Roquin-1/2 and Regnase-1 thereby allowing translation of the previously repressed mRNAs. Roquin-1/2 and Regnase-1 targets include co-stimulatory receptors, inflammatory cytokines and transcription factors. Adapted from (Jeltsch and Heissmeyer, 2016; Jeltsch *et al.*, 2014).

The function of the resulting N-terminal cleavage product which contains the ROQ-domain required for mRNA binding is currently not clear. Recently, we were able to show that in the absence of full length Roquin proteins, the Roquin-1$^{aa1-510}$ fragment was still able to regulate ICOS and Regnase-1 expression, but was not functional in the regulation of other targets, like Ox40 (Behrens *et al.*, 2021).

1.3 Gross anatomy and function of the pancreas

The pancreas is part of the gastrointestinal system and is responsible for the production of digestive enzymes as well as for the secretion of hormones related to the energy metabolism. The pancreas is made up of two parts. The smaller endocrine pancreas which accounts for 1-2% of the pancreatic mass produces hormones, like insulin and glucagon. The rest of the organ is made up from the exocrine pancreas, comprised of acinar and duct cells as well as the associated connective tissue, nerves and blood vessels (Longnecker, 2021). It is subdivided into lobules that are

surrounded by a thin capsule of connective tissue, and each lobule consists of acini, which are groups of large, tightly packed secretory epithelial cells, the acinar cells, surrounding a lumen (Liggitt and Dintzis, 2018). In this work only aspects concerning the exocrine portion of the pancreas will be discussed.

1.3.1 Pancreatic ductal adenocarcinoma

Pancreatic ductal adenocarcinoma (PDAC) is the most common form of pancreatic cancer and is the fourth leading cause of cancer related death. Over the last 20 years the number of yearly diagnosed new cases has doubled, from 196 000 cases in 1990 to 441 000 new cases in 2017, and the incidence is projected to increase over the next decade due to an increased average age of the population in developed countries (Klein, 2021; Rahib et al., 2014). Even though survival rates for patients suffering from pancreatic cancers have slightly improved in the last decades, owing to better diagnostic and imaging tools, they still remain very low. Currently, the estimated 5-year survival rate for pancreatic cancer is ~9% in Europe and the USA (Rahib *et al.*, 2014; Siegel et al., 2021). The poor prognosis arises in parts from late-stage diagnosis, since PDAC is nearly asymptomatic during early stages and forms distant metastasis early in development, preventing successful surgical resection in the majority of patients. Furthermore, PDAC is resistant to most conventional therapies due to its dense tumor microenvironment and it accumulates a number of genetic alterations (Kleeff et al., 2016).

1.3.2 Carcinogenesis in the pancreas is a multistep process

Acinar-to-ductal metaplasia (ADM) is generally considered to be the first step in PDAC development (Kanda et al., 2012; Orth et al., 2019; Storz, 2017). It is a normal and reversible process which occurs in response to stress (by inflammation or injury) and is characterized by the dedifferentiation or trans-differentiation of acinar cells into embryonic progenitor cells with duct-like properties (Pinho et al., 2011). This process is believed to be important for the regeneration of acinar cells and for the maintenance of a healthy pancreas (Liou et al., 2013; Storz, 2017). However, upon acquisition of the oncogenic Kras mutation, acinar cells can no longer re-differentiate, expression of ductal genes (cytokeratin-19, mucin-1) is initiated and precancerous pancreatic intraepithelial neoplasia (PanIN) develops (Kopp et al., 2012). Oncogenic Kras by itself

can only drive tumor development in the initiation phase, for further progression of PanINs to PDAC additional pro-tumorigenic events are necessary, including inflammation (Guerra et al., 2011; Guerra et al., 2007; Liou *et al.*, 2013), accumulation of additional gene mutations and further amplification of *Kras* signaling (Ji et al., 2009; Mueller et al., 2018).

The next step in PDAC development is the progression of ADMs to PanIN1A, PanIN1B and PanIN2 lesions **(Fig. 6).** Additional inactivation in tumor suppressor genes (*Tp53, Brca2* and *Smad4*) cause further progression of these preneoplastic lesions into high-grade PanIN3 and PDAC (Hruban et al., 2000; Storz, 2017). Already in the early precancerous PanIN1 and PanIN2 lesions cells have been shown to acquire invasive properties by undergoing epithelial-to-mesenchymal transition (EMT). Interestingly, EMT and dissemination was shown to be linked to inflammation (Rhim et al., 2012).

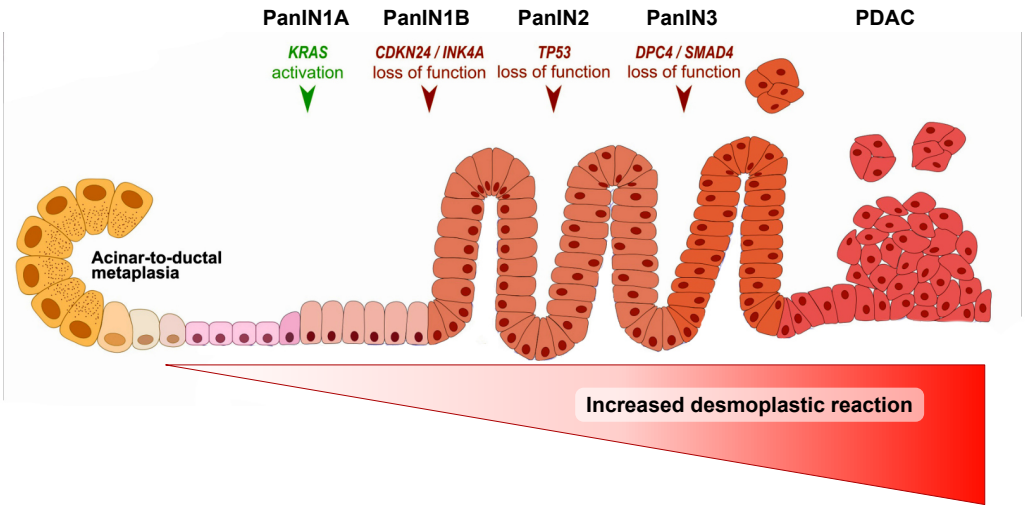

Fig. 6: Schematic representation of PDAC development.

Schematic overview of the development of PDAC. Acinar cells undergo acinar-to-ductal metaplasia (ADM) in response to environmental changes in the pancreas and acquire properties associated with duct cells. Upon acquisition of an oncogenic Kras mutation ADMs progress into low-grade PanIN1A lesions. Additional acquisition of genetic alterations leads to progression of PanINs to PDAC. Immune cells play an important role in this progression and higher grades of preneoplastic lesions are correlated with more pronounced desmoplastic reactions and stronger immune cell infiltrations into the tissue. Image modified from (Liot et al., 2021).

Histologically, PanINs are microscopic lesions that are made up of neoplastic epithelium and can be subdivided according to the grade of dysplasia. PanIN1A and PanIN1B lesions are low grade lesions characterized by tall columnar epithelial cells and basally located nuclei, and in the case of PanIN1B lesions, papillary architecture. PanIN2 and PanIN3 lesions are mid- to high-grade lesions characterized by papillary epithelium and moderate to extensive cytological atypia, respectively. Complete loss of cellular polarity is usually observed in PanIN3 lesions (Brosens et al., 2015).

1.3.3 $Kras^{G12D}$-driven models of PDAC development

An activating Kras mutation is present in >90% of pancreatic cancers (Drosten et al., 2018; Hezel et al., 2006). The development of the $Kras^{LSL\text{-}G12D}$ mouse allowed the expression of the activating mutation at physiological levels (Jackson et al., 2001). This mouse harbors a STOP cassette which is flanked by LoxP sites upstream of the G>D mutation and allows for tissue specific expression of the mutant Kras allele via Cre-mediated recombination. Hingorani and colleagues were later able to establish a mouse model that recapitulates pancreatic cancer formation via the known PanIN1 to PanIN3 progression by crossing the $Kras^{LSL\text{-}G12D}$ mouse to mice expressing a Cre recombinase under the pancreas specific promotors *Pdx1* and *Ptf1a* (p48) (Hingorani et al., 2003).

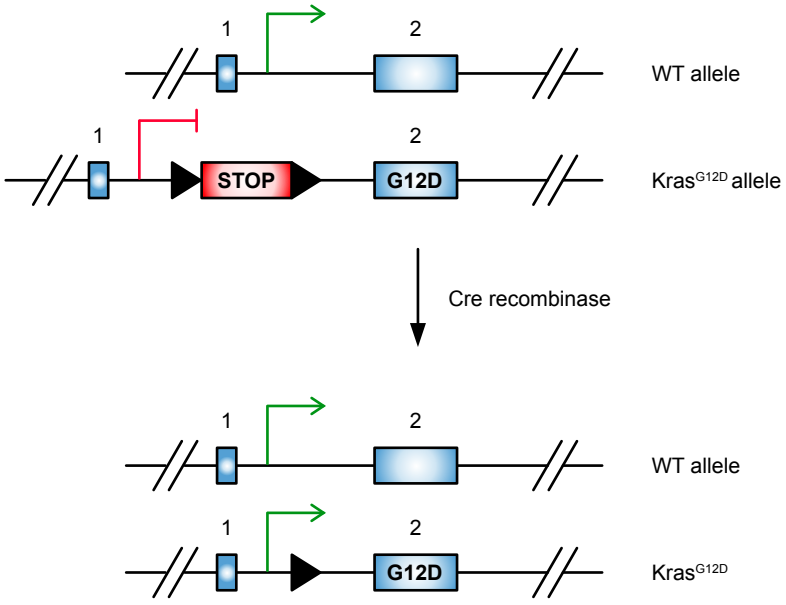

Fig. 7: The $Kras^{G12D}$ mouse model.

Schematic of cre mediated induction of the constitutively active $Kras^{G12D}$ mutation. Based on (Hingorani *et al.*, 2003; Jackson *et al.*, 2001).

Premalignant lesions were detected in all mice harboring the $Kras^{G12D}$ mutation and could progress via the preneoplastic PanIN lesions to invasive carcinoma, supporting the stepwise progression model of PDAC which had been proposed based on observations in human samples (Hingorani *et al.*, 2003; Hruban *et al.*, 2000).
Since invasive carcinoma in these mice occurred very rarely and at an old age, this mouse model allowed investigations of the contributions of the four most common genetic alterations detected in pancreatic cancer samples (Hruban *et al.*, 2000; Schutte et al., 1997; Yachida et al., 2012). It was possible to identify that loss of the tumor suppressor genes *Cdkn2a* and/or inactivating mutations in *Trp53* in combination with the $Kras^{G12D}$ driver mutation dramatically increased tumor aggressiveness and strongly decreased survival (Aguirre et al., 2003; Bardeesy et al., 2006a; Hingorani et al., 2005). Loss of *Smad4* and *Tgfbr2* in combination with the pancreas specific $Kras^{G12D}$ mutation also significantly decreased median survival and led to the development of PDAC precursor lesions or well-differentiated PDAC, respectively (Bardeesy et al., 2006b; Ijichi et al., 2006). In addition to mutations in these key driver genes, a plethora of other genetic alterations have been identified, revealing an immense genetic heterogeneity in PDAC (Bailey et al., 2016; Biankin et al., 2012; Jones et al., 2008).

1.3.4 Tumor microenvironment and inflammation

One hallmark of pancreatic cancers is the formation of a dense desmoplastic stroma consistent of extracellular matrix (ECM) proteins (collagens, fibronectin and laminin), glycoproteins, proteoglycans and glycosaminoglycans as well as growth factors. This stroma can make up to 90% of the tumor and is thought to be derived from cancer-associated fibroblasts (CAF), which are activated pancreatic stellate cells, and from infiltrating immune cells (Dougan, 2017; Kleeff *et al.*, 2016).
Stromal stellate cells have been suggested to promote cancer cell survival, proliferation and migration, thus, facilitating the establishment of a cancer stem cell niche (Apte et al., 2013; Hamada et al., 2012). Other functions of pancreatic stellate cells include promotion of vascularization (Patel et al., 2014), sequestration of tumor-suppressive $CD8^+$ T cells (Ene-Obong et al., 2013), induction of T cell apoptosis (Tang et al., 2012), as well as the recruitment of myeloid-derived suppressor cells (MDSC) (Mace et al., 2013a; Mace et al., 2013b) into the tumor stroma. These processes lead

to the release of cytokines which promote further activation of stellate cells (Ma et al., 2013; Öhlund et al., 2017; Shi et al., 2014). Furthermore, cancer cells themselves have been suggested to induce stellate cell proliferation (Apte *et al.*, 2013) creating a vicious circle. On the other hand, protective roles have also been attributed to the stroma, suggesting that stroma function may be highly context dependent (Kleeff *et al.*, 2016; Özdemir et al., 2014; Rhim et al., 2014).

Analysis of samples taken from human patients as well as mouse models of pancreatic cancer have provided evidence that inflammation is strongly involved in driving PDAC progression, and it is considered to be one of the biggest risk factors for the development of pancreatic cancer (Cobo et al., 2018; Guerra *et al.*, 2011; Guerra *et al.*, 2007). It is a commonly accepted concept, that inflammation can greatly affect the tumor microenvironment (TME) by influencing both tumor and stromal cell plasticity, and can play a dual role in carcinogenesis. On the one hand, it can have pro-tumorigenic functions by suppressing anti-tumor responses and inducing tumor-promoting pathways in epithelial and cancer cells. On the other hand, it can play an anti-tumorigenic role through immune surveillance and eradication of malignant cells (Greten and Grivennikov, 2019). There is more and more evidence arising for the existence of “cancer-promoting inflammation” suggesting that the immune system is involved in tumor initiation and progression through, for example, the production of inflammatory mediators. Inhibition of inflammation has also been associated with improved prognosis (Grivennikov et al., 2009; Ridker et al., 2017; Rothwell et al., 2011; Rothwell et al., 2012).

A low degree of inflammation in tissues is normal and important to maintain tissue homeostasis following insults or environmental stress (Medzhitov, 2008). Inflammatory responses in tissues arise due to local proliferation of tissue-associated macrophages (TAM) and dendritic cells (DCs), recruitment of pro-inflammatory cells from the bone marrow and lymphoid tissue and/or by activation and differentiation of inflammatory cells that have been recruited into the tissue (Greten and Grivennikov, 2019; Huber et al., 2020). Inflammation in the pancreas can be caused by both the innate as well as the adaptive immune system, and acinar cells respond to inflammation induced stress through ADM to be able to maintain a healthy function.

Although, as described above, inflammation has been strongly linked to the development and progression of pancreatic cancer, it is still not clear by which

mechanisms inflammation drives the acquisition of pro-tumorigenic properties in acinar cells. Several genetically-engineered mouse models of PDAC development exist, which heavily rely on the presence of oncogenic Kras signaling in combination with at least one additional pro-tumorigenic genetic alteration or the induction of acute or chronic inflammation. However, not all cancers exhibit genetic alterations prior to an inflammatory response. So how does inflammation drive cancer development in this context? To date, mouse models of inflammation-induced spontaneous development of neoplasia in the pancreas are still lacking.

2. Aims of this work

- To investigate the T cell intrinsic and extrinsic effects of Roquin hypomorph or loss-of-function or deficiency on other immune cells (Section 4.1).

- To define the *trans*-effect of Roquin-1/2-deficient T cells in the development of chronic inflammation of the pancreas and pancreatic cancer (Section 4.2).

- To identify the mechanism by which Roquin-1/2-deficient T cells lead to the development of pancreas cancer (Section 4.3).

3. Material and Methods

3.1 Material

3.1.1 Mice

All mice used in this work were on a C57BL/6 background, housed under specific pathogen-free (SPF) conditions under a 12h/12h dark/light cycle, 20-24°C and 45-65% humidity in accordance with the Ludwig-Maximilian-Universität München and Helmholtz-Zentrum-München institutional, state and federal guidelines. All procedures involving *in vivo* manipulations were approved by the local government (Regierung von Oberbayern, TVA numbers 55.2-2532.Vet_02_17_159 and 55.2-2532.Vet_02-18-10).

The *Rc3h1/2*$^{fl/fl}$ transgenic mice harbor loxP-sites around exons 4-6 of the Roquin-1 encoding gene *Rc3h1* (Bertossi *et al.*, 2011) and around exon 4 of the Roquin-2 encoding gene *Rc3h2* (Vogel *et al.*, 2013).

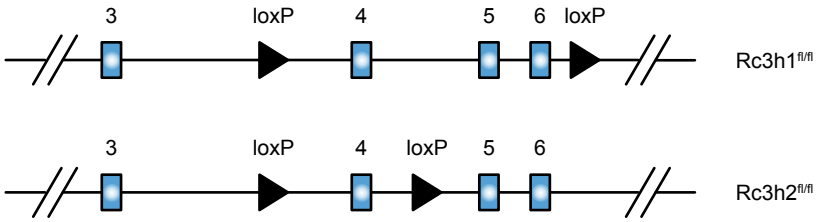

Fig. 8: Schematic representation of genetically modified alleles in *Rc3h1* and *Rc3h1*.
Schematic overview over targeting strategy in *Rc3h1* and *Rc3h2*. Position of loxP sites flanking exons 4-6 in Roquin-1 (*Rc3h1*) and exon 4 in Roquin-2 (*Rc3h2*) are indicated by black triangles.

To induce gene recombination mice with loxP-flanked gene regions were crossed to either *Cd4*-Cre (Lee et al., 2001; Sawada et al., 1994) or *Cd4*-CreERT2 (Sledzinska et al., 2013) mice. In these mice Cre recombinase is expressed under the *Cd4* promotor, resulting in a T cell-specific deletion of Roquin-1/2 proteins. *Cd4*-CreERT2 mice express a Cre recombinase which is fused to estrogen-receptor 2 (ERT2) under the *Cd4* promotor. This allows inducible deletion of loxP flanked sites in $CD4^+$ T cells following tamoxifen treatment. To achieve inducible deletion in any type of cell mice with loxP-flanked gene regions were crossed to CreERT2 mice.

Following mouse lines were used in this work:

Mouse line	Name
CD4-cre	WT
CD4-creERT2	WT
Rc3h1/2$^{fl/fl}$	WT
Rc3h1/2$^{fl/fl}$*; Cd4*-cre	DKO^{T}
Rc3h1/2$^{fl/fl}$*; Cd4*-creERT2	iDKO^{T}
Zc3h12a$^{fl/fl}$; *Cd4*-creERT2	iKO^{T}
Rc3h1/2$^{fl/fl}$*; Zc3h12a*$^{fl/fl}$; *Cd4*-creERT2	iTKO^{T}
Rc3h1$^{M199R/M199R}$	San/san
Sh2d1a-/-	SapKO
IL6Ra-/-	IL6Rα KO
CD80-/-; CD86-/-	CD80/CD86 KO
μMT	
ICOS-/-	
C57BL/6, IFNγR$^{-/-}$ B6.129S7-*Ifngr1*^{tm1Agt}/J	IFNγR-/- (kindly provided by Prof. Dr. Heiko Adler)
LSL-Kras^{G12D}*; p48cre*	Kras^{G12D}
B6.SJL-Ptprca Pepcb/BoyJ	CD45.1^{+}

Table 1: Mouse lines used in this work.

Overview over all mouse lines used in this work and denominations used to describe these lines.

3.1.2 Cell culture and cell lines

HEK293 cells, *Rc3h1/2*$^{fl/fl}$*;* creERT2; LSL-*hCAR* mouse embryonic fibroblasts (MEF) cell lines (Vogel et al., 2013) and primary pancreatic cancer cell lines were kept in cell line medium (DMEM supplemented with 10% (v/v) FCS, 1% Pen-Strep and 10mM HEPES pH7.4). Primary T cells were cultivated in T cell medium (DMEM supplemented with 10% (v/v) FCS, 100U/ml Pen-Strep, 10mM HEPES pH7.4, 1x non-essential amino acids and 50μM β-Mercaptoethanol). Primary cancer cells were cultivated in Tumor medium (DMEM supplemented with 10% (v/v) FCS, 1% Pen-Strep).

Cell line culture medium	Supplier	Concentration
DMEM (Dulbecco's modified eagle medium, 4.5g/l D-glucose, L-Glutamine, Pyruvate added)	Thermo Fisher Scientific	
FCS	Anprotech	10% (v/v)
Penicillin-Streptomycin (10 000 U/ml and 10 000 µg/ml)	Gibco	100U/ml, 100µg/ml
1M HEPES-Buffer pH 7.4	Gibco	10mM
T cell medium	**Supplier**	**Concentration**
DMEM (Dulbecco's modified eagle medium, 4.5g/l D-glucose, L-Glutamine, Pyruvate added)	Thermo Fisher Scientific	
FCS	Anprotech	10% (v/v)
Penicillin-Streptomycin (10 000 U/ml and 10 000 µg/ml)	Gibco	100U/ml, 100µg/ml
1M HEPES-Buffer pH 7.4	Gibco	10mM
1M β-Mercaptoethanol	Gibco	50µM
100x MEM non-essential amino acids	Gibco	1x
Tumor medium	**Supplier**	**Concentration**
DMEM (Dulbecco's modified eagle medium, 4.5g/l D-glucose, L-Glutamine, Pyruvate added)	Thermo Fisher Scientific	
FCS	Anprotech	10% (v/v)
Penicillin-Streptomycin (10 000 U/ml and 10 000 µg/ml)	Gibco	100U/ml, 100µg/ml

Table 2: Cell culture medium compositions for cell lines and primary T cells.

Cell Line	Species
Rc3h1/2$^{fl/fl}$; creERT2; LSL-*hCAR*	*Mus musculus*
HEK293	*Homo sapiens*

Table 3: Cell lines used in this work.

3.1.3 Oligonucleotides

All oligonucleotides were obtained from MWG Eurofins, salt-free purified and reconstituted with sterile ddH_2O according to manufacturers' instructions to achieve a final stock concentration of 100pM.

Name	Sequence (5' – 3')	Application
*Cd86*cds for	CACCATGGACCCCAGATGCACCATGGG	Cloning
*Cd86*cds rev	TCACTCTGCATTTGGTTTTGCTGAA	Cloning
Csf3 3'UTR for	ATCTAGATAAACGCGACCTGAGCAGAAAGCCCTTTCC	Cloning
Csf3 3'UTR rev	ATCGAATTCTAATCCGCAAGCTTGGCTATAGTGAC	Cloning
Csf3 ΔARE for	CCTGAGCAGAAAGCCCTTTGACAAAGACGAGAAAATG	QC
Csf3 ΔARE rev	CATTTTCTCGTCTTTGTCAAAGGGCTTTCTGCTCAGG	QC
Csf3 SLBmut for	GGAACACTGCTGTTTAATATTTAAACAGGGATGTCTT GTCCCCCG	QC
Csf3 SLBmut rev	CGGGGGACAAGACATCCCTGTTTAAATATTAAACAGC AGTGTTCC	QC
pEGFP for	TTCGCCCTTGTCGACATGGTGAGCAAGGGCGAGG	Cloning
pEGFP rev	TCGAATTCTACGCGTTTATCTAGATCCGGTGGATCCC GG	Cloning
Nfkbid 1-263 for	ATCTAGATAAACGCGGACCGAAACCCAGAACCTGGA	Cloning
Nfkbid 1-263 rev	ATCGAATTCTACGCGCTAGAGTGTTTCACAGAAACAA TC	Cloning
Kras-WT-UP1	CACCAGCTTCGGCTTCCTATT	Genotyping
Kras-URP-LP1	AGCTAATGGCTCTCAAAGGAATGTA	Genotpying
KrasG12Dmut-UP	CCATGGCTTGAGTAAGTCTGC	Genotpying

Table 4: Oligonucleotides for cloning and genotyping of primary cancer cell lines.
All 3'UTRs were cloned using the Takara In-Fusion Cloning system. Mutations were introduced using the QuickChange II Site-Directed Mutagenesis system. QC: QuickChange.

Name	Sequence (5‘–3‘)	UPL probe
YHWAZ for	CGC TAA TAA TGC AGT TAC TGA GAG A	2
YHWAZ rev	TTG GAA GGC CGG TTA ATT TT	2
Rpl13a for	ATCCCTCCACCCTATGACAA	108
Rpl13a rev	GCCCCAGGTAAGCAAACTT	108
Cd86 for	GAAGCCGAATCAGCCTAGC	107
Cd86 rev	CAGCGTTACTATCCCGCTCT	107
Cd40lg for	ACGTTGTAAGCGAAGCCAAC	89
Cd40lg rev	TATCCTTTCTTGGCCCACTG	89
Csf3 for	GCTGCTGGAGCAGTTGTG	17
Csf3 rev	GGGATCCCCAGAGAGTGG	17
Il6 for	TCT AAT TCA TAT CTT CAA CCA AGA GG	78
Il6 rev	TGG TCC TTA GCC ACT CCT TC	78
Il22 for	TGACGACCAGAACATCCAGA	94
Il22 rev	AATCGCCTTGATCTCTCCAC	94
Il17a for	GCT GAG CTT TGA GGG ATG AT	74
Il17a rev	CAG GGA GAG CTT CAT CTG TGT	74
Pdcd1 for	TGCAGTTGAGCTGGCAAT	81
Pdcd1 ref	GGCTGGGTAGAAGGTGAGG	81
Cxcr5 for	GAATGACGACAGAGGTTCCTG	13
Cxcr5 rev	GCCCAGGTTGGCTTCTTAT	13
Bcl6 for	CTGCAGATGGAGCATGTTGT	4
Bcl6 rev	GCCATTTCTGCTTCACTGG	4

Table 5: Universal Probe Library (UPL) probe and oligonucleotides used for RT-qPCR analysis.

3.1.4 Chemicals and Consumables

Description	Supplier
1.5ml centrifuge tubes	Eppendorf
2x RNA loading dye	Thermo Scientific
15ml tubes	Sarstedt
2-Isopropanol	Roth
2ml centrifuge tubes	Eppendorf
4'OH-tamoxifen	Sigma
50ml tubes	Sarstedt
5ml tubes	Eppendorf
96-well plate, V-bottom	Roth
Acrylamide 4K (30%)	AppliChem
Agarose	Biozym
Album Fraction V	Roth
Aluminium foil	Universal
Ammonium-peroxide sulfate (APS)	Roth
Ampicillin	AppliChem
β-Mercaptoethanol	Roth
β-Mercaptoethanol, cell culture	Thermo Fisher

Barrier food wrap	Saran
Bradford Reagent	Bio-Rad
Brefeldin A	Sigma StemCell Technologies
BSA (98%)	Sigma
Calcium chloride	Roth
Cannula 26g (Fine-Ject Needle only 0,45 x 25mm)	VWR
CASY cups	Ols-bio
CASY ton	Ols-bio
Cell culture dish (100mm)	BD
Cell culture dish (150mm)	VWR
Cell culture flasks (25, 75, 175 cm2)	BD
Cell culture plates	Falcon Sarstedt
Cell strainer (40µM, 100µM)	Corning
CellTrace Violet Cell Proliferation Kit	Thermo Fisher
Chloroform	Sigma
Chloroquine	Sigma
Complete Protease Inhibitor Cocktail Tablets	Roche
Corn Oil	Sigma
Cryo Tubes	Thermo Scientific
DH5α chemically competent E. coli	In house production
DMSO	Sigma
DNase/ RNase-free H2O	Invitrogen
dNTP Set	Thermo Fisher
DTT (Dithiothreitol)	AppliChem
Dulbecco's Modified Eagle Medium (DMEM) low glucose	Invitrogen
ECL reagent	GE Healthcare Invitrogen in-house
ecoLab Einmal-Küvetten	Neolab
EDTA	Roth
Ethanol (100%)	Roth
Ethanol (denatured)	Roth
Ethidiumbromid - solution 0.07 % "dropper-bottle"	AppliChem
FACS-Tubes non-sterile (Falcon, 5ml)	VWR
Fetal Calf Serum (FCS)	Sigma Anprotech
Fixable Viablity Dye eF780	Thermo Fisher
Fixation and Developing Solution	Agfa
FrameStar 384 Well qPCR Platte, LC480, weiß, mit Folie	Brooks/4-titude
Glass pipettes 5 ml,10 ml	Hirschmann ®
Glassware	Schott
Glycerol	Roth
HBSS, no calcium, no magnesium, no phenol red	Thermo Fisher
HEPES Buffer (1M)	Invitrogen
Immobilon PVDF Membrane	Merck Millipore
Injekt-F Solo 1mL ohne Kanüle	Ryma-Pharm

Ionomycin	Calbiochem StemCell Technologies
Isopropanol bucket	Merck
Kanamycin	Roth
Laboratory film	Parafilm®
LB Agar	AppliChem
LB Medium (Miller)	Roth
Live/Dead Fixable Blue Dead Cell Stain Kit	Thermo Fisher
LIVE/DEAD™ Fixable Violet Dead Cell Stain Kit, for 405 nm excitation	Thermo Fisher
Methanol	Roth
MgCl2 solution (25 mM)	PCR Perkin Elmer
Milk powder	Roth
MilliQ water	Millipore
Motor for pellet pestle	Sigma
Bio-Plex Pro™ Mouse Cytokine Standard 23-Plex, Group I	Bio Rad
NEAA (100x)	Thermo Fisher
NeoLab sample cup, 200 ml, PP, sterile	NeoLab
NeoLab Skalpell blades steril, Nr. 20, 12	NeoLab
Neubauer Counting Chamber	Roth
Nitrile gloves	NitriSense
NP-40	Sigma
Nunc MaxiSorp™ flat-bottom ELISA Plates	Thermo Fisher
Paraformaldehyde	Merck KGaA
Pasteur pipettes	Brand
PCR tubes	Thermo
Pellet pestle, polypropylene, disposable	Sigma
Penicillin / Streptomycin (Pen-Strep)	Thermo Fisher
Petri Dishes	Greiner
Pipette (5ml, 10ml, 25ml)	Greiner Bio One
Pipette tips	Rainin
PMA (Phorbol-12-myristate-13-acetate)	Calbiochem StemCell Technologies
Polyamide/Nylon filter 41µm	RCT
Polybrene	Sigma
PVDF Membrane	Merck Millipore
qPCR Optical Clear Seal	Brooks/4-titude
RNALater	Sigma
Saponin	VWR
Sodium acid (NaN3)	Roth
Sodium dodecyl sulfate (SDS)	Roth
Sodium pyruvate solution 100 mM, sterile-filtered, BioReagent	Sigma
Sterile Filter tips	Kisker
Syringe 1ml with needle (26G) Omnican	Ryma-Pharm
Syringe 30ml Omnifix® Luer Lock Solo	Ryma-Pharm
Syringe filter 0.45 µM	VWR
Syringe omnifix luer 5mlsterile	VWR
Tamoxifen	Sigma

TEMED	Roth
Epredia™ Cassette II Biopsy Tissue Casette in Tube Packs	Fisher scientific
Tris-HCl pH 7.5	Invitrogen
Trypan blue	Roth
Trypsin/Ethylenediaminetetraacetic acid (EDTA) (0.05%)	Invitrogen
Tween-20	AppliChem
UltraComp eBeads™ Compensation Beads	Thermo Fisher
Whatman Blotting Paper 20x25cm	VWR
X-ray films	Röntgen Bender

Table 6: Overview over chemicals and consumables used in this work.

3.1.5 Kits, Markers, Enzymes

Kits	Supplier
Bio-Plex Pro™ Mo Cyto Group I 23-Plex	Bio Rad
Bio-Plex Pro™ Mouse Cytokine Th17 Group III	Bio Rad
DNeasy® Blood&Tissue Kit	Qiagen
DuoSet ELISA Ancillary Reagent Kit 2	R&D Systems
EasySep™ Mouse CD4+ T Cell Isolation Kit	Stem Cell Technologies
EasySep™ Mouse CD8+ T cell Isolation Kit	Stem Cell Technologies
EasySep™ Mouse MDSC (CD11b+Gr1+) Isolation Kit	Stem Cell Technologies
EasySep™ Mouse Naïve CD4+ T Cell Isolation Kit	Stem Cell Technologies
EasySep™ Mouse T Cell Isolation Kit	Stem Cell Technologies
eBioscience™ Annexin V Apoptosis Detection Kit	Thermo Fisher
FastGene Gel/PCR Extraction Kit	Nippon Genetics
FastGene Plasmid Mini Kit	Nippon Genetics
Foxp3 staining buffer set	eBioscience
In-Fusion® HD Cloning Kit	Takara Clontech
Light Cycler® 480 pobes master	Roche
Mouse G-CSF DuoSet ELISA	R&D Systems
Nucleobond® Xtra Midi/Maxi	Macherey-Nagel
NucleoSpin Gel and PCR Clean Up Kit	Macherey-Nagel
NucleoSpin RNA	Macherey-Nagel
PureYield Plasmid Miniprep System	Promega
QuikChange II XL Site-Directed Mutagenesis Kit	Agilent Technologies
RNA Clean & Concentrator™-5	Zymogen Research
Universal Probe Library	Roche

Table 7: Kits used in this study

Markers	Supplier
DNA 2-log-ladder	Biolabs
RiboRuler HR RNA ladder	Thermo Scientific
Protein Marker VI prestained 10-245 kDa	AppliChem

Table 8: Markers used in this study

Enzymes	Supplier
Aprotinin	Sigma
Collagenase II	Thermo Fisher
Gateway® BP clonase enzyme mix	Life technologies
Gateway® LR clonase II enzyme mix	Life technologies
Pfu Ultra High Fidelity 100U	Agilent
Proteinase-K	Sigma
Q5® High-Fidelity DNA Polymerase	New England BioLabs
RevertAid Reverse Transcriptase	Qiagen
RNAse inhibitor	Promega
Taq Polymerase	Invitrogen New England BioLabs In-house

Table 9: Enzymes

3.1.6 Buffers

Buffer	Composition
Blocking buffer	5% Milk powder TBS
DNA lysis buffer	10mM Tris-HCl, pH 8.5 5mM EDTA 0.2% SDS (w/v) 200mM NaCl
Freezing medium (2x)	20% DMSO FCS
FACS Buffer	2% FCS 1mM EDTA PBS
HBS (2x) pH 6.95-7.05	280mM NaCl 50mM HEPEs 1.5mM Na_2HPO_4
Laemmli buffer (4x)	200mM Tris-HCl, pH 6.8 8% SDS (w/v) 40% Glycerol (v/v) 0.01% Bromphenol blue (w/v) 10% β-Mercaptoethanol (added fresh before use)
LB Agar	LB medium 1.5% Bacto agar (w/v)
LB Medium	1.0% Tryptone (w/v) 0.5% Yeast extract (w/v) 1.0% NaCl (w/v)
Meister lysis buffer (2x)	40 mM Tris-HCl pH 7.5 300 mM NaCl 0.5% NP-40 3mM $MgCl_2$
PBS	137mM NaCl 2.7mM KCl

	10mM Na_2HPO_4, pH 7.4
Saponin buffer	0.5% Saponin 1% BSA PBS
SDS running buffer	20mM Tris 200mM Glycine 0.1% SDS
TAC lysis buffer	13mM Tris 140mM NH_4Cl, pH 7.2
TBE (1x)	89mM Tris-borate 2mM EDTA, pH 8.0
TBS (1x)	50mM Tris-HCl, pH 8.0 150mM NaCl
TBS-T	TBS with 0.05% Tween-20
T cell buffer	2% FCS 1mM EDTA PBS
Transfer buffer	25mM Tris 39mM Glycine 20% Methanol (v/v)

Table 10: Buffers

3.1.7 Antibodies

Antibody	Clone	Dilution/ c_{Final}	Supplier	Application
anti-CD3	2C11	0.5µg/ml	in house production	cell culture
anti-CD4	GK1.5	1:400	invitrogen	FC
anti-CD8a	53-6.7	1:400	eBioscience	FC
anti-CD11b	M1/70	1:200	eBioscience	FC
anti-CD11c	N418	1:200	BioLegend	FC
anti-CD19	6D5	1:300	BioLegend	FC
anti-CD25	PC61.5	1:200	invitrogen	FC
anti-CD28	37.5N	2.5µg/ml	in house production	cell culture
anti-CD38	90	1:200	BioLegend	FC
anti-CD44	IM7	1:200	Biolegend	FC
anti-CD45.1	A20	1:100	eBioscience	FC
anti-CD45.2	104	1:100	eBioscience	FC
anti-CD45R (B220)	RA3-6B2	1:200	eBioscience	FC
anti-CD62L	MEL-14	1:200	invitrogen	FC
anti-CD69	H1.2F3	1:200	BD	FC
anti-CD86	GL1	1:100	eBioscience	FC
anti-CD95	15A7	1:200	eBioscience	FC
anti-CD103	2E7	1:200	eBioscience	FC
anti-CD127	A7R34	1:200	eBioscience	FC
anti-CD134 (Ox40)	OX-86	1:200	eBioscience	FC
anti-CD154 (CD40L)	MR1	1:200	invitrogen	FC
anti-CD185 (CXCR5)	L138D7	1:50	BioLegend	FC
anti-CD223 (LAG3)	eBioC9B7W	1:200	eBioscience	FC
anti-CD278 (ICOS)	C398.4A	1:200	eBioscience	FC

anti-CD279 (PD1)	J43	1:100	invitrogen	FC
anti-CD326 (EpCAM)	G8.8	1:100	invitrogen	FC
anti-CD274 (PDL1)	MIH5	1:200	invitrogen	FC
anti-b-actin	C4	1:5000	SantaCruz	WB
anti-Bcl6	K112-91	1:50	BD	FC
anti-Foxp3	FJK-16s	1:100	invitrogen	FC
anti-GCSF	67604	1:100	R&D Systems	FC
anti-mouse G-CSF	67604	25µg/injection	R&D Systems	*In vivo*
anti-CD114 (G-CSFR)	polyclonal	1:50	R&D Systems	FC
anti-GFP	7.1 and 13.1	1:1000	Roche	WB
anti-GL-7	GL-7	1:200	eBioscience	FC
anti-Granzyme B	Granzyme B	1:100	eBioscience	FC
anti-Gr1	RB6-8C5	1:800	eBioscience	FC
anti-IFNγ	Xmg1.2	10µg/ml	in house production	cell culture
anti-IFNγ	XGM1.2	1:200	invitrogen	FC
anti-IgD	11-26c.2a	1:200	BioLegend	FC
anti-IL-4	11B11	10µg/ml	in house production	cell culture
anti-IL-17A	eBio17B7	1:100	invitrogen	FC
InVivoMab anti-mouse IL-17A, IgG1, kappa	17F3	50µg/injection	BioXCell	*In vivo*
InVivoMab mouse IgG1 isotype control, IgG1, kappa	MOPC-21	50µg/injection	BioXCell	*In vivo*
anti-Ki67	SolA15	1:200	invitrogen	FC
anti-KLRG1	2F1	1:200	eBioscience	FC
anti-Ly6C	HK1.4	1:400	BioLegend	FC
anti-NK1.1	PK136	1:200	eBioscience	FC
anti-Perforin	eBioOMAK-D	1:20	eBioscience	FC
Rat IgG1 Isotype Control	43414	25µg/injection	R&D Systems	*In vivo*
anti-Roquin	3F12	1:10	in house production	FC
anti-RoRγt	Q31-378	1:100	BD	FC
anti-TCRγδ	eBioGL3	1:200	invitrogen	FC
anti-TCRβ	H57-597	1:200	eBioscience	FC
anti-Tbet	eBio4B10	1:100	eBioscience	FC
anti-Tim3	RMT3-23	1:200	eBioscience	FC
FcR	4G8	1:200	in house production	FC
Rabbit-anti-hamster IgG	Polyclonal	50µg/ml	Anprotech	cell culture

Table 11: Antibodies used for flow cytometry, western blotting, cell culture and in vivo manipulations.

In house produced antibodies were generated by the monoclonal antibody facility at the Helmholtz Center Munich. FC: Flow cytometry, WB: Western blot

3.1.8 Cytokines

Cytokine	Supplier	Application
hIL-2	Novartis	T cell culture
rmIL-6	R&D systems	T_H17
rmIL-12 p70	StemCell Technologies	T_H1
rhTGF-β1	R&D systems	T_H17

Table 12: Cytokines.

3.1.9 Plasmids

Viruses for retroviral transductions were produced in HEK293 cells using DNA-plasmids. The MSCV-hICOS-GFP-Nfkbid(1-263)-IRES-Thy1.1 plasmid was kindly provided by Dr. Nina Kronbeck for use as template. All MSCV-pEGFP plasmids were linearized using MluI.

Destination vector	Insert
KMV-ccdb-IRES-GFP	*CD86cds*
MSCV-pEGFP	*Nfkbid(1-263)*
MSCV-pEGFP	*Csf3* 3‘UTR
MSCV-pEGFP	*Csf3* 3’UTR ΔARE
MSCV-pEGFP	*Csf3* 3’UTR SLBmut
MSCV-pEGFP	*Csf3* 3’UTR ΔARE SLBmut

Table 13: Retroviral expression plasmids used for transductions of MEF and T cells.

Entry vector	Insert
pCR8/GW/TOPO	CD86cds

Table 14: Entry vectors used for Gateway cloning.

3.1.10 Instruments and Softwares

Device	Company
-20°C freezer	Liebherr
-80°C freezer	Thermo Scientific
37°C bacterial incubator	New Brunswick innova® 44 Incubator Shaker Series
37°C mammalian cell incubator	New Brunswick
4°C fridge	Liebherr
Airflow Controler Hood	Waldner
Autoclave (Varioklav)	H+R
BD FACS Canto II	Beckman Dickinson
BD Fortessa 5 Laser	Beckman Dickinson
Casettes for SDS-PAGE	Life Technologies
Casy Cell Counter	Innovartis

Centrifuges	Eppendorf 5417R (1.5ml tubes) New Brunswick Galaxy 170S (1.5ml tubes) Thermo Scientific Heraeus Multifuge X3R (15 and 50ml tubes) Hettich Rotanta 460R (15 and 50ml tubes)
Film cassettes	VWR
Fluorescence microscope	Leica
Freezing box with isopropanol	Roth
Gel cassette for SDS gels	Bio-Rad
Gel Doc™ XR+	Bio-Rad
Gel electroporation chamber	Bio-Rad
Ice machine	Scotsman
Light cycler 480® II	Roche
Luminex 100/BioPlex	BioRad
Magnet stirrer	IKA
Microwave	LG
Neubauer counting chamber	Brand
Optimax Developer	Protec
pH-Meter	InoLab pH 720
Photometer	Eppendorf
Pipetboy	Eppendorf
Pipettes	Rainin
Power supply	Bio-Rad
SD semi-dry transfer cell	Biorad
Shaker	ST5 CAT Neolabs
Spectrophotometer	Nanodrop ND100, Peqlab
Thermoblock (shaker)	Eppendorf
Thermoblocks	Eppendorf ThermoStat plus Eppendorf ThermoMixer F1.5 Eppendorf Thermomixer compact
Thermocycler	Analytic Jena Biozym
Thermomixer 5436	Eppendorf
Tissue culture hood	Clean Air
Vacuum pump	VWR
VersaMax microplate reader	Molecular devices
Vortex Genie 2	Scientific Industries
Waterbath	GFL
X-ray machine	Xstrahl RS225

Table 15: Instruments

Software	Supplier	Application
Affinity Designer v 1.10.4	Serif	Image processing
ApE v 2.0.49.10	https://jorgensen.biology.utah.edu/wayned/ape/	Sequence alignment
Aperio ImageScope v 12.3.3	Leica Biosystems	Image analysis
BD FACS Diva Software v 8.0.1	Beckman Dickinson	Data acquisition
BioPlex Manager v 6.2	Bio-Rad	Luminex analysis
Endnote™ v 20.2	Clarivate	Organization of references and citations
FlowJo v 10	Treestar	Data analysis for flow cytometry
Image Lab v 5.2.1	Bio-Rad	Data acquisition and processing
Light Cycler 480 gene scanning software v 1.5.1	Roche	Data acquisition
Microsoft® Excel	Microsoft	Data processing
Microsoft® PowerPoint		
Microsoft® Word		
Prism v. 7.0	GraphPad	Data processing
R v 4.1.1	GNU (https://cran.r-project.org)	Data processing
RStudio v 1.4.1717	GNU (https://www.rstudio.com)	Data processing
SoftMax Pro 7.0.3	Molecular Devices	Data acquisition

Table 16: Softwares

3.2 Methods

3.2.1 Molecular Biology

3.2.1.1 Polymerase chain reaction

DNA fragments were amplified by polymerase chain reaction (PCR) using gene-specific forward (FW) and reverse (RV) primers and heat-stable DNA Polymerases. Cycling times and temperatures were primer and polymerase-specific. **Table 17** shows a typical PCR reaction for the Q5 polymerase supplied by New England Biolabs.

Reaction	**Cfinal**	**Volume for a 25µl reactions [µl]**
5x Q5 Reaction Buffer	1x	5
10µM FW Primer	0.5µM	1.25
10µM Rev Primer	0.5µM	1.25
10mM dNTPs	200µM	0.5
template DNA	<1000ng	variable
nuclease-free H_2O		up to 25µl
Q5 Polymerase (Hot start)	0.02U/µl	0.25
Temperature	**Time**	**Step**
98°C	30s	Initial Denaturation
98°C	10s	35 cycles
50-72°C	30s	
72°C	30s/kb	
72°C	2min	Final extension

Table 17: Reagents and cycle conditions for a standard PCR reaction.

For a standard PCR reaction mix 1-100ng of template DNA were mixed with reaction buffer, dNTPs, forward and reverse primers as well as a heat-stable polymerase. Final concentrations are indicated in **Table 17**. For PCRs using the Taq polymerase supplied by invitrogen 1mM $MgCl_2$ was added to the reaction mix. For cloning a hot-start protocol was employed to reduce unspecific amplification. For hot-starts the reaction was allowed to go through the initial denaturation step before addition of the polymerase.

Initial denaturation was performed at 95°-98°C depending on the polymerase used, followed by 30-35 cycles of denaturation, annealing at a primer specific temperature, and elongation at 72°C. A final elongation step at 72°C was performed for 2-10min

depending on the length of the amplified fragment. **Table 9** shows an overview of all polymerases used in this study.
PCR products were size separated by agarose gel electrophoresis. For small fragments 2% (w/v) and for large construct 1% (w/v) agarose in 1xTBE buffer were used. Fragments were visualized by UV light and correct bands were excised, DNA purified using the FastGene Gel/PCR Extraction kit according to manufacturers' instructions.

3.2.1.2 Cloning

To generate expression plasmids for retroviral transductions different cloning techniques were used. An overview of the plasmids used in this work as well as the sequences of the primer pairs are listed in **Table 13** and **Table 4**, respectively.

In-Fusion® HD:
The In-Fusion® HD Cloning kit (Takara Bio) is based on Gibson assembly which allows site-directed integration of a DNA insert into a linearized plasmid. The proprietary In-Fusion enzyme mix is designed to recognize 15 base pairs (bp) overlaps between the fragment and the target plasmid allowing precise and efficient insertion of PCR fragments. This technique was employed to generate all MSCV-pEGFP-3'UTR constructs listed in **Table 13** according to manufacturers' instructions. Briefly, 10-200ng purified PCR fragment was mixed with 50-200ng linearized vector in a 2:1 molar ratio, followed by the addition of 1µl 5x In-Fusion HD Enzyme Premix and dH_2O to achieve a final reaction volume of 5µl. The reaction was incubated for 15min at 50°C and cloning products were transformed into competent DH5α E. coli cells.

Gateway® Cloning:
The retroviral expression vector containing the CD86CDS was generated by Gateway® cloning (Thermo Scientific), which is based on gene recombination of *att*-sites contained in the entry (pCR8/GW/TOPO) and destination (KMV-ccdb-IRES-GFP) vector. Gateway® Cloning was performed according to manufacturers' instructions. In short, to generate an entry clone, a PCR fragment of the CD86 CDS flanked by *att*B sites was generated and inserted into the donor vector using the BP Clonase II enzyme mix. The donor vector was transformed into competent cells, grown

at 37°C O/N in kanamycin containing growth medium and isolated using the Nuclebond® Xtra Midi kit resulting in an entry clone containing the insert of interest flanked by *att*L sites. The transfer from the gateway entry clone into the destination vector was achieved using the Invitrogen LR Clonase II enzyme mix which catalyses the recombination between the *att*L sites contained in the entry clone and the *att*R sites contained in the destination vector. Competent DH5α E. coli cells were transformed with the product of the LR reaction and appropriate clones were selected based on ampicillin resistance.

QickChange II XL Site-directed mutagenesis:

Mutations and deletions in the G-CSF 3'UTR were introduced using the QickChange XL Site-directed mutagenesis kit (Agilent Technologies) according to manufacturers' instructions. Briefly, MSCV reporter plasmids were PCR amplified using primer which contained the desired mutation flanked by gene-specific sequences 5' and 3' of the mutation. The high-proof-reading Pfu polymerase was used for these PCR reactions. The resulting PCR product was digested using *Dpn* I restriction enzyme (10U per reaction), followed by transformation into competent DH5α E. coli.

Successful cloning or mutagenesis was confirmed by specific restriction enzyme digestion and DNA sequencing (Eurofins Genomics and GATC).

3.2.1.3 Transformation

Chemically competent DH5α E. coli cells (in house production) were thawed on ice and gently mixed with plasmid DNA. Bacterial suspensions were incubated on ice for 30min, followed by a heat shock at 42°C for 45s and 5min incubation on ice. Pre-warmed SOCs outgrowth medium was added and bacteria were incubated at 37°C for 1h. Cells were plated onto dishes containing LB Agar supplemented with an appropriate antibiotic (100µg/ml) and grown at 37°C over-night (O/N) or at room temperature (RT) for 2 days (d).

3.2.1.4 Bacterial culture and isolation of plasmid DNA

To isolate plasmid DNA transformed *E. coli* bacteria were grown in LB medium supplemented with 100µg/ml ampicillin. For small-scale preparations 2ml cultures were used (mini-preps), for large-scale preparations (midi-preps) bacteria were grown

in 200ml LB medium. Bacterial cultures were grown at 37°C, 160rpm for ~12h. Bacterial suspensions were centrifuged (4122xg, 4°C) and plasmid DNA was isolated using the FastGene Plasmid Mini Kit or the Nucleobond® Xtra Midi/Maxi kit for mini-preps or midi-preps, respectively, following manufacturers' instructions.

3.2.1.5 Agarose Gel Electrophoresis

DNA and RNA fragments were separated by size using agarose gel electrophoresis (0.8-2% (w/v) agarose in TBE, 0.5 µg/ml ethidium bromide. DNA separations was performed at 80-100V, RNA separation was performed at 60V for 1h to avoid RNA degradation. Bands were visualized using UV light (254-366nm) on the Gel Doc™ XR+ instrument (Bio-Rad).

3.2.2 Cell Biology

3.2.2.1 Cell Counting

The Casy cell counter was used according the manufacturers' instructions to determine cell numbers unless specifically stated otherwise. For accurate readings all cells were pre-diluted 1:10 before measuring cell numbers. MEF and HEK as well as bone marrow cells were counted using a Neubauer counting chamber and trypan blue to visualize dead cells. Four quadrants were counted and cell numbers were determined using the following equation:

$$cell\ number\ (per\ ml) = \frac{counted\ number}{4}\ x\ DF\ x\ 10^4$$

DF: Dilution Factor

3.2.2.2 Cryo-conservation of cell lines

Cells were counted and resuspended in their respective culture medium at a density of >10x10^6 cells per ml. Cells were mixed 1:1 with 2x freezing medium (20% DMSO in FCS) and immediately frozen at -80°C in isopropanol freezing buckets. To thaw cells, cells were briefly warmed in a water bath at 37°C. Ice cold culture medium was added drop by drop to partially thawed cells. Cells were then taken up in ice cold culture medium (at least 10x freezing volume) and washed 3x in cold culture medium.

Cells were plated and kept at 37°C, 10%CO_2 for at least two passages before performing experiments.

3.2.2.3 Maintenance of eucaryotic cell lines

Adherent cells lines (HEK293 and MEF cells) were kept at 37°C, 10% CO_2 in cell line culture medium (DMEM supplemented with 10% fetal calf serum (FCS), 100U/ml Penicillin-Streptomycin (Pen-Strep) and 10mM HEPES-Buffer). Cells were passaged when they reached 80-90% confluency. Cell line medium was removed, cells were washed with PBS and incubated with 0.05% Trypsin-EDTA at 37°C for 5min. Cells were resuspended in fresh cell line culture medium and seeded at the desired cell density for maintenance or further experiments.

3.2.2.4 Isolation and cultivation of primary lymphocytes

For primary T cell cultures, mice were sacrificed by cervical dislocation and lymph nodes as well as peripheral and mesenteric lymph nodes were dissected. For naïve T cell isolations mesenteric lymph nodes were omitted. Organs were mechanically disrupted, passed through a 100µm filter and erythrocytes were lysed using a tris-ammonium-chloride (TAC) lysis buffer. Lymphocyte suspensions were then passed through a 40µm filter and resuspended in T cell isolation buffer (2% FCS, 1 mM EDTA in PBS) at a density of $1.0x10^8$ cells/ml. Naïve or total $CD4^+$ T cells were isolated using the EasySep™ Mouse Naïve CD4+ T Cell Isolation Kit or the EasySep™ Mouse CD4+ T Cell Isolation Kit, respectively. For $CD8^+$ T cell isolation the EasySep™ Mouse CD8+ T cell Isolation Kit and for $CD3^+$ T cell isolation the EasySep™ Mouse T Cell Isolation Kit were used. All T cell isolations were performed following manufacturers' instructions.

Purified $CD4^+$ and $CD8^+$ T cells either used immediately for *in* vivo experiments or were taken up in T cell medium (DMEM supplemented with 10% (v/v) FCS, 100U/ml Pen-Strep, 10mM HEPES pH7.4, 1x non-essential amino acids and 50µM β-Mercaptoethanol) and cultured *in vitro.* A schematic overview over the *in vitro* culture conditions is shown in **Fig. 9**.

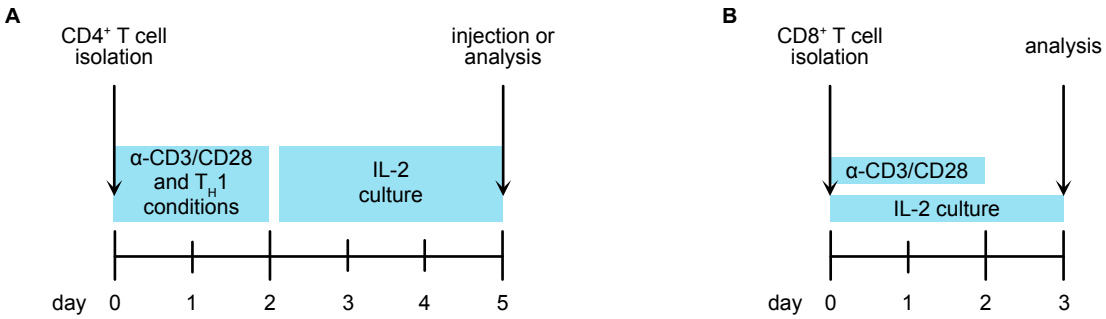

Fig. 9: Schematic representation of *in vitro* T cell activation conditions.
(A) $CD4^+$ T cells were isolated and stimulated with anti-CD3/anti-CD28 under T_H1 skewing conditions for 40h and expanded in IL-2 containing medium for 3 days before analysis or use for adoptive transfer experiments. **(B)** $CD8^+$ T cells were stimulated with anti-CD3/anti-CD28 in the presence of IL-2 and further expanded in IL-2 containing medium before analysis.

Unless otherwise stated all primary $CD4^+$ T cell cultures were kept under T_H17 skewing conditions. For this $CD4^+$ T cells were taken up in T cell medium containing 0.1µg/ml anti-CD3, 1µg/ml anti-CD28, 10µg/ml anti-IL-4 and 10ng/ml rmIL-12 (**Table 12**) and plated on rabbit-anti-hamster IgG pre-coated plates at a density of 4-5x10^6 cells/ml/well for 40-48h. $CD4^+$ T cells were taken up in IL-2 containing T cell medium (200U/ml) and cultured for additional 2-3 days at 37°C, 10% CO_2. Fresh IL-2 containing medium was added daily to maintain the cells at a density of 0.5-1x10^6 cells/ml (**Fig. 9**).
$CD8^+$ T cells were activated using 0.5µg/ml anti-CD3, 1µg/ml anti-CD28 and 700U/ml IL-2 for 40-48h. $CD8^+$ T cells were taken up in IL-2 containing medium (700U/ml) and expanded for the indicated amounts of time. Fresh IL-2 containing medium was added daily to maintain the cells at a density of 0.5-1x10^6 cells/ml (**Fig. 9**).
For Multiplex analysis WT or DKO^T $CD4^+$ T cells were activated using anti-CD3 and anti-CD28 on rabbit-anti-hamster coated plates without any skewing conditions for 48h. Supernatants were flash frozen and passed on to Barbara Mosetter (AG Noessner) for multiplex analysis.

3.2.2.5 Isolation of bone marrow

Hind legs were dissected, femurs and tibas were removed, washed in PBS and sterilized in 100% Isopropanol for 2min. Bone marrow was flushed out of the bones using 5ml syringes with 26G needles, passed through 40µm cell strainers and washed with T cell medium twice. Red blood cells were lysed using TAC buffer and cell

numbers were determined. Bone marrow cells were either used immediately or cryo-preserved for future use.

3.2.2.6 *In vitro* deletion of loxP-flanked genes by 4'OH-tamoxifen

To induce deletion of loxP-flanked genes *in vitro Rc3h1/2*$^{fl/fl}$; creERT2; LSL-*hCAR* mouse embryonic fibroblasts (MEF cells) were treated with 0.32µM 4'hydroxy (OH)-tamoxifen for 5 days (**Fig. 10A**). Fresh 4'-OH-tamoxifen containing medium was added daily. To induce *in vitro* deletion of loxP-flanked sites in T cells, purified *Cd4*creERT2 expressing CD4$^+$ T cells were isolated and treated with 1µM 4'OH-tamoxifen for 24h (**Fig. 10B**). Cells were washed with fresh T cell medium 3 times prior to *in vitro* stimulation and expansion as described in section 3.2.2.4.

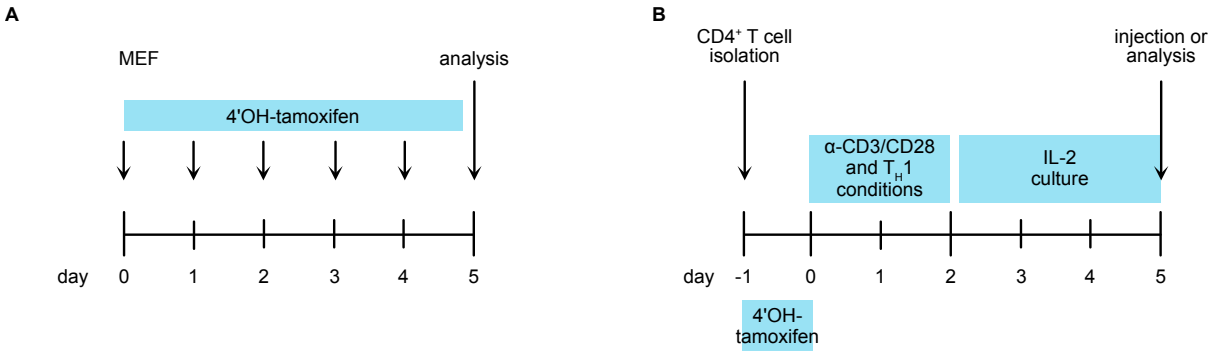

Fig. 10: Schematic representation of *in vitro* deletion conditions.
To induce deletion in **(A)** *Rc3h1/2*$^{fl/fl}$; creERT2; LSL-*hCAR* MEF or **(B)** *Rc3h1*$^{fl/fl}$; *Cd4*creERT2 T cells (iDKO^T), cells were treated with 4'OH-tamoxifen for 5d or 24h, respectively. T cells were then activated and expanded *in vitro* for and MEF cells were analyzed immediately after 4'OH tamoxifen treatment was terminated.

3.2.2.7 *In vitro* differentiation

To generate T cell supernatants for subsequent enzyme-linked immunosorbent assays (ELISA) naïve CD4$^+$ T cells were isolated as described in section 3.2.2.4 and differentiated *in vitro*. Cells were taken up in T cell medium containing 0.1µg/ml anti-CD3 and 1µg/ml anti-CD28 as well as T_H1 (10µg/ml anti-IL-4, 10ng/ml rmIL-12) or T_H17 (10µg/ml anti-IL-4, 10µg/ml anti-IFNγ, 20ng/ml rmIL-6, 5ng/ml rhTGFβ) skewing cytokine mixes at a density of 0.25x10^6 cells/ml and 50 000 cells were seeded into each well of a 96-well flat bottom plate pre-coated with rabbit-anti-hamster IgG. Each

condition was set up in triplicate, tissue culture supernatants were collected on d1, d2 and d3 after initial stimulation and flash frozen for future analysis.

3.2.2.8 Transfection of HEK293 T cells and retrovirus production

Retroviruses were produced in HEK293 cells using Calcium-phosphate-precipitation. Plasmids used for retroviral transductions are listed in **Table 13** and both contain a long terminal repeat (LTR) sequences flanking a SV-40 promotor and the transgene. For transfections HEK293 cells were seeded at a density of $8x10^6$ cells per 15cm dish, left to adhere O/N and treated with 100µM chloroquine for 1h at 37°C, 10% CO_2. The transfection mix was prepared by mixing 50µg of plasmid DNA, 5µg packaging vector pCl-Eco (containing the viral packaging and envelope genes *gag-pol* and *env*), 125mM $CaCl_2$ and H_2O to make up a final volume of 1250µl. An equal volume of HBS (pH 6.95-7.05) was added to the transfection mix under vigorous vortexing. The mix was allowed to incubate at RT for 15min prior to drop wise addition to the chloroquine treated HEK293 cells. After 6h of incubation at 37°C, 10% CO_2 the medium containing the transfection mix was replaced by fresh cell line medium and the transfected HEK293 cells were incubated at 37°C, 10% CO_2. Supernatant containing the virus was collected 12h and 24h after exchange of the cell culture medium, filtered through a 0.45µm syringe filter and used immediately for transductions.

3.2.2.9 Retroviral transduction of MEF and T cells

To achieve stable integration of transgenes into the genomes of MEF or T cells retroviral transductions were performed. One day prior to transductions MEF cells were seeded into 6-well tissue culture plates at a density of $0.05x10^6$ cells per well. $CD4^+$ T cells were isolated and stimulated *in vitro* under T_H1 skewing conditions 40h before addition of the virus. For MEF and T cell transduction the respective medium was removed and replaced by 2ml or 10ml virus mixed with 5µg/ml polybrene, respectively, per well of a 6-well plate. Cells were spin infected at 300g, 32°C for 2h (MEF cells) or 860g, 18°C for 1h (T cells) and incubated at 37°C, 10% CO_2 for 4-6h. Virus was removed and replaced with fresh cell line culture medium for MEF cells. T cells were taken up in IL-2 containing T cell medium following virus removal and expanded for 2d *in vitro* prior to *i.v.* injection into WT recipient mice. Successful transduction was confirmed by flow cytometry.

3.2.2.10 *Ex vivo* stimulation of CD4 T cells

To asses cytokine expression in *ex vivo* isolated cells, splenocytes were taken up in T cell medium at a density of 1-2x10^6 cells/ml and stimulated with 20nM PMA and 1µM ionomycin for 1h at 37°C. Subsequently, 10µg/ml Brefeldin A in PMA/ionomycin containing T cell medium was added and cells were incubated at 37°C, 10% CO_2 for 3h. PMA and Ionomycin activate signaling pathways just downstream of the TCR and CD28, so that cytokines are newly produced by T cells. Brefeldin A is used to inhibit protein transport from the golgi apparatus, thus trapping the cytokines inside the cytoplasm, which allows subsequent cytokine detection by flow cytometry (section 3.2.2.11).

3.2.2.11 Cell Trace Violet labelling and co-culture conditions

For co-culture experiments $CD4^+$, $CD8^+$ and $CD11b^+$ $Gr1^+$ cells were isolated using the EasySep™ Mouse $CD4^+$ T Cell Isolation Kit, EasySep™ Mouse $CD8^+$ T Cell Isolation Kit and EasySep™ Mouse MDSC ($CD11b^+Gr1^+$) Isolation Kit, respectively. T cells were labelled with 5µM cell trace violet (CTV) in PBS supplemented with 0.1% FCS for 20min according to manufacturers' instructions. The labelling reaction was quenched with pre-warmed T cell medium.

For suppression assays WT CTV labelled $CD8^+$ T cells were resuspended in T cell medium containing 0.5µg/ml anti-CD3, 1µg/ml anti-CD28 and 0.05x10^6 T cells were seeded into each well of a rabbit-anti-hamster coated 96-well plate. Unlabelled $CD11b^+$ $Gr1^+$ cells from WT or DKO^T mice were added at ratios of 1:1, 2:1, 4:1, 8:1 and 16:1 (T cells:$CD11b^+$ $Gr1^+$ cells). As control samples T cells incubated without any $CD11b^+$ $Gr1^+$ cells or without anti-CD3, anti-CD28 antibodies were used.

To assess stimulatory capacities of $CD11b^+$ $Gr1^+$ cells isolated from WT or DKO^T mice, these cells were mixed with WT CTV labelled $CD4^+$ or $CD8^+$ cells in the presence of soluble 0.1µg/ml anti-CD3, 1µg/ml anti-CD28 or 0.5µg/ml anti-CD3, 1µg/ml anti-CD28, respectively. Cells were seeded into uncoated 96-well plates at the ratios indicated above.

Co-cultures were incubated at 37°C, 10% CO_2 for 72h and T cells were then analysed by flow cytometry for CTV dilution as a marker of proliferation and surface expression of activation markers.

3.2.2.12 Antibody staining for flow cytometry

All staining steps described below were performed in the dark. Single cell-suspensions were washed with PBS and stained with either fixable blue viability dye or fixable viability dye eF780 (Thermo Scientific) in PBS for 20min on ice. For the detection of surface proteins cells were stained with the appropriate antibodies diluted in FACS buffer (2% FCS, 1mM EDTA in PBS) for 20min on ice. For staining of surface T_{FH} cell markers, cells were first stained with a viability dye, followed by a 5min pre-incubation in FACS buffer containing rat serum (Stem Cell Technologies) and Fc block, before the appropriate 2x antibody mixture in FACS buffer was added. Cells stained for T_{FH} surface markers were incubated for 45min on ice. All antibodies and dilutions used for flow cytometry are listed in **Table 11.**

Following surface staining cells were fixed using the Foxp3 Fixation/Permeabilization buffer set (eBioscience) for 30min on ice. After fixation cells were washed with permeabilization buffer once and resuspended in the appropriate antibody mix diluted in permeabilization buffer. Intracellular staining was performed for 30min on ice.

For intracellular cytokine staining, surface-stained cells were fixed in 4% Paraformaldehyde (PFA) in PBS for 12-15min at RT. Fixed cells were washed with saponin once and stained with the appropriate antibody mix diluted in saponin buffer for at least 30min at RT.

Cells were filtered through 41µm polyamide/nylon filters (RCT) and data was acquired using the BD FACS Canto II or BD LSR Fortessa instruments. Data analysis was performed with FlowJo (Treestar). An exemplary gating strategy is shown in **Fig. 11.**

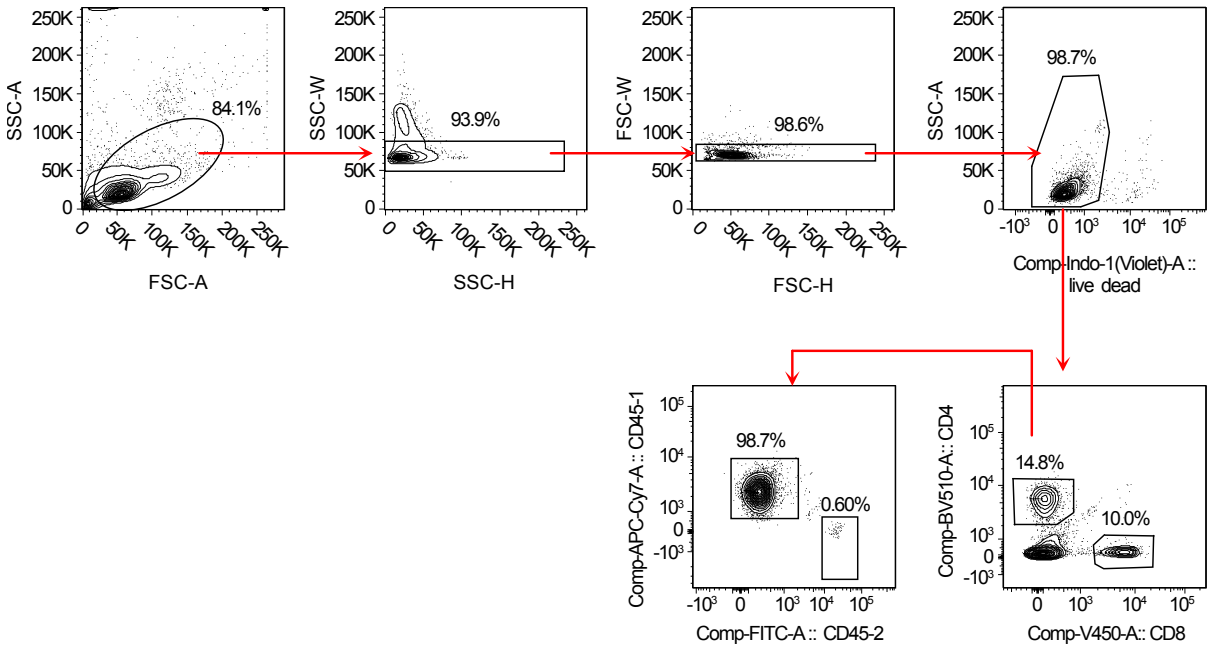

Fig. 11: Example gating strategy used for flow cytometry data analysis.
To analyze data obtained by flow cytometry cells were gated on lymphocytes (FSC-A/SSC-A), single cells (SSC-H/SSC-W and FSC-H/FSC-W), followed by a gating for live cells (Indo-1(violet)-A neg). Live cells were further gated according to the population of interest. Here, an example gating for adoptive T cell transfers is shown, where live cells are further gated on $CD4^+$ T cells followed by analysis of recipient ($CD45.1^+$) or donor ($CD45.2^+$) cells.

3.2.3 *In vivo* techniques

3.2.3.1 Adoptive T cell transfers

$CD4^+$, $CD8^+$ or $CD3^+$ T cells were isolated from female donor mice as described in section 3.2.2.4. After isolation cells were washed in sterile PBS three times, counted and resuspended in sterile PBS at a density of $13.3x10^6$ cells/ml. $1.5\text{-}2x10^6$ cells in a total volume of 150µl were injected intravenously (i.v.) into 10-12 weeks-old congenically marked recipient mice. Recipient mice were sacrificed on day 8, 14 or 49 after transfer and scored at least once per week throughout the course of the experiments.

3.2.3.2 *In vivo* deletion of loxP-flanked sites using tamoxifen

To delete loxP-flanked sites *in vivo* T cells isolated from female *Cd4*creERT2 or creERT2 mice with floxed alleles encoding for *Rc3h1/2* and/or *Zc3h12a* were injected into congenically marked recipients. One day after injection recipient mice were fed

5mg tamoxifen twice a day for two days by oral gavage (total dose of 20mg per mouse). Mice were sacrificed at least 6 days after the first gavage treatment.

3.2.3.3 Bone marrow chimeras

10-12 weeks-old LSL-Kras^{G12D}; p48cre mice were lethally irradiated on two subsequent days using the XSTrahl 225 X-ray device with tungsten cathode (radiation hardened). Irradiation was performed with a 0.5mm Cu filter; 5.5 Gy; 195 kV and 15mA settings. Irradiated mice were injected *i.v.* with 5x10^6 bone marrow cells isolated from WT or *Rc3h1/2*$^{fl/fl}$; *Cd4*cre mice 4-5h after the second irradiation. Mice received water supplemented with antibiotics (2.5% Baytril®) during the first two weeks after reconstitution and were sacrificed 5.5-6 weeks after irradiation.

3.2.3.4 Generation of primary pancreatic cancer cell lines for exome sequencing

LSL-Kras^{G12D}; p48cre mice reconstituted with bone marrow isolated from either WT or DKO^T mice were sacrificed 5.5-6 weeks after reconstitution, when tumors were palpable in the abdominal area. Pancreata were removed and 2-3 ~3mm^2 pieces were cut out from each identified tumor region. Care was taken not to resect fat or healthy appearing pancreas tissue. Tumor pieces were put into high glucose DMEM supplemented with 20% FCS and 100U/ml Penicillin-Streptomycin. From each tumor one additional piece was incubated in RNAse later at 4°C for 24h and subsequently stored at -20°C for future RNA isolation.

Tumors were digested in high glucose DMEM supplemented with 20% FCS, 100U/ml Penicillin-Streptomycin and 200U/ml Collagenase II. Digestions were performed for at least 18h at 37°C, 800rpm. Following digestion collagenase II containing medium was replaced with tumor medium (10% FCS, 100U/ml Penicillin-Streptomycin in DMEM) and cultured at 37°C, 5% CO_2. Cells were initially seeded into 6-well plates (Falcon), expanded in T175 flasks and cryo-preserved as soon as possible (before reaching passage 10). Cells were allowed to reach 100% confluence before passaging and were passaged as long as contaminating stromal cells or fibroblasts could be detected. Successful removal of stromal cells/fibroblasts was assessed by PCR. A cell line was considered to be pure, when the unrecombined Kras^{G12D} band could no longer be detected (**Fig. 12).**

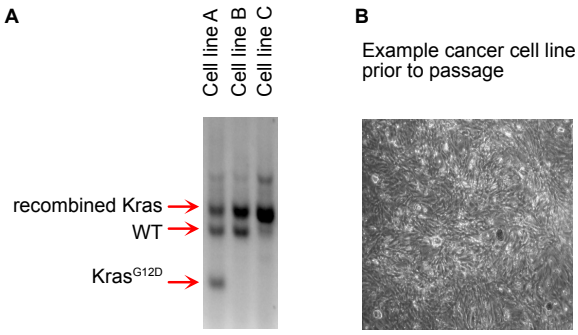

Fig. 12: Generation of primary pancreas cancer cell lines.
(A) 2% agarose gel used to assess removal of stromal cells and fibroblasts from primary cancer cell lines. Cell line A contains both stromal contamination as well as cancer cells as assessed by the presence of the $Kras^{G12D}$ and a recombined Kras band, respectively. Cell lines B and C are examples of two cancer cell lines that do not contain any stromal contaminations. **(B)** Example image of a primary cancer cell line at 100% confluence.

3.2.3.5 *In vivo* cytokine neutralization

For *in vivo* neuralization of G-CSF bone marrow chimeras were generated as described above. Treatment with anti-G-CSF neutralizing antibodies or with isotype controls was initiated one week after irradiation. Mice were injected intraperitoneally (i.p.) with 25µg anti-G-CSF or isotype control twice per week. Site of injection was alternated between treatments and mice were sacrificed 5 weeks after reconstitution. For *in vivo* neutralization of IL-17A 10 weeks-old *Rc3h1/2*$^{fl/fl}$; *Cd4*cre mice were injected i.p. with 50µg anti-IL-17A neutralizing antibody or isotype control twice per week for 10 weeks. Site of injection was alternated between treatments.

3.2.4 Biochemical methods

3.2.4.1 Protein extraction, SDS-PAGE and immunoblotting

To assess protein expression cells were harvested, washed with ice-cold PBS once and lysed in 2x Meister lysis buffer supplemented with protease inhibitor and DTT just before use. The volume of lysis buffer was equal to the pellet size. Cell were vortexed thoroughly, lysed on ice for 20min and the protein-containing lysate was cleared from cell debris by centrifugation (13000xg, 15min, 4°C). Protein concentrations were determined by Bradford assay using the Bio-Rad Protein assay dye according to manufacturers' instructions. 25-50µg protein lysate were denatured in 4x Laemmli

loading buffer, boiled at 95°C for 5min and loaded on 8-10% SDS-polyacrylamide gels. A pre-stained size marker was used to determine protein sizes. Electrophoresis was performed in SDS running buffer at 100V, followed by wet transfer onto PVDF membranes. Blotting was performed at 4°C either at 40V O/N or at 100V for 90min.
For detection of specific proteins, membranes were blocked in 5% milk in TBS, followed by O/N incubation with primary antibodies at 4°C with constant agitation. Primary antibodies were diluted either in 1% milk in TBS-T for hybridoma supernatants (anti-Roquin 3F12) or in 5% BSA in TBS-T for commercially available antibodies. Membranes were washed with TBS-T three times and incubated with the appropriate horseradish peroxidase (HRP)-conjugated secondary antibody diluted in 1% milk in TBS-T for 1h at RT. After incubation with the secondary antibody, membranes were washed three times with TBS-T and signals were detected on X-Ray films using either self-made or commercially available ECL substrate depending on the expected band intensity.

3.2.4.2 Organ preparation for immunohistochemistry and quantification of positive cells

For immunohistological staining pancreas tissue was dissected and fixed in 4% paraformaldehyde for 5 days. Tissue embedding in paraffin, preparation of 2µm tissue sections and histological stainings were performed by Dr. Jessica Zoeller, Jenny Hetzer and Danijela Heide from the AG Heikenwälder (DKFZ Heidelberg) as described in (Jeltsch *et al.*, 2014). Images were generated by scanning whole tissue sections with a Leica SCN400 slide scanner. Whole tissue sections were quantified using Aperio ImageScope (Leica) following instructions from Dr. Katja Steiger.
Percent tissue remodeling in pancreata dissected from $Kras^{G12D}$ mice reconstituted with either WT or DKO^{T} bone marrow was determined by measuring the surface of all areas affected by tumor and or high grade panIN lesions and normalizing it to the total pancreas area. A similar approach was taken to quantify the portions of tissue affected by pancreas pathology in DKO^{T} mice treated with IL-17A neutralizing antibodies. Only areas which showed clear deviations from normal pancreatic tissue were used for this analysis.
To quantify cells in pancreas tissue stained positive for different markers (e.g. CD3 for T cells, Ly6G for neutrophils) three high-power fields (i.e. 20x magnification) were selected and counted by hand. Cell counts were normalized to the area of the counted

high-power field (in mm^2) and average cell counts for three high-power fields were determined for each biological replicate. To quantify cells in tissues from $Kras^{G12D}$ mice reconstituted with either WT or DKO^T bone marrow high-power fields were selected randomly. To quantify cells in tissues obtained after neutralization of IL-17A areas affected by pathological changes were selected. Representative pictures of scanned whole tissue sections were taken using Aperio ImageScope.

3.2.4.3 Enzyme-linked immunosorbent assay

Enzyme-linked immunosorbent assays (ELISA) were performed using the Mouse G-CSF DuoSet® ELISA kit (R&D Systems) according to manufacturers' instructions. In brief, all reagents and standards were reconstituted or diluted as specified in the kit instructions. ELISA plates were coated with capture antibody (2µg/ml in PBS) at RT O/N. All reagents were warmed to RT and samples were thawed on ice. All subsequently described steps were carried out at RT. Plates were washed with wash buffer, blocked with reagent diluent for 1h, followed by incubation with serum diluted in reagent diluent, undiluted tissue culture supernatants (TCS) or G-CSF standard (serially diluted in reagent diluent). As blanks reagent diluent or unconditioned T cell medium was used. Plates were washed with wash buffer three times, followed by an incubation with biotinylated detection antibody (200ng/ml in reagent diluent) for 2h, three additional washing steps and incubation with streptavidin-HRP diluted in reagent diluent for 45min. Subsequently substrate solution was added for 20min and the reaction was stopped by the addition of stop solution. Optical density was immediately determined using a microplate reader set to 450nm. For wavelength corrections readings at 540nm were substracted from all values. All readings were blank corrected and G-CSF concentrations were extrapolated using the 4-parameter-logistic-fit function in GraphPad Prism.

3.2.5 RNA and DNA methods

3.2.5.1 RNA isolation and cDNA synthesis

RNA was isolated from T cells or tumor tissue using the column-based RNeasy Kit with on column gDNA (genomic DNA) removal. Isolation was performed according to manufacturers' instructions. RNA isolated from T cells was reversed transcribed using

the RevertAid RT Kit following manufacturers' instruction and remaining RNA was stored at -80°C.

For RNA isolation from pancreas tissue 20mg tissue were mechanically disrupted in 8ml ice cold Trizol reagent. 2x2ml were transferred into Eppendorf tubes and cleared by centrifugation (12000xg, 5min, 4°C). 1ml clear supernatant from each tube was used for RNA isolation by standard phenol-chloroform extraction, followed by an RNA clean up step using RNA Clean & Concentrator^{TM} columns. RNA was eluted in DPEC treated H_2O and RNase inhibitor was added to each sample. RNA was reverse transcribed using the Quantitect RT Kit.

Before reverse transcription RNA integrity and quality was confirmed by agarose gel electrophoresis. Quality of RNA isolated from primary tumors was assessed on the Bioanalyser (by Dr. Taku Kureha).

3.2.5.2 Real-Time qPCR

Gene expression was quantified using the UPL Probe Library System by Roche and the Roche Light Cycler instrument. The UPL system is based on a combination of gene-specific intron spanning primer pairs with a sequence specific fluorescent probe. Calculation of expression levels was performed using the ΔCp method and was based on fluorescence intensity during the amplification. All values were normalized to one or two housekeeper genes for analysis of expression levels in T cells or pancreas tissue, respectively.

3.2.5.3 Genomic DNA isolation

Genomic DNA (gDNA) was isolated from primary tumor cell lines and paired tails from LSL-Kras^{G12D}; p48cre mice reconstituted with either WT or DKO^{T} bone marrow using the DNeasy Blood&Tissue Kit following manufacturers' instructions. Mouse tails were cut into small pieces and lysed at 56°C in a proteinase K containing lysis buffer for 6h under continuous agitation prior to gDNA isolation.

3.2.5.4 RNA Sequencing, Whole Exome Sequencing and Bioinformatical analysis

RNA and gDNA was isolated from primary tumors or primary cell lines obtained from LSL-Kras^{G12D}; p48cre mice reconstituted with either WT or DKO^{T} bone marrow as described above. As reference tissue gDNA isolated from tails of these mice was used

and paired with the respective gDNA sample obtained from cell lines or tumors for anlaysis.

Library preparation, RNA Sequencing, Whole Exome Sequencing (WES) and bioinformatical analysis were performed by Dr. Sebastian Müller (AG Rad, TU Munich) as described in (Mueller *et al.*, 2018). A list of significantly deregulated genes is attached in **appendix 2**.

Sequencing data for WT and DKO^{T} $CD4^{+}$ T cells was generated by Dr. Nina Kronbeck. It is available from (https://www.ncbi.nlm.nih.gov/geo/query/acc.cgi?acc=GSE152961). A list of significantly up and down regulated genes between WT and DKO^{T} $CD4^{+}$ T cells is attached in **appendix 1**.

3.2.6 Statistical Analysis

All statistical analysis was performed using Prism 7 (GraphPad). One-tailed student's t-tests were used for comparisons between two experimental groups. For three or more experimental groups One-way-ANOVA was used and an appropriate post-hoc test was applied to correct for multiple comparisons. The test used for analysis is indicated in the figure legends. Results were considered significant if the p value was <0.05. To extrapolate concentrations for ELISAs 4-parameter-logistic-fit was used to generate standard curves and concentrations were extrapolated using the extrapolate function of Prism. Unless otherwise stated all data shown in this study is presented as mean $\pm$ standard error of mean (SEM).

Visual representations of RNA sequencing data were generated using the ggplot2 package in R Studio. The code use to generate volcano and enrichment plots based on sequencing data provided by the bioinformaticians as excel sheets is available in **Appendix 4.**

4. Results

4.1 Roquin-1/2-deficient T cells affect WT immune cells in *trans*

4.1.1 Dissecting T cell intrinsic and extrinsic effects of Roquin-1/2-deficiency

DKO^T mice that lack Roquin proteins in peripheral T cells and mice harboring a systemic Roquin-1^{M199R} mutation show strong auto-immune and auto-inflammatory phenotypes characterized by splenomegaly, lymphadenopathy, expansion of the $CD4^+$ and $CD8^+$ effector memory T cell compartment, as well as accumulation of T_{FH} and GC B cells (Jeltsch and Heissmeyer, 2016; Jeltsch *et al.*, 2014; Linterman *et al.*, 2009b; Vinuesa *et al.*, 2005; Vogel *et al.*, 2013). Interestingly, deletion of Roquin proteins in T_{regs} also resulted in an expanded effector-memory compartment in CD4+ T_{conv} and $CD8^+$ T cells, and accumulation of $Foxp3^-$ $PD1^{int}$ $CXCR5^{int}$ pre-T_{FH} cells (Essig *et al.*, 2017).

Loss-of-function of Regnase-1, another RNA-binding protein that shares an overlapping target set with the Roquin proteins, either systemically or conditionally in peripheral T cells, also leads to the development of severe autoimmune and autoinflammatory pathologies, characterized by splenomegaly, lymphadenopathy, production of anti-nuclear antibodies, accumulation of activated T cells, elevated immunoglobulin levels and accumulation of plasma cells (Akira, 2013; Liang et al., 2010; Matsushita et al., 2009; Miao et al., 2013; Mino *et al.*, 2015; Mino and Takeuchi, 2015; Uehata et al., 2013).

These observations challenge the current belief that Roquin proteins control T cell activation and differentiation only in a T cell intrinsic manner and pose the question how Regnase-1 contributes to phenotypes observed in Roquin mutant mice.

The first part of this work focuses on dissecting T cell intrinsic versus the T cell extrinsic effects of Roquin protein loss-of-function, and I also discuss contributions from Regnase-1 to cell intrinsic function, since these data resulted in a recent manuscript (Behrens *et al.*, 2021).

To analyze acute and temporally resolved effects of Roquin or Regnase-1 deficiency, I adoptively transferred $CD45.2^+CD3^+$ T cells isolated from mice, that allowed inducible Roquin-1/2 ($iDKO^T$), Regnase-1 (iKO^T) and combined Roquin-1/2; Regnase-1 ($iTKO^T$) deletion, into WT $CD45.1^+$ recipient mice. Deletion was induced by feeding the

recipient mice tamoxifen und the transferred cells were then assessed for their ability to proliferate within the host 8d after transfer **(Fig. 13A).**

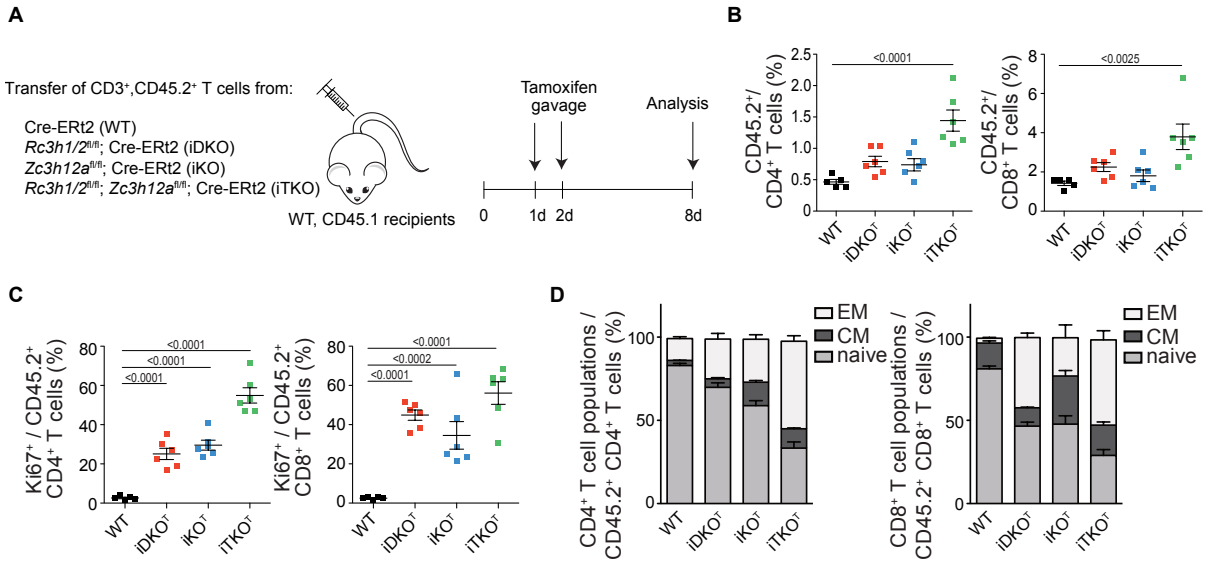

Fig. 13: Roquin-1/2 or Regnase-1 deficiencies causes enhanced activation and proliferation of T cells.

(A) Schematic of experimental set-up to assess T cell intrinsic effects on T cell activation and proliferation. **(B)** Portion of transferred WT, iDKO^T, iKO^T, iTKO^T cells on the day of analysis. **(C)** Proliferation of transferred cells. **(D)** Analysis of the memory compartments of transferred cells. Statistical significance was determined by one-way ANOVA, with Dunnett's post hoc test. All data are presented as Mean ± SEM. Adapted from (Behrens *et al.*, 2021) and reproduced with permission of Springer Nature.

Transferred T cells from all genotypes could readily be detected 8 days after transfer **(Fig. 13B**), all inducible knock-out but not the WT T cells became activated and strongly proliferated **(Fig. 13C,D)** within the WT recipients, with strongest effects observed in the cells that harboured a combined ablation of Roquin-1/2 and Regnase-1 (iTKO^T).

Since T cell specific Roquin deletion is associated with an accumulation of PD-1^{hi}CXCR5^{hi}Bcl6$^+$ T follicular helper cells (T_{FH}) and induction of GC B cells (GL7$^+$, CD95$^+$, IgD$^-$) (Vogel *et al.*, 2013), we were wondering whether this occurred in a normal, non-inflammatory environment with a functional WT regulatory T cell (T_{reg}) compartment. We transferred naïve CD45.2$^+$ CD4$^+$ T cells from WT or inducible knock-out donors into CD45.1$^+$ recipients, treated the recipient mice with tamoxifen to induce deletion of floxed alleles and analyzed the transferred T cells on d8 or d49 after transfer **(Fig. 14A)** to assess short- and long-term effects.

As expected, 8 days after transfer all inducible knock-out cells spontaneously acquired a T_{FH} phenotype, with the strongest effects observed in iKO^T cells **(Fig. 14B,C)** rather than in the combined knock-out. When we analyzed the transferred cells 49d after transfer, we could only find back iKO^T and $iTKO^T$ cells, whereas WT and $iDKO^T$ cells had completely disappeared from the recipient mice **(Fig. 14D)**.

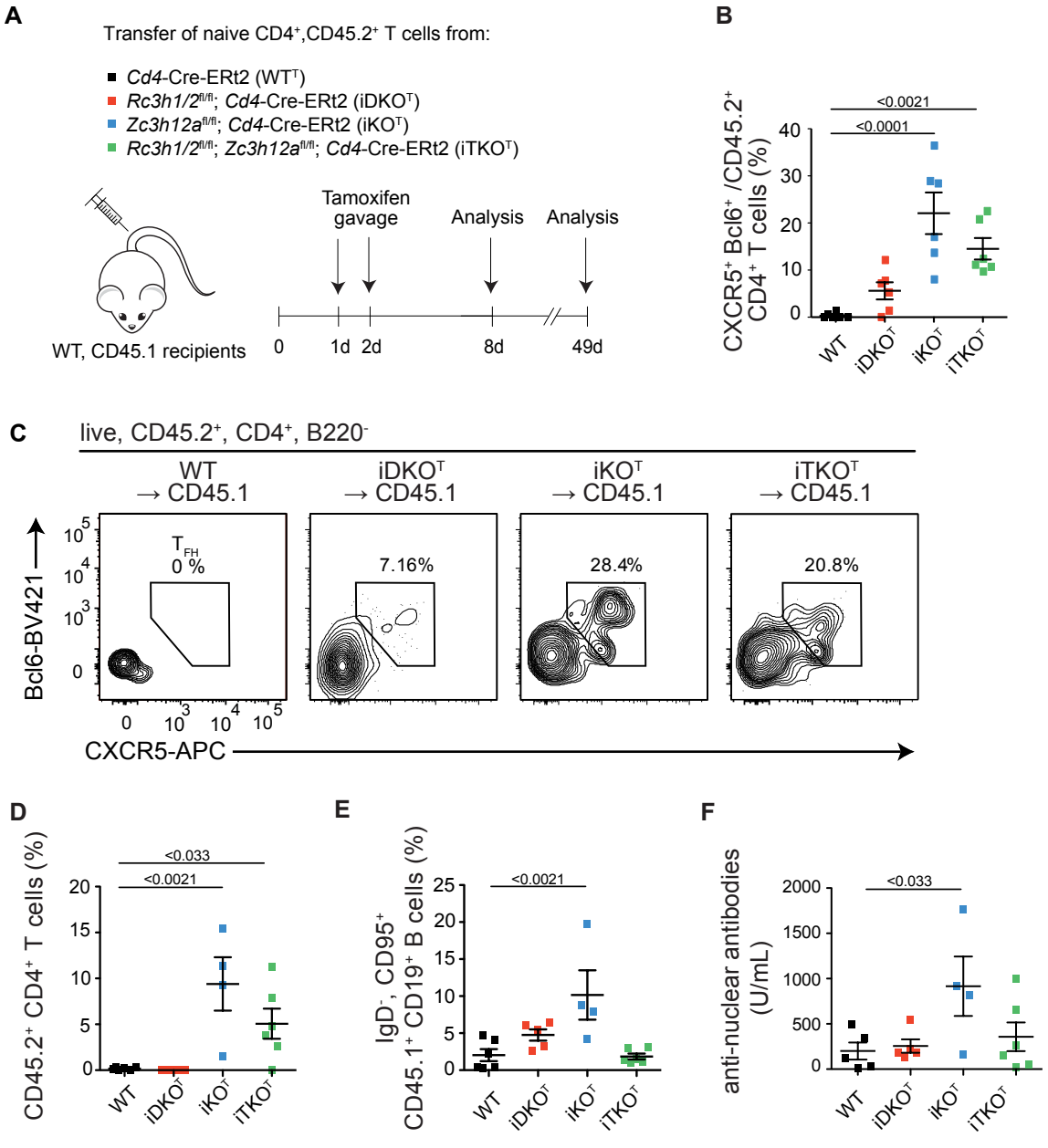

Fig. 14: Roquin-1/2 and Regnase-1 deficiency causes enhanced T_{FH} differentiation.

(A) Schematic representation of adoptive transfer conditions. **(B)** Quantification of injected T_{FH} cells and **(C)** representative plots 8d after transfer. **(D)** Quantification of transferred WT or knock out cells 49d after adoptive transfer. **(E)** Quantification of endogenous GC B cells 49d after adoptive transfer of WT or knockout $CD4^+$ T cells. **(F)** Quantification of anti-nuclear antibodies in the sera of recipient mice 49d

after adoptive transfer (ANA-ELISAs were performed by Elaine Wong). Data presented as Mean ± SEM. Statistical significance was determined by one-way ANOVA with Dunnett's post hoc test. For each group 4-6 biological replicates were analyzed. Taken from (Behrens *et al.*, 2021) and reproduced with permission of Springer Nature.

Interestingly, even though iDKO^{T} cells were no longer detectable within the recipient mice, they still caused an expansion in endogenous GC B cells **(Fig.14E)**. A similar effect on GC B cells was observed for iKO^{T} but not for iTKO^{T} cells 7 weeks after transfer further supporting a T cell extrinsic role of Roquin loss-of-function. Only iKO^{T} cells were able to transfer autoimmunity as assessed by the production of anti-nuclear antibodies (ANAs) in the sera of CD45.1^{+} recipients 7 weeks after transfer **(Fig.14F).**

We next wanted to identify whether the observed phenotypes of Roquin loss-of-function are specific for Roquin function in T cells or could also involve contributions from non-T cells. To answer this question, we analyzed mice that contained the M199R mutation on one allele of Roquin-1 (*Rc3h1*^{M199R}) and the other allele in a floxed configuration. Mice that harbor only one heterozygous M199R allele do not develop a phenotype at young age (Ellyard et al., 2012), i.e. *Rc3h1*$^{M199R/fl}$ only develop a phenotype if the floxed allele is deleted in the presence of a *cre* recombinase. We combined these mice with either *Cd4-Cre* or *Vav-Cre* to induce a T cell specific or hematopoietic cell specific deletion, respectively **(Fig.15).**

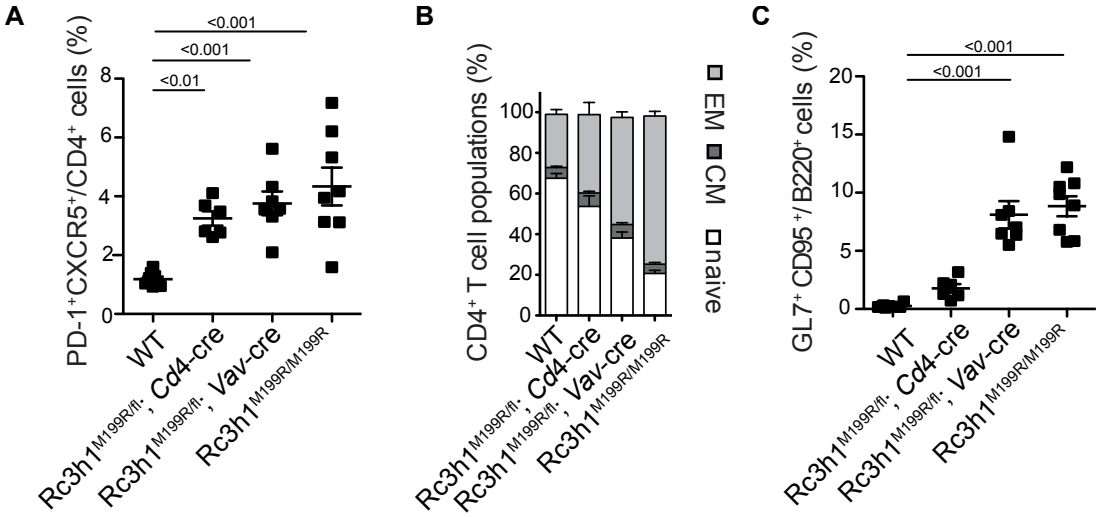

Fig. 15: Roquin loss-of-function leads to a T cell intrinsic T_{FH} differentiation.
Frequencies of **(A)** T_{FH}, **(B)** CD4^{+} memory populations and **(C)** GC B cells in the spleens of 9-14-weeks-old WT, *Rc3h1*$^{M199R/fl}$;*Cd4*-Cre, *Rc3h1*$^{M199R/fl}$;*Vav*-Cre and *Rc3h1*$^{M199R/M199R}$ (*sanroque*) mice. Data are

representative for at least 5 biological replicates per group and presented as Mean ± SEM. Statistical significance was determined by one-way ANOVA with Bonferroni post-hock test. Taken from (Behrens *et al.*, 2021) and reproduced with permission of Springer Nature. This experiment was performed by Dr. Gesine Behrens.

Roquin loss-of-function in the hematopoietic system, i.e. by expression Cre from the *Vav* promotor, caused a much stronger T cell activation and GC B cell accumulation **(Fig. 15B,C)** than T cell specific deletion. On the other hand, T_{FH} differentiation was comparable in the *Cd4-Cre* and the *Vav-Cre* models of Roquin-1 loss-of-function **(Fig. 15A)**, meaning that T_{FH} differentiation involves regulatory inputs only from Roquin function in T cells, whereas extrinsic contributions from non-T cells can play a role in T cell activation and GC B cell accumulation.

In the adoptive transfer model with congenically marked cells, it is also possible to analyze how the host reacts to the transfer of cells. Unexpectedly, when we analyzed the T cell compartments of recipient CD45.1$^+$ mice, it became apparent that iDKO^T T cells could also induce T_{FH} differentiation in *trans* which was not the case for iKO^T or iTKO^T cells **(Fig. 16).**

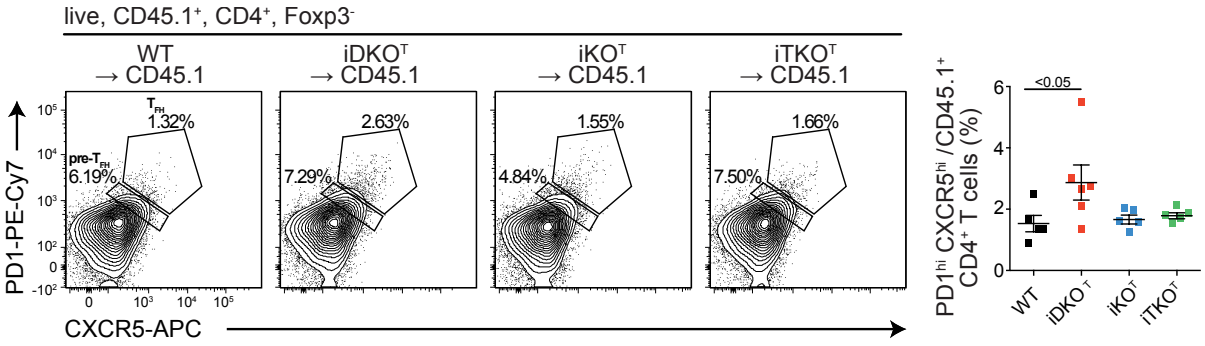

Fig. 16: Roquin-1/2 but not Regnase-1 deficient T cell cause enhanced T_{FH} differentiation in *trans.* Representative plots and quantification of endogenous T_{FH} cells in WT recipients that were adoptively transferred with WT, iDKO^T, iKO^T or iTKO^T T cells. Data presented as Mean ± SEM. Statistical significance was determined by one-way ANOVA with Dunnett's post hoc test. For each group 4-6 biological replicates were analyzed.

Taken together, these data together with previously published report, support the hypothesis that ablation of the RNA-binding proteins Roquin-1/2 in T cells, on the one hand affects the T cell compartment in a cell intrinsic manner, on the other hand it leads to inappropriate production of one or more factors that affect other cells, among

others T cells in *trans*. Whereas the effects of Regnase-1 loss appear to be predominantly cell intrinsic. Based on these observations we hypothesized that Roquin-1 and Roquin-2 deficiency in T cells leads to an inappropriate expression of a factor that works in *trans* by affecting other cells to promote autoimmune and autoinflammatory responses and pathology.

Thus, the remainder of this work will focus on the T cell extrinsic effects of DKO^{T} cells, aiming to comprehensively describe the *trans* effect on bystander cells trying to identify one or several *trans*-acting factors.

4.1.2 Optimization of adoptive transfer conditions

To be able to study the *trans* effect induced by DKO^{T} cells and to confirm the robustness of the effect, I first optimized the adoptive transfer conditions **(Fig. 17)**. Three different conditions were assessed. First, naïve cells were isolated from WT or $iDKO^{T}$ donor mice and transferred into $CD45.1^{+}$ WT recipients. Recipient mice were force-fed with tamoxifen on two consecutive days to induce acute deletion of floxed alleles **(Fig. 17A).** Second, $CD4^{+}$ T cells were isolated from WT or DKO^{T} mice, differentiated *in vitro* under T_H1 conditions and expanded in IL-2 containing medium for 2 days, prior to injection into $CD45.1^{+}$ recipient mice **(Fig. 17B)**. In a third approach, floxed alleles were deleted by *in vitro* hydroxytamoxifen treatment, prior to T_H1 differentiation, expansion and injection into $CD45.1^{+}$ recipient mice **(Fig.17C).** Recipient mice were sacrificed on d8 after transfer, splenocytes were analyzed by flow cytometry and sera were flash-frozen for later analyses.

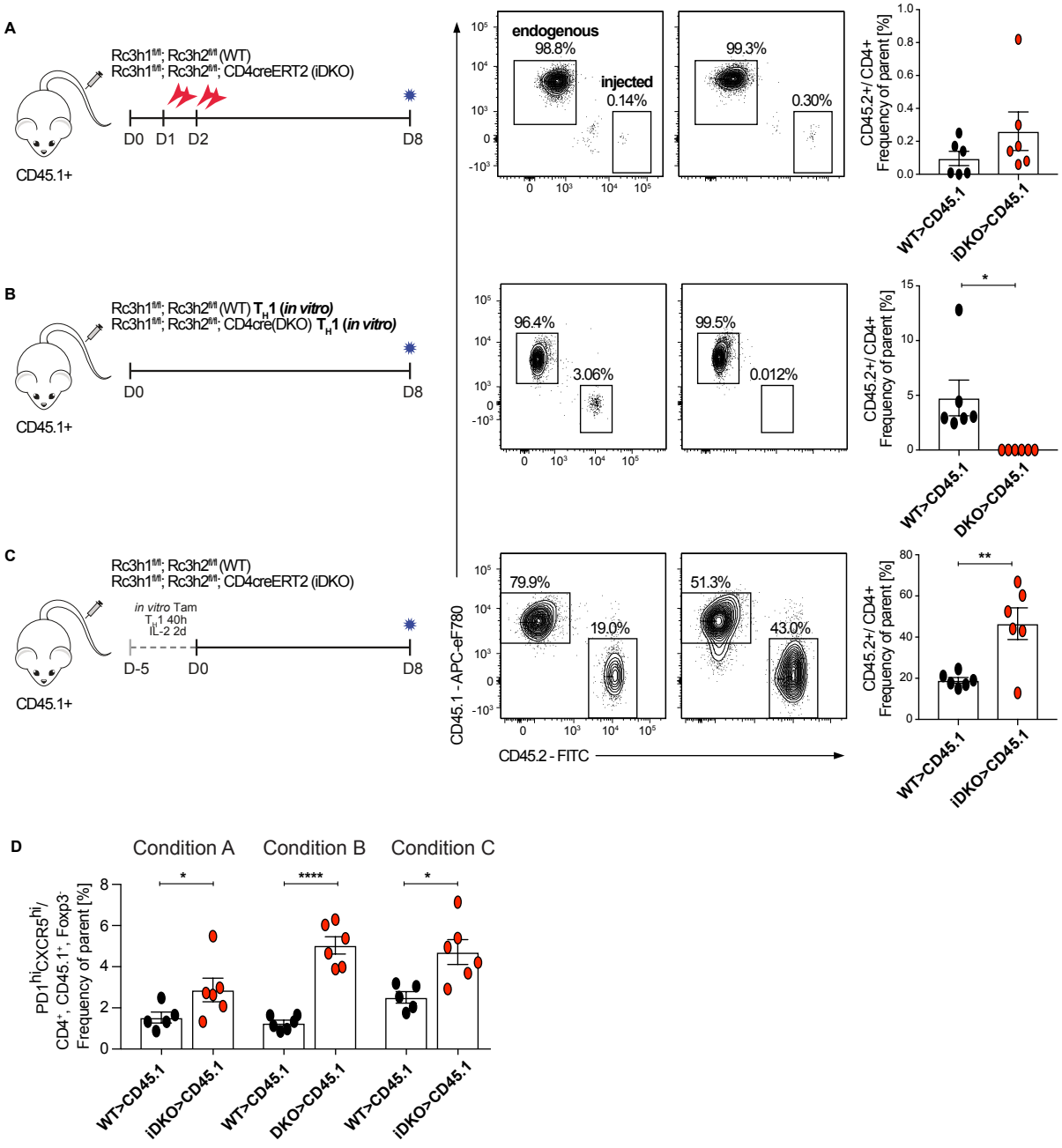

Fig. 17: Optimization of adoptive transfer conditions.

Schematic representations of adoptive transfer conditions used throughout this work. **(A)** $CD4^+$ T cells were isolated from WT or $iDKO^T$ donor mice and directly injected into WT, CD45.1 recipient. WT mice were treated with Tamoxifen 4 times on two consecutive days. **(B)** WT and DKO^T $CD4^+$ T cells were activated *in vitro* under T_H1 conditions, expanded in IL-2 for 2 days and injected into WT, $CD45.1^+$ recipients. **(C)** $CD4^+$ T cells were isolated from WT or $iDKO^T$ donor mice and treated with hydroxy-tomoxifen *in vitro*, then stimulated under T_H1 conditions and expanded in IL-2 for 2 days prior to injection into WT, $CD45.1^+$ recipient mice. Recipient mice were sacrificed on day 8 post injection. **(D)** Quantifications of endogenous T_{FH} cells 8d post transfer under conditions A-C. Representative plots and quantifications are shown. Data presented as Mean ± SEM. Statistical significance was determined

by unpaired, one-tailed t-test. For each group 6 biological replicates were analyzed. * p<0.05, ** p< 0.01, **** p<0.0001.

In the first transfer condition, naïve T cells were transferred followed by an acute deletion within the host, but only very few transferred T cells could be re-isolated after 8 days and only slightly more transferred iDKO^{T} cells were present than transferred WT T cells **(Fig. 17A).** Also in the second condition, the transfer of *in vitro* activated DKO^{T} T_H1 cells showed that these cells were no longer detectable within the WT host after 8d **(Fig. 17B).** When iDKO^{T} cells were treated with hydroxytamoxifen *in vitro* they strongly proliferated within the WT recipient, so that on day 8 after transfer there was a 1:1 ratio between the endogenous, CD45.1^{+} and the transferred T cells. The transferred WT T cells were also present at a higher frequency compared to the other conditions **(Fig. 17C).** All conditions were able to robustly induce an accumulation of endogenous CD45.1^{+} T_{FH} cells **(Fig. 17D).**

Due to the ease of handling and smaller burden for the recipient mice, condition B was used for all adoptive transfers of CD4^{+} T cells. Condition A was used, when CD8^{+} or total CD3^{+} T cells were transferred. Since in condition C the DKO^{T} cell expansion within the WT host was very strong, I decided not to use this condition for any of the following experiments, since under these circumstances it was not possible to distinguish between a real *trans*-effect or secondary changes caused by the strong expansion and competition with donor cells.

4.1.3 Roquin deficient CD4^{+} T cells induce activation and T_{FH} differentiation

To assess the full extent of DKO^{T} T cell mediated *trans*-effects, we analyzed different endogenous immune cell compartments of WT recipient mice **(Fig. 18).** For this purpose, we transferred *in vitro* activated T_H1 cells taken from WT or DKO^{T} mice into CD45.1^{+} recipients and analyzed the recipient mice 8 days after transfer. Although the majority of injected DKO^{T} donor cells had disappeared **(Fig. 17B)**, the spleens of mice that received DKO^{T} cells were strongly enlarged compared to mice that received WT T_H1 cells **(Fig. 18A**). Interestingly, Roquin deficient CD4^{+} T cells induced strong activation, expansion of the memory compartment as well as proliferation in endogenous CD8^{+} T cells from the CD45.1^{+} host **(Fig. 18B,C)**. Furthermore, endogenous CD8^{+} T cells downregulated surface CD8 expression in response to the

presence of DKO^{T} CD4^{+} T cells **(Fig. 18D)** also pointing at increased bystander CD8^{+} T cell activation.

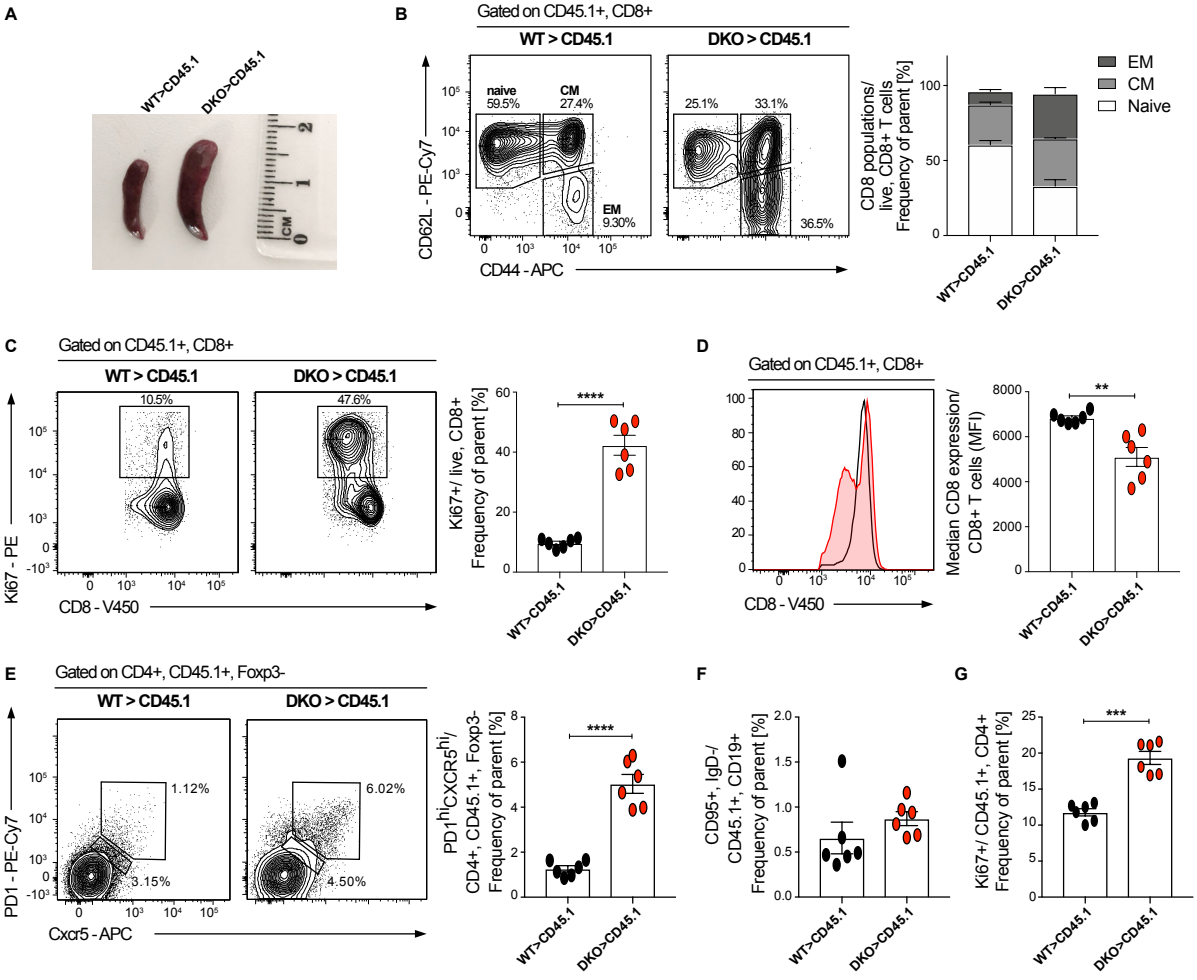

Fig. 18: DKO^{T} cells induce bystander CD8^{+} T cell activation and T_{FH} differentiation.
(A) Representative image showing spleens taken from WT recipient mice 8 days after WT or DKO^{T} T cell transfer. **(B)** Endogenous CD8^{+} T cell populations, **(C)** proliferation and **(D)** surface CD8 expression 8 days after WT or DKO^{T} T cell transfer. **(E)** T_{FH} differentiation of endogenous CD4^{+} T cells, **(F)** accumulation of GC B cells and **(G)** proliferation of endogenous CD4^{+} T cells in response to WT or DKO^{T} T cell transfer. Representative plots and quantifications are shown. Data presented as Mean ± SEM. Statistical significance was determined by unpaired, one-tailed t-test. For each group 6 biological replicates were analyzed. ** p< 0.01, *** p<0.001, **** p<0.0001.

Similar to the observations made in **Fig.16**, transfer of *in vitro* activated DKO^{T} also lead to an accumulation of endogenous, CD45.1^{+}, PD1^{hi} CXCR5^{hi} T_{FH} cells and a slight increase in endogenous GC B cells **(Fig.18E,F)**. Endogenous CD45.1^{+} CD4^{+} T cells proliferated stronger after DKO^{T} cell transfer than after WT T cell transfer **(Fig. 18G)**

as assessed by Ki67 staining. The effects on endogenous CD4$^+$ T cell proliferation were not as strong as the effects on the endogenous CD8$^+$ T cell compartment.

We were wondering whether similar *trans* effects could also be produced by Roquin-1/2-deficient CD8$^+$ T cells. To test this, CD8$^+$ T cells were isolated from WT or iDKO^T mice, transferred into CD45.1$^+$ recipient mice (**Fig. 17A**), which were treated with tamoxifen to induce deletion of floxed alleles. 8 days after transfer splenocytes of recipient mice were analyzed **(Fig. 19).**

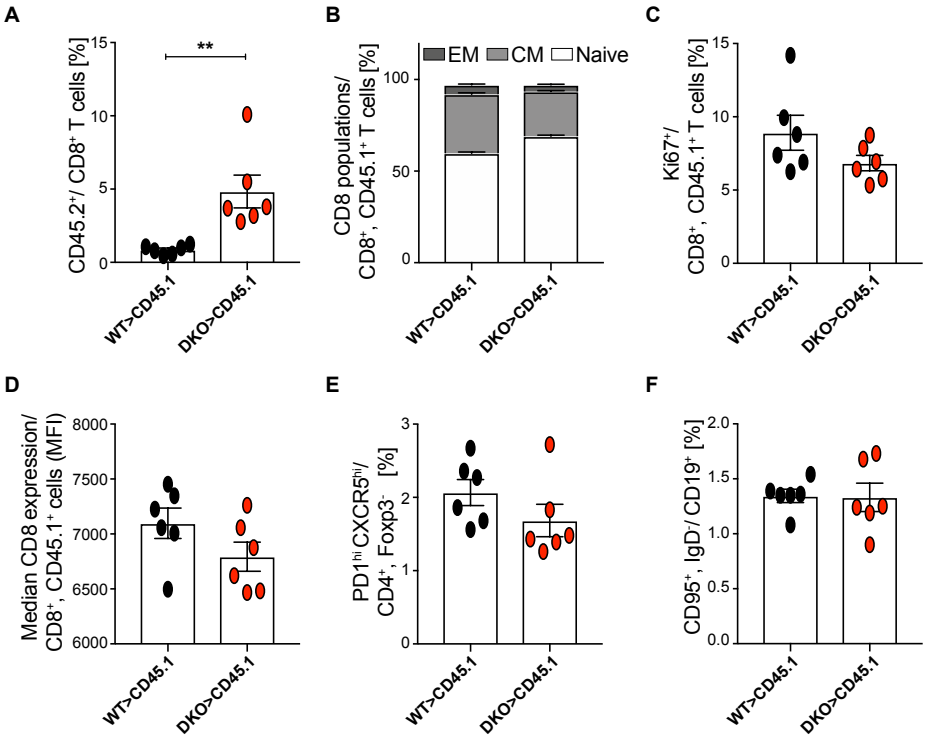

Fig. 19: DKO^T CD8$^+$ T cells do not induce the *trans*-effect.
(A) Persistence of injected CD8$^+$ T cells in WT hosts 8 days after transfer **(B)** Endogenous CD8$^+$ T cell populations, **(C)** proliferation and **(D)** surface CD8 expression 8 days after WT or DKO^T T cell transfer. **(E)** T_{FH} differentiation of endogenous CD4$^+$ T cells and **(F)** accumulation of GC B cells in response to WT or DKO^T T cell transfer. Quantifications of cell populations are shown. Data presented as Mean ± SEM. Statistical significance was determined by unpaired, one-tailed t-test. For each group 6 biological replicates were analyzed. ** p< 0.01.

Transferred Roquin-1/2 deficient CD8$^+$ T cells expanded within the WT host better that WT cells **(Fig. 19A).** However, contrary to Roquin-1/2 deficient CD4$^+$ T cells, transfer of Roquin-1/2 deficient CD8$^+$ T cells did not lead to an increased activation and proliferation of endogenous CD45.1$^+$ T cells **(Fig. 19B-D).** Accumulation of

endogenous T_{FH} or GC B cells could also not be observed after transfer of $CD8^+$ $iDKO^T$ cells **(Fig. 19E,F).**

Taken together, these data suggest that Roquin-1/2 deficient $CD4^+$ but not $CD8^+$ T cells, are able to produce one or several factors that can affect bystander T cells in *trans.* These factors caused activation and proliferation of bystander $CD8^+$ T cells, and induced differentiation of endogenous T_{FH} cells.

4.1.4 *Trans* effect does not occur secondary to increased cell death of DKO^T cells

Since activated DKO^T $CD4^+$ T cells nearly completely disappeared from the WT recipients, but the *trans* effect remained, we were wondering whether this effect could be explained by increased apoptosis of DKO^T cells due to strong activation (Kabelitz and Janssen, 1997). In other words, transferred DKO^T cells could undergo more programs of apoptosis or necrosis within the WT host and release intracellular molecules that trigger an immune response (Rock and Kono, 2008).

To answer this question, we took advantage of the inducible knock-out transfer system **(Fig. 17A)**, transferring total $CD3^+$ T cells and treating the recipient mice with tamoxifen to induce deletion. On day 8 after transfer, we assessed apoptosis of the transferred cells by Annexin V staining.

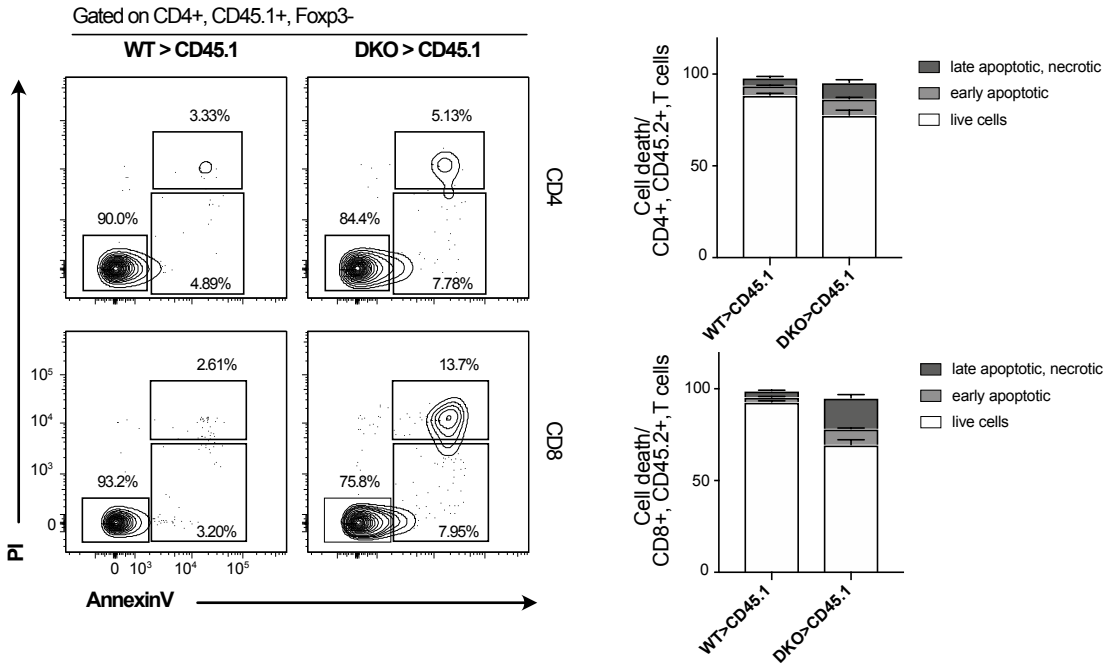

Fig. 20: Apoptosis of DKO^T T cells within WT recipients is comparable to WT T cells.
CD3$^+$ cells from WT;creERT2 or Roquin-1/2$^{fl/fl}$; creERT2 mice were isolated, injected into WT recipients and recipients were treated with tamoxifen gavage to induce deletion. On day 8 after transfer apoptosis of injected CD4$^+$ (upper panel) and CD8$^+$ (lower panel) T cells was assessed by annexin V staining. Representative plots and quantifications are shown. Data presented as Mean ± SEM. Statistical significance was determined by unpaired, one-tailed t-test. For each group 6 biological replicates were analyzed.

The majority of transferred WT cells was viable 8d after transfer. Both CD4$^+$ and CD8$^+$ Roquin-1/2-deficient T cells showed a slight increase in late apoptotic and necrotic cells after transfer as compared to mice that received WT donor cells. CD8$^+$ DKO^T cells were more prone to cell death than CD4$^+$ DKO^T cells **(Fig.20).**
Since cell death was increased more in CD8$^+$ DKO^T cells than in CD4$^+$ cells, which did not affect the endogenous immune system of the host, and the increase in dead or dying cells was negligible compared to WT donor cells, we concluded that the *trans*-acting factor is likely secreted by or expressed on viable CD4$^+$ DKO^T cells.

4.1.5 The t*rans*-effect is independent of IFNγ and IL-6 signalling

T_{FH} differentiation has been linked to excess IFNγ (Lee *et al.*, 2012) and IL-6 signaling is crucial for T_{FH} differentiation (Nurieva *et al.*, 2008). Moreover, IFNγ (Lee *et al.*, 2012; Pratama *et al.*, 2013) and IL-6 (Jeltsch *et al.*, 2014; Tan *et al.*, 2014) have been

proposed to be directly regulated by Roquin proteins, and DKO^T cells do produce higher levels of IFNγ, as determined by intracellular cytokine staining (Jeltsch *et al.*, 2014). We asked whether one of these cytokines may be responsible for the *trans*-effect.

To answer this question, we performed adoptive T cell transfers of *in vitro* activated DKO^T **(Fig. 17B)** into WT, IFNγR-/- and IL6Rα-/- mice. IFNγR-/- mice cannot respond to IFNγ but have an otherwise normal immune system with normal T helper cell responses (Huang et al., 1993). IL6Rα-/- mice have impaired IL-6 signaling (McFarland-Mancini et al., 2010) and a reduced ability for T_{FH} differentiation (Nish et al., 2014).

On day 8 after transfer recipient mice were assessed for reduced activation of endogenous $CD8^+$ T cells and/or reduced differentiation of endogenous T_{FH} cells in the knockout recipients as compared to the WT recipient mice. As reference untreated age-matched WT mice housed under identical conditions in the same animal facility were used **(Fig. 21).**

Transfer of DKO^T $CD4^+$ T cells into WT or knockout recipient mice caused a similar downregulation of surface CD8 on recipient $CD8^+$ T cells **(Fig. 21A,B),** as well as comparable expansion of the memory compartment and proliferation of endogenous $CD8^+$ T cells **(Fig. 21C-F).**

Results

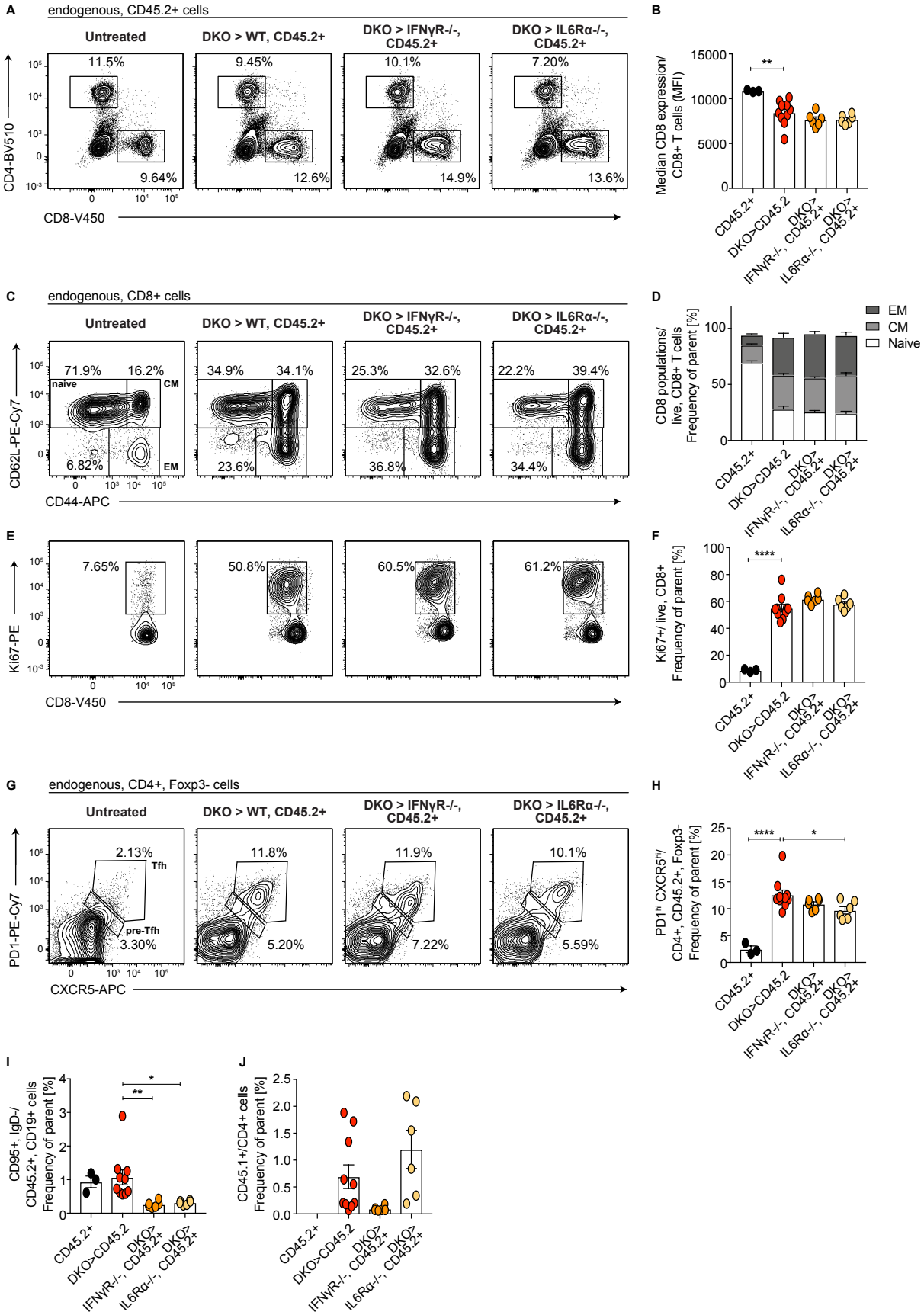
A
endogenous, CD45.2+ cells
Untreated
DKO > WT, CD45.2+
DKO > IFNγR-/-, CD45.2+
DKO > IL6Rα-/-, CD45.2+
11.5%
9.64%
9.45%
12.6%
10.1%
14.9%
7.20%
13.6%
CD4-BV510
CD8-V450
B
Median CD8 expression/ CD8+ T cells (MFI)
15000
10000
5000
0
**
CD45.2+
DKO>CD45.2
DKO> IFNγR-/-, CD45.2+
DKO> IL6Rα-/-, CD45.2+
C
endogenous, CD8+ cells
Untreated
DKO > WT, CD45.2+
DKO > IFNγR-/-, CD45.2+
DKO > IL6Rα-/-, CD45.2+
71.9%
16.2%
naive
CM
6.82%
EM
34.9%
34.1%
23.6%
25.3%
32.6%
36.8%
22.2%
39.4%
34.4%
CD62L-PE-Cy7
CD44-APC
D
CD8 populations/ live, CD8+ T cells Frequency of parent [%]
100
50
0
EM
CM
Naive
CD45.2+
DKO>CD45.2
DKO> IFNγR-/-, CD45.2+
DKO> IL6Rα-/-, CD45.2+
E
7.65%
50.8%
60.5%
61.2%
Ki67-PE
CD8-V450
F
Ki67+/ live, CD8+ Frequency of parent [%]
100
80
60
40
20
0
****
CD45.2+
DKO>CD45.2
DKO> IFNγR-/-, CD45.2+
DKO> IL6Rα-/-, CD45.2+
G
endogenous, CD4+, Foxp3- cells
Untreated
DKO > WT, CD45.2+
DKO > IFNγR-/-, CD45.2+
DKO > IL6Rα-/-, CD45.2+
2.13%
Tfh
pre-Tfh
3.30%
11.8%
5.20%
11.9%
7.22%
10.1%
5.59%
PD1-PE-Cy7
CXCR5-APC
H
PD1hi CXCR5hi/ CD4+, CD45.2+, Foxp3- Frequency of parent [%]
25
20
15
10
5
0
****
*
CD45.2+
DKO>CD45.2
DKO> IFNγR-/-, CD45.2+
DKO> IL6Rα-/-, CD45.2+
I
CD95+, IgD-/ CD45.2+, CD19+ cells Frequency of parent [%]
4
3
2
1
0
*
**
CD45.2+
DKO>CD45.2
DKO> IFNγR-/-, CD45.2+
DKO> IL6Rα-/-, CD45.2+
J
CD45.1+/CD4+ cells Frequency of parent [%]
2.5
2.0
1.5
1.0
0.5
0.0
CD45.2+
DKO>CD45.2
DKO> IFNγR-/-, CD45.2+
DKO> IL6Rα-/-, CD45.2+

Fig. 21: The t*rans*-effect is independent of IFNγ and IL-6 signaling.
DKO^T cells were adoptively transferred into IFNγR -/- and IL6Rα -/- recipient mice. Recipient mice were sacrificed 8d after transfer. **(A)** Representative plots and **(B)** quantifications of surface CD8 downregulation. **(C,D)** Memory compartments of endogenous $CD8^+$ T cells and **(E,F)** their proliferation. **(G,H)** Endogenous T_{FH} cell differentiation and **(I)** GC B cell formation in the recipient mice. **(J)** Persistence of injected $CD4^+$ T cells within the WT host. Data presented as Mean ± SEM. Statistical significance was determined by one-way ANOVA with Dunnett's post hoc test. WT mice injected with DKO^T cells were used as control group. * p<0.05, ** p<0.01, *** p<0.001, **** p<0.0001.

Furthermore, impaired IFNγ or IL-6 signaling in recipient mice did not have any effects on the DKO^T T cell induced differentiation of endogenous T_{FH} cells **(Fig. 21G,H**). Only in IL6Rα-/- recipient mice there was a slight decrease in T_{FH} cells compared to the DKO^T injected WT recipient group. However, the levels were still significantly higher than in age matched untreated WT mice **(Fig. 21G,H).** Interestingly, both IFNγR-/- and IL6Rα-/- recipient mice, produced less GC B cells in response to DKO^T T cells compared to the WT recipient group **(Fig. 21I).** Persistence of DKO^T T cells within the IFNγR-/- host but not in WT or IL6Rα-/- recipients was impaired **(Fig. 21J)**.
These data suggest, that the DKO^T T cell induced endogenous $CD8^+$ activation and T_{FH} differentiation of endogenous $CD4^+$ T cells within the recipient mice does not depend on functional IL-6 or IFNγ signaling in recipient cells. These findings suggested that DKO^T T cell produced IFNγ or IL-6 are not the *trans*-acting factors.

4.1.6 DKO^T T cell induced T_{FH} differentiation is independent of ICOS expression

ICOS is a co-stimulatory molecule that has been shown to be crucial for T_{FH} differentiation (Akiba *et al.*, 2005; Crotty, 2014) and in ICOS-/- mice T_{FH} differentiation is strongly impaired (Choi *et al.*, 2011; Nurieva *et al.*, 2008). Thus, we analyzed whether ICOS signaling was required for DKO^T T cell induced T_{FH} differentiation. To test this, $CD4^+$ T cells from WT or Roquin-$1/2^{fl/fl}$ mice were isolated, activated *in vitro* with anti-CD3/anti-CD28 under T_H1 conditions and deletion of Roquin proteins was induced by introducing a cre recombinase by retroviral transduction. Transduced WT and DKO^T T cells were cultured for 3-4 days and adoptively transferred into ICOS-/- hosts. Recipient mice sacrificed on d6, 7 and 8 after transfer and the endogenous T_{FH} cells were analyzed.

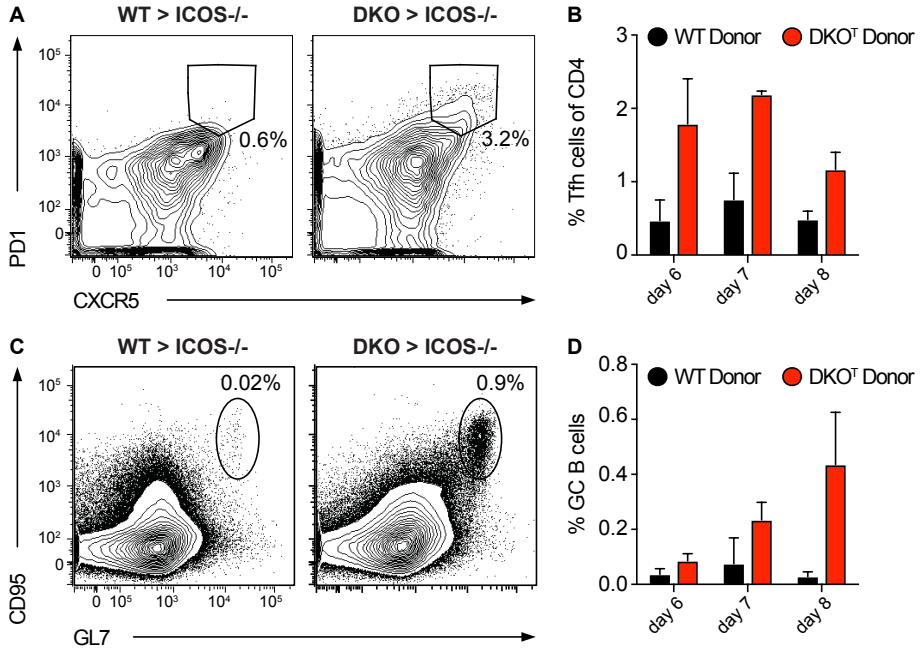

Fig. 22: DKO^T T cells induce T_{FH} differentiation in the absence of ICOS signaling.
Adoptive transfer of *in vitro* activated and deleted WT or DKO^T cells into ICOS-/- recipients. **(A)** Representative plots and **(B)** quantifications of endogenous T_{FH} cells analyzed on d6, d7 or d8 after transfer. **(C, D)** Plots and quantifications of recipient GC B cells on d6, d7 and d8 after transfer. Two biological replicates per day per group were analyzed. Data presented as Mean ± SEM. This experiment was performed by Dr. Stephanie Edelmann.

Interestingly, DKO^T cells were able to induce T_{FH} cell differentiation in ICOS-/- recipients **(Fig. 22A,B)**. Whereas, ICOS-/- mice that received WT T cells showed almost undetectable endogenous T_{FH} frequencies. Concomitant with the increase in endogenous T_{FH} cells also GC B cells appeared increased in ICOS-/- recipient mice **(Fig. 22C,D)**.

These data suggest, that the *trans*-acting factor produced by DKO^T CD4$^+$ T cells can induce T_{FH} differentiation and GC B cell formation independently of ICOS signaling.

4.1.7 Analyzing co-stimulatory signals as *trans*-factor that activates bystander cells

So far, I determined that only DKO^T CD4$^+$ T cells induce the *trans*-effect in WT bystander CD4$^+$, CD8$^+$ T cells and GC B cells. The effect did not correlate with increased apoptosis in the transferred T cells and was independent of ICOS, IL-6 or IFNγ signaling in the recipient T cells. We next tested whether the DKO^T T cell induced T_{FH} differentiation and bystander CD8$^+$ activation required CD28 co-stimulation, the

presence of B cells or SAP signaling in a series of adoptive transfer experiments into various knockout animals. In these recipients we asked whether or not DKO^T T cells induced endogenous $CD8^+$ T cell activation and proliferation **(Fig. 23)** and/or T_{FH} differentiation **(Fig. 24)**.

Specifically, we analyzed the *trans*-effect in µMT, CD80/86 KO and SapKO mice. µMT mice (Kitamura et al., 1991) lack mature B cells and therefore the ability to form cognate T cell-B cell interactions which are required for T_{FH} differentiation (Haynes *et al.*, 2007; Johnston *et al.*, 2009). SapKO mice (Czar et al., 2001) lack an intracellular adaptor molecule which binds SLAM family surface receptors. These mice have impaired T_{FH} development and function and cannot stably interact with B cells (Cannons et al., 2010; Kamperschroer et al., 2008; Linterman *et al.*, 2009b; Qi *et al.*, 2008). CD80/CD86 KO mice (Borriello et al., 1997) cannot provide co-stimulation to T cells and T cell proliferation is reduced in these mice (Grujic et al., 2010). Furthermore, since T cells in these mice do not receive signals via CD28 engagement, T_{FH} cell differentiation is impaired (Watanabe et al., 2017; Wing et al., 2014).

DKO^T cells induced $CD8^+$ T cell activation in SapKO and very strongly in CD80/CD86 KO recipients **(Fig. 23A,B)**. Endogenous $CD8^+$ in WT, SapKO and CD80/CD86 KO recipients proliferated in response to DKO^T cells. The strongest effects were observed in CD80/CD86 KO recipients **(Fig. 23C,D)**, suggesting the possibility that DKO^T cells may be able to provide a co-stimulatory signal that potently activates bystander T cells that lack CD28 stimulation. In µMT mice DKO^T cells did not affect endogenous $CD8^+$ T cells involving B cells as critical component of the *trans*-effect.

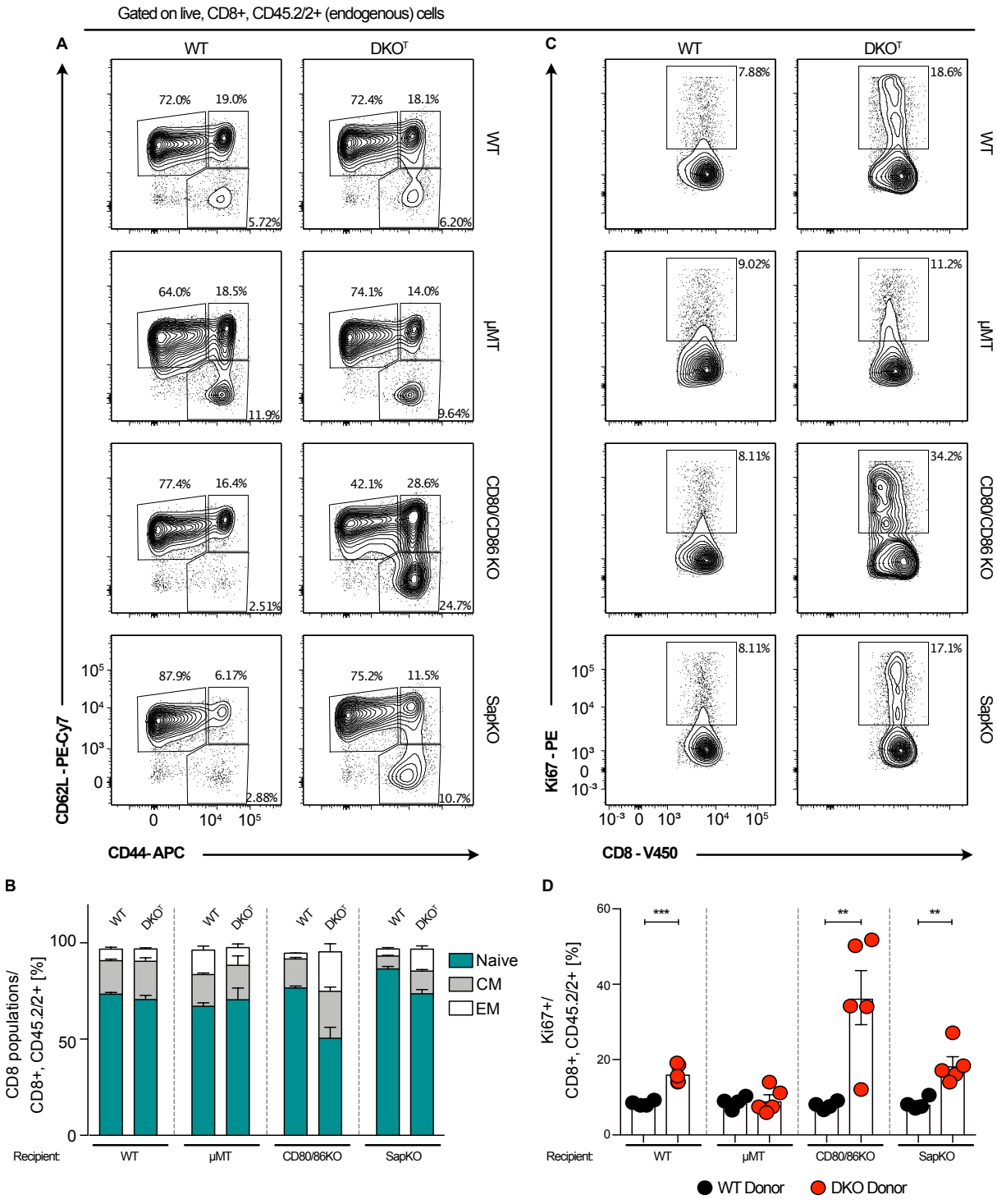

Fig. 23: DKO^T T cells induced *trans* – effect on bystander CD8$^+$ T cells in WT, µMT, CD80/CD86 KO and SapKO recipients.

WT or DKO^T cells were activated *in vitro* and transferred into different knockout recipients as indicated in the figure. **(A)** Representative plots showing endogenous CD8 T cell activation and **(B)** quantifications of naïve and memory populations. **(C)** Representative plots showing proliferation of endogenous CD8$^+$ T cells 8 days after WT or DKO^T T cell transfer and **(D)** quantifications of Ki67$^+$ endogenous CD8$^+$ T cells. Data presented as Mean ± SEM. Statistical significance was determined by unpaired, one-tailed t-test. ** p<0.01, *** p<0.001.

We next analyzed the ability of DKO^T T cells to induce T_{FH} differentiation and GC B cell accumulation in recipient mice. The levels of endogenous T_{FH} cells after DKO^T T cell transfer were comparable to those in WT T cells injected animals in µMT and CD80/CD86 KO recipients **(Fig. 24A,B)**. Interestingly, DKO^T T cells were able to induce T_{FH} differentiation but not GC B cell accumulation in SapKO recipient mice **(Fig. 24A-C)**. The effects were however weaker than the effects observed in WT recipients.

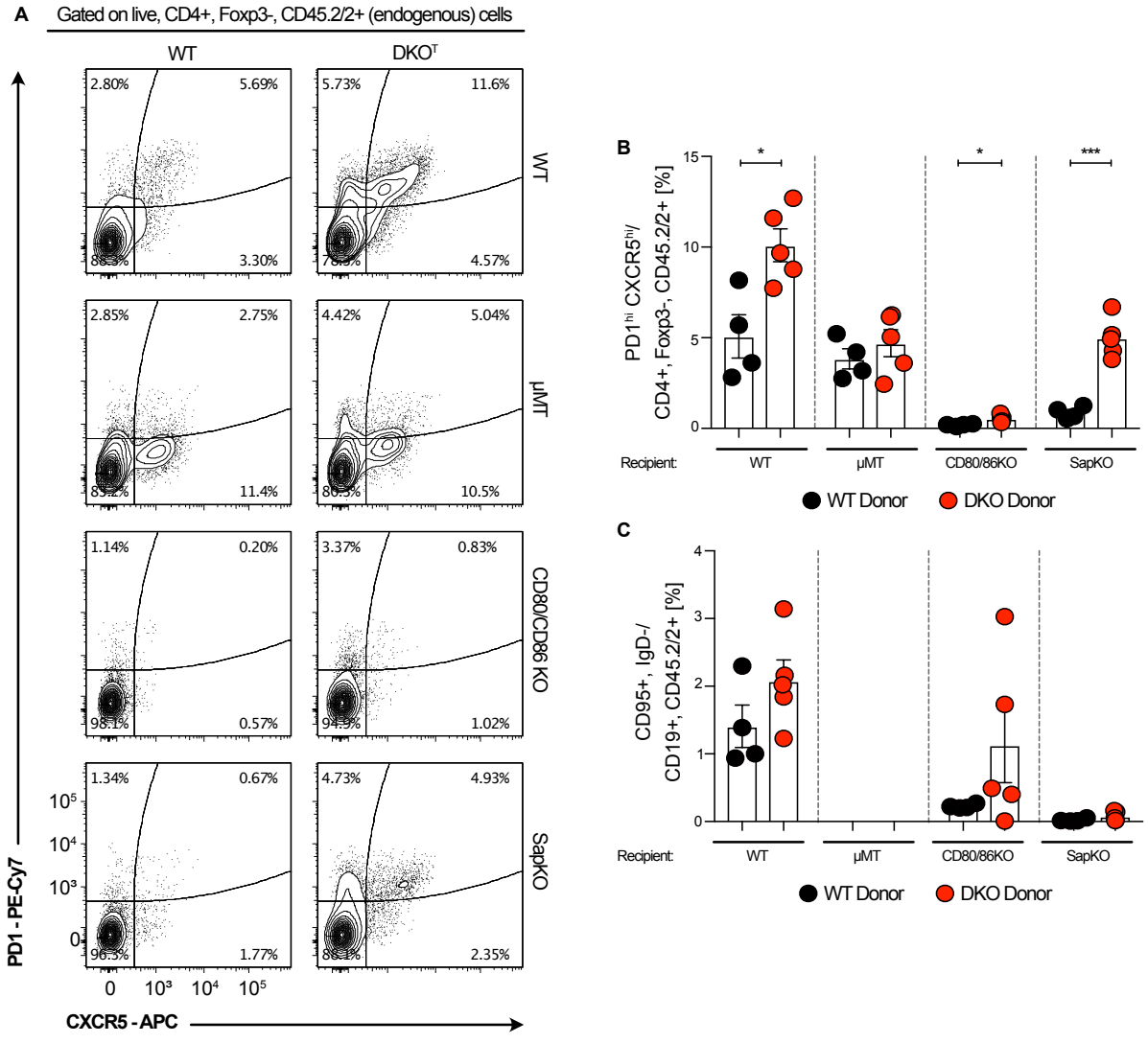

Fig.24: DKO^T T cells induced T_{FH} differentiation in WT, µMT, CD80/CD86 KO and SapKO recipients.

WT or DKO^T cells were activated *in vitro* and transferred into different knockout recipients as indicated in the figure. **(A)** Representative plots showing endogenous T_{FH} differentiation and **(B)** quantifications of T_{FH} cells 8 days after WT or DKO^T T cell transfer. **(C)** Quantifications of GC B cells 8 days after transfer. Data presented as Mean ± SEM. Statistical significance was determined by unpaired, one-tailed t-test. * $p<0.05$, *** $p<0.001$.

Taken together, these data suggest that DKO^{T} CD4^{+} T cells may express a factor that can provide co-stimulatory signal to bystander CD8^{+} T cells, leading to the observed increase in activation and proliferation. Furthermore, the *trans*–acting factor appears to be able to replace or bypass intracellular Sap signaling and thus lead to increased T_{FH} differentiation in WT CD4^{+} T cells. However, CD4^{+} T cell co-stimulation requires B cells potentially as endogenous APCs for T_{FH} differentiation, which cannot be circumvented by one or more factors produced by DKO^{T} CD4^{+} T cells.

4.1.8 CD4+ T cells from DKO mice express elevated levels of CD86 on their surface

To identify molecules that may be responsible for the observed *trans*-effect I analyzed a RNASeq data set that was previously acquired by Dr. Nina Kronbeck. For this, RNA from *in vitro* deleted, activated and expanded WT or DKO^{T} $T_{H}1$ cells was sequenced, and differentially expressed genes between the two genotypes were determined.

In total 174 genes were significantly upregulated and 35 were significantly downregulated in DKO^{T} $T_{H}1$ cells as compared to WT $T_{H}1$ cells. As cut-off values a log2fc$\geq$1 (i.e. at least a two-fold increase in expression) and p $\leq$0.05 were selected. To confirm that the cut-off criteria were appropriate, we checked whether we could detect known Roquin targets among the significantly upregulated genes. Indeed *Icos, Tnfrsf4, Ctla4* and *Zc3h12a* were all included in the gene list **(Fig. 25A).**

Since in part 4.1.4 we had determined that the *trans* effect is not caused by molecules released by dying DKO^{T} cells, we made an assumption that the *trans*-acting factor must either be expressed on the surface or secreted by DKO^{T} CD4^{+} T cells. We therefore identified all surface expressed and secreted molecules among the 174 significantly upregulated genes **(Fig. 25B)**, followed by a literature search to identify molecules that are known to induce CD8^{+} T cell activation and/or promote T_{FH} differentiation, and subsequent validation of interesting hits by qPCR. Since Roquin proteins function as repressors of mRNA expression, I did not analyze genes that were down-regulated in DKO^{T} cells any further.

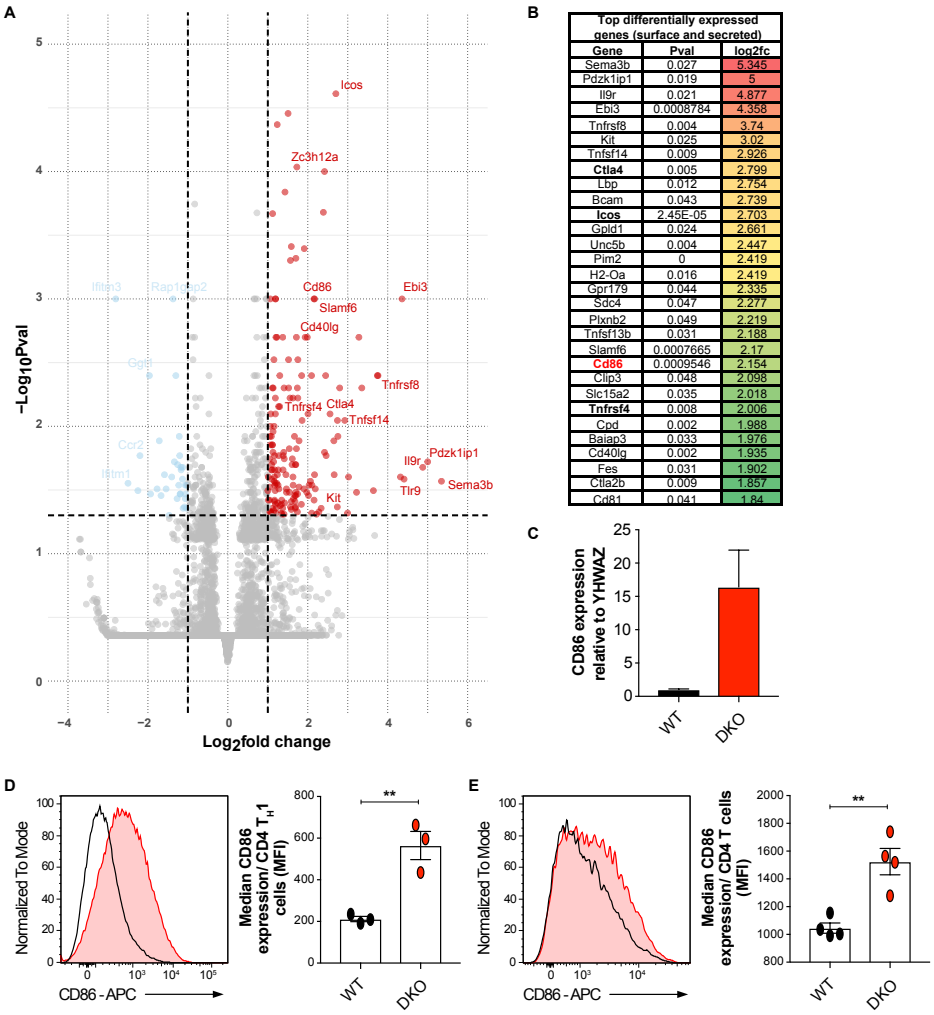

Top differentially expressed genes (surface and secreted)		
Gene	Pval	log2fc
Sema3b	0.027	5.345
Pdzk1ip1	0.019	5
Il9r	0.021	4.877
Ebi3	0.0008784	4.358
Tnfrsf8	0.004	3.74
Kit	0.025	3.02
Tnfsf14	0.009	2.926
Ctla4	0.005	2.799
Lbp	0.012	2.754
Bcam	0.043	2.739
Icos	2.45E-05	2.703
Gpld1	0.024	2.661
Unc5b	0.004	2.447
Pim2	0	2.419
H2-Oa	0.016	2.419
Gpr179	0.044	2.335
Sdc4	0.047	2.277
Plxnb2	0.049	2.219
Tnfsf13b	0.031	2.188
Slamf6	0.0007665	2.17
Cd86	0.0009546	2.154
Clip3	0.048	2.098
Slc15a2	0.035	2.018
Tnfrsf4	0.008	2.006
Cpd	0.002	1.988
Baiap3	0.033	1.976
Cd40lg	0.002	1.935
Fes	0.031	1.902
Ctla2b	0.009	1.857
Cd81	0.041	1.84

Fig. 25: DKO^{T} T$_{H}$1 cells express CD86.

(A) Differentially expressed genes in WT and DKO^{T} T$_{H}$1 cells. **(B)** Significantly upregulated surface expressed or secreted molecules in DKO^{T} T cells. Cut-off values were log2fc≥1 and p ≤0.05. **(C)** qPCR analysis of CD86 expression in DKO^{T} T$_{H}$1 cells. **(D)** WT and DKO^{T} CD4^{+} T cells were *in vitro* differentiated towards T$_{H}$1, expanded in IL-2 medium for 2d and surface CD86 expression was determined by flow cytometry. **(E)** Surface CD86 expression on WT and DKO^{T} CD4^{+} T cells *ex vivo.* Data are representative for at least 3 biological replicates. Data presented as Mean ± SEM. Statistical significance was determined by unpaired, one-tailed t-test. ** p<0.01.

The co-stimulatory molecule, CD86, which is normally expressed on APCs appeared to be a very interesting candidate for the *trans* acting factor. Its transcript level was ~15 fold increased in DKO^{T} T$_{H}$1 cells compared to WT T$_{H}$1 cells **(Fig.25 C)**, and it was strongly upregulated on protein level in both, *in vitro* activated DKO^{T} T$_{H}$1 and *ex vivo* isolated total DKO^{T} CD4^{+} T cells **(Fig.25 D,E)** but not on WT CD4^{+} T cells.

CD40L was also upregulated in the RNAseq data set **(Fig.25 A,B)** and if overexpressed on DKO^{T} cells would explain the *trans*-effect. However, when we checked for CD40L expression by qPCR as well as on protein level in *ex vivo* isolated cells, there were no differences between WT and DKO^{T} T cells **(Fig.26 A,B).**

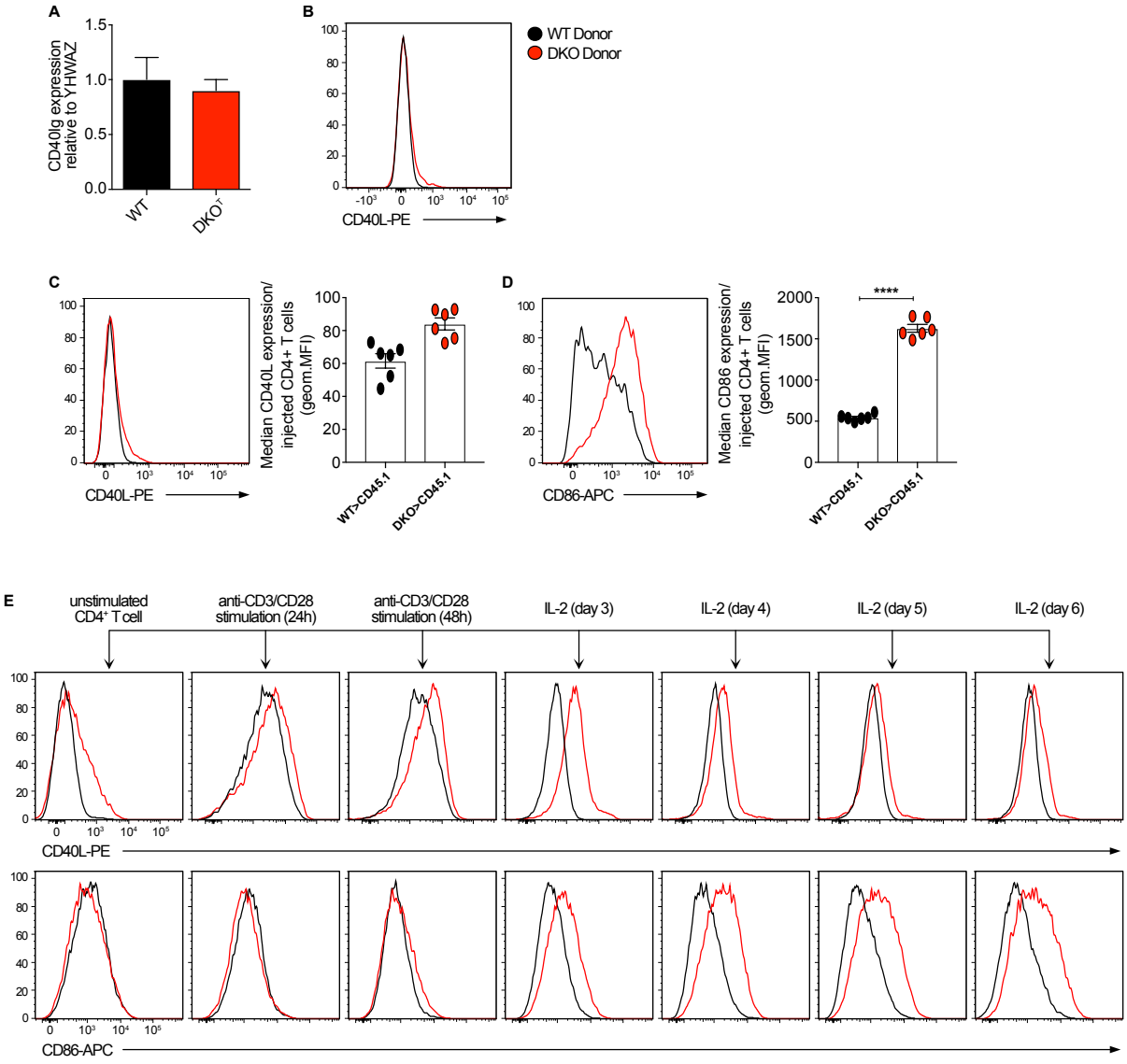

Fig. 26: CD86 but not CD40L is continuously elevated on DKO^{T} cells.

(A) qPCR analysis of CD40L levels in WT and DKO^{T} T_H1 cells. **(B)** *Ex vivo* CD40L expression on CD4^{+} T cells taken from WT and DKO^{T} mice. **(C)** CD40L and **(D)** CD86 expression on donor T cells isolated from WT recipients 8 days after adoptive transfer. **(E)** Kinetics of CD40L and CD86 expression on WT and DKO^{T} T cells on *in vitro* stimulated CD4^{+} T cells. IL-2 (day 4) is equivalent to donor T cells that are used for adoptive transfer experiments. Data are representative for at least 3 biological replicates. Data presented as Mean ± SEM. Statistical significance was determined by unpaired, one-tailed t-test. ** p<0.01, **** p<0.0001.

Furthermore, when analyzing donor WT and DKO^{T} CD4^{+} T cells 8 days after adoptive transfer, we could only detect elevated CD86 expression but not CD40L expression **(Fig. 26C,D)**. CD40L was elevated on DKO^{T} CD4^{+} T cells shortly after *in vitro* T cell activation, but from day 4 after stimulation, which is also the day that was used as day 0 for adoptive transfer experiments, CD40L levels returned to similar levels as in WT cells. CD86 expression on the other hand was continuously elevated on activated DKO^{T} cells **(Fig.26 E)**, further supporting the hypothesis that CD86 may be (one of) the *trans*-acting factor(s).

Since CD86 is upregulated on DKO^{T} cells and co-stimulation is necessary for both, efficient T cell activation as well as T_{FH} differentiation, we were wondering whether CD86 may be the *trans*-acting factor that can, at least in parts explain the observed effect.

We hypothesized, that if CD86 is indeed the *trans*-acting factor, overexpression of CD86 in WT T cells would reproduce the effects observed in recipients after DKO^{T} T cell transfer. Overexpression of CD86 in DKO^{T} T cells would enhance the effect. To test this hypothesis, I cloned the CD86 coding sequence into a KMV-IRES-GFP vector and retrovirally transduced WT and DKO^{T} $T_{H}1$ cells prior to adoptive transfer. To confirm successful transduction, I checked for GFP expression by flow cytometry. WT, DKO^{T}, WT+CD86 and DKO^{T}+CD86 T cells were transferred into WT recipients and endogenous CD8^{+} T cells and T_{FH} cells were analyzed on d8 after transfer.

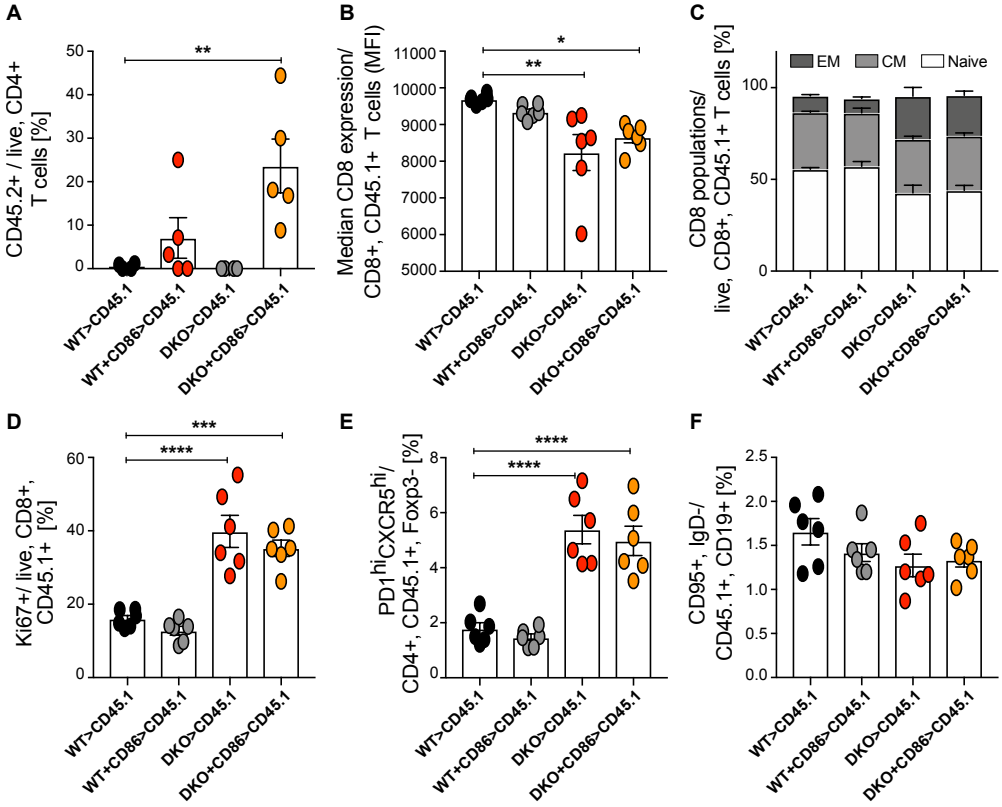

Fig. 27: CD86 overexpression on WT cells does not cause a *trans*-effect.

WT, DKO^{T}, WT+CD86 overexpression and DKO^{T}+CD86 overexpression were transferred into WT recipients. Splenocytes were analyzed 8 days after transfer. **(A)** Persistence of injected cells within the WT recipient. **(B)** Down-regulation of surface CD8 on endogenous CD8^{+} T cells. **(C)** Endogenous CD8^{+} memory populations. **(D)** Proliferation of endogenous CD8^{+} T cells. **(E)** T_{FH} differentiation of endogenous CD4^{+} T cells and **(F)** GC B cells in WT recipients. Data are representative for 6 biological replicates per group. Data presented as Mean ± SEM. Statistical significance was determined by one way ANOVA with Dunnett's post hoc test. * p<0.05, ** p<0.01, *** p<0.001, **** p<0.0001.

CD86 overexpression on both WT and DKO^{T} cells improved their persistence within the recipient mice **(Fig. 27A)**. However, we could not observe increased endogenous CD8^{+} T cell activation **(Fig. 27B,C)** or proliferation **(Fig. 27D)** in mice that received WT cells overexpressing CD86. CD86 over-expression on WT cells did furthermore not lead to an increased T_{FH} differentiation **(Fig. 27E)**. The *trans* effect was also not exacerbated when DKO^{T} cells overexpressing CD86 were transferred as compared to normal DKO^{T} cells **(Fig. 27B-E)**. There were no effects on GC B cells in any of the groups **(Fig. 27F)**.

Taken together these data suggest that even though CD86 may be a *trans*-acting factor which is responsible for the effects observed for bystander CD8^{+} T cells, it is not likely to lead to the increased T_{FH} cell differentiation in WT recipients. Furthermore, CD86 by itself is not sufficient to induce or exacerbate the DKO^{T} cell induced *trans*-

effect, meaning that there must be additional factors causing the observed changes in the host immune cell compartment.

In summary, I showed that Roquin proteins control T cell activation and differentiation in a T cell intrinsic as well as T cell extrinsic manner. When adoptively transferred into WT recipients Roquin-1/2-deficient T cells robustly induced bystander T cell activation and led to a differentiation of recipient $CD4^+$ T cell into the T_{FH} subset. DKO^T cell induced T_{FH} cell differentiation did not require IFNg, IL-6 or ICOS signaling in recipient cells. It was independent of co-stimulation or SAP signaling but did require interactions with B cells. Furthermore, DKO^T cells could provide co-stimulatory signals that potently activated bystander T cells which lack CD28 stimulation. Several molecules that could be responsible for the observed *trans*-effect were identified in an mRNASeq experiment and two promising candidates, CD86 and CD40L were validated. Overexpression of CD86 on WT or DKO^T cells did not induce or exacerbate the *trans*-effect in WT recipient mice. CD40L was excluded as potential *trans*-acting factor, since CD40L expression on WT and DKO^T cells only differed immediately following *in vitro* T cell activation. Expression levels were similar from d4 of *in vitro* culture which reflects the conditions used for the adoptive transfer experiments.
Even though, in addition to CD86, several other promising candidates for the *trans*-acting factor were detected in the mRNASeq data, we were not able to pursue the search for the *trans*-acting factor beyond this point. Experimentally addressing all potential candidates would have required a significantly higher amount of time and more sophisticated genetic and experimental systems. To date there is no robust *in vitro* T_{FH} differentiation assay, meaning that all validation steps need to be carried out *in vivo*, which puts additional time and legal constraints on this type of validation.

4.2 Roquin-1/2-deficient T cells induce early preneoplastic changes in the exocrine pancreas

As described in the first part of this work, Roquin-1/2-deficient T cells can strongly affect other immune cells in *trans*, causing strong T cell activation, inappropriate T_{FH} differentiation as well as accumulation of GC B cells. We have furthermore observed pathological changes in the lung including the thickening of arterial walls and spontaneous development of gastritis in mice harboring a T cell-specific knock-out of Roquin proteins. Furthermore, these mice produce pancreas-antigen recognizing autoantibodies (Jeltsch *et al.*, 2014), suggesting that Roquin-deficient T cells may also produce factors that affect non-immune cells in *trans*. Therefore, the focus of the second part of this work will be on the role of DKO^T T cells and Roquin-mediated regulation of mRNAs in the development of pancreas pathology.

4.2.1 DKO^T mice develop pancreas pathology and immune cell infiltration

To assess whether DKO^T mice develop any kind of pancreas pathology we collected pancreata from WT and DKO^T mice at various ages, fixed and analyzed them by histology. All histological stainings described in this work were performed in collaboration with AG Heikenwälder from the DKFZ in Heidelberg.

Mice with conditional ablation of Roquin proteins in T cells (DKO^T) but not WT mice spontaneously developed pancreas pathology. The incidence of DKO^T mice exhibiting pancreas pathologies was highest in 20-weeks-old animals, with 50% of the analyzed animals showing pathological changes **(Fig. 28).**

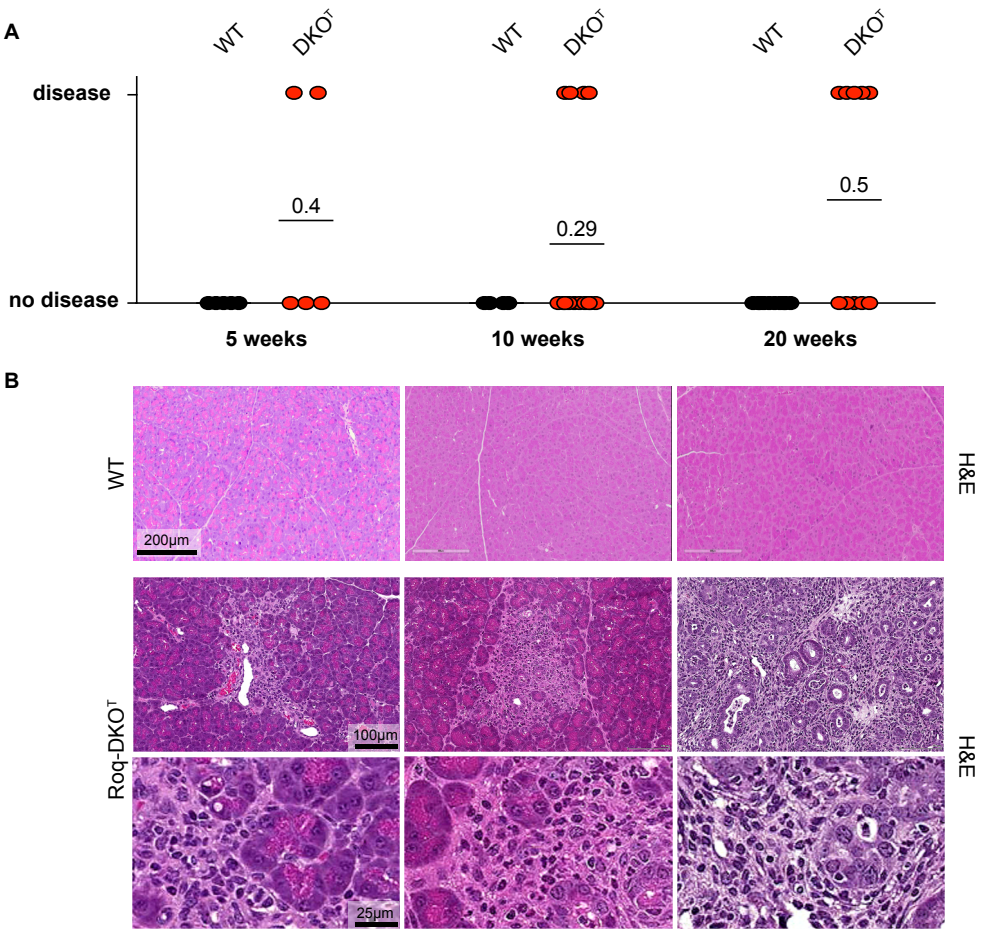

Fig. 28: Mice with Roquin-1/2 deficiency in T cells spontaneously develop pancreas pathology. **(A)** Quantification of the incidence of pathological changes in pancreata of WT and DKO^{T} mice at various ages. Mean incidence in each age group is indicated where applicable. **(B)** Exemplary H&E pancreas sections from WT (upper row) and DKO^{T} mice at different ages showing pathological changes at a low (middle row) and high (lower row) magnification. Samples were collected by Dr. Desheng Hu (AG Heissmeyer), staining and analysis of the sections were performed by Dr. Jessica Zoeller (AG Heikenwälder).

In an earlier publication our group has shown that the overactive T cell compartment in DKO^{T} cells caused lung inflammation in these mice (Jeltsch *et al.*, 2014). We were wondering whether this could also be true for the spontaneous development of pancreas pathology. Therefore, we looked for immune cell infiltrations in pancreas draining lymph nodes (panLN) and in pancreas tissue.

When comparing T cell compartments in the panLN, there were no differences between the frequencies of CD4^{+} and CD8^{+} T cell, whereas in the spleen there was a strong reduction of CD4^{+} and a marked increase of CD8^{+} T cells **(Fig. 29A-C).**

However, similar to what is known for splenic T cells, the majority of T cells in the panLN were activated effector memory (EM) T cells **(Fig. 29D,E)**.

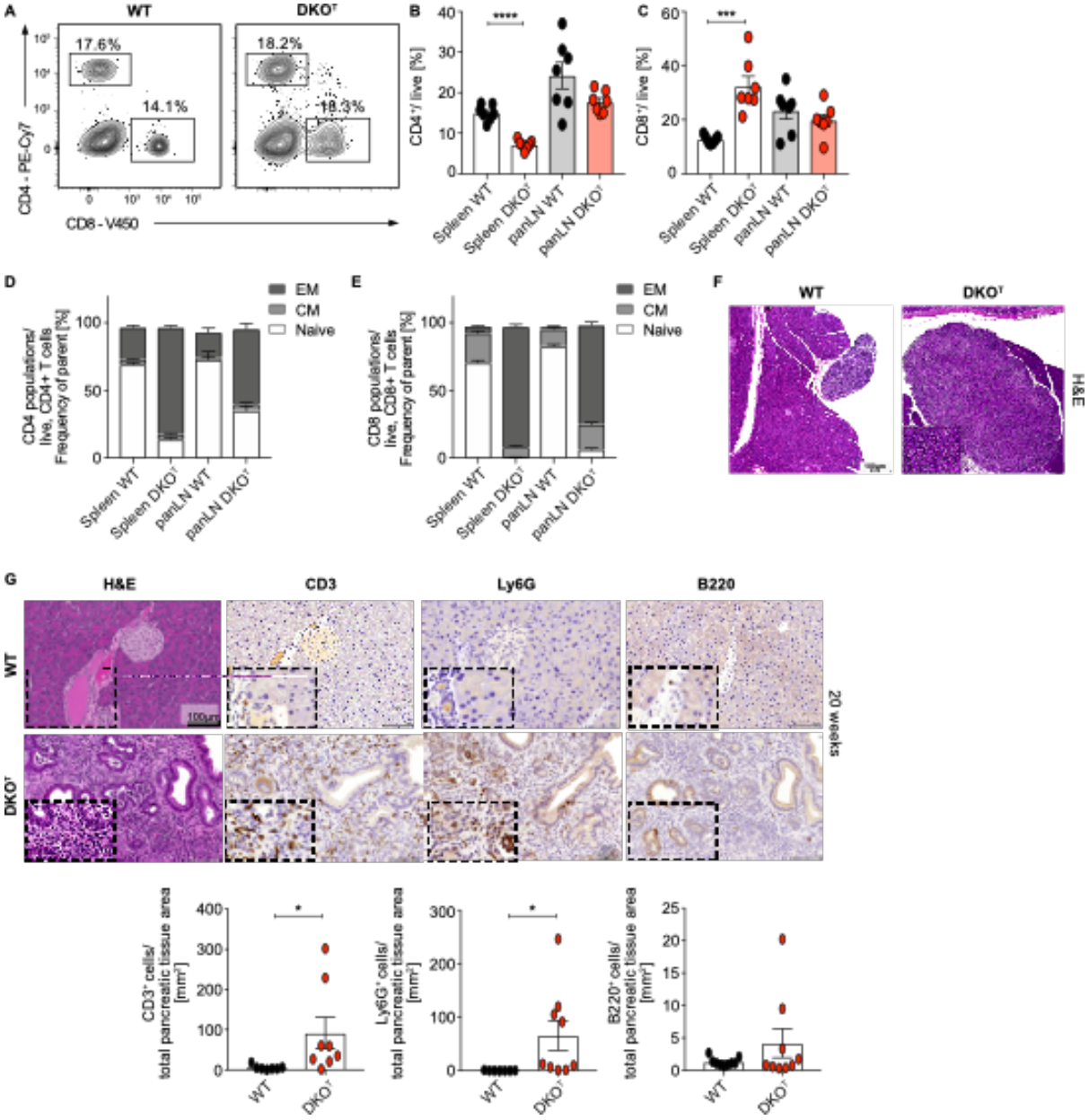

Fig. 29: Pancreas pathology is characterized by strong immune cell infiltration into pancreas draining lymph nodes and tissue

(A) Representative plots of CD4$^+$ and CD8$^+$ T cell populations in WT and DKO^T pancreas draining lymph nodes (panLN). **(B, C)** Quantifications of total CD4$^+$ and CD8$^+$ T cells in spleens and panLN. **(D, E)** Quantification of memory CD4$^+$ and CD8$^+$ T cell compartments. **(F)** Representative H&E image of panLN in WT and DKO^T mice. **(G)** Immunohistology of pancreas sections showing infiltrating CD3$^+$, Ly6G$^+$ and B220$^+$ cells and quantifications thereof. Data presented as Mean ± SEM. Statistical significance was determined by unpaired, one-tailed t-test. Histological stainings and quantifications of pancreas sections were performed by Dr. Jessica Zoeller.

The panLN were strongly enlarged in DKO^T mice, pointing towards an accumulation of inflammatory cells in the pancreas microenvironment **(Fig. 29F)**. Furthermore, there was a strong infiltration of $CD3^+$ and $Ly6G^+$ cells into the pancreas tissue of DKO^T mice **(Fig. 29G)**.

Concomitant with the observed infiltration of $Ly6G^+$ cells into the tissue, there was also an increase in $CD11b^+$ $Ly6G^+$ cells in the spleen and panLN of DKO^T mice **(Fig. 30A, B).** Since $CD11b^+$ $Ly6G^+$ cells are a very heterogeneous population consisting of both, inflammatory and suppressive cells (Bronte et al., 2016), this population was analyzed in more detail. First, we determined that the $CD11b^+$ $Ly6G^+$ population in DKO^T mice predominantly consisted of $Ly6C^{int}$ neutrophils **(Fig. 30C)**.

To assess whether these cells had suppressive functions that could affect T cells, co-cultures were performed. For this $CD11b^+$ $Ly6G^+$ cells from WT or DKO^T mice were isolated and mixed with CTV labelled $CD8^+$ T cells at different ratios. Co-cultures were then mixed with anti-CD3 and anti-CD28 antibodies and seeded onto rabbit-anti-hamster coated plates to achieve optimal stimulation of the T cells. 72h after activation $CD8^+$ T cell proliferation was assessed by CTV-dilution **(Fig. 30D)**.

WT $CD8^+$ T cells proliferated equally independent how many $CD11b^+$ $Gr1^+$ cells were present in the co-cultures. Interestingly, proliferation of $CD8^+$ T cells appeared to be slightly increased when they were co-cultured with DKO^T $CD11b^+$ $Gr1^+$ cells at a 1:1 ratio as compared to $CD8^+$ T cell proliferation without addition of $CD11b^+$ $Gr1^+$ cells or WT $CD11b^+$ $Gr1^+$ **(Fig. 30D)**, suggesting that these cells did not have suppressive functions.

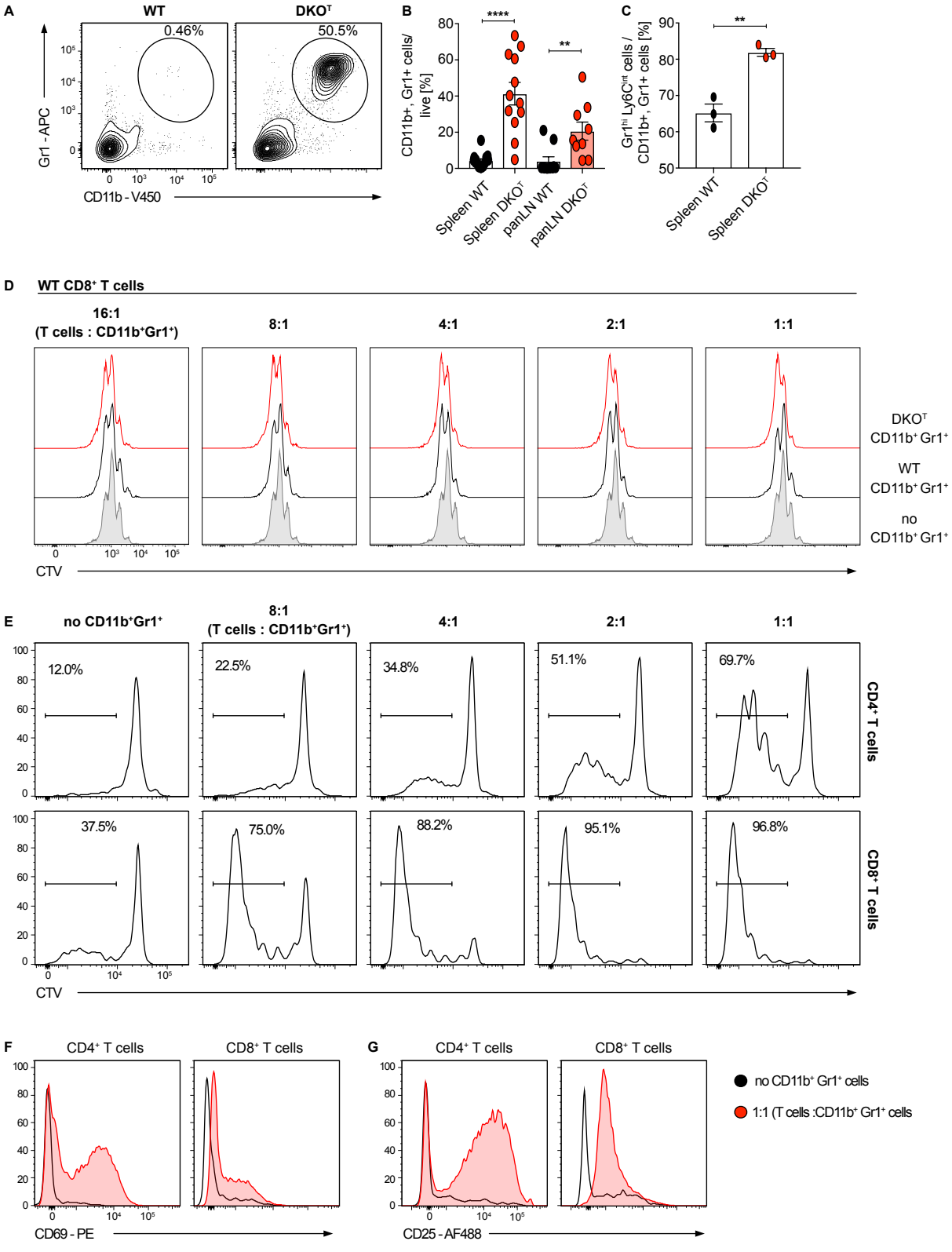

Fig. 30: Proinflammatory neutrophils infiltrate into the pancreata of DKO^T mice.

(A) Representative plots showing CD11b$^+$ Gr1$^+$ populations in the pancreas draining lymph nodes and **(B)** quantification of CD11b$^+$ Gr1$^+$ cell populations in spleens and pancreas draining lymph nodes of WT and DKO^T mice. **(C)** Quantification of the neutrophil population within splenic CD11b$^+$ Gr1$^+$ cells. **(D)** Representative plots of CTV dilution assays after co-culture with CD11b$^+$ Gr1$^+$ cells isolated from WT

or DKO^{T} mice and cultured under optimal stimulation conditions for 72h. **(E)** Representative plots of CTV dilution assays after co-culture of WT CD4^{+} and CD8^{+} T cells with splenic CD11b^{+} Gr1^{+} cells isolated from DKO^{T} mice and cultured under suboptimal stimulation conditions. Expression of **(F)** CD69 and **(G)** CD25 on the T cell surface after co-culturing them with DKO^{T} CD11b^{+} Gr1^{+} cells. All data presented as Mean ± SEM. At least 3 biological replicates were analyzed per group. Statistical significance was determined by unpaired, one-tailed t-test.

To formally test whether these CD11b^{+} Gr1^{+} cells promote T cell activation, we repeated the co-culture experiment with suboptimal stimulation conditions. CD11b^{+} Ly6G^{+} cells from DKO^{T} mice were isolated and mixed with CTV labelled CD4^{+} or CD8^{+} T cells at different ratios. Co-cultures were then mixed with soluble anti-CD3 and anti-CD28 antibodies and CTV dilution as well as the expression of activation markers were assessed 72h later. Both, CD4^{+} and CD8^{+} T cells showed increased proliferation in response to co-culturing with CD11b^{+} Ly6G^{+} cells in a dose dependent manner **(Fig. 30E).** There was also an increased expression of the activation markers CD69 and CD25 following co-culture **(Fig. 30F,G)**, suggesting that these cells rather exert activation of T cells instead of suppressive functions.

Taken together these data suggest, that pancreas pathology in DKO^{T} mice is characterized by strong infiltration of T cells and the systemic induction of pro-inflammatory neutrophils.

4.2.2 T_{FH} and T_H17 cells are the predominant T cells population in the pancreas microenvironment

CD3^{+} T cells were one of the two strongly expanded immune cell compartments in the panLN as well as pancreas tissue. Since DKO^{T} mice exhibit spontaneous activated T cells, a systemic skewing towards T_{FH} and T_H17 cells, and these cells are likely to cause lung inflammation in these mice (Jeltsch *et al.*, 2014; Vogel *et al.*, 2013), the CD4^{+} T cell compartment was analyzed in more detail.

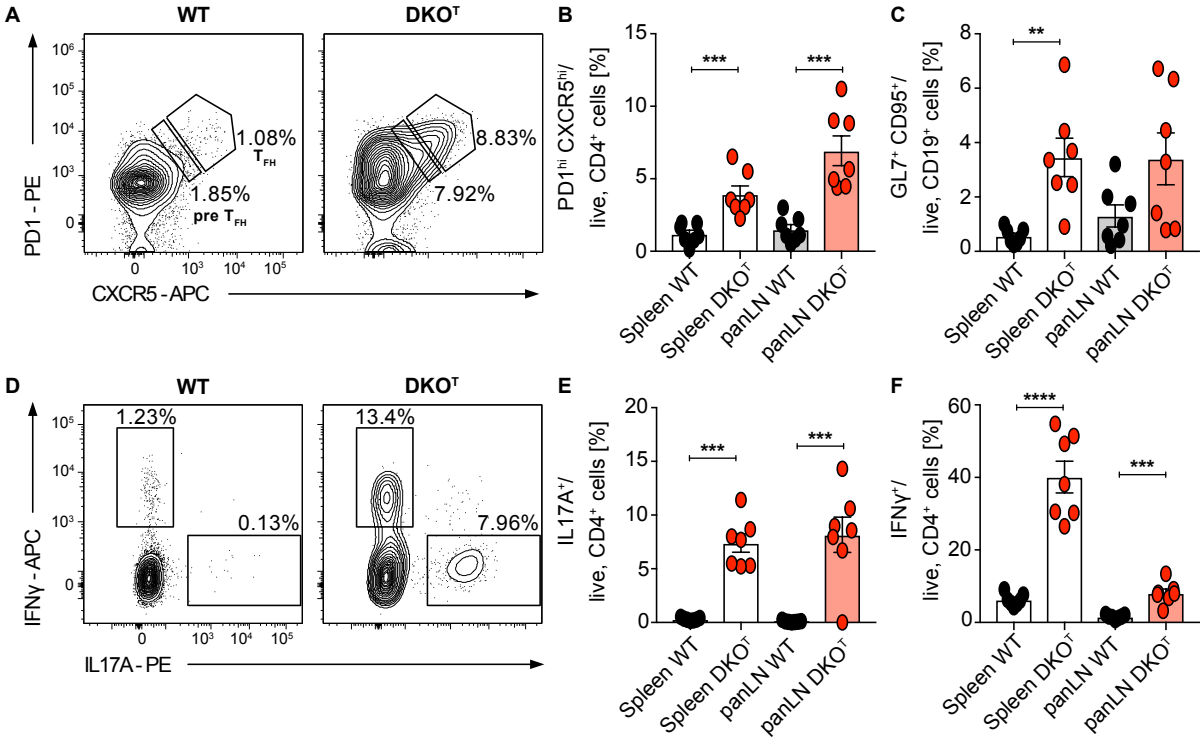

Fig. 31: T_{FH} and T_H17 cells accumulate in the pancreas draining lymph nodes in DKO^T mice. Representative plots showing **(A)** the T_{FH} cell population in panLN. Quantification of **(B)** T_{FH} cells and **(C)** GC B cells in spleens and panLN of WT and DKO^T mice. Representative plots showing **(D)** the T_H17 cell population in panLN. Quantification of **(E)** IL-17A producing cells and **(F)** IFNγ producing cells in spleens and panLN of WT and DKO^T mice. All data presented as Mean ± SEM. At least 7 biological replicates were analyzed per group. Statistical significance was determined by unpaired, one-tailed t-test. ** p< 0.01, *** p<0.001, **** p <0.0001. panLN: pancreas draining lymph nodes.

There was an accumulation of T_{FH} cells in the pancreas draining lymph nodes in DKO^T mice, concomitant with an increase in GC B cells **(Fig. 31A-C)**. Furthermore, there was a strong increase in IL-17A producing T_H17 cells and a slight increase in IFNγ producing T_H1 cells **(Fig. 31D-F).** The increase of IFNγ producing $CD4^+$ T cells in panLN, although significant, was small compared to the systemic frequencies of IFNγ producing $CD4^+$ T cells in DKO^T mice.

We next assessed whether gene expression of T_{FH} and T_H17 cells can be detected in pancreas tissue. We analyzed RNA isolated from pancreas tissue or from the draining lymph nodes for markers associated with these two T cell subsets.

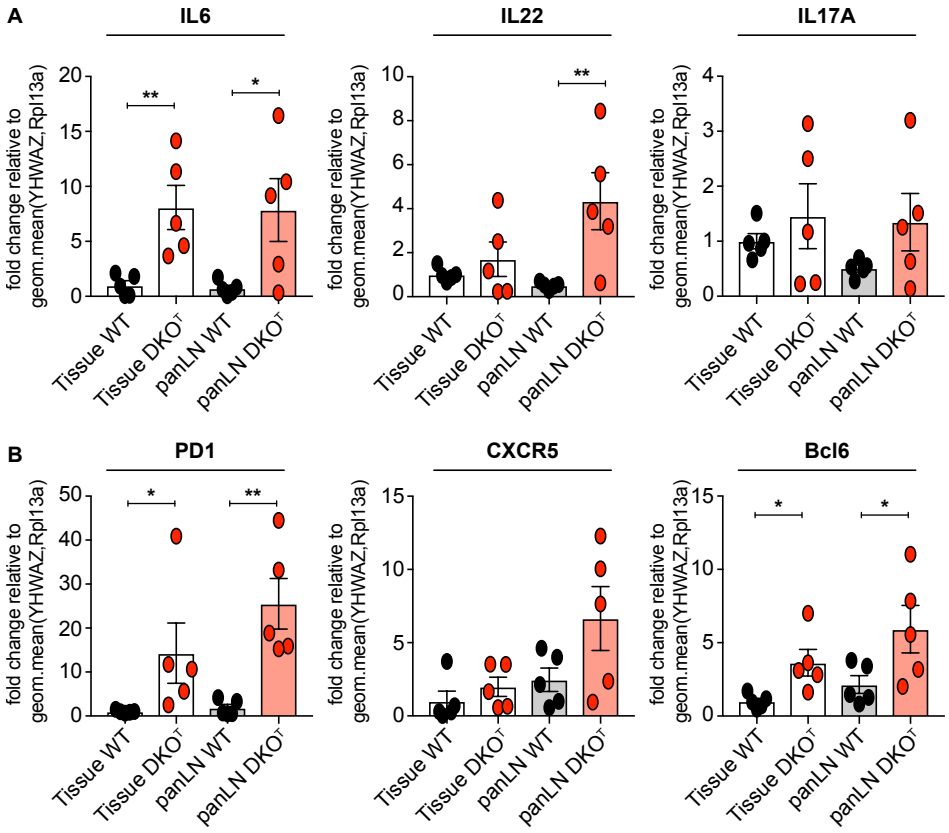

Fig. 32: T_{FH} and T_H17 associated markers are present in pancreas tissue.
qPCR analysis of markers associated with **(A)** T_H17 and **(B)** T_{FH} cells in pancreas tissue compared to panLNs in WT and DKO^T mice. All data presented as Mean fold change ± SEM normalized to the geometric mean Cp value of YHWAZ and Rpl13a. At least 4 biological replicates were analyzed per group. Statistical significance was determined by unpaired, one-tailed t-test. * $p<0.05$, ** $p< 0.01$. panLN: pancreas draining lymph nodes.

Transcripts characteristic for both, T_H17 and T_{FH} cells were increased in panLN as well as in the tissue **(Fig. 32A,B).** Interestingly, *Il6* and *Il22* transcripts were also elevated **(Fig. 32A),** two proinflammatory cytokines that are linked to T_H17 cells and have been closely associated with tumor development and progression (Lesina et al., 2011; Perusina Lanfranca et al., 2020).

Taken together these data point towards a potential role of T_H17 or T_{FH} cells in the development of pancreas pathology in the DKO^T mouse model.

4.2.3 Pancreatitis leads to the development of pre-neoplastic lesions the in pancreata of DKO^T mice

The strong immune cell infiltration into pancreas tissue and draining lymph nodes point towards an inflammatory reaction in the pancreas of DKO^T mice. To confirm this and to assess whether the chronic inflammation in the DKO^T mouse model leads to a deregulated proliferation and increased apoptosis, we performed immunohistological staining of pancreas sections taken from 20-weeks-old DKO^T mice.

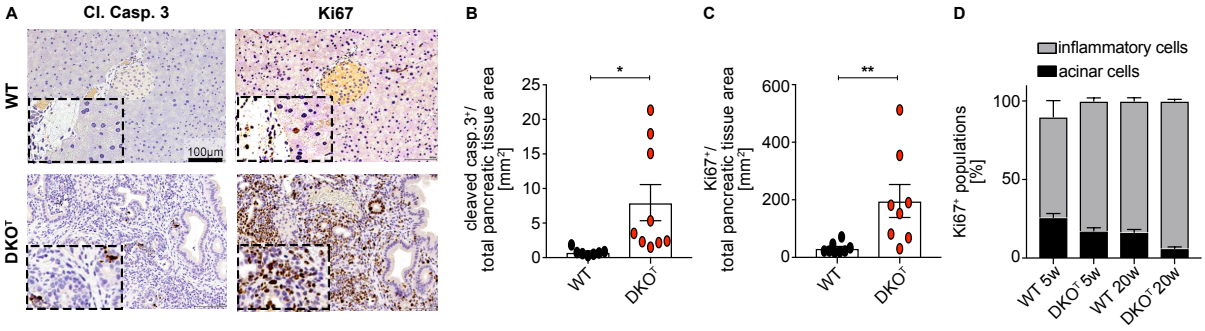

Fig. 33: DKO^T cells suffer from pancreatitis.

(A) Representative immunohistology sections with cleaved caspase 3 and Ki67 staining in WT and DKO^T mice. Quantification of **(B)** cleaved caspase 3$^+$ and **(C)** Ki67$^+$ cells normalized to total pancreatic tissue area. **(C)** Proportion of Ki67$^+$ acinar and inflammatory cells in 6- and 20-weeks-old WT and DKO^T mice. Samples were collected by Dr. Desheng Hu, stainings and quantifications were performed by Drs. Jessica Zoeller and Gaia Bianco. All data presented as Mean ± SEM. Statistical significance was determined by unpaired, one-tailed t-test. * $p<0.05$, ** $p<0.01$.

DKO^T mice had an elevated number of cleaved caspase 3$^+$, i.e. apoptotic cells as well as an increased number of Ki67$^+$, i.e. proliferating cells in pancreas tissue **(Fig. 33A-C).** The majority of proliferating cells were infiltrating immune cells **(Fig. 33D)**, suggesting that DKO^T mice do indeed suffer from pancreatitis (Bhatia, 2004; Pergolini et al., 2019; Scholzen and Gerdes, 2000).

Since DKO^T mice show strong signs of pancreatitis and chronic pancreatitis is a major risk factor for the development of pancreatic cancer (Kirkegård et al., 2017). We therefore examined whether the pathological changes observed in the pancreata of DKO^T mice exhibit signs of neoplasia. To test this hypothesis, pancreas sections were stained for Claudin 18 and alcian blue. Claudin 18 is a tight-junction protein which is normally expressed in the stomach and lung, and whose function it is to maintain

epithelial cell polarity (Tsukita and Furuse, 2000). It is also expressed in pancreatic cancer cells and can be used as an early marker to identify neoplastic lesions (Karanjawala et al., 2008; Tanaka et al., 2011). Alcian blue is used for the detection of acidic mucins, that are typically contained within PanIN lesions derived from acinar cells (Johnson et al., 2019; Kopp *et al.*, 2012; Lee et al., 2019).

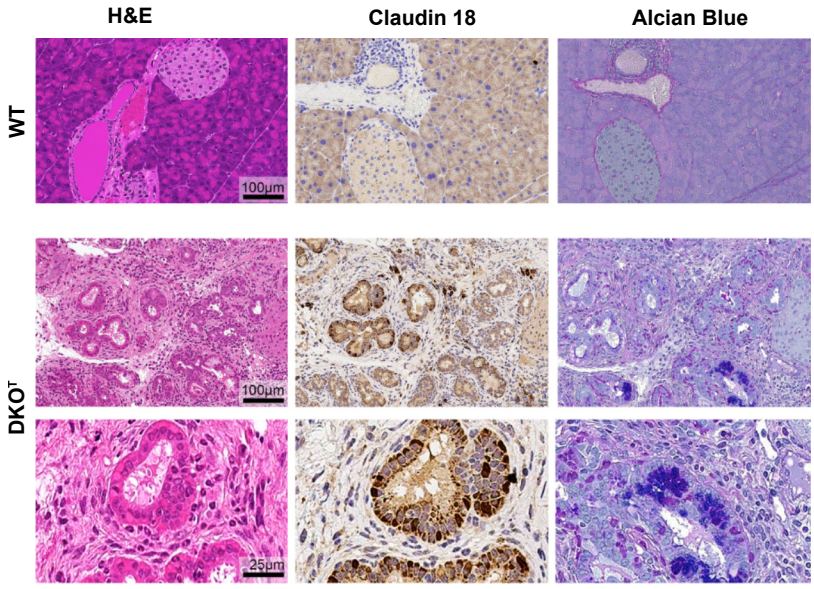

Fig. 34: Pancreata of DKO^T mice exhibit sign of early pre-neoplastic changes and panIN lesions. Pancreata of WT and DKO^T mice were fixed and analyzed by immunohistology. Representative images of WT pancreata (upper panel) and DKO^T pancreata at two magnifications (lower panels) stained with anti-Claudin 18 or alcian blue. Samples were collected by Dr. Desheng Hu. Staining and analysis was performed by Dr. Jessica Zoeller.

Pancreata from 20-weeks-old DKO^T mice contained both Claudin 18 positive as well as alcian blue positive cells **(Fig. 34 lower two panels)**, whereas WT pancreata did not contain any cells positive for these markers **(Fig. 34 upper panels)**, supporting the hypothesis that DKO^T mice spontaneously develop pre-neoplastic lesions in their pancreata.

Taken together, these data support a model in which activated Roquin deficient T cell infiltrate into pancreatic tissue, where predominantly T_H17 accumulate and produce one or several factors that on the one hand attract inflammatory neutrophils into the pancreas microenvironment, and, on the other hand act on the pancreas tissue directly to promote pathological changes. Infiltration of pro-inflammatory cells leads to

pancreatitis which in turn promotes pre-neoplastic changes in the pancreas tissue of DKO^{T} mice.

4.2.4 Roquin deficiency in T cells acts synergistically with the Kras^{G12D} mutation to promote PDAC development

Since Roquin deficiency in T cells drives pancreatitis and leads to the spontaneous development of PanIN lesions in the DKO^{T} mouse model, we were wondering whether DKO^{T} cell driven inflammation can act synergistically with mutations in acinar cells that are known to accelerate PDAC development. To address this question, we took advantage of a genetically engineered mouse model, which expresses constitutively active Kras^{G12D} specifically in acinar cells (Hingorani *et al.*, 2003; Jackson *et al.*, 2001). These mice spontaneously develop PanIN lesions which stepwise progress to higher grades as the mice age. In very low frequencies and only at the age of > 6months these precursor lesions have the potential to progress to invasive and/or metastatic PDAC (Hingorani *et al.*, 2003).

We lethally irradiated the 10-11 weeks old LSL-Kras^{G12D}; p48cre mice and reconstituted them with either WT or DKO bone marrow. 5 – 6 weeks after reconstitution mice were sacrificed and spleens, pancreata and blood were collected for analysis. Changes in the immune compartments were analyzed by flow cytometry, and development of pancreatic cancer was assessed by immunohistology **(Fig. 35A).**

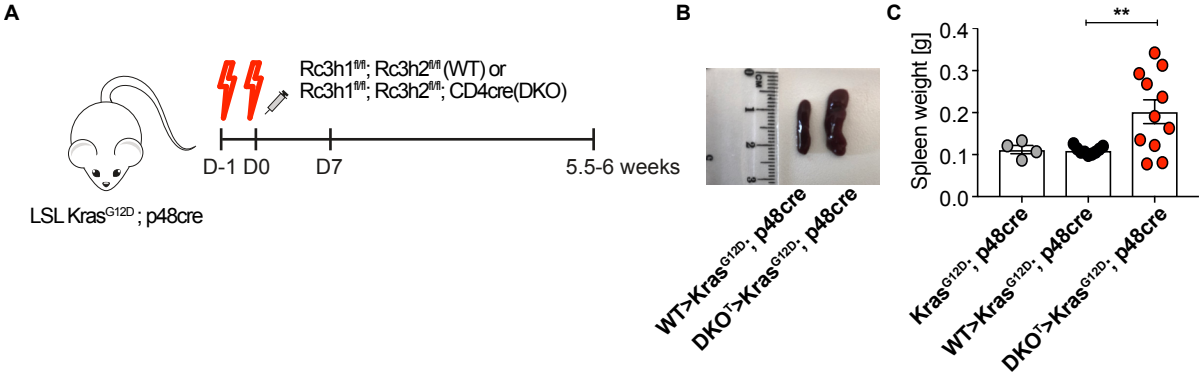

Fig. 35: Experimental set up of Kras^{G12D} Bone marrow chimeras.

(A) LSL-Kras^{G12D} mice were lethally irradiated and reconstituted with either WT or DKO^{T} bone marrow. Mice were sacrificed and organs were analyzed 5-6 weeks after reconstitution. **(B)** Representative images of spleens taken from WT or DKO^{T} reconstituted mice and **(C)** their respective weights. Data is representative of at least 15 animals per group analyzed in two independent experiments. Statistical

data are presented as Mean ± SEM. Statistical significance was determined by unpaired, one-tailed t-test. Untreated controls show reference weight in untreated LSL-Kras^{G12D}; p48cre mice. ** p<0.01.

5-6 weeks after reconstitution Kras^{G12D} mice that received DKO^{T} bone marrow showed marked swelling in the abdominal region of their body and significant signs of pain. Therefore, the mice were sacrificed earlier than the planned end of experiment. Upon necropsy we determined bloody ascites in the majority of Kras^{G12D} mice reconstituted with DKO^{T} bone marrow but not in mice reconstituted with WT bone marrow or untreated animals. The spleens of DKO^{T} bone marrow reconstituted mice were significantly bigger than spleen taken from mice reconstituted with WT bone marrow **(Fig. 35B,C).**

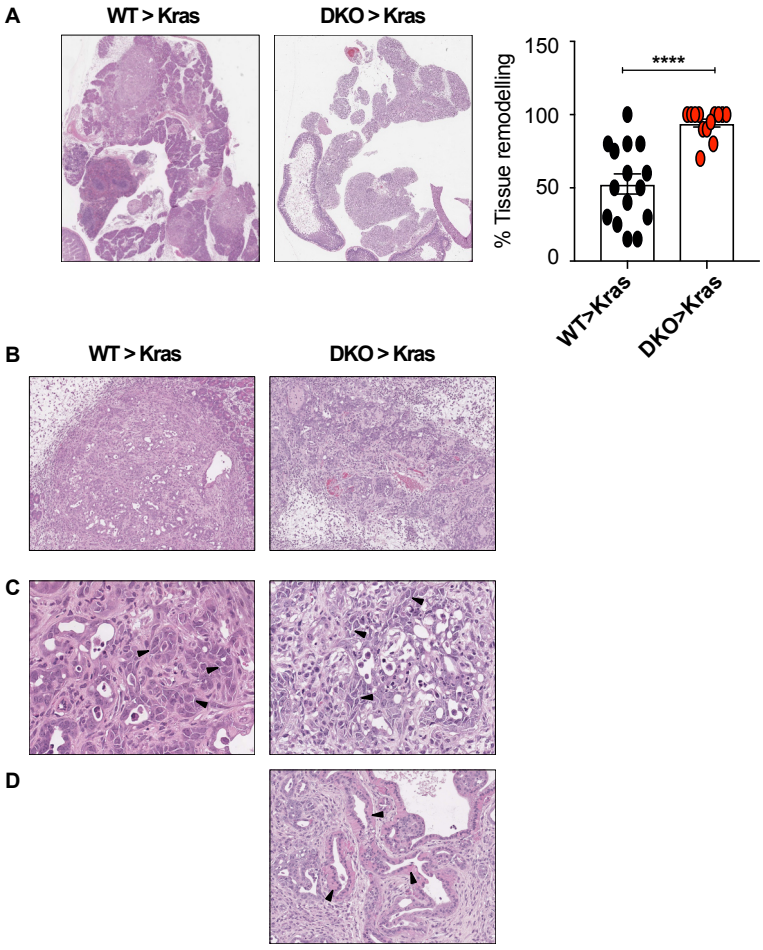

Fig. 36: DKO^{T} bone marrow accelerates carcinoma development in Kras^{G12D} mice.
(A) Representative overview over a whole pancreas taken from Kras^{G12D} mice reconstituted with either WT or DKO^{T} bone marrow showing the extent of tissue remodeling (left) and quantification thereof (right). **(B)** Higher magnification of pancreata from WT and DKO^{T} reconstituted Kras^{G12D} mice affected by tissue remodeling. **(C)** Both groups show signs of loosened intracellular contacts (black arrows). **(D)** Intracellular hyalinosis in DKO^{T} reconstituted Kras^{G12D} mice (black arrows). Data is representative of at

least 15 animals per group analyzed in two independent experiments. Statistical data are presented as Mean ± SEM. Statistical significance was determined by unpaired, one-tailed t-test. Histological stainings were performed by AG Heikenwälder (Jenny Hetzer and Danijela Heide). Pathological analysis was performed by Dr. Katja Steiger. **** p< 0.0001.

Upon initial inspection pancreata of $Kras^{G12D}$ mice reconstituted with DKO^{T} bone marrow were stiffer than those from mice that received WT bone marrow. We performed histological stainings to assess whether mice reconstituted with DKO^{T} bone marrow had indeed developed cancer. We could detect invasive carcinoma in both groups with loosened intracellular contacts **(Fig. 36A-C).** However, the portion of remodeled tissue was significantly higher in mice reconstituted with DKO^{T} bone marrow, with the majority of mice showing up to 100% tissue remodeling **(Fig. 36A, B).** Furthermore, we observed intracellular hyalinosis in mice reconstituted with DKO^{T} bone marrow but not in mice reconstituted with WT bone marrow **(Fig. 36D).**

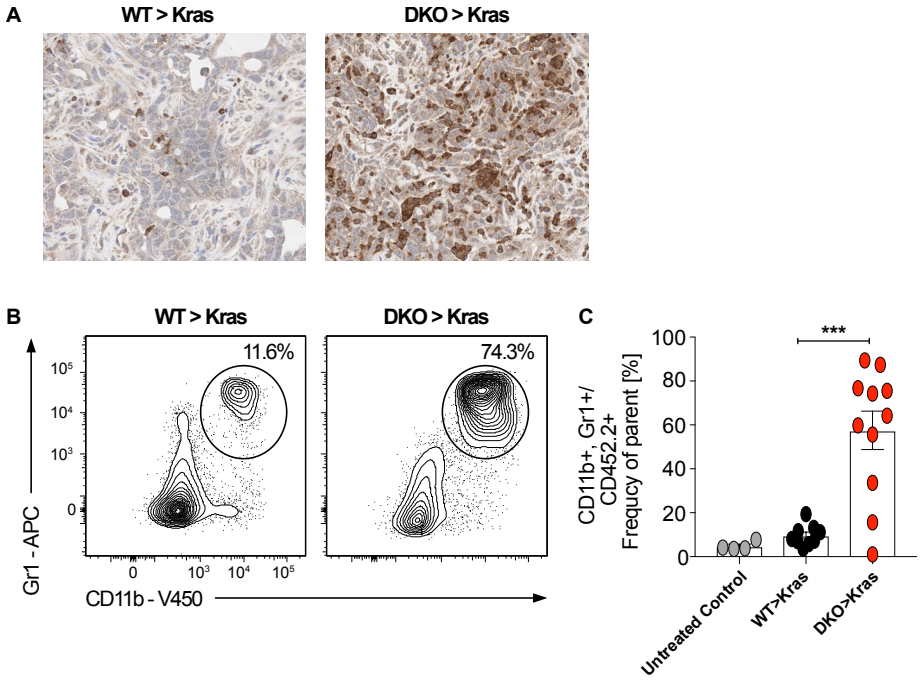

Fig. 37: Reconstitution of $Kras^{G12D}$ mice with DKO^{T} bone marrow causes an accumulation of neutrophils.

(A) Representative pancreas sections stained with anti-Ly6G. **(B)** Representative FACS plots of $CD11b^{+}$ $Gr1^{+}$ cells in spleens of mice reconstituted with WT or DKO^{T} bone marrow and **(C)** quantification thereof. Data is representative of at least 10 animals per group analyzed in two independent experiments. Statistical data are presented as Mean ± SEM. Statistical significance was determined by unpaired, one-tailed t-test. Untreated controls show reference levels of immune cell populations in untreated LSL-$Kras^{G12D}$; p48cre mice. Histological staining was performed by AG Heikenwälder (Jenny

Hetzer and Danijela Heide). Analysis of histology sections was performed following instructions by Dr. Katja Steiger. *** p<0.001.

The most prominent difference between the two groups was an accumulation of Ly6G$^+$ neutrophils in the pancreatic tissue of DKO^T bone marrow reconstituted mice **(Fig. 37 A)**. In the spleen, an accumulation of CD11b$^+$ Gr1$^+$ cells was also the most prominent phenotype in Kras^{G12D} mice reconstituted with DKO^T bone marrow, phenocopying the DKO^T mouse model **(Fig. 37B,C).**

Upon further analysis of the immune cell compartment, it became apparent that detection of CD4$^+$ T cells showed a reduction in DKO^T bone marrow reconstituted animals, as there were significantly less CD4$^+$ T cells compared to the WT reconstituted group, although proliferation of these cells was comparable between the two genotypes **(Fig. 38A,B).** Interestingly, even though there were fewer CD4$^+$ T cells in DKO^T reconstituted animals, there was an increase in IL-17A and IFNγ producing cells **(Fig. 38F,G).**

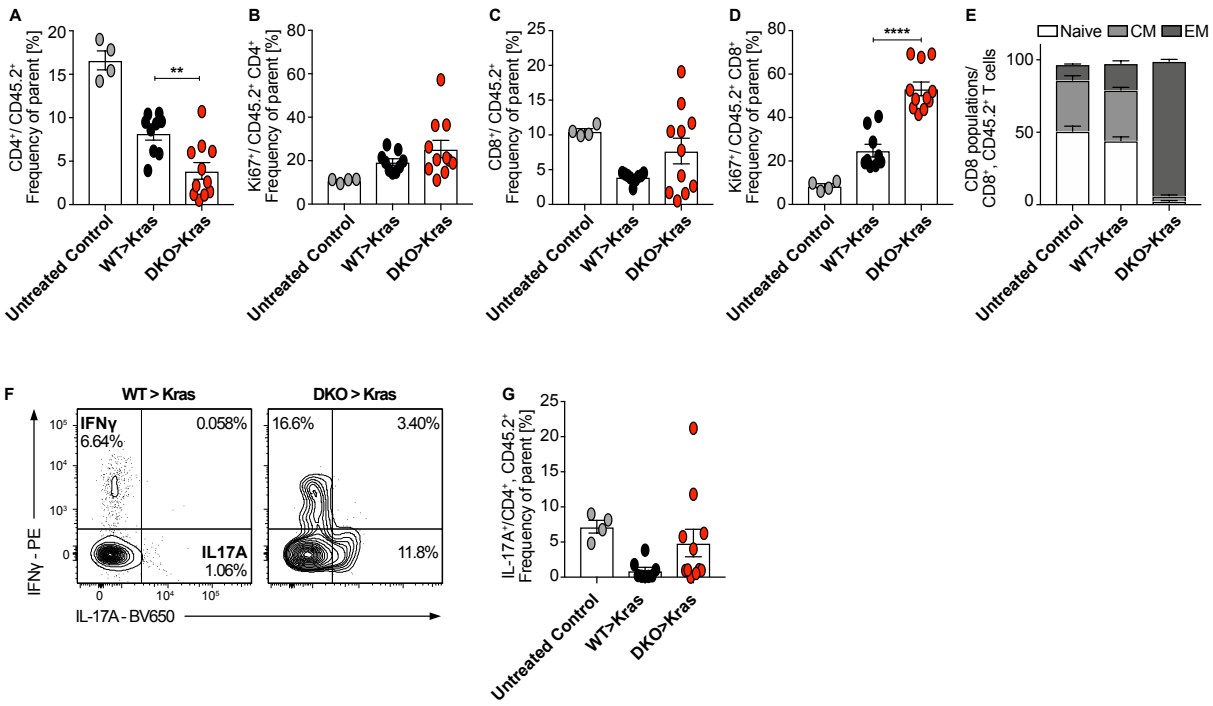

Fig. 38: CD4$^+$ produce IL-17A in DKO^T reconstituted Kras mice.

(A) Frequency and **(B)** proliferation of donor CD4$^+$ T cells in Kras^{G12D} recipient mice. **(C)** Frequency and **(D)** proliferation of donor CD8$^+$ T cells in Kras^{G12D} recipient mice. **(E)** Memory populations of donor CD8$^+$ T cells. **(F)** Representative plots and **(G)** quantification showing donor IL-17A producing CD4$^+$ T cells. Data is representative of at least 10 animals per group analyzed in two independent experiments. Statistical data are presented as Mean ± SEM. Statistical significance was determined by unpaired,

one-tailed t-test. Untreated controls show reference levels of immune cell populations in untreated LSL-Kras^{G12D}; p48cre mice. * p<0.05, ** p<0.01, **** p<0.0001.

CD8^{+} T cells in the DKO^{T} bone marrow reconstituted mice appeared increased compared to WT bone marrow reconstituted animals, predominantly acquired an effector memory phenotype **(Fig. 38C-E)** and strongly upregulated exhaustion markers (PD-1, LAG3 and TIM3) as compared to the WT reconstituted group **(Fig. 39).**

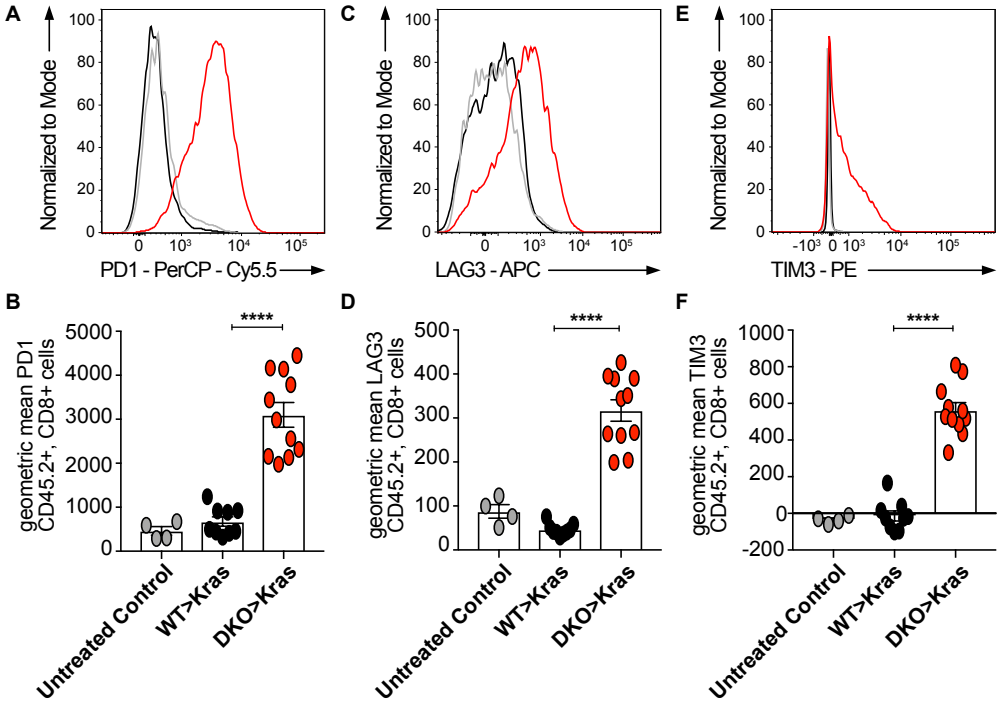

Fig. 39: CD8^{+} T cells in DKO^{T} reconstituted Kras^{G12D} mice are exhausted.
Representative histograms showing **(A)** PD-1, **(C)** LAG3 and **(E)** TIM3 expression on the surface of WT or DKO^{T} reconstituted Kras^{G12D} mice. Quantification of surface expression of **(B)** PD-1, **(D)** LAG3 and **(F)** TIM3. Data is representative of at least 10 animals per group analyzed in two independent experiments. Statistical data are presented as Mean ± SEM. Statistical significance was determined by unpaired, one-tailed t-test. Untreated controls show reference levels of exhaustion marker expression on CD8^{+} T cells of untreated LSL-Kras^{G12D}; p48cre mice. **** p<0.0001.

4.2.5 Reconstitution of Kras^{G12D} mice with DKO^{T} bone marrow does not promote chromosomal aberrations

Genomic instabilities can cause deregulated expression levels of oncogenes and tumor suppressor genes, which can drive tumor progression (Harada et al., 2008; Hata et al., 2018; Kou et al., 2020). Acute and chronic inflammation have been shown to induce DNA damage which may have the potential to cause genomic rearrangements and drive malignancies in the pancreas (Kay et al., 2019; Kiraly et al., 2015). Furthermore, it has been recently published that genomic rearrangement associated increases in the Kras dosis as well as loss of *Cdk2n* gene expression, promote PDAC development (Mueller *et al.*, 2018). We hypothesized that in our Kras^{G12D} bone marrow chimera model, DKO^{T} T cell-induced inflammation leads to chromosomal rearrangements and the amplification of the *Kras* locus, which may accelerate the development of pancreas cancer.

To test this hypothesis, LSL-Kras^{G12D}; p48cre mice were lethally irradiated and reconstituted with either WT or DKO^{T} bone marrow. Five weeks after reconstitution mice were sacrificed and pancreas tumors were dissected. Since pancreatic tumors are known to have a high stromal content (Hosein et al., 2020), stable cell lines were established from primary tumors for subsequent genetic analysis. Purity of the cell lines was confirmed by PCR to ensure complete removal of contaminating fibroblasts as described in section 3.2.3.4 **(Fig.12).** Genomic DNA was extracted from cell lines and from tails as reference tissue and whole exome sequencing (WES) was performed in collaboration with AG Rad. In total, it was possible to establish five cell lines derived from tumors taken from DKO^{T} reconstituted Kras^{G12D} mice (two of these cell lines D13A and D13B were derived from different tumor sites in one mouse) and two cell lines from tumors taken from WT reconstituted Kras^{G12D} mice. Samples were analyzed for copy number aberrations (CNA) and loss of heterozygosity (LOH).

No LOH was detected in any of the cell lines. To check for gains or losses in certain regions of each chromosome we analyzed WES data using CopywriteR (Kuilman et al., 2015). CNA profiles and segmentation values for all chromosomes were plotted against each other to identify common instabilities between the groups. The majority of samples showed deletions on chromosomes 4 and 12, however the effects were very mild. No significant amplifications were detected on any of the chromosomes **(Fig. 40)**.

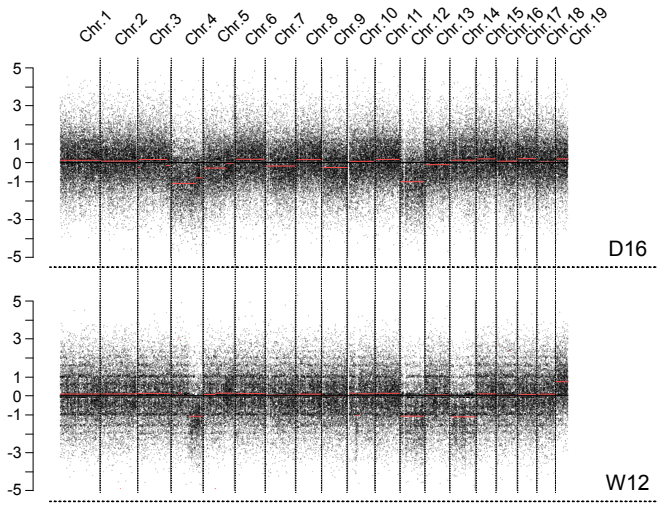

Fig. 40: Tumors derived from WT or DKO^{T} reconstituted Kras mice show losses on chromosomes 4 and 12.

Representative CNA profiles obtained from tumor cell lines derived from DKO^{T} (top panel) and WT (bottom panel) reconstituted Kras^{G12D} mice. Library preparation and bioinformatical analysis of CNAs were performed by Dr. Sebastian Mueller (AG Rad). CNA: Copy number aberration.

Genes affected by CNA were cross-referenced against the CGC database to determine genes that are known to be associated with cancer. The data set obtained from W11 did not yield any hits for cancer associated genes. The gene lists of remaining samples were compared to each other to identify commonly affected genes. Cut-off segmentation values were set to $\log_2$fc changes $-0.5 \leq x \geq 0.5$, where a mean segmentation value of -0.5 means a heterozygous deletion and a segmentation value of 0.5 is equivalent to a gain of a single copy, i.e. trisomy. Only genes that showed CNAs in 3 or more samples were considered. Genes affected by CNA are summarized in table **(Table 18)** and a full list of all affected genes is available in **Appendix 3.** Contrary to our hypothesis, we did not detect amplification of the *Kras* locus (Chr. 6: 145162425-145195965 bp) in any of the samples. However, the majority of cell lines exhibited a loss in Cdk2na and Cdk2nc **(Table 18).**

To our surprise, there were no major differences in CNAs between tumors derived from WT or DKO^{T} bone marrow reconstituted Kras^{G12D} mice, i.e. all CNAs detected in the DKO^{T} tumor cell lines were also present in WT tumor cell lines **(Table 18)**. These data suggest, that DKO^{T} T cell-induced inflammation and accelerated tumor progression in Kras^{G12D} bone marrow chimeras does is not a consequence of enhanced chromosomal instability or specific rearrangement events.

Altered gene copy numbers						
Chr.	Start (bp)	End (bp)	Gene symbol	decreased in #Samples	increased in #Samples	altered in WT
4	89274471	89294653	Cdkn2a	4		y
4	109660876	109667189	Cdkn2c	2	1	y
4	109280268	109387817	Eps15	2	1	y
4	94599385	94599795	Gm12657	4	1	y
4	101152367	101265282	Jak1	3	3	y
4	95049034	95052222	Jun	4	1	y
4	116702279	116708406	Mmachc	2	1	y
4	116807723	116819440	Mutyh	2	1	y
4	115000159	115043196	Stil	2	1	y
4	115056426	115071755	Tal1	3	1	y
12	52503972	52571975	Arhgap5	3		y
12	107910403	108003602	Bcl11b	3		y
12	38779380	38870484	Etv1	3		y
12	57540628	57546916	Foxa1	3		y
12	102469135	102497907	Golga5	3		y
12	78226379	78684772	Gphn	3		y
12	73901375	73947530	Hif1a	3		y
12	76937269	76962201	Max	3		y
12	70011435	70113717	Nin	3		y
12	56531958	56536908	Nkx2-1	3		y
12	79297282	79814690	Rad51b	3		y
12	105216750	105222793	Tcl1	3		y
12	101834043	101913267	Trip11	3		y
12	91384563	91549808	Tshr	3		y

Table 18: Commonly affected genes by copy number alterations in tumors derived from WT or DKO^{T} Kras^{G12D} bone marrow chimeras.

Cut-off segmentation values were set to $\log_2$fc changes $-0.5 \leq x \geq 0.5$. Genes that were affected by copy number changes in ≥ 3 primary tumor cell lines are listed. Bioinformatical analysis was performed by AG Rad.

4.2.6 Comparison of transcriptional profiles between WT and DKO^{T} reconstituted Kras^{G12D} mice

In addition to WES analysis of the primary tumor cell lines, we also performed mRNA sequencing on the cell lines as well as on bulk primary tumor tissue, to determine which genes or pathways were important drivers of the accelerated cancer development in the DKO^{T} reconstituted Kras^{G12D} bone marrow chimera model.

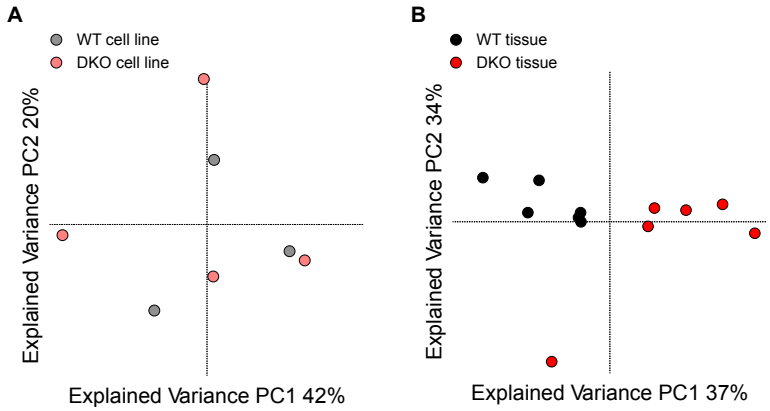

Fig. 41: PCA analysis of RNAseq data.

Unsupervised clustering of RNAseq results from **(A)** tumor cell lines and **(B)** bulk tumor tissue derived from WT and DKO^{T} reconstituted $Kras^{G12D}$ mice. Bioinformatic analysis was performed by AG Rad.

Principal component analysis (PCA) of RNAseq results revealed that the established tumor cell lines from the WT or DKO^{T} group did not cluster by genotype **(Fig. 41A)**, whereas clear clusters were observed when primary tumor tissue was analyzed **(Fig. 41B)**. Thus, the subsequent analysis was focused on the sequencing data obtained from primary tumors. Only one tumor (D12) appeared to be a clear outlier in the PCA analysis **(Fig. 41B)** and was therefore removed from further analyses.

In total we could identify 15940 genes when comparing primary tumors dissected from WT and DKO^{T} reconstituted $Kras^{G12D}$ mice. 312 genes were significantly downregulated, and 121 genes were significantly upregulated in DKO^{T} induced tumors. Interestingly, among the upregulated genes we found several matrix metalloproteases as well as genes associated with neutrophils **(Fig. 42A)**.

Fig. 42: Differentially expressed genes and enriched pathways in DKO^{T} induced tumors.
(A) Volcano plot showing significantly up- and downregulated genes in DKO^{T} versus WT induced tumors in the Kras^{G12D} bone marrow chimera model. Cut off values for significantly deregulated genes were a log2Fold change of ≥ 1 and padj ≤ 0.05. **(B)** KEGG pathway enrichment analysis showing the top 5 enriched pathways in tumors derived from DKO^{T} Kras^{G12D} bone marrow chimera. **(C)** GO term analysis showing the top 5 strongest enriched biological processes. Bioinformatical analysis was performed by AG Rad. KEGG: Kyoto Encyclopedia of Genes and Genomes, GO: Gene ontology.

We next performed enrichment analyses to identify the key deregulated pathways and biological processes **(Fig. 42B,C)**. The p53 and IL-17 signaling pathways as well as

ECM-receptor interaction pathways were among the five strongest upregulated KEGG pathways in DKO^{T} reconstituted $Kras^{G12D}$ mice **(Fig. 42B**). The biological processes that were strongest affected were predominantly related to extracellular matrix reorganization **(Fig. 42C)**.

Taken together these data suggest, that in our $Kras^{G12D}$ bone marrow chimera model there is an acceleration of the prototypic $Kras^{G12D}$ driven pancreas transformation. This acceleration is caused by DKO^{T} T cells induced changes in the pancreas stroma and microenvironment, but not by an accumulation of genetic aberrations in the pre-neoplastic lesions.

4.3 Pancreas pathology in Roquin-1/2-deficient mice is driven by IL-17A and G-CSF signalling

DKO^T T cells are able to produce one or more factors that affect both immune cells and non-immune cells of the pancreas, leading to the spontaneous development of pancreas pathology. This factor can act synergistically with the $Kras^{G12D}$ mutation accelerating cancer progression. We thus addressed the identity of the *trans*-acting factor and the mechanisms contributing to the spontaneous development of pre-neoplastic lesions in the DKO^T mouse model.

4.3.1 G-CSF is strongly deregulated in DKO^T mice and $Kras^{G12D}$ Chimeras receiving DKO^T bone marrow

To assess the contribution of cytokines and other soluble factors in the development of pancreas pathology as well as the accelerated tumorigenesis in $Kras^{G12D}$ mice reconstituted with DKO^T bone marrow, I performed multiplex analysis on the sera taken from WT and DKO^T mice as well as $Kras^{G12D}$ recipient mice 5 weeks after reconstitution.

I hypothesized that, if there was a soluble factor that could drive the observed pancreas pathology in the DKO^T mouse model, it would also be strongly involved in the accelerated tumorigenesis in the bone marrow chimera system. Therefore, such a factor should be deregulated to a similar extent in both models.

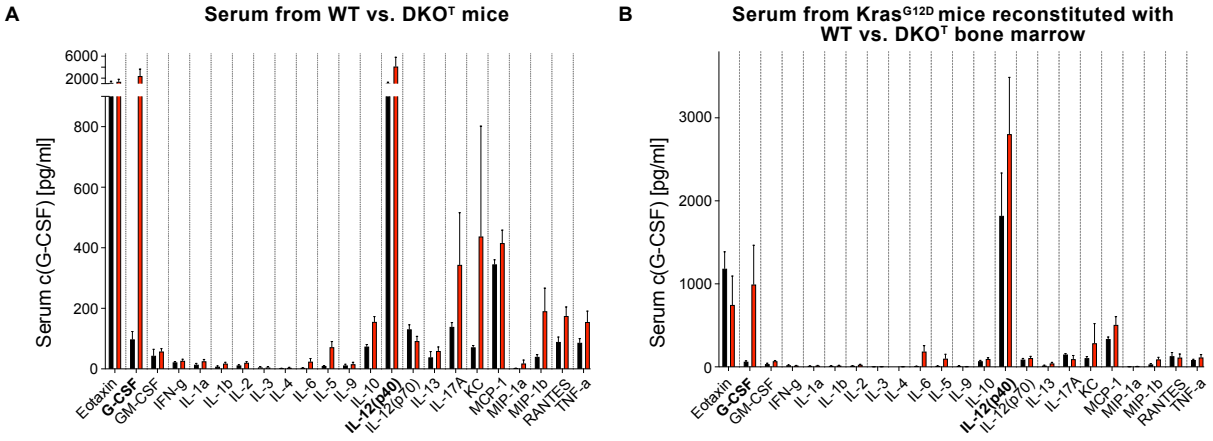

Fig. 43: Roquin deficiency in T cells leads to a systemic elevation of G-CSF levels.
Luminex analysis of sera taken from **(A)** WT and DKO^{T} mice, and **(B)** Kras^{G12D} bone marrow chimeras 5.5 weeks after reconstitution with either WT or DKO^{T} bone marrow. Statistical data are presented as Mean ± SEM. Data are representative for at least 5 biological replicates per group. Luminex measurements were performed in collaboration with AG Noessner.

As expected, DKO^{T} mice exhibited elevated systemic levels of IL-6, IL-17A and TNFα Interestingly, and unexpectedly, multiplex analysis revealed very high systemic G-CSF levels that were almost 1000fold higher compared to WT mice **(Fig. 43A)**. Furthermore, elevations in systemic KC, MIP-1b as well as RANTES levels were observed in DKO^{T} mice. All of these molecules have previously been implicated in cancer development and progression (Huber *et al.*, 2020; Singh et al., 2018).

When comparing the cytokine profiles of DKO^{T} mice with the cytokine profiles obtained from Kras^{G12D} mice reconstituted with either WT or DKO^{T} bone marrow, it became evident that systemic G-CSF levels were strongest deregulated with an approximately 1000fold increase as compared to WT reconstituted counterparts also in this model **(Fig.43B).**

Another cytokine that was elevated in both models was IL-12(p40). However, the difference between IL-12(p40) levels in WT vs. DKO^{T} was not as pronounced as for G-CSF. Since G-CSF has been linked to cancer development, progression and poor prognosis we focused on G-CSF and IL-12(p40) was not further pursued in this work.

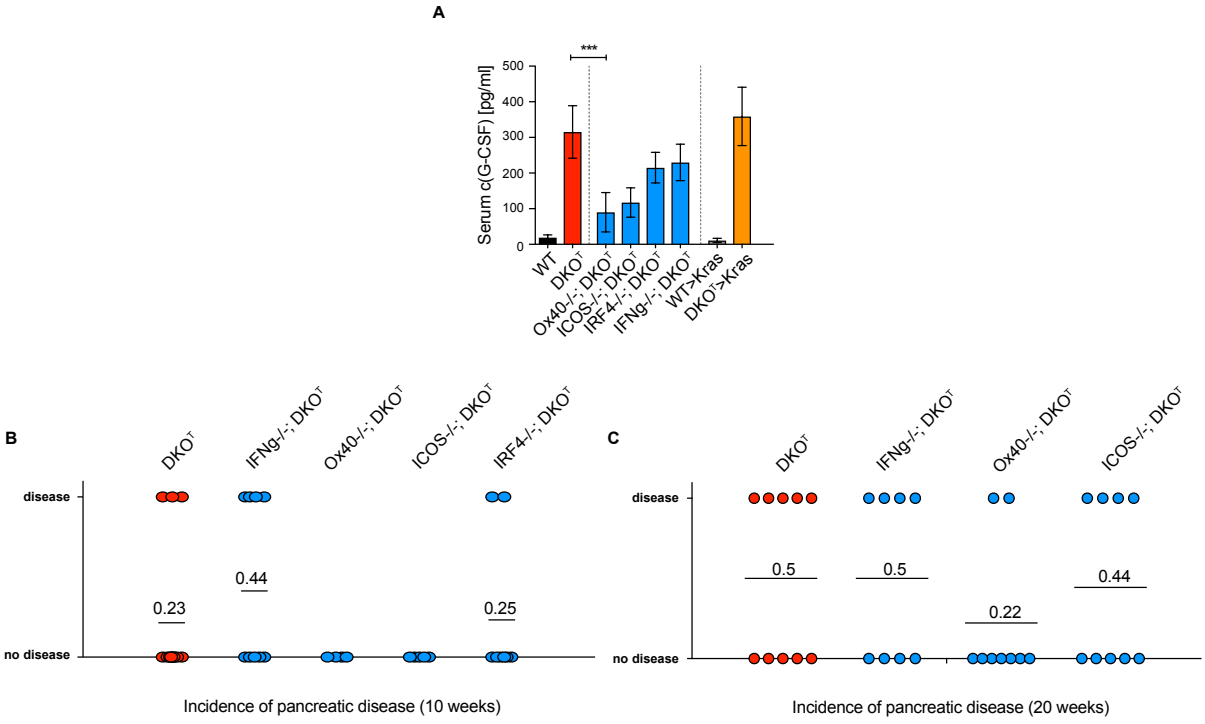

Fig. 44: Systemic G-CSF levels are reduced in TKO mice with an improved pancreas phenotype. **(A)** Serum G-CSF levels were determined in WT, DKO^T and Kras^{G12D} mice reconstituted with WT or DKO^T bone marrow and compared to serum levels in triple knock out mice with systemic deletions of Roquin targets in addition to T cells specific Roquin deletion. Data presented as Mean ± SEM. Data are representative for at least 6 biological replicates per group. **(B)** Incidence of pancreatic disease in 10-weeks-old triple knock out mice compared to DKO^T mice. **(C)** Incidence of pancreatic disease in 20-weeks-old triple knock out mice compared to DKO^T mice. TKO mice were crossed by Dr. Desheng Hu and incidence of disease was determined by Dr. Jessica Zoeller.

To validate the multiplex results and investigate a link between G-CSF levels and pancreas pathology in mice with Roquin-1/2-deficient T cells, I measured systemic G-CSF levels in sera from WT and DKO^T mice, as well as in sera taken from triple KO mice that were systemically lacking individual Roquin targets combined with conditional Roquin deletion in T cells. Sera of 20-weeks-old DKO^T mice exhibited increased G-CSF levels, confirming the initial multiplex findings. Only the 20-weeks-old Ox40-/-; DKO^T mice had significantly decreased systemic G-CSF levels as compared to DKO^T mice. G-CSF levels were also slightly decreased in 10 weeks old ICOS-/-; DKO^T mice but the difference was not statistically significant **(Fig. 44A**). Interestingly, the Ox40-/-; DKO^T mice were also the only mice, that exhibited a partial rescue with regards to incidence of pancreas pathology at the age of 20 weeks. 10-

weeks-old ICOS-/-; DKO^T mice showed a reduced incidence of pancreas pathology compared to DKO^T mice. At the age of 20 weeks these differences could no longer be detected **(Fig. 44B,C).**

ELISA measurements of G-CSF levels in $Kras^{G12D}$ mice 5.5 weeks after reconstitution with DKO^T bone marrow were comparable to the levels observed in 20 weeks old DKO^T mice, confirming the multiplex findings.

Taken together, these data correlate systemic G-CSF levels with the incidence of pancreas pathology in mice with Roquin-1/2-deficient T cells, implicating G-CSF function in this spontaneous model of pancreas pathology.

4.3.2 G-CSF is directly regulated by Roquin family proteins via its 3'UTR

Since systemic G-CSF levels were associated with the development and progression of pancreas pathology, I was wondering whether G-CSF could be a direct Roquin target. There have been previous reports, that have associated G-CSF with Roquin (Braun *et al.*, 2018; Leppek *et al.*, 2013), however direct regulation of G-CSF by Roquin proteins has not been proven to date. To identify potential Roquin binding sites, the folding of the G-CSF 3'UTR was simulated using RNAfold (Gruber et al., 2015). Several AU rich elements (AREs), stem loop (SL) structures as well as one prototypical constitutive decay element (CDE) were present in the 3'UTR **(Fig. 45).** The two stem loops, SLA and B, have been previously described and SLB is known to be necessary for post-transcriptional regulation of the cytokine (Braun *et al.*, 2018; Brown et al., 1996; Putland et al., 2002).

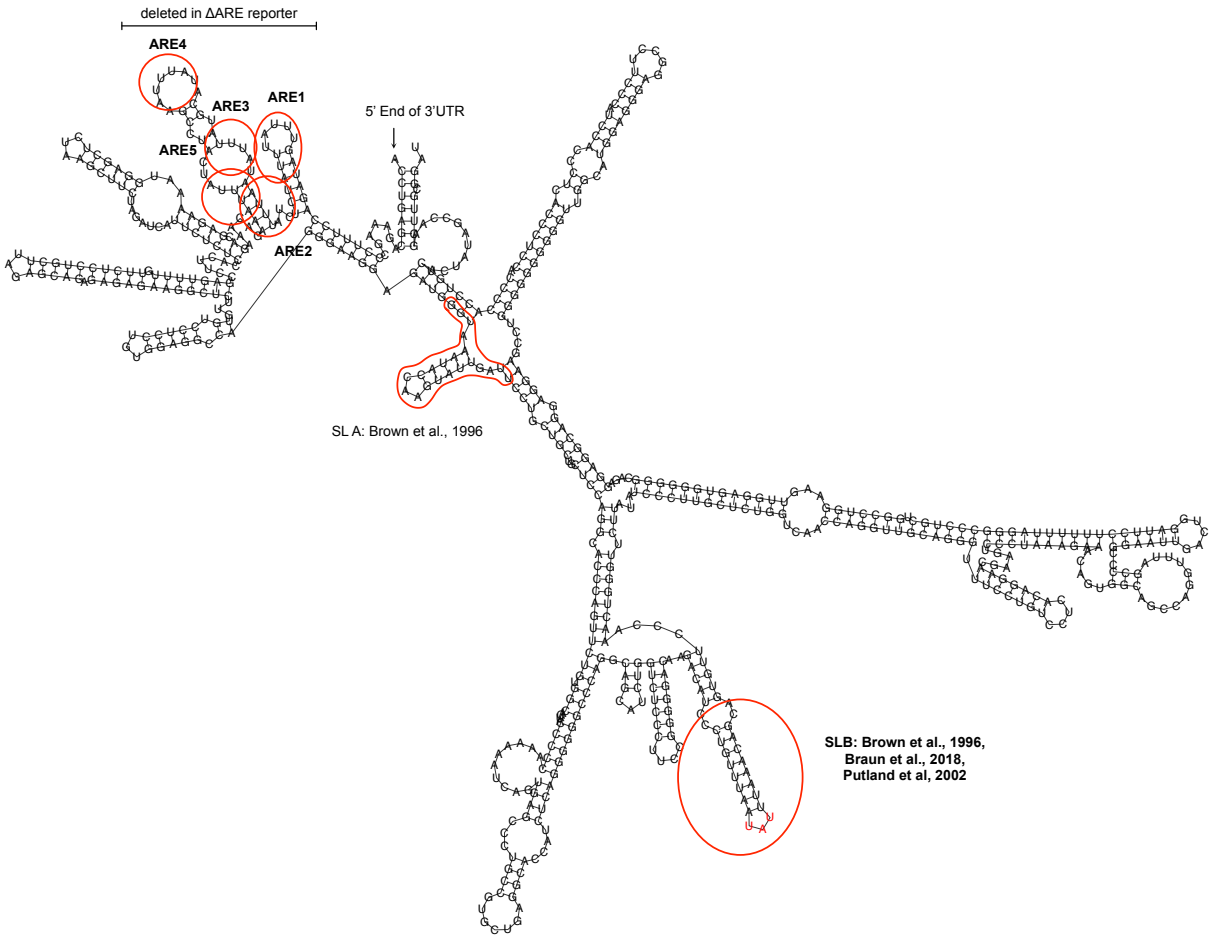

Fig. 45: Secondary structure of the G-CSF 3'UTR.

Folding of the G-CSF 3'UTR was predicted using the RNAfold web server (Hofacker et al., 1994). AREs as well as stem loop structures that have previously be suggested to be involved in post-transcriptional regulation are circled in red. ARE: AU-rich elements. Regions that have been mutated for reporter

assays are indicated. ΔARE reporter constructs lack the indicated areas. In SLBmut constructs the UAU sequence marked in red was replaced by a AUA sequence. SL: stem loop.

To formally test, whether Roquin can directly regulate G-CSF expression by binding to its 3'UTR reporter assays were performed. The G-CSF 3'UTR was amplified from cDNA acquired from cultured DKO^{T} T_H1 cells and inserted into a MSCV vector downstream of the GFP coding sequence. As a positive control, a portion of the *Nfkbid* 3'UTR, *Nfkbid* 1-263, was coupled to the GFP reporter (Essig *et al.*, 2018). To assess whether the ARE and/or SLB (CDE) played a role in Roquin dependent regulation of G-CSF several mutations were introduced into the G-CSF 3'UTR. Roquin-$1^{fl/fl}$; Roquin-$2^{fl/fl}$; Ert2-Cre; LSL-hCAR MEF cells were retrovirally transduced with the various GFP reporter constructs. Transduced MEF cells were split in two on day 2 after transduction. Half of the cells was treated with Hydroxytamoxifen for five days to delete Roquin-1 and Roquin-2 and GFP expression was assessed by flow cytometry and western blot. To confirm successful Roquin deletion the removal of the Stop cassette in front of the hCAR reporter was measured by anti-CAR staining and flow cytometry, and Roquin deletion was additionally confirmed directly by western blot **(Fig. 46 A,D)**.

GFP levels were strongly increased following Roquin deletion when the reporter was linked to either the 3'UTR of *Nfkbid* 1-263 or G-CSF. Deletion of the portion of the G-CSF 3'UTR that contained the AREs or a mutation in the SLB both reduced the fold regulation of the reporter by Roquin, whereas only a combination of ARE deletion and SLB mutation led to a complete abrogation of regulation **(Fig. 46B-D)**. This means that Roquin proteins can directly or indirectly regulate the G-CSF via the AREs as well as the CDE, and absence of both regulatory elements is required for complete de-repression.

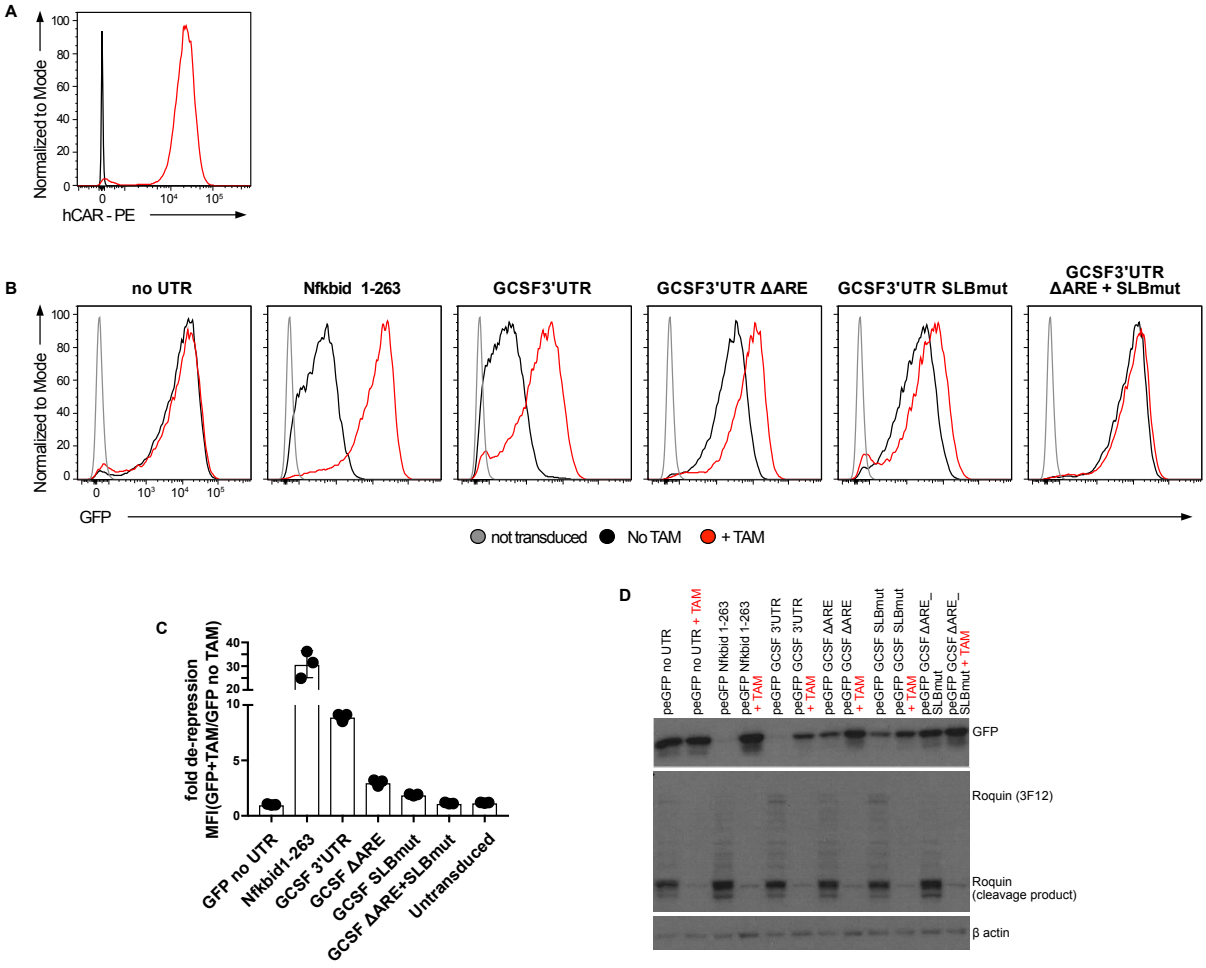

Fig. 46: G-CSF 3'UTR is directly regulated by Roquin.

Roquin-1/2$^{fl/fl}$; creERT2; LSL-hCAR MEF cells were transduced with GFP reporters with a WT or mutated G-CSF 3'UTR and treated with hydroxytamoxifen to induce Roquin deletion. **(A)** hCAR expression on MEF cells without (black curve) and with hydroxytamoxifen treatment (red curve) as a measure for Roquin deletion. **(B)** Representative plots showing GFP expression without (black curve) and with hydroxytamoxifen treatment (red curve). **(C)** Quantification of fold change of GFP gMFI, i.e. fold de-repression, after Roquin deletion. Data presented as Mean ± SEM **(D)** Western blot analysis of transduced MEF cells without and with hydroxytamoxifen treatment. Data are representative for three independent experiments.

Recently strong evidence has emerged showing that the Roquin ROQ domain can indeed directly bind CDE-ARE tandem structures. One such structure is present in SLB of the G-CSF 3'UTR (Binas et al., 2020; Braun *et al.*, 2018) **(Fig. 45)** and further supporting direct regulation of G-CSF by Roquin. AREs are not prototypical Roquin target structures but are known to be regulated by other RBPs, like TTP, Butyrate response factor1 (ZFP36L1) and K-homology splicing regulatory protein (KSRP)

(Beisang and Bohjanen, 2012). Thus, we cannot exclude that additional proteins other than Roquin repress the G-CSF 3'UTR via the ARE-region. However, the fact that both, the ARE-region as well as SLB are required for full repression, suggests a potential Roquin interaction with both *cis*-elements **(Fig. 46).**

4.3.3 G-CSF is produced by Roquin-1/2-deficient CD4 T cells *in vitro* and *in vivo*

G-CSF is known to be produced by a variety of cells, including cancer cells and other immune cells, but, to my knowledge, G-CSF production by T cells has not been reported to date. Since systemic G-CSF levels were elevated in DKO^{T} mice which have a T cell specific Roquin deficiency and I have shown that the G-CSF 3'UTR can be regulated by Roquin proteins, I was wondering whether deletion of Roquin in T cells could cause them to produce this cytokine even though it would normally be suppressed.

To test this hypothesis, we first assessed the ability of DKO^{T} CD4^{+} and CD8^{+} T cells to produce G-CSF *in vitro*. For this total CD4^{+} and CD8^{+} T cells were isolated from WT or DKO^{T} mice and stimulated with plate-bound anti-CD3/anti-CD28 antibodies without subset skewing antibodies (T_H0 culture conditions). Tissue culture supernatants were collected on days 1, 2 and 3 and flash frozen. Since, both, IL-17A producing T_H17 T cells and IFNγ producing T_H1 cells were expanded in DKO^{T} mice, both of these conditions were also included. G-CSF levels in the tissue culture supernatant were determined by ELISA **(Fig. 47A).**

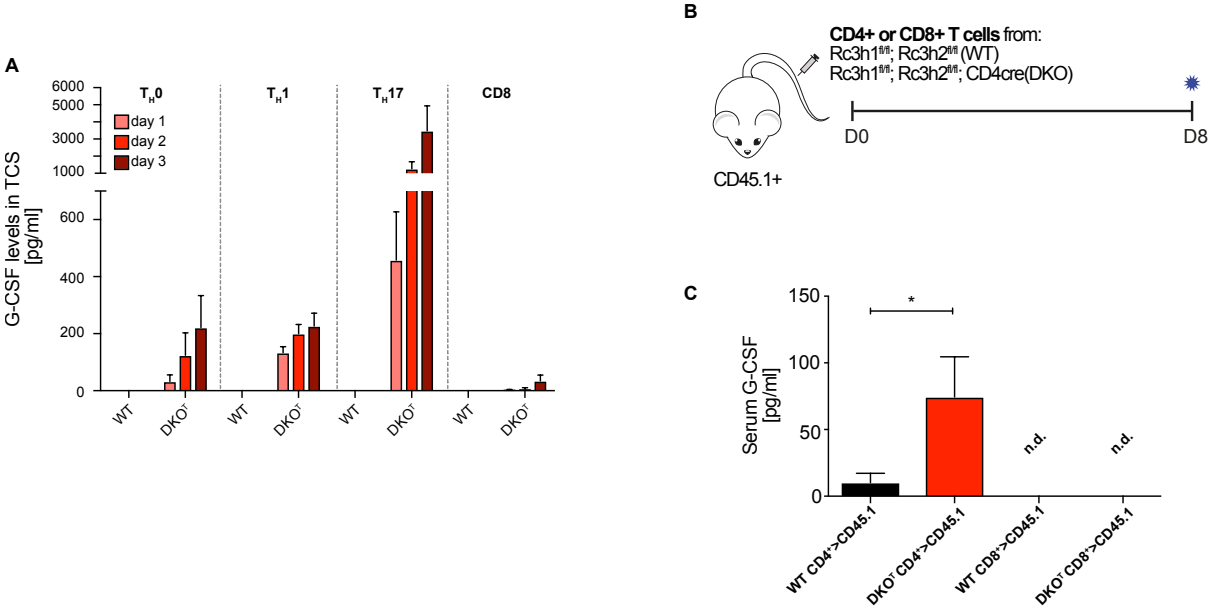

Fig. 47: Roquin1/2-deficient CD4$^+$ T cells produce G-CSF *in vitro* and *in vivo*.
(A) Total CD4$^+$ or CD8$^+$ or naïve CD4$^+$ T cells and were cultured *in vitro* under T_H0, T_H1 or T_H17 conditions, respectively. G-CSF levels in supernatants taken on days 1-3 were determined by ELISA. **(B)** Schematic showing adoptive transfer conditions used prior to the detection of serum G-CSF levels. **(C)** Serum G-CSF levels in WT, CD45.1$^+$ mice that were adoptively transferred with either WT or DKO^T T_H1 cells or CD8$^+$ cells. Data presented as Mean ± SEM. Data are representative for 6 biological replicates per group. ELISA: Enzyme linked immunosorbent assay. N.d.: not detectable. * $p<0.05$.

G-CSF was present in tissue culture supernatants from CD4$^+$ DKO^T cells cultured under T_H0, T_H1 and T_H17 conditions, but was not detectable in supernatants taken from WT CD4$^+$ cells and WT or DKO^T CD8 cells. G-CSF accumulated in the supernatants over time. Interestingly, when DKO^T CD4$^+$ cells were kept under T_H17 polarizing conditions G-CSF levels were significantly higher than in any other condition **(Fig. 47A),** pointing towards a link between Th17 cells and/or IL-17 signaling and G-CSF production.
In a second approach, I assessed the ability of DKO^T T cells to produce G-CSF *in vivo*. For this, I analyzed sera taken from mice that were adoptively transferred with either CD4$^+$ or CD8$^+$ T cells from WT or DKO^T mice **(Fig. 47B)** 8 days after transfer. Interestingly, G-CSF was not detectable in mice that received WT or DKO^T CD8$^+$ T cells. Mice that had received DKO^T CD4$^+$ cells, on the other hand, showed a marked increase in systemic G-CSF levels **(Fig. 47C).** Taken together, these data show that Roquin-1/2-deficiency in T cells leads to an inappropriate production of G-CSF by CD4$^+$ but not CD8$^+$ T cells *in vitro* and *in vivo.* The effect is further exacerbated under Th17 conditions, pointing towards a role of T cell produced IL-17 in the amplification of G-CSF production.

4.3.4 G-CSF neutralization in Kras^{G12D} bone marrow chimeras attenuates tumor progression

Since G-CSF levels were strongly elevated in the DKO^T Kras bone marrow chimera model and I observed a strong expansion of the CD11b$^+$, Gr1$^+$ compartment, I was wondering whether G-CSF drives accelerated tumor progression and neutrophil generation or expansion. To test this hypothesis, 10-12-weeks-old Kras^{G12D}; p48cre mice were reconstituted with WT or DKO^T bone marrow and treated with G-CSF

neutralizing antibodies or isotype controls. Five weeks after reconstitution, mice were sacrificed and pancreata were analyzed by histology **(Fig. 48A)**.

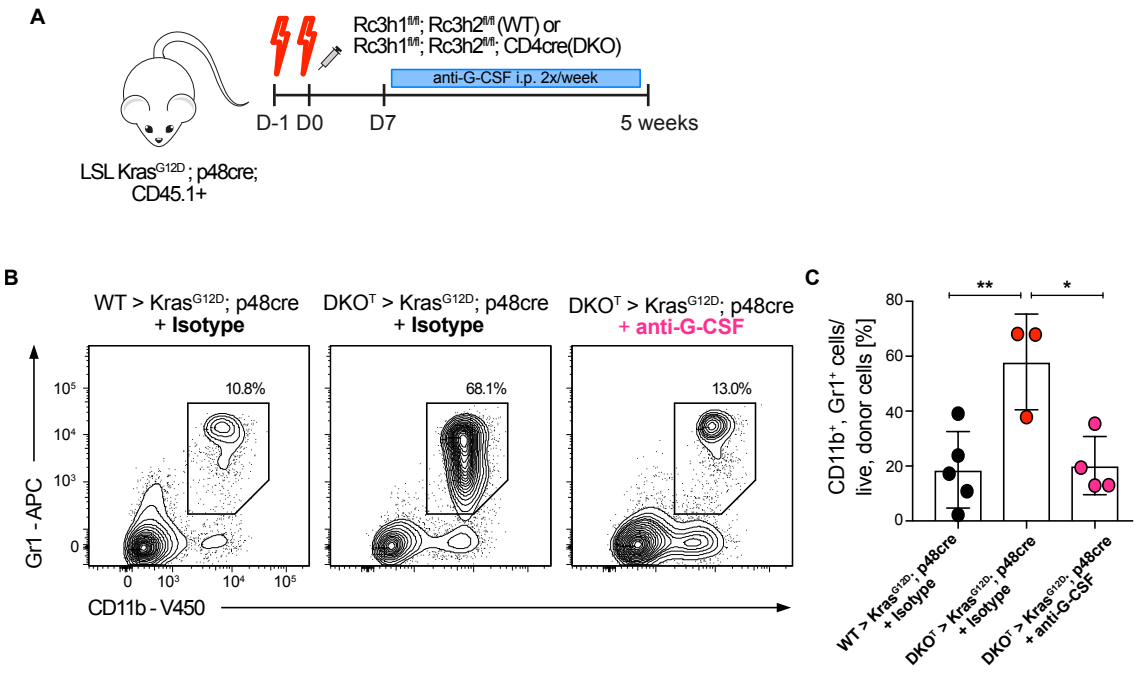

Fig. 48: G-CSF neutralization in DKO^{T} Kras^{G12D} leads to a decrease in CD11b^{+} Gr1^{+} cells.
(A) Schematic representation of experimental setup. **(B)** Representative plots showing CD11b^{+}Gr^{+} cells in spleens from bone marrow chimeras and **(C)** quantifications thereof. Data presented as Mean ± SEM. Data are representative for at least 3 biological replicates per group. Statistical significance was determined by one-way ANOVA with Dunnett's post hoc test. * p<0.05, ** p<0.01.

Importantly, the frequencies of CD11b^{+}, Gr^{+} neutrophils were reduced to similar levels as in WT bone marrow reconstituted Kras^{G12D} mice **(Fig. 48B,C)** in response to anti-G-CSF neutralizing antibody treatment showing that G-CSF neutralization predominantly affected the neutrophil compartment.

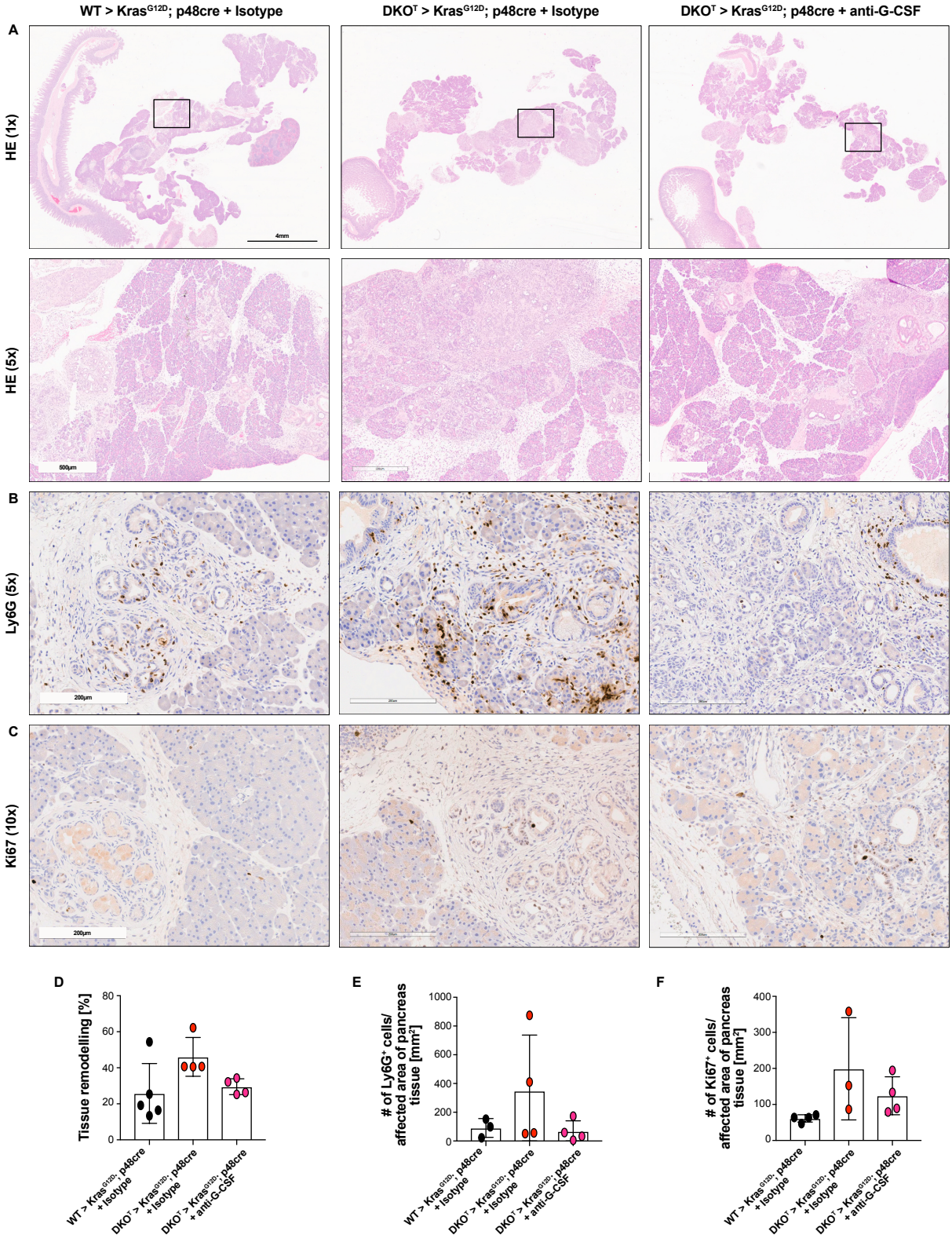

Fig. 49: G-CSF neutralization in Kras^{G12D} DKO^{T} bone marrow chimera model decelerates pancreas tumor progression.

(A) Representative H&E sections of pancreata taken from WT and DKO^{T} reconstituted Kras^{G12D} mice treated with anti-GCSF or isotype control. Upper panel: overview over whole pancreas. Black box marks the area that was used for higher magnification images (lower panel) and immunostainings for **(B)** Ly6G^{+} and **(C)** Ki67^{+} cells. **(D)** Quantification of the portion of remodeled tissue compared to the total

pancreas area. Quantifications of infiltrating **(E)** Ly6G$^+$ and **(F)** Ki67$^+$ cells in pancreas tissue. Each point represents average cell count in three high power fields (20x magnification) per pancreas. Data are representative for at least 4 biological replicates per group. Statistical significance was determined by one-way ANOVA with Dunnett's post hoc test.

DKO^T bone marrow reconstituted Kras^{G12D} mice showed an improved pancreatic phenotype after anti-G-CSF treatment, with a reduction in pancreatic tissue that exhibited tissue remodeling, i.e. complete disruption of normal acinar structures. Different from control mice that received isotype antibody controls pancreata from anti-G-CSF treated mice contained areas with acinar cells that had a normal appearance interspersed in areas clearly showing neoplasia. In fact, the tissue phenotype of anti-GCSF treated mice was very similar to Kras^{G12D} mice reconstituted with WT bone marrow. In contrast, the pancreata from mice reconstituted with DKO^T bone marrow that were treated with the isotype control revealed more areas containing acinar cells with prominent pathological changes **(Fig. 49A,D)**. Anti-G-CSF treatment also reduced the infiltration of Ly6G+ neutrophils into pancreas tissue **(Fig. 49B,E)** as well the number of actively proliferating cells **(Fig. 49C,F).**

Taken together, these data point towards a role of G-CSF in the accelerated progression of pancreas cancer at least in Kras^{G12D} mice reconstituted with DKO^T bone marrow. Cancer progression appears to be functionally linked to an accumulation of neutrophils in the lymphoid organs as well as in the neoplastic pancreas tissue.

4.3.5 IL-17A neutralization in DKO^T mice rescues pancreas pathology

In the DKO^T mouse model T_H17 cells are the predominant T cell subset present in the pancreas draining lymph nodes and IL-17 signaling was identified as one major pathway associated with in the DKO^T T cell-driven tumorigenesis in the Kras^{G12D} bone marrow chimera model. Furthermore, several publications have linked the IL-17A/G-CSF axis with cancer development and progression, as well as with neutrophil recruitment and metastasis (Coffelt et al., 2015; Jin et al., 2019; Mucciolo et al., 2021).

I, therefore, wanted to investigate whether T_H17 skewing and chronically increased IL-17A as apparent in the DKO^T mouse are promoting the development of pancreas pathology and pre-neoplastic changes. To test this, 10-weeks-old DKO^T mice were

treated with either an IL-17A neutralizing antibody or an isotype control (i.p.) for 10 weeks. At the age of 20 weeks, when the incidence of pancreas pathology in DKO^T mice is highest, mice were sacrificed and the development of pancreas pathology was assessed by histology. Furthermore, serum G-CSF levels or changes in the immune compartment were analyzed by ELISA or flow cytometry, respectively.

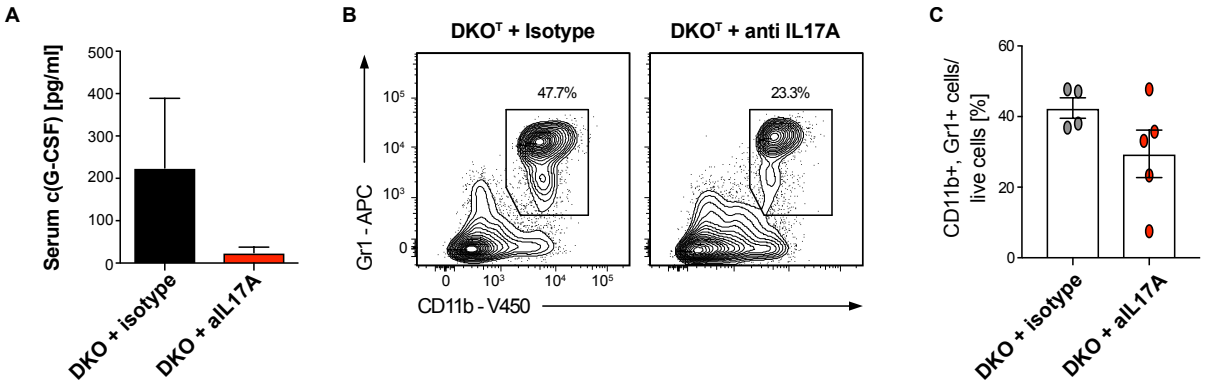

Fig. 50: IL-17A neutralization in DKO^T mice reduces G-CSF levels and neutrophils.
(A) Serum G-CSF levels in DKO^T mice treated with IL-17A neutralizing antibody for 10 weeks. **(B)** Representative plots showing neutrophils in anti-IL-17A treated DKO^T mice and **(C)** quantifications thereof. Data presented as Mean ± SEM. Data are representative for at least 5 biological replicates per group. Statistical significance was determined by unpaired, one-tailed t test.

Treatment of DKO^T mice with IL-17A neutralizing antibodies caused a stark decrease of systemic G-CSF levels **(Fig. 50A)** as well as a reduction of splenic CD11b$^+$ Gr1$^+$ cells in the spleens in anti-IL-17A treated mice **(Fig. 50B,C).** This means that the increased systemic G-CSF levels and neutrophil accumulation in the DKO^T mice are strongly affected by high IL-17A production by T_H17 cells.

To assess the effects of IL17A neutralization on the development of pancreas pathology, I analyzed pancreatic H&E sections. Since I started treatment with neutralizing antibodies in 10-weeks-old mice, both groups were exposed to the same cytokine milieu initially. It was likely that both groups would exhibit some sort or pathological changes in their pancreata. I hypothesized, that elimination of IL-17A from the system of DKO^T mice could slow down the development of pathology and prevent the formation of pre-neoplastic lesions. Therefore, I determined the portions of pancreatic tissue area that were affected by pathology in relationship to the whole pancreas and quantitatively assessed progression of pancreatic disease. DKO^T mice

treated with IL-17A neutralizing antibodies exhibited less and smaller areas with pathological changes **(Fig. 51A, black boxes, B)**. The majority of pancreas tissue showed no abnormalities.

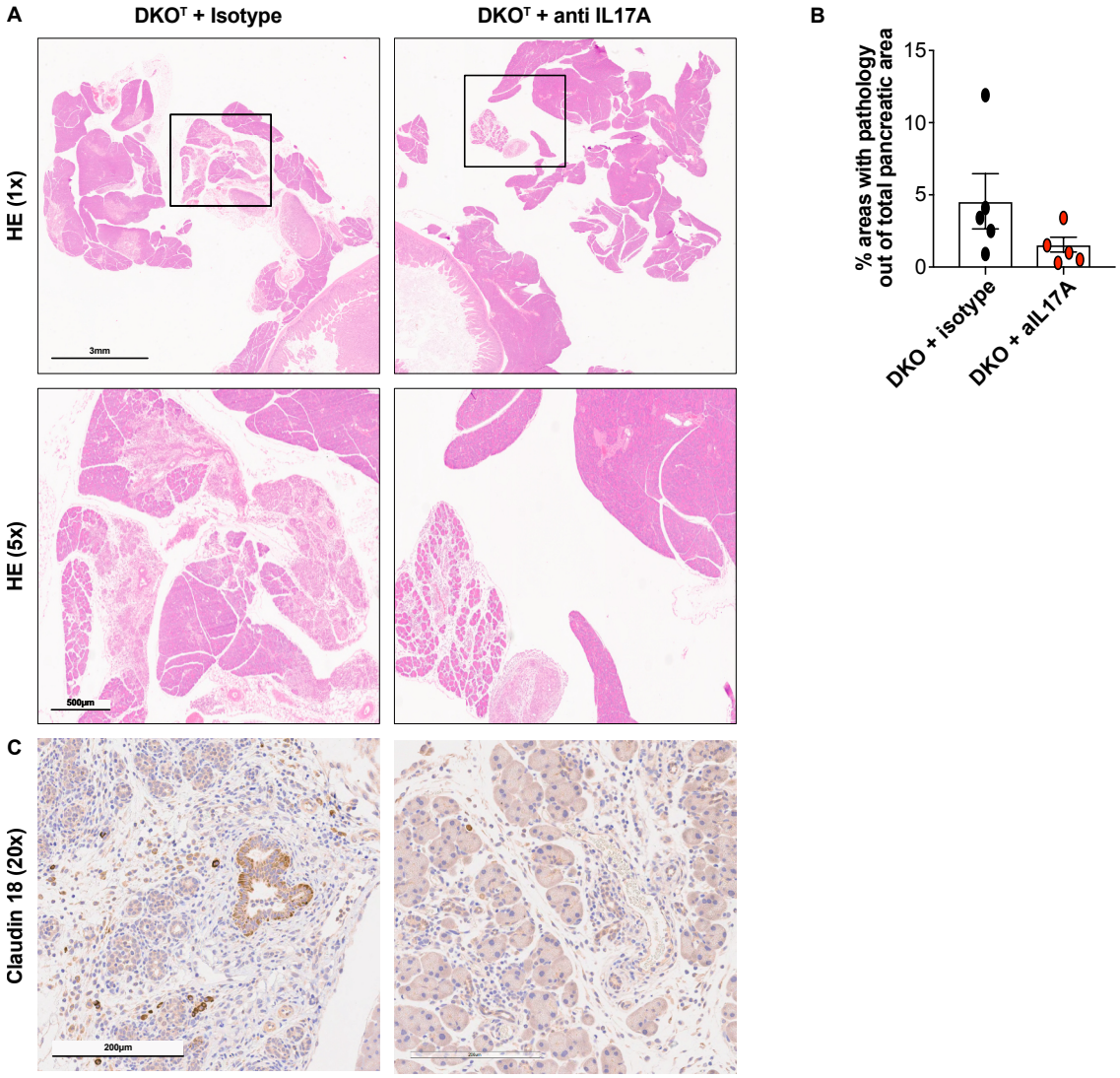

Fig. 51: IL-17A neutralization improves pancreas phenotype in 20-weeks-old DKO^T mice.
(A) Representative H&E sections showing the whole pancreas (upper panel) of DKO^T mice treated with anti-IL17A neutralizing antibody or an isotype control. Black boxes mark areas selected for higher magnification images (lower panel). **(B)** Quantification of the percentage of pancreatic areas affected by pathological changes. **(C)** Pancreas sections stained for Claudin 18. Data presented as Mean ± SEM. Data are representative for at least 5 biological replicates per group. Statistical significance was determined by unpaired, one-tailed t test. Histological stainings were performed by AG Heikenwälder (Danijela Heide, Jenny Hetzer).

To further confirm the nature of the lesions, Claudin 18 staining was performed to identify whether these changes were early pre-neoplastic transformations. Indeed, DKO^T mice had Claudin 18 positive cells within the areas of the pancreas that exhibited pathologies, whereas no Claudin-18 positive cells could be detected in tissues taken from DKO^T mice treated with IL-17A neutralizing antibodies **(Fig. 51C).**

Neutralization of IL-17A in DKO^T mice strongly reduced the infiltration of $Ly6G^+$ neutrophils **(Fig. 52A,B)** similar as the effects observed on $CD11b^+$ $Gr1^+$ cells. Furthermore, less CD3+ T cells **(Fig. 52C)** infiltrated into pancreas tissue after neutralization of IL-17A.

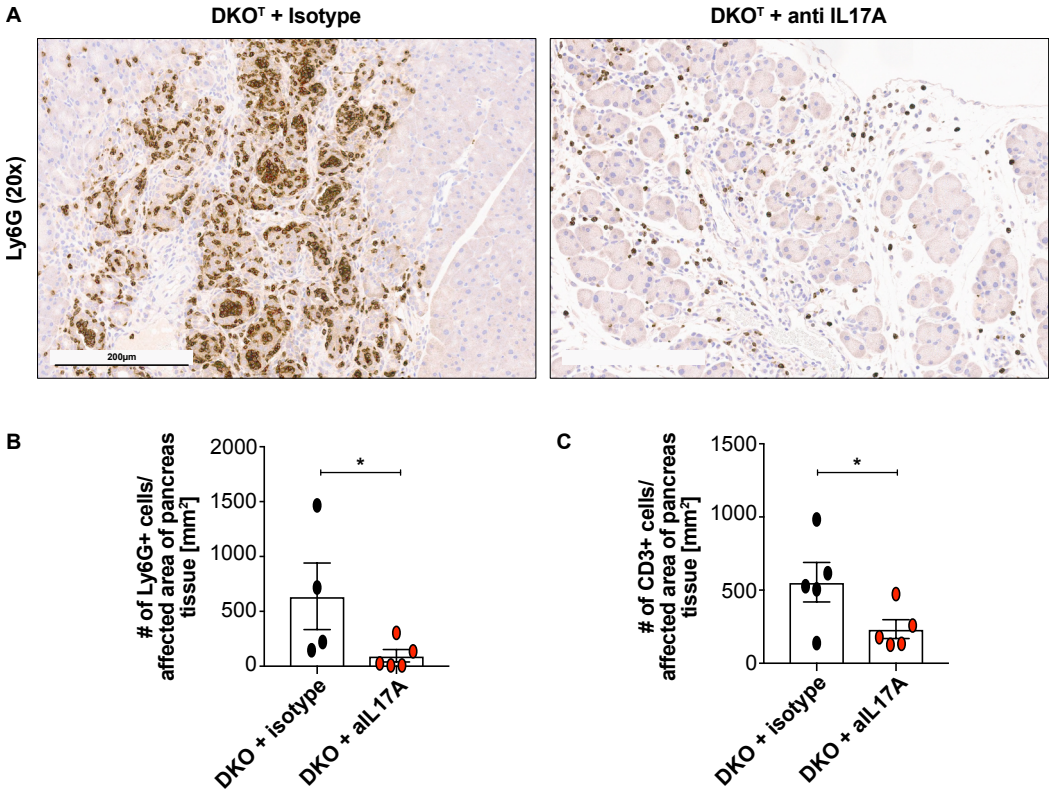

Fig. 52: IL-17A neutralization reduces immune cell infiltration into pancreas tissue of DKO^T mice. **(A)** Representative immunohistology stainings showing $Ly6G^+$ cells in pancreas tissue of DKO^T mice treated with anti-IL17A or isotype control and **(B)** quantifications thereof. **(C)** Quantification of tissue infiltrating $CD3^+$ T cells. Each point represents the average cell count in three high power fields (20x magnification) per pancreas. Data are representative for 5 biological replicates per group. Statistical significance was determined by unpaired, one-tailed t test. * $p<0.05$.

Taken together these data support the hypothesis, that T_H17 cells and the production of IL-17A in the DKO^T mouse model drives local inflammation and neoplastic transformations in the pancreas.

In summary, in the second part of this work I focused on extrinsic effects of Roquin-1/2-deficient T cells during the development of pancreas pathology and early stages of neoplasia. Mice with Roquin-1/2-deficiency in T cells spontaneously developed pancreas pathology and low grade pre-neoplastic panIN lesions. Higher incidence of pancreas pathology was correlated with a higher age of DKO^T mice. In these mice, inflammatory $CD11b^+$ $Gr1^+$, T_H17 and T_{FH} cells accumulated, both systemically as well as locally in the pancreas draining lymph node and $Ly6G^+$ neutrophils infiltrated into pancreas tissue. Reconstitution of mice harboring and acinar cell-specific $Kras^{G12D}$ mutation with bone marrow taken from DKO^T mice lead to accelerated cancer development and progression, due to a local accumulation of inflammatory cells in the pancreas microenvironment.

Pancreas pathology in DKO^T mice as well as cancer progression in $Kras^{G12D}$ mice reconstituted with DKO^T bone marrow is correlated with strongly elevated systemic G-CSF levels. Neutralization of G-CSF in $Kras^{G12D}$ mice reconstituted with DKO^T bone marrow lead to an improved pancreas phenotype, comparable to the phenotype observed in $Kras^{G12D}$ mice which were reconstituted with WT bone marrow.

$CD4^+$ T cells isolated from DKO^T mice produced G-CSF both *in vivo* and *in vitro* suggesting that Roquin proteins play a role in preventing tissue inappropriate expression of some target genes. However, systemic elevation of G-CSF levels in DKO^T mice was predominantly caused by IL-17A producing T_H17 cells rather than $CD4^+$ T cell produced G-CSF. Neutralization of IL-17A in these mice strongly reduced G-CSF levels, neutrophil infiltration into the pancreas and pancreas pathology, suggesting that local inflammation and formation of pre-neoplastic panIN lesions is driven by IL-17A producing T_H17 cells.

5. Discussion

In this project, cell-extrinsic consequences of Roquin-1 and Roquin-2 deficiencies in T cells were studied.

In the first part of the thesis, I focused on the extrinsic effect Roquin-1/2-deficent T cells have on other immune cells. First of all, I demonstrated that Roquin-1/2 loss-of function in T cell has both cell intrinsic as well as cell extrinsic consequences, whereas loss-of-function of Regnase-1 controls T cell activation and differentiation in an intrinsic manner. In adoptive transfer experiments, I showed that DKO^{T} T cells cause bystander activation of WT $CD8^{+}$ T cells, bystander T_{FH} differentiation of WT $CD4^{+}$ T cells and concomitant accumulation of GC B cells. T_{FH} cell differentiation did not require IFNγ, IL-6 or ICOS signaling in recipient cells. It was independent of SAP signaling but did require interactions with B cells. Furthermore, DKO^{T} cells were able to replace co-stimulatory signals that potently activated bystander T cells which lacked normal B7-mediated CD28 stimulation. Several molecules that could be responsible for the observed *trans*-effect were identified in an mRNASeq experiment and two promising candidates were further investigated.

The second part of the thesis focused on extrinsic functions of DKO^{T} cells that affected non-immune cells. Specifically, I showed that mice with conditional Roquin-1/2 deletion in T cells spontaneously developed pancreas pathology and pre-neoplastic low grade PanIN lesions. In these mice, inflammatory $CD11b^{+}$ $Gr1^{+}$, $T_{H}17$ and T_{FH} cells accumulated, both systemically as well as locally in the pancreas draining lymph node and $Ly6G^{+}$ neutrophils infiltrated into pancreas tissue. Reconstitution of mice harboring an acinar cell-specific $Kras^{G12D}$ mutation with bone marrow taken from DKO^{T} mice led to accelerated cancer development and progression, due to a local accumulation of inflammatory cells in the pancreas microenvironment.

The third part of the thesis was dedicated to the identification of molecules and mechanisms involved in the spontaneous development of pancreas pathology in DKO^{T} mice. I showed tissue inappropriate production of G-CSF by DKO^{T} $CD4^{+}$ T cells and demonstrated that Roquin proteins regulated the expression of this cytokine through the 3'UTR of the G-CSF encoding mRNA. Furthermore, I demonstrated that IL-17A producing $T_{H}17$ cells drive spontaneous development of pancreas pathology in DKO^{T} mice by increasing systemic G-CSF levels and the recruitment of pro-inflammatory neutrophils into the pancreas.

Discussion

5.1 Roquin-1/2-deficiency in T cells affects other immune cells in *trans*

5.1.1 T cell extrinsic and intrinsic functions of Roquin-1/2 and Regnase-1 deficiencies

In a collaborative research project on Roquin-1/2 and Regnase-1 function and physical interaction and as part of a recently accepted manuscript (Behrens *et al.*, 2021) I analyzed phenotypes of mice with Roquin-1/2 and Regnase-1 deficiencies in T cells. The findings from these analyses comprised T cell intrinsic and extrinsic effects and describe an essential molecular interaction of these RNA-binding proteins in the prevention of autoimmunity. The described interaction of these RBPs in post-transcriptional gene regulation address a longstanding controversy whether these RBPs regulate their overlapping target set cooperatively (Jeltsch and Heissmeyer, 2016; Jeltsch *et al.*, 2014) or separately (Mino *et al.*, 2015).

Specifically, we found out that $CD4^+$ and $CD8^+$ T cells isolated from $iDKO^T$, iKO^T and $iTKO^T$ mice spontaneously acquired activation phenotypes and $CD4^+$ T cells upregulated T_{FH} associated markers **(Fig. 13 and Fig. 14).** Both, Roquin-1/2 and Regnase-1 contributed equally to the T cell intrinsic phenotypes and a combined ablation of both RBPs, exacerbated the T cell intrinsic phenotype, suggesting that these RBPs cooperate in the same pathways (Behrens *et al.*, 2021). Regnase-1-deficiency also imparted a T cell intrinsic pro-survival phenotype which could not be observed in DKO^T or TKO^T cells as evidenced by increased persistence of iKO^T cells within the WT recipients. Neither T cells derived from $iDKO^T$ nor $iTKO^T$ mice were able to survive within WT recipients **(Fig. 14).** Since Regnase-1 expression is controlled by Roquin and Regnase-1 cooperative post-transcriptional regulation, Regnase-1 protein levels are strongly increased in DKO^T T cells (Behrens *et al.*, 2021; Braun *et al.*, 2018; Jeltsch *et al.*, 2014). Given Regnase-1-deficiency seemed to promote T cell persistence (**Fig. 14** and (Uehata *et al.*, 2013)) increased Regnase-1 levels in $iDKO^T$ T cells can potentially explain the loss of these cells after adoptive transfer.

T cells from $iDKO^T$ and iKO^T donors induced an increase in WT GC B cells after adoptive transfer. In mouse models that address Roquin-1 loss-of function in the hematopoietic versus the T cell compartment **(Fig. 15)**, we found that the involved spontaneous T cell activation and GC B cell accumulation also had T cell extrinsic components. My analysis of the endogenous the $CD4^+$ T cell compartment in WT mice after adoptive transfer of either $iDKO^T$, iKO^T or $iTKO^T$ T cells, revealed a T cell extrinsic

role of Roquin-1/2-deficiency but not Regnase-1-deficiency on T_{FH} differentiation. Peripheral Regnase-1-/- $CD4^+$ T cells have previously been suggested to be able to activate immune cells in *trans* (Uehata et al., 2013). This is in line with the observed effects on GC B cells and an induction of ANAs in my long term adoptive transfer experiments (Behrens *et al.*, 2021).

5.1.2 Characterization of the *trans*-effect induced by DKO^T T cells

Having established that adoptive transfer of DKO^T T cells into WT recipient mice also drives T_{FH} differentiation in WT T cells, I aimed to characterize the *trans*-effect in detail and to identify affected cells. I hypothesized that Roquin-1/2 deficient T cells inappropriately produce factors that work in *trans* and affect other cells of the immune and non-immune cell compartments.

I established three experimental set ups, all of which robustly induced T_{FH} differentiation in WT recipient mice **(Fig. 17).** Transfer of T cells combined with Tamoxifen inducible deletion of Roquin-1 and Roquin-2 proteins encoding alleles induced T cell intrinsic as well as T cell extrinsic effects. Furthermore, this inducible system allowed to study the contribution of $CD8^+$ Roquin-1/2-deficient T cells to the effect, since no conditional $CD8^+$ T cell specific knock out was available to us. However, this set up was more stressful for the recipient mice, and was therefore not further pursued.

T_H1 cells are one of the predominant $CD4^+$ effector T cell subsets in DKO^T mice (Jeltsch *et al.*, 2014). Using *in vitro* activated and differentiated T_H1 cells isolated from WT or DKO^T mice with constitutive or inducible expression of the cre recombinase robustly induced the *trans*-effect on WT T_{FH} cells. Surprisingly, whereas DKO^T T_H1 cells derived from *Cd4*-cre donors were almost completely cleared by the recipient mice 8 days after transfer, DKO^T T_H1 cells that were treated with 4'OH-Tamoxifen prior to *in vitro* differentiation strongly expanded within the WT host, making up half of the $CD4^+$ T cell population on day 8 after transfer **(Fig. 17).** I decided to mainly focus on the DKO^T T_H1 transfer condition to exclude secondary changes caused by the strong expansion and competition with donor cells.

Besides driving T_{FH} differentiation in recipient mice, adoptive transfer of DKO^T T cells also strongly induced bystander activation and increased proliferation of recipient $CD8^+$ T cells, accompanied by a down-regulation of surface CD8 expression on these

cells. These effects were caused exclusively by Roquin-1/2-deficient $CD4^+$ T cells, since adoptive transfer of $CD8^+$ DKO^T cells did not recapitulate any of the described effects **(Fig. 18 and Fig. 19).**

Adoptively transferred DKO^T T cells were nearly completely cleared from the WT host on the day of analysis, however the *trans*-effect remained. Given that DKO^T T cells show a strong activation phenotype, I was wondering whether these cells underwent activation induced cell death (Kabelitz and Janssen, 1997), which would lead to an increased release of factors that can be taken up by WT DCs and presented or cross-presented to endogenous T cells. It has been previously reported that murine DCs can take up cell fragments or soluble peptides from apoptotic virus infected cells and activate MHC class I-restricted $CD8^+$ T cells through cross-presentation (Albert et al., 1998a; Albert et al., 1998b; Fossum and Rolstad, 1986). Adoptively transferred WT and DKO^T T cells showed similar levels of apoptosis and necrosis, suggesting that factors released during apoptosis are not likely to cause the observed *trans*-effect.

Given that on the one hand, adoptively transferred DKO^T cells have increased proliferative capacity **(Fig. 13C)** and do not undergo increased cell death **(Fig.20),** but on the other hand DKO^T $CD4^+$ T cells (but not DKO^T $CD8^+$ T cells **(Fig. 17 and Fig. 19)**) disappear from the recipients' system, questions arise concerning the fate of these cells. One possibility is that these cells home or infiltrate into different tissues of the recipient mice which would be in line the fact that mice with T cell-specific ablation of Roquin-1/2 show T cell infiltrates in lung tissue (Jeltsch *et al.*, 2014) and mice harboring a homozygous Roquin-1^{M199R} mutation show lymphocytic infiltrations into kidneys (Choi et al., 2019). It would be interesting to ask whether DKO^T $CD4^+$ cells that infiltrate into tissues lead to pathological changes? However, this question was beyond the scope of this study and should be addressed in future work.

5.1.3 Dissecting the role of IFNγ, IL-6 and ICOS signaling

I next assessed the role of IFNγ, IL-6 and ICOS signaling as potential *trans*-acting factors, as all three molecules have been shown to be important in T_{FH} differentiation (Choi *et al.*, 2011; Lee *et al.*, 2012; Nurieva *et al.*, 2008). All three molecules have been proposed to be directly regulated by Roquin proteins and are known to be excessively produced by DKO^T T cells (Jeltsch *et al.*, 2014; Lee *et al.*, 2012; Pratama *et al.*, 2013; Tan *et al.*, 2014). Adoptive transfer of i*n vitro* differentiated or DKO^T T_H1

cells into IFNγR-/-, IL6Rα-/- or ICOS-/- recipient mice did not prevent aberrant T_{FH} differentiation of recipient $CD4^+$ T cells **(Fig. 21 and Fig. 22)**.

Previous studies showed that lack of IFNγ receptor on T cells from sansan mice strongly reduced their intrinsic ability to differentiate into T_{FH} cells and that excessive IFNγ signaling leads to an enhanced Bcl-6 expression specifically in T cells (Lee *et al.*, 2012; Zhou and Ono, 2005). My data suggests that the *trans*-acting factor which is produced by DKO^T $CD4^+$ T cells seems to be able to bypass a potential need for IFNγ signaling.

Bcl6 expression is induced by STAT3 and repressed by STAT5 signaling (Nurieva et al., 2012; Oestreich et al., 2012; Walker et al., 2013). The *trans*-acting factor may therefore be able to activate the STAT3 signaling pathway and in this way promote T_{FH} differentiation. One molecule, which is known to induce both STAT3 and STAT1 signaling as well as transient Bcl6 expression is IL-6 (Hirano et al., 1997; Nurieva *et al.*, 2009) and mice deficient in IL-6 had significantly impaired production of early T_{FH} cells in response to acute viral infections (Choi et al., 2013a). Therefore, I expected that in recipient mice which are lacking IL6Rα and are not able to respond to IL-6 signaling endogenous T_{FH} differentiation should be impaired. To my surprise, adoptive transfer of DKO^T T cells also induced endogenous T_{FH} cells. Since the effects on endogenous T_{FH} cells were only moderately reduced in comparison to adoptive transfer of DKO^T T cells into WT recipients, these findings suggested that IL-6 signaling in this system may be involved but does not play crucial roles. Other studies have suggested that IL-6 signaling can be almost entirely replaced by IL-27 induced activation of STAT3 signaling (Batten et al., 2010; Harker et al., 2013; Vijayan et al., 2016). IL-27 is a cytokine which belongs to the IL-12/IL-6 family and is made up of two subunits, IL-27p28 and EBI3, which for a heterodimeric complex and can signal via gp130, one of the subunits of the IL-6 receptor (Hall et al., 2012; Yoshida and Hunter, 2015). Signaling via IL-6 and IL-27 have also been described to induce overlapping gene signatures (Hirahara et al., 2015). Ebi3, on the other hand, was one of the top hits when comparing mRNA profiles between WT and DKO^T T cells **(Fig. 25)** and IL-27 was also increased in the sera of DKO^T mice. Additionally, IL-27 has been linked to an increase of memory $CD8^+$ T cells in response to vaccination and cancer and to promote $CD8^+$ T cell function *in vitro* (Liu et al., 2013; Morishima et al., 2005; Pennock et al., 2014). In conjunction with previously published literature my results point towards a role of Ebi3 in the development of the DKO^T $CD4^+$ T cell-mediated *trans*-

effect on T_{FH} differentiation and $CD8^+$ T cell activation in WT recipient mice. Interestingly, when I simulated folding of the Ebi3 3'UTR using RNAfold, I did not detect any structures that would suggest obvious recognition of this RNA by Roquin proteins. However, this analysis should be reassessed in light of the most recent findings concerning Roquin interactions with some targets that have unconventional binding sites (Binas *et al.*, 2020; Braun *et al.*, 2018). The possibility, that the observed *trans*-effect may be caused by transfer of DKO^T cells through molecules that may not be direct targets but appear deregulated as a secondary effect of Roquin-1/2-deficiency, further complicates the search for the *trans*-acting factor. Ebi3 is an interesting candidate, however time constraints did not allow to further pursue this molecule with sophisticated mouse genetics in the course of this study, but an investigation of its function as *trans*-acting or disease-driving factor in the DKO^T mouse should be addressed in future work.

T_{FH} differentiation is highly dependent on ICOS signaling, which is required both during early priming of T cells by DCs as well as during B cell:T cell interaction. And T_{FH} differentiation is severely impaired when ICOS signaling is abrogated (Akiba *et al.*, 2005; Choi *et al.*, 2011; Gigoux et al., 2009). So how is it possible, that adoptive transfer of DKO^T cells can drive the T_{FH} program in ICOS-/- T cells **(Fig. 22)** ICOS in T_{FH} differentiation has been shown to induce Bcl6 expression which in turn leads to the upregulation of CXCR5 (Choi *et al.*, 2011). However, Bcl6 expression can also be enhanced by other factors, one of which is IL-21, one of the effector cytokines of T_{FH} cells (Nurieva *et al.*, 2009). ICOS signaling leads to an increase of IL-21 and IL-21 together with IL-6 drive T_H1 differentiation (Bauquet et al., 2009; Eto *et al.*, 2011; Hiramatsu et al., 2010). Given that DKO^T $CD4^+$ cells acquire a T_{FH} phenotype upon adoptive transfer into WT recipient mice **(Fig. 14)**, I can speculate that the *trans*-effect in ICOS-/- recipients can be explained by possible IL-21 production by transferred Roquin-1/2-deficient T cells which, potentially in collaboration with increased IL-27 (or Ebi3) levels **(Fig. 25)**, drives T_{FH} differentiation of recipient cells. Furthermore, it is possible that CD28 signals can compensate for ICOS deficiency.

5.1.4 Dissecting the contribution of B cells, SAP signaling and co-stimulation to the *trans*-effect

T_{FH} cells are necessary for the development of functional germinal centers, which give rise to high-affinity antibody producing memory B cells and plasma cells (Allen et al., 2007; Crotty, 2019). As described in the introduction, several molecular pathways and interactions with DCs and B cells are required for T_{FH} differentiation. SAP is an intracellular adapter molecule which interacts with SLAM family receptors on T and B cells. Its expression in $CD4^+$ T cells is crucial for the prolonged interaction of T cells with their cognate B cell but is not required for T cell interactions with DCs, and SAP-deficient mice show severely decreased GC T_{FH} cell numbers (Cannons *et al.*, 2010; Cannons et al., 2011; Qi *et al.*, 2008). µMT mice lack mature B cells and cannot form cognate T cell:B cell interactions (Haynes *et al.*, 2007; Johnston *et al.*, 2009), which severely impairs T_{FH} cell development (Choi *et al.*, 2011).

The fact, that DKO^T T cells are able to induce T_{FH} differentiation in SapKO mice but not in µMT mice, suggests that early DC interaction and the presence of B cells but not prolonged interactions between T and B cells are required for the *trans*-effect. DKO^T T cell-mediated T_{FH} differentiation in SapKO mice was decreased when compared to WT mice **(Fig. 24).** These data point towards the possibility that DKO^T $CD4^+$ T cells can induce early T_{FH} differentiation in a DC dependent manner but the *trans*-effect overrides the normal requirement for prolonged T cell:B cell interactions and essential signals from B cells.

Co-stimulation of T cells by CD28 interaction with its ligands CD80 and CD86 is an important step in T cell activation and is required for the differentiation into effector subsets (Janeway and Medzhitov, 2002). CD28-deficient mice have impaired GC formation and T cells derived from these mice show reduced CXCR5 or Ox40 expression. However, in the san/san mouse, T cell intrinsic defects in T_{FH} differentiation due to CD28 ablation can be overcome by ICOS overexpression caused by defective *Icos* mRNA repression (Linterman *et al.*, 2009a; Walker et al., 1999). To test whether co-stimulation was required for the *trans*-effect, I adoptively transferred WT or DKO^T $CD4^+$ T cells into CD80/CD86 KO recipients. Even though these mice do express CD28 on T cells, signaling via CD28 does not occur, due to the absence of both ligands on APCs. Thus, no co-stimulatory signal is available for T cells in these mice. Consistent with a need for co-stimulation for T_{FH} differentiation, adoptive transfer of DKO^T $CD4^+$ T cells did not induce T_{FH} differentiation in CD80/CD86 KO mice **(Fig.**

24). Surprisingly, the *trans*-effect on the endogenous $CD8^+$ T cell compartment was striking **(Fig. 23)**. Adoptive transfer of DKO^T $CD4^+$ T cells induced strong activation and proliferation of $CD8^+$ T cells in CD80/CD86 KO mice. These data suggests that the molecular requirements for the *trans*-effect on T_{FH} level are different from the requirement for the *trans*-effect on the level of $CD8^+$ T cell activation, and that DKO^T CD4 T cells may produce several *trans*-acting factors that affect different cells in different manners. These data also point towards the ability of DKO^T T cells to provide a co-stimulatory signal to bystander $CD8^+$ T cells, possibly via CD28 engagement.

This notion is supported by results obtained from analyzing an RNA sequencing data set, where differential gene expression between WT and DKO^T T_H1 cells was determined **(Fig. 25).** Two strongly upregulated surface expressed molecules on DKO^T T cells were CD86 as well as CD40L, both of which have the potential to cause the *trans*-effect described in this study. CD40-CD40L interactions between T cells and DCs during the priming stage of T_{FH} development are known to be crucial for effective T_{FH} differentiation. And CD40L deficiency leads to reduced T_{FH} cell numbers (Bossaller *et al.*, 2006; Choi *et al.*, 2011; MacLennan, 1994). However, in validation experiments it became apparent that CD40L, was not likely to cause the *trans*-effect, since DKO^T $CD4^+$ T cells at the time of transfer did not show increases on transcript or protein level. In DKO^T T_H1 cells CD40L, expression was only elevated 48h after anti-CD3/anti-CD28 stimulation and returned to similar levels as observed on WT cells immediately after **(Fig. 26).**

On the other hand, CD86, a ligand for CD28 and CTLA-4, which is constitutively expressed on APCs (Boussiotis et al., 1993; Hathcock et al., 1994; Lanier et al., 1995), was strongly elevated in DKO^T $CD4^+$ T cells both, on the transcript as well as on the protein level. Furthermore, CD86 expression increased over time on *in vitro* cultivated DKO^T T_H1 cells and strongly elevated expression was observed in adoptively transferred DKO^T T cells after re-isolation from WT recipient mice. These findings provide a possible explanation for the strong activation of $CD8^+$ T cells in CD80/CD86 KO mice in response to adoptive transfer of DKO^T T cells. DKO^T T cells may be able to interact with CD28 on the surface of recipient T cells and thus lead to increased activation and proliferation. This opens up the possibility that DKO^T $CD4^+$ T cells are able to replace the function as APCs by possibly directly interacting with recipient T cells.

As CD86 appeared to be a good candidate that may explain at least parts of the observed *trans* effect, I tested whether overexpression of CD86 in WT cells could induce the *trans*-effect. Overexpression of CD86 on WT cells did not induce increased T_{FH} differentiation or CD8+ T cell activation. Also, overexpression of CD86 on DKO^T T cells did not exacerbate the *trans*-effect(s) **(Fig. 27)**. These results do not rule out CD86 as a potential *trans*-acting factor, since this experiment has several limitations. It is not clear how long CD86 is expressed in transduced T cells after transfer into WT recipient mice. It can well be, that it is downregulated shortly after transfer, before it can exert an effect. Since CD86 expression on DKO^T cells is already very high **(Fig. 25 and Fig. 26)** it is possible that the requirement for CD86 co-stimulation by DKO^T cells are already satisfied by the existing levels, and thus further overexpression, cannot exacerbate the effect. Furthermore, these data and the described effects in different knock-out systems suggest, that the *trans*-effect cannot be reduced down to one single event or deregulated molecule. It may rather develop due to the concerted effect of a number of directly and indirectly deregulated molecules in DKO^T cells. Furthermore, there is a high possibility that the factor(s) that induce T_{FH} differentiation or $CD8^+$ T cell activation may be different.

A better way to assess the contributions of CD86 to the *trans*-effect would be to generate DKO^T mice with additional either systemic or T cell specific CD86 knock out and use $CD4^+$ T cells isolated from these mice for adoptive transfer experiments or to transfer DKO^T $CD4^+$ T cells into CD28-/- hosts. However, the acquisition and establishment of these new mouse lines did not fit into the time frame of this study. Another possibility is to use the CRISPR/Cas9 technology to delete CD86 in DKO^T T cells, which should also give more reliable results on the role of CD86 in the DKO^T T cell-induced *trans*-effect. Currently, I am gearing up to establish the technology to perform this experiment.

5.1.5 Summary of findings and future perspectives

In the first part of this thesis, I have aimed to comprehensively describe the *trans*-effect exerted by DKO^T $CD4^+$ T cells on WT T_{FH} and T_H1 cells, and I have attempted to identify molecules that may cause or contribute to the *trans*-effect. The findings derived from a series of adoptive transfer experiments are summarized in Fig. 5.1.5.

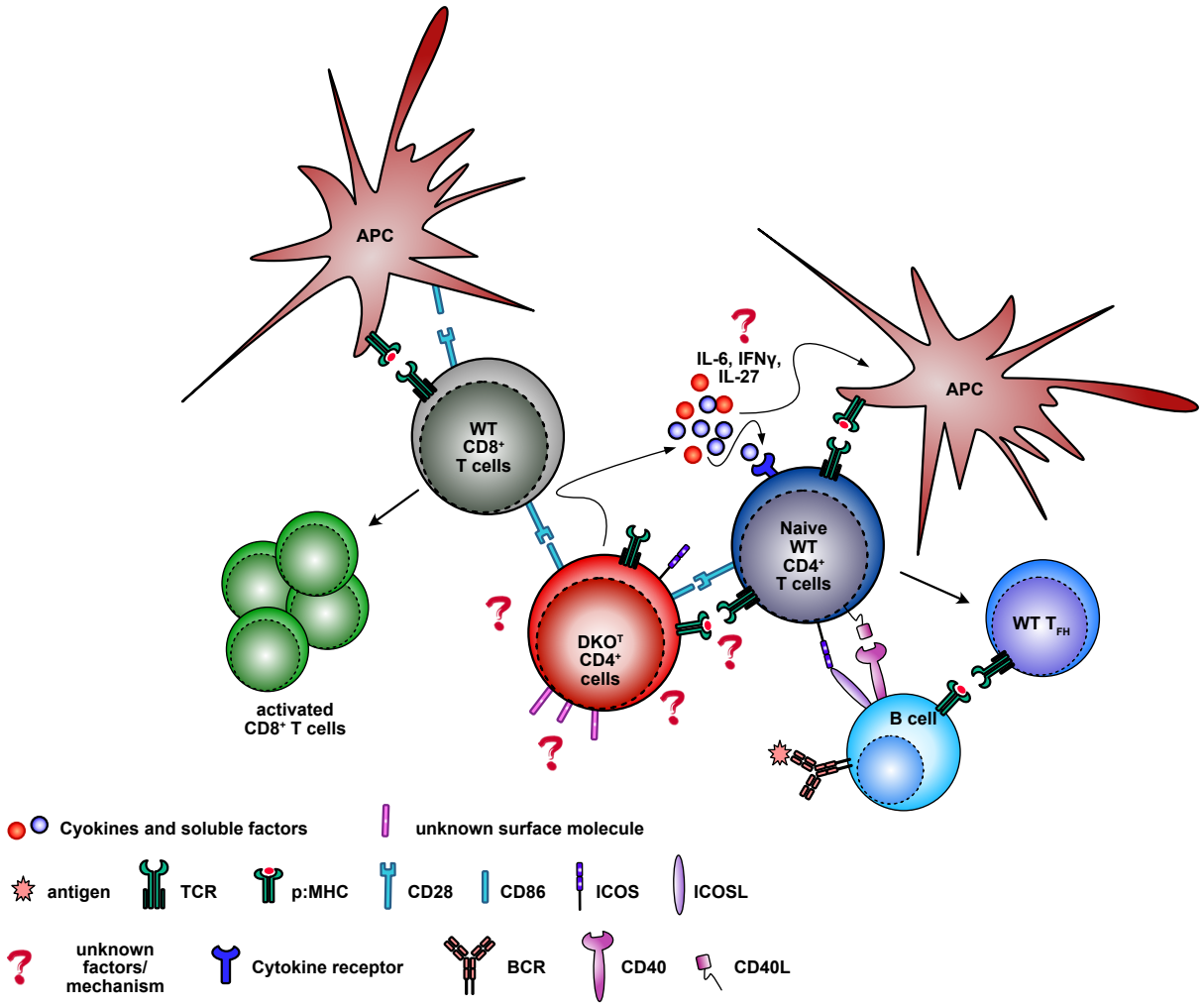

Fig. 53: Schematic overview over T cell extrinsic functions of Roquin-1/2 deficiency.
Roquin-1/2-deficient T cells induce bystander activation of $CD8^+$ WT T cells as well as a bystander $CD4^+$ differentiation into T_{FH} cells. T_{FH} cell differentiation does not require IFNγ, IL-6 or ICOS signaling in recipient cells. It is independent of SAP signaling but does require interactions with B cells. DKO^T cells were able to replace co-stimulatory signals that potently activated bystander T cells which lacked normal B7-mediated CD28 stimulation.

As detailed in the first part of the discussion, a number of questions still remain to be addressed. For instance, it is not clear what happens to the adoptively transferred DKO^T T cells inside the WT recipient mice. I did not find signs of elevated apoptosis and these cells strongly proliferated, however I cannot detect them in the spleens of the recipient mice 8 days after transfer. Thus, it is important to address the fate of these cells with a focus on trafficking and homing to tissues, especially given that T cells in DKO^T mice have the potential to cause organ inflammation and damage, as described in Sections 4.2 and 4.3 in this study as well as in (Jeltsch *et al.*, 2014).

Furthermore, the results obtained in this work, point towards the possibility that DKO^T T cells may be able to induce activation comparable to APCs. However, it is not clear whether these cells can also present antigen to bystander T cells or whether they affect WT APCs, for example via increased licensing of WT DCs through CD40-CD40L interactions, which then act on WT T cells and lead to increased T_{FH} differentiation and CD8$^+$ T cell activation. T cell activation and differentiation normally requires TCR interaction with a cognate p:MHC complex (signal 1), which is important for T_{FH} differentiation (Benson et al., 2015; Tam et al., 2016). In this study, I only addressed the contributions of signal 2 (i.e. co-stimulation) and signal 3 (cytokine milieu) to the *trans*-effect. Whether or not WT T cells receive signal 1 from the transferred DKO^T T cells, and if yes, what is the antigen that is required for the *trans* effect, remains to be answered in future work. One possibility to assess the contribution of TCR signaling would be to generate triple knock out mice with systemic deletion of MHC II in addition to T cell-specific ablation of Roqui-1 and Roquin-2, and use these mice to generate mixed bone marrow chimeras. In this system, the contribution of antigen presentation by DKO^T cells to the *trans*-effect can be confirmed or ruled out unambiguously.

Even though, in addition to CD86, several other promising candidates for the *trans*-acting factor were detected in the mRNASeq data (e.g. Ebi3, Tnfsf13b (APRIL), Tnfsf14 (LIGHT)) **(Fig. 25)**, we were not able to pursue the search for the *trans*-acting factor beyond this point. Experimentally addressing all potential candidates would have required a significantly higher amount of time and more sophisticated genetic systems for experimentation. Due to the multifaceted way of T_{FH} differentiation, we also expect multiple factors to be involved in the *trans*-effect. To date there is no robust *in vitro* T_{FH} differentiation assay available, meaning that all validation steps need to be carried out *in vivo*, involving mouse genetics and legal constraints of this type of validation, which again extends the required time frame.

5.2.1 Roquin-1/2-deficiency in T cells drives spontaneous development pancreas pathology

In the second and third part of this study, I focused on T cell extrinsic effects in DKO^T mice which are directed towards non-immune cells, namely towards acinar cells of the exocrine pancreas. I aimed to describe the pancreas phenotype in DKO^T mice in detail

and identified the mechanism whereby Roquin-1/2-deficient T cells act in concert with pro-inflammatory neutrophils to cause pancreas pathology. Since phenotype and mechanism are closely related to each other, they will be discussed together.

5.2.2 Pancreas phenotype in DKO^{T} mice is driven by chronic inflammation

In previous studies, Roquin-1/2-deficiency in T cells or systemic hypomorphic function in sanroque mice have been associated with inflammatory conditions in different organs and DKO^{T} mice have been shown to produce antibodies directed towards pancreas tissue antigens (Choi *et al.*, 2019; Jeltsch *et al.*, 2014; Linterman *et al.*, 2009b). When analyzing pancreas tissue taken from WT and DKO^{T} mice of various ages, it became apparent that DKO^{T} mice were prone to develop pathological changes of the pancreas, leading up to pre-neoplastic low grade PanIN lesions **(Fig. 28 and Fig. 34)**. The incidence of pancreas pathology increased with age **(Fig. 28)** and was characterized by immune cell infiltration into pancreas tissue and draining LNs **(Fig. 29)**, systemic and local expansion of T_H17, T_{FH} **(Fig. 31)** and CD11b^{+} Gr1^{+} cells **(Fig. 30)**, and increased proliferation of inflammatory cells in the pancreas tissue **(Fig. 29 and Fig. 33)**. These data suggest that DKO^{T} mice suffered from inflammation in the pancreas tissue which over time culminated in the development of pre-neoplastic lesions. Chronic pancreatitis is one of the major risk factors linked to the development of pancreatic cancer and inflammation is also one of the hallmarks of cancer (Hanahan and Weinberg, 2011).

A widely used model to study the relationship of inflammation and the development of pancreas cancer is cearulein induced pancreatitis. Treatment of mice with cearulein triggers inflammation, necrosis and transient formation of ADMs (Lampel and Kern, 1977). Upon resolution of inflammation ADMs readily transdifferentiated into normal acinar cells, and progression to PanIN and PDAC could only be observed in the presence of oncogenic Kras signaling. Several groups investigated the relationship between pancreatitis and the development of PanIN lesion, showing that caerulein induced chronic pancreatitis as well as short recurrent boosts of pancreatitis could indeed drive PanIN development in the presence of oncogenic Kras signaling (Guerra *et al.*, 2011; Guerra *et al.*, 2007). *In vivo* lineage trancing experiments identified that chronic inflammation played a major role in EMT (epithelial-to-mesenchymal

transition) and in the acquisition of cancer stem cell like properties, and promoted invasiveness (Rhim *et al.*, 2012).

All the above-described studies about inflammation-induced pancreas cancer development and progression was assessed in the context of genetically engineered mouse models that harbor one or more known cancer driving mutations, at least one of which was an oncogenic Kras mutation. In contrast, DKO^{T} mice develop low grade, pre-neoplastic panIN lesions spontaneously, showing that chronic inflammation in the pancreas due to Roquin-1/2-deficiency in T cells drives neoplasia before signaling from mutant Kras proteins engages the formation of the tumor. To my knowledge, the DKO^{T} mouse is the first mouse model with spontaneous, T cell-driven pancreas neoplasia occuring independently from pro-tumorigenic genetic alterations in acinar cells. Moreover, this model does not require any additional manipulations, like high-fat diet or caerulein treatment (Dennaoui et al., 2021; Kong et al., 2020).

A recent study provides some intriguing evidence on the mechanisms by which inflammation induces tumorigenesis in the absence of oncogenic activation. Del Poggetto and colleagues, were able to show, that inflammatory events lead to long-lasting transcriptional and epigenetic changes in acinar cells facilitating ADM and upon promoting tumor development upon Kras activation. Interestingly, acinar cells appeared to be able to develop epithelial memory, which was mediated by IL-6 signaling. Importantly, induction of oncogenic signaling long after the inflammation has been resolved still triggered the development and progression of cancer (Del Poggetto et al., 2021). In a back-to-back publication, more mechanistic insights into the role of the adaptive immune system during tumorigenesis were provided by a large scale CRISPR screen in wild-type versus immune deficient mice. According to this study, in the context of a wild-type immune system, genetic alterations that lead to loss of tumor suppressor genes are selected based on their ability to evade immune surveillance (Martin et al., 2021). In the context, of the DKO^{T} mouse model and based on the findings, from these two recent studies, I would speculate that inflammation induced through Roquin-1/2-deficient T cells leads to ADM reprogramming and possibly induces mutations in some of the affected cells. The cells that have acquired changes which facilitate neoplasia are selected thereby causing the formation of panIN lesions in the pancreata of DKO^{T} mice. However, this speculation remains to be confirmed in future studies but poses an intriguing explanation for the observed pathologies.

5.2.3 DKO^{T} cells accelerate carcinogenesis in Kras^{G12D} mice

Having established that Roquin-1/2-deficient T cells can affect acinar cells in *trans* and lead to the formation of pre-neoplastic lesions, I was wondering whether these cells can accelerate carcinogenesis when combined with the Kras^{G12D} mutation, a known cancer driving mutation present in a number of different cancers. Indeed, when young, lethally irradiated mice with an acinar cell specific Kras^{G12D} mutation were reconstituted with DKO^{T} bone marrow they developed invasive carcinoma affecting almost the whole pancreas area within 5.5-6 weeks of reconstitution **(Fig. 36)**. On the other hand, also mice reconstituted with WT bone marrow developed carcinoma, however, this development was significantly less extensive than in the DKO^{T} group. Mice with constitutively active Kras signaling spontaneously develop pre-neoplastic lesions but need an additional stimulus to drive cancer progression (Hingorani *et al.*, 2003; Hingorani *et al.*, 2005). This stimulus can be provided in form of tissue damage caused by inflammation (Guerra *et al.*, 2011; Guerra *et al.*, 2007). In this study, it is likely that the observed carcinogenesis in both groups is in part caused by radiation induced inflammation (Multhoff and Radons, 2012). However, mice reconstituted with DKO^{T} bone marrow show a significantly stronger pancreas phenotype, showing that Roquin-1/2-deficient T cells accelerate Kras^{G12D}-driven cancer progression.

Both, Roquin-1 and Roquin-2 proteins have been previously linked to different types of cancers. One study established the role of Roquin-2 in the prevention of breast cancer progression. The authors determined that in tumor cells several factors that promoted angiogenesis, like ENG, END1, VEGFB and PDGFC, were directly regulated by Roquin-2. Furthermore, reduced Roquin-2 expression in cancer cell correlated with increased expression of pro-angiogenic factors and was suggested with increased vascularization in the tumor microenvironment (Zhou et al., 2021). One of the most striking observations I made upon necropsy of Kras^{G12D} mice reconstituted with DKO^{T} bone marrow, was the presence of bloody ascites (see section 4.2.4), which could also be explained by the increased presence of pro-angiogenic factors in this system. However, the question arises as to which cells are the source of these factors? Another recent study has linked Roquin-1 downregulation to cancer progression by promoting cell-cycle arrest. It was suggested that Roquin-1 can directly regulate mRNA stability of genes associated with cell-cycle progression and suppress aberrant

proliferation of cancer cells. Furthermore, Roquin-1 downregulation was associated with poor prognosis in multiple cancers (Lu et al., 2020).

In T cells it is currently not known whether Roquin-1 and Roquin-2 regulate pro-angiogenic or cell-cycle promoting mRNAs. To date it is not known whether regulation of Roquin proteins is important in acinar cells and whether it can also contribute to neoplasia. While there is substantial knowledge on the regulation of Roquin proteins through MALT-1 cleavage in T cells, other pathways may be involved in the regulation of Roquin proteins in other cell types. For instance, it has been suggested that in B cells Roquin-2 stability is regulated by KLHL6 and PTPN14 (Choi et al., 2018a; Choi et al., 2018b). The above-described studies underline the importance of assessing whether Roquin proteins are also involved in other models of pancreatitis and can be detected in the pancreas tumor samples from patients to determine whether these proteins are indeed downregulated or cleaved in T cells infiltrating the pancreas tissue or even in the cancer cells themselves.

Throughout the time of this study, I and other colleagues have put a lot of effort into generating a monoclonal antibody which can specifically detect cleaved Roquin, which would allow us to assess Roquin cleavage in pancreas tissue. However, even though we have generated a number of promising candidates, this antibody could not yet be fully established and validated. Another possibility to detect Roquin cleavage or downregulation in an indirect manner, is to assess the upregulation of known prototypic Roquin targets, for example *Nfkbid*. In collaboration with the AG Heikenwälder we are currently validating an in-house-produced monoclonal antibody for the application in histological samples and are hoping to make use of this indirect measure to assess Roquin function in pancreas tissue in future.

Genomic instability has also been proposed to be a hallmark of cancer, since it can be detected in most cancer types and inflammation has been shown to be able to induce such instabilities (Hanahan and Weinberg, 2011; Kay *et al.*, 2019; Kiraly *et al.*, 2015). A recent study has aligned genomic rearrangements causing an increased Kras dosis as well as the acquisition of additional tumor driving mutations to PDAC development (Mueller *et al.*, 2018). To compare mutations that arise in the context of DKO^{T} T cell induced pancreas inflammation I generated primary cancer cell lines from $Kras^{G12D}$ mice reconstituted with WT or DKO^{T} bone marrow and in collaboration with the AG Rad, we performed WES analysis and defined genomic rearrangement events **(Fig. 40 and Table 18)**. Furthermore, we performed sequencing of RNA isolated from

the cell lines or primary cancer tissue, which, in addition to the cancerous cells, also contains fibroblasts, stroma and infiltrating immune cells **(Fig. 41 and Fig. 42)**. These experiments revealed that similar genetic instabilities occurred in association with accelerated tumor progression in mice that were subjected to DKO^T bone marrow reconstitution.

5.2.4 Pancreas pathology in DKO^T mice is driven by the IL-17A/G-CSF signaling axis

So far, I have gathered some strong evidence that pancreas pathology in DKO^T mice is caused by excess inflammation in the tissue. But how does inflammation translate into spontaneous development of neoplasia and tumor progression in the bone marrow chimera setting? To answer this question, I performed multiplex analysis on sera obtained from WT and DKO^T mice as well as on sera taken from $Kras^{G12D}$ mice reconstituted with WT or DKO^T bone marrow **(Fig. 43).** G-CSF in particular caught my attention, due to the observed immense upregulation occurring in both models **(Fig. 43).** Decreased G-CSF levels were also associated with decreased incidence of pancreas pathology in DKO^T mice with combined systemic Ox40 deficiency **(Fig. 44).** Interestingly, DKO^T $CD4^+$ T cells but not $CD8^+$ T cells were able to produce G-CSF *in vitro* and *in vivo*, with cells from the T_H17 subset being the best G-CSF producers **(Fig. 47).** Neutralization of G-CSF in $Kras^{G12D}$ mice reconstituted with DKO^T bone marrow reduced the portion of remodeled pancreas tissue, displaying a histology comparable to that of mice, which were reconstituted with wild-type bone marrow **(Fig. 48 and Fig. 49)**. Furthermore, neutralization of IL-17A in DKO^T mice, reduced systemic G-CSF levels and ameliorated the pancreatic phenotype **(Fig. 50 and Fig. 51).** Neutralization of either IL-17A or G-CSF caused marked reduction of $Ly6G^+$ cell infiltration into the pancreas tissue as well as reduced frequencies of systemic $CD11b^+$ $Gr1^+$ cells **(Fig. 48 and Fig. 50)**. These results placed IL-17A signaling in DKO^T upstream of G-CSF and neutrophil recruitment. In the context of my data showing that Roquin deficient T cells can and do produce G-CSF themselves this finding suggests that the T cell produced G-CSF plays only a minor role in the DKO^T mouse model of pancreas pathology. Rather an increased IL-17A production in DKO^T mice causes the systemic elevation of G-CSF, and both molecules act in a coordinated manner to recruit other pro-inflammatory cells that drive spontaneous development of neoplasia.

IL-17A signaling has been linked to cancer progression in several studies, however the molecular mechanisms of how IL-17 signaling achieves this effect are still not completely understood (Zhao et al., 2019). In lung cancer the altered local microbiota has been shown to promote tumor development in a manner that depends on γδT cells and IL-17 production, presumably by promoting the expansion of neutrophils which cause tumor cell proliferation (Jin *et al.*, 2019). An earlier study suggested that mammary tumors were also able to induce IL-17 producing γδT cells. These cells led to increased G-CSF levels, by so-far undefined mechanisms and caused an accumulation of neutrophils which ultimately promoted metastasis in distant organs (Coffelt *et al.*, 2015). IL-17 affected tumor associate fibroblasts, promoted fibrosis and recruited granulocytes and myeloid derived suppressor cells, thus creating an immune suppressive microenvironment (Mucciolo *et al.*, 2021). Furthermore, IL-17 has been shown to induce IL-6 and G-CSF production by lung cancer cells and in 3T3 fibroblasts and to recruit neutrophils (Akbay et al., 2017; Cai et al., 1998). In turn, G-CSF not only causes neutrophil mobilization, but also increases neutrophil proliferation, maturation and affects their function, creating a more suppressive, pro-tumorigenic environment and promoting survival and migration of cancer cells (Karagiannidis et al., 2020; Kumar et al., 2014; Yang et al., 2014). My results are in line with these studies, suggesting that also in the DKO^{T} mouse model tumor development and progression is mediated via the IL-17A/G-CSF axis. In this model DKO^{T} T_H17 cells release IL-17 which can act on other cells and especially on pancreatic epithelial cells, which release G-CSF in response to IL-17A stimulation. G-CSF in turn causes an increased mobilization and recruitment of pro-inflammatory neutrophils which drive further inflammation. Additionally, I have shown, that Roquin-1/2-deficient T cells can produce G-CSF which may, at least in part, contribute to the neutrophil recruitment, but T cell produced IL-17A rather G-CSF is the main driver of the pancreas phenotype and accelerated tumor progression in the $Kras^{G12D}$ bone marrow chimera model.

5.2.5 Role of Roquin-1/2 proteins in the suppression of tissue inappropriate expression of G-CSF

G-CSF was strongly upregulated in mice with T cell specific Roquin-1/2-deficiencies, but T cells are not known to secrete G-CSF. My data now make the case for a function of Roquin proteins in T cells to prevent tissue inappropriate expression of G-CSF in

addition to the known regulation of mRNAs that are typically expressed in T cells. As described above, DKO^{T} CD4^{+} T cells produced G-CSF both *in vitro* and *in vivo* **(Fig. 47)** and the 3'UTR of the G-CSF encoding *Csf3* mRNA contains a CDE element, a prototypical Roquin target loop, as well as several AREs **(Fig. 45).** In G-CSF reporter assays I furthermore showed, that Roquin does indeed regulate the G-CSF 3'UTR and that both the CDE containing SLB as well as the AREs are necessary for efficient suppression **(Fig. 46).**

Earlier studies have provided some evidence that G-CSF may be regulated by Roquin. When endogenous Roquin was immunoprecipitated in cell lysates obtained from LPS-stimulated macrophages *Csf3* was found among the top ten enriched mRNAs. However, since the CDE consensus sequence known at that time, could not be detected in the G-CSF 3'UTR it was not further considered (Leppek *et al.*, 2013).

Recently evidence from many different groups have proposed that a more relaxed sequence instead of the initially defined CDE consensus sequence is recognized. Moreover, the Roquin ROQ domain was shown to directly bind CDE-ARE tandem structures (Binas *et al.*, 2020; Braun *et al.*, 2018). Such a tri-loop structure is present in SLB of the G-CSF 3'UTR and in HEK293 cells this loop was shown to be important for mRNA repression by Roquin (**Fig. 46** and (Braun *et al.*, 2018) further supporting the notion of direct regulation of G-CSF encoding mRNA by Roquin. Interestingly, post-transcriptional regulation of G-CSF via a stem-loop destabilizing element (SLDE) located in the 3'UTR has also been proposed years before Roquin proteins were described. This SLDE did in fact contain the CDE-ARE stem-loop now known to be directly bound by Roquin (Putland *et al.*, 2002).

Direct regulation G-CSF SLB by Roquin has been verified, based on computational structure predictions and in luciferase assays (Braun *et al.*, 2018). However, this recent publication did not investigate additional contributions of the ARE to Roquin mediated regulation, which had been proposed for the Ucp3 mRNA (Binas *et al.*, 2020). AREs were initially not considered to be Roquin target structures but are known to be regulated by other RBPs, like TTP, Butyrate response factor1 (ZFP36L1) and K-homology splicing regulatory protein (KSRP) (Beisang and Bohjanen, 2012; Fu and Blackshear, 2017; Stoecklin *et al.*, 2003). Here I show that Roquin regulates G-CSF 3'UTR not only through the CDE-ARE stem-loop but also through interactions with the ARE region. I cannot exclude that additional proteins other than Roquin repress the G-CSF 3'UTR via the ARE-region. It is not yet clear, whether Roquin can directly bind

to the ARE region in the G-CSF 3'UTR or whether the regulation I observed is caused by indirect effect, however, the fact that both, the ARE-region as well as SLB are required for full repression, suggests a potential Roquin interaction with both *cis*-elements **(Fig. 46)**. These questions should be addressed in future work through detailed structure and function analyses. Furthermore, recently Dr. Taku Kureha established a robust CLIP (UV cross-linking and immunoprecipitation) protocol in our lab, based on protein and RNA crosslinking followed by immunoprecipitations, which enables the detection of direct mRNA targets as well as the identification of binding sites at a single nucleotide resolution. In future work, direct binding of Roquin proteins to AREs in the 3'UTR of *Csf3* and other mRNAs will be assessed using this technique.

5.2.6 A model for spontaneous development of pancreas pathology in DKO^{T} mice

Taken together, when integrating the data on pancreas pathology in DKO^{T} mice as presented in the second and third parts of this study with previously published mechanisms the following mechanism for the spontaneous development of pancreas neoplasia in DKO^{T} mice can be involved **(Fig. 54)**. Roquin-1/2-deficiency in T cells promotes an aberrant differentiation program towards T_H17 and T_{FH}. Both cell populations are elevated in the spleen but preferentially expand in pancreas draining lymph nodes and can potentially also infiltrate into pancreas tissue. Differentiation of both subtypes is further increased by elevated systemic IL-6 levels, which can originate from both DKO^{T} T cells and other immune cells (Jeltsch *et al.*, 2014; Tan *et al.*, 2014). DKO^{T} T_H17 cells secrete high levels of IL-17A which binds to IL-17Rα. This receptor is strongly expressed on neutrophils and exocrine pancreatic cells, and is further upregulated on pancreatic cells that harbor an oncogenic Kras mutation (McAllister et al., 2014; Uhlén et al., 2015). IL-17 signaling leads to increased secretion of G-CSF from pancreatic epithelial cells (Bharadwaj et al., 2007; Zhao *et al.*, 2019). In addition to their known effector cytokines, DKO^{T} T_H17 cells also produce G-CSF. Together, IL-17 and G-CSF recruit CD11b^{+} Gr1^{+} pro-inflammatory neutrophils.

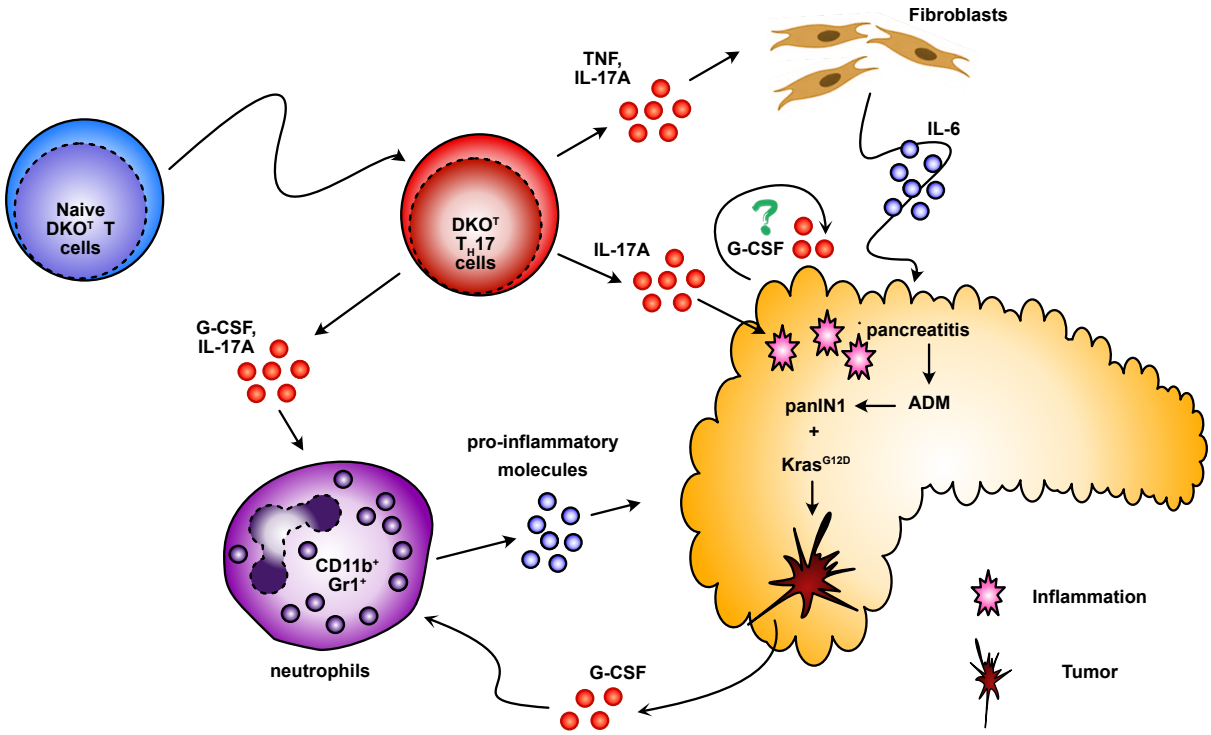

Fig. 54: A model for the development of pancreas cancer through inflammation induced by Roquin-1/2-deficient T cells.

T cells from DKO^{T} mice furthermore produce high levels of TNFα which in collaboration with IL-17A induces high IL-6 production by fibroblasts (Jeltsch *et al.*, 2014), and infiltrating myeloid cells further increase the IL-6 levels in the DKO^{T} mouse. In fact, elevated IL-6 levels are closely linked to pancreas cancer development and progression (Bharadwaj *et al.*, 2007; Lesina *et al.*, 2011; Zhang et al., 2013).
All these events, drive chronic inflammation in the pancreas which leads to an accumulation of damaging events and drives ADM and low grade PanIN development. This strong inflammation may then affect the exocrine cells of the pancreas (Uhlén *et al.*, 2015), trigger an increase of pro-angiogenic factors, increase the vascularization and even attract more immune cell infiltration. In the context of oncogenic Kras signaling, this strong inflammation then causes neoplasia and progression.

5.2.7 Future perspectives

In this study, I was able to show that Roquin-1/2-deficient T cells spontaneously induce pancreas pathology in an IL-17A/G-CSF dependent manner. In in the presence of oncogenic Kras Roquin-1/2-deficient T cells accelerate tumor progression. To my

knowledge, this is the first mouse model in which PanIN lesions develop spontaneously in response to sustained inflammation and do not require an experimental induction of oncogenic Kras signaling.

However, several questions still remain to be answered. For instance, we currently do not know whether Roquin cleavage in T cells also occurs in human pancreatitis, ADMs and PDAC. Therefore, it is important to establish tool which allow the detection of Roquin inactivation T cells in patient samples either directly or through the detection of upregulation of prototypic Roquin targets.

Furthermore, two very recent studies suggested that inflammation induced memory in acinar cells which makes them more prone to tumor development when an additional cancer driving mutation occurs at a later time and that cells which downregulate tumor suppressors are preferentially selected in the presence of cells from the adaptive immune system. Therefore, it is quite intriguing to investigate whether Roquin-1/2-deficient T cells in the DKO^{T} mouse induce responses including epigenetic changes and impose selection of genetically altered acinar cells. This would also explain the fact, that not all DKO^{T} mice spontaneously develop pathology.

In this study, I showed that Roquin proteins can play a role in preventing tissue inappropriate expression of G-CSF and I have also provided some evidence for the ability to regulate 3'UTRs via AREs which are not part of the CDE-ARE stem-loop consensus structure. Whether this regulation takes place by direct or indirect mechanisms needs to be investigated in future studies.

I have also provided evidence that pancreas pathology in the DKO^{T} mice is mediated through the IL-17A/G-CSF axis. This leads to a recruitment of $CD11b^{+}$ $Gr1^{+}$ neutrophils into the pancreas draining lymph nodes and also to the expansion of $CD11b^{+}$ $Gr1^{+}$ cells in secondary lymphoid organs. However, so far, I did not directly prove the role of these cells in pancreas pathology. Currently, I am gearing up to perform Gr1 neutralization experiment similar to the IL-17A neutralization described in section 4.3.5. to prove the direct effect of $CD11b^{+}$ $Gr1^{+}$ cells in the development of PanIN lesions in DKO^{T} mice. For me, this experiment could provide final proof for my hypothesis how Roquin-deficient T cells can induce pathophysiological changes in the pancreas.

6. Conclusion

The RNA-binding proteins Roquin-1 and Roquin-2 play crucial roles in multiple cells of the immune system. In T cells, these proteins are required to control aberrant activation and differentiation. In this work, I focused on the T cell extrinsic effects of Roquin-1/2-deficiencies. Adoptive transfer experiments revealed that Roquin-1/2-deficient T cells induce activation of bystander $CD8^+$ T cells as well as an aberrant differentiation of wild-type $CD4^+$ T cells into the T_{FH} subset. Roquin-1/2-deficiency in T cells furthermore caused a spontaneous development of pre-neoplastic panIN lesions in the pancreata of conditional knock-out mice. I have described a mouse model in which T cell-driven inflammation leads to the spontaneous development of pancreas cancer via the IL-17A/G-CSF/neutrophil axis without a requirement for genetic activation of oncogenic Kras signaling. The findings presented in this work elucidate the complex role of post-transcriptional gene regulation in the prevention of autoinflammation and pancreatic cancer, and provide a valuable tool for future studies on the mechanisms linking pancreatitis and cancer development.

References

Abernathy, E., and Glaunsinger, B. (2015). Emerging roles for RNA degradation in viral replication and antiviral defense. Virology *479-480*, 600-608. 10.1016/j.virol.2015.02.007.

Acosta-Rodriguez, E.V., Napolitani, G., Lanzavecchia, A., and Sallusto, F. (2007a). Interleukins 1beta and 6 but not transforming growth factor-beta are essential for the differentiation of interleukin 17-producing human T helper cells. Nature immunology *8*, 942-949. 10.1038/ni1496.

Acosta-Rodriguez, E.V., Rivino, L., Geginat, J., Jarrossay, D., Gattorno, M., Lanzavecchia, A., Sallusto, F., and Napolitani, G. (2007b). Surface phenotype and antigenic specificity of human interleukin 17-producing T helper memory cells. Nature immunology *8*, 639-646. 10.1038/ni1467.

Aggarwal, S., Ghilardi, N., Xie, M.H., de Sauvage, F.J., and Gurney, A.L. (2003). Interleukin-23 promotes a distinct CD4 T cell activation state characterized by the production of interleukin-17. J Biol Chem *278*, 1910-1914. 10.1074/jbc.M207577200.

Aguirre, A.J., Bardeesy, N., Sinha, M., Lopez, L., Tuveson, D.A., Horner, J., Redston, M.S., and DePinho, R.A. (2003). Activated Kras and Ink4a/Arf deficiency cooperate to produce metastatic pancreatic ductal adenocarcinoma. Genes & development *17*, 3112-3126. 10.1101/gad.1158703.

Akbay, E.A., Koyama, S., Liu, Y., Dries, R., Bufe, L.E., Silkes, M., Alam, M.M., Magee, D.M., Jones, R., Jinushi, M., et al. (2017). Interleukin-17A Promotes Lung Tumor Progression through Neutrophil Attraction to Tumor Sites and Mediating Resistance to PD-1 Blockade. J Thorac Oncol *12*, 1268-1279. 10.1016/j.jtho.2017.04.017.

Akiba, H., Takeda, K., Kojima, Y., Usui, Y., Harada, N., Yamazaki, T., Ma, J., Tezuka, K., Yagita, H., and Okumura, K. (2005). The role of ICOS in the CXCR5+ follicular B helper T cell maintenance in vivo. Journal of immunology (Baltimore, Md. : 1950) *175*, 2340-2348. 10.4049/jimmunol.175.4.2340.

Akira, S. (2013). Regnase-1, a ribonuclease involved in the regulation of immune responses. Cold Spring Harb Symp Quant Biol *78*, 51-60. 10.1101/sqb.2013.78.019877.

Akkaya, M., Traba, J., Roesler, A.S., Miozzo, P., Akkaya, B., Theall, B.P., Sohn, H., Pena, M., Smelkinson, M., Kabat, J., et al. (2018). Second signals rescue B cells from activation-induced mitochondrial dysfunction and death. Nature immunology *19*, 871-884. 10.1038/s41590-018-0156-5.

Albert, M.L., Darnell, J.C., Bender, A., Francisco, L.M., Bhardwaj, N., and Darnell, R.B. (1998a). Tumor-specific killer cells in paraneoplastic cerebellar degeneration. Nat Med *4*, 1321-1324. 10.1038/3315.

Albert, M.L., Sauter, B., and Bhardwaj, N. (1998b). Dendritic cells acquire antigen from apoptotic cells and induce class I-restricted CTLs. Nature *392*, 86-89. 10.1038/32183.

Allen, C.D., Okada, T., and Cyster, J.G. (2007). Germinal-center organization and cellular dynamics. Immunity *27*, 190-202. 10.1016/j.immuni.2007.07.009.

Alt, F.W., Blackwell, T.K., DePinho, R.A., Reth, M.G., and Yancopoulos, G.D. (1986). Regulation of genome rearrangement events during lymphocyte differentiation. Immunological reviews *89*, 5-30. 10.1111/j.1600-065x.1986.tb01470.x.

Anderson, P. (2010). Post-transcriptional regulons coordinate the initiation and resolution of inflammation. Nature reviews. Immunology *10*, 24-35. 10.1038/nri2685.

References

Apte, M.V., Wilson, J.S., Lugea, A., and Pandol, S.J. (2013). A starring role for stellate cells in the pancreatic cancer microenvironment. Gastroenterology *144*, 1210-1219. 10.1053/j.gastro.2012.11.037.

Arnold, C.N., Campbell, D.J., Lipp, M., and Butcher, E.C. (2007). The germinal center response is impaired in the absence of T cell-expressed CXCR5. European journal of immunology *37*, 100-109. 10.1002/eji.200636486.

Artyomov, M.N., Lis, M., Devadas, S., Davis, M.M., and Chakraborty, A.K. (2010). CD4 and CD8 binding to MHC molecules primarily acts to enhance Lck delivery. Proceedings of the National Academy of Sciences of the United States of America *107*, 16916-16921. 10.1073/pnas.1010568107.

Athanasopoulos, V., Barker, A., Yu, D., Tan, A.H., Srivastava, M., Contreras, N., Wang, J., Lam, K.P., Brown, S.H., Goodnow, C.C., et al. (2010). The ROQUIN family of proteins localizes to stress granules via the ROQ domain and binds target mRNAs. Febs j *277*, 2109-2127. 10.1111/j.1742-4658.2010.07628.x.

Bailey, P., Chang, D.K., Nones, K., Johns, A.L., Patch, A.M., Gingras, M.C., Miller, D.K., Christ, A.N., Bruxner, T.J., Quinn, M.C., et al. (2016). Genomic analyses identify molecular subtypes of pancreatic cancer. Nature *531*, 47-52. 10.1038/nature16965.

Ballesteros-Tato, A., León, B., Graf, B.A., Moquin, A., Adams, P.S., Lund, F.E., and Randall, T.D. (2012). Interleukin-2 inhibits germinal center formation by limiting T follicular helper cell differentiation. Immunity *36*, 847-856. 10.1016/j.immuni.2012.02.012.

Barber, D.L., Wherry, E.J., and Ahmed, R. (2003). Cutting edge: rapid in vivo killing by memory CD8 T cells. Journal of immunology (Baltimore, Md. : 1950) *171*, 27-31. 10.4049/jimmunol.171.1.27.

Bardeesy, N., Aguirre, A.J., Chu, G.C., Cheng, K.H., Lopez, L.V., Hezel, A.F., Feng, B., Brennan, C., Weissleder, R., Mahmood, U., et al. (2006a). Both p16(Ink4a) and the p19(Arf)-p53 pathway constrain progression of pancreatic adenocarcinoma in the mouse. Proceedings of the National Academy of Sciences of the United States of America *103*, 5947-5952. 10.1073/pnas.0601273103.

Bardeesy, N., Cheng, K.H., Berger, J.H., Chu, G.C., Pahler, J., Olson, P., Hezel, A.F., Horner, J., Lauwers, G.Y., Hanahan, D., and DePinho, R.A. (2006b). Smad4 is dispensable for normal pancreas development yet critical in progression and tumor biology of pancreas cancer. Genes & development *20*, 3130-3146. 10.1101/gad.1478706.

Batten, M., Ramamoorthi, N., Kljavin, N.M., Ma, C.S., Cox, J.H., Dengler, H.S., Danilenko, D.M., Caplazi, P., Wong, M., Fulcher, D.A., et al. (2010). IL-27 supports germinal center function by enhancing IL-21 production and the function of T follicular helper cells. The Journal of experimental medicine *207*, 2895-2906. 10.1084/jem.20100064.

Bauquet, A.T., Jin, H., Paterson, A.M., Mitsdoerffer, M., Ho, I.C., Sharpe, A.H., and Kuchroo, V.K. (2009). The costimulatory molecule ICOS regulates the expression of c-Maf and IL-21 in the development of follicular T helper cells and TH-17 cells. Nature immunology *10*, 167-175. 10.1038/ni.1690.

Behrens, G., Edelmann, S.L., Raj, T., Kronbeck, N., Monecke, T., Davydova, E., Wong, E.H., Kifinger, L., Giesert, F., Kirmaier, M.E., et al. (2021). Disrupting Roquin-1 interaction with Regnase-1 induces autoimmunity and enhances antitumor responses. Nature immunology. 10.1038/s41590-021-01064-3.

Beisang, D., and Bohjanen, P.R. (2012). Perspectives on the ARE as it turns 25 years old. Wiley Interdiscip Rev RNA *3*, 719-731. 10.1002/wrna.1125.

References

Benson, R.A., MacLeod, M.K., Hale, B.G., Patakas, A., Garside, P., and Brewer, J.M. (2015). Antigen presentation kinetics control T cell/dendritic cell interactions and follicular helper T cell generation in vivo. Elife *4*. 10.7554/eLife.06994.

Bertossi, A., Aichinger, M., Sansonetti, P., Lech, M., Neff, F., Pal, M., Wunderlich, F.T., Anders, H.J., Klein, L., and Schmidt-Supprian, M. (2011). Loss of Roquin induces early death and immune deregulation but not autoimmunity. The Journal of experimental medicine *208*, 1749-1756. 10.1084/jem.20110578.

Bettelli, E., Carrier, Y., Gao, W., Korn, T., Strom, T.B., Oukka, M., Weiner, H.L., and Kuchroo, V.K. (2006). Reciprocal developmental pathways for the generation of pathogenic effector TH17 and regulatory T cells. Nature *441*, 235-238. 10.1038/nature04753.

Bharadwaj, U., Li, M., Zhang, R., Chen, C., and Yao, Q. (2007). Elevated Interleukin-6 and G-CSF in Human Pancreatic Cancer Cell Conditioned Medium Suppress Dendritic Cell Differentiation and Activation. Cancer research *67*, 5479-5488. 10.1158/0008-5472.Can-06-3963.

Bhatia, M. (2004). Apoptosis versus necrosis in acute pancreatitis. Am J Physiol Gastrointest Liver Physiol *286*, G189-196. 10.1152/ajpgi.00304.2003.

Biankin, A.V., Waddell, N., Kassahn, K.S., Gingras, M.C., Muthuswamy, L.B., Johns, A.L., Miller, D.K., Wilson, P.J., Patch, A.M., Wu, J., et al. (2012). Pancreatic cancer genomes reveal aberrations in axon guidance pathway genes. Nature *491*, 399-405. 10.1038/nature11547.

Binas, O., Tants, J.N., Peter, S.A., Janowski, R., Davydova, E., Braun, J., Niessing, D., Schwalbe, H., Weigand, J.E., and Schlundt, A. (2020). Structural basis for the recognition of transiently structured AU-rich elements by Roquin. Nucleic Acids Res *48*, 7385-7403. 10.1093/nar/gkaa465.

Bolognani, F., and Perrone-Bizzozero, N.I. (2008). RNA-protein interactions and control of mRNA stability in neurons. J Neurosci Res *86*, 481-489. 10.1002/jnr.21473.

Borriello, F., Sethna, M.P., Boyd, S.D., Schweitzer, A.N., Tivol, E.A., Jacoby, D., Strom, T.B., Simpson, E.M., Freeman, G.J., and Sharpe, A.H. (1997). B7-1 and B7-2 have overlapping, critical roles in immunoglobulin class switching and germinal center formation. Immunity *6*, 303-313. 10.1016/s1074-7613(00)80333-7.

Bossaller, L., Burger, J., Draeger, R., Grimbacher, B., Knoth, R., Plebani, A., Durandy, A., Baumann, U., Schlesier, M., Welcher, A.A., et al. (2006). ICOS deficiency is associated with a severe reduction of CXCR5+CD4 germinal center Th cells. Journal of immunology (Baltimore, Md. : 1950) *177*, 4927-4932. 10.4049/jimmunol.177.7.4927.

Bour-Jordan, H., Esensten, J.H., Martinez-Llordella, M., Penaranda, C., Stumpf, M., and Bluestone, J.A. (2011). Intrinsic and extrinsic control of peripheral T-cell tolerance by costimulatory molecules of the CD28/B7 family. Immunological reviews *241*, 180-205. 10.1111/j.1600-065X.2011.01011.x.

Boussiotis, V.A., Freeman, G.J., Gribben, J.G., Daley, J., Gray, G., and Nadler, L.M. (1993). Activated human B lymphocytes express three CTLA-4 counterreceptors that costimulate T-cell activation. Proceedings of the National Academy of Sciences of the United States of America *90*, 11059-11063. 10.1073/pnas.90.23.11059.

Brannan, K., Kim, H., Erickson, B., Glover-Cutter, K., Kim, S., Fong, N., Kiemele, L., Hansen, K., Davis, R., Lykke-Andersen, J., and Bentley, D.L. (2012). mRNA decapping factors and the exonuclease Xrn2

function in widespread premature termination of RNA polymerase II transcription. Mol Cell *46*, 311-324. 10.1016/j.molcel.2012.03.006.

Braun, J., Fischer, S., Xu, Z.Z., Sun, H., Ghoneim, D.H., Gimbel, A.T., Plessmann, U., Urlaub, H., Mathews, D.H., and Weigand, J.E. (2018). Identification of new high affinity targets for Roquin based on structural conservation. Nucleic Acids Res *46*, 12109-12125. 10.1093/nar/gky908.

Braun, J.E., Huntzinger, E., Fauser, M., and Izaurralde, E. (2011). GW182 proteins directly recruit cytoplasmic deadenylase complexes to miRNA targets. Mol Cell *44*, 120-133. 10.1016/j.molcel.2011.09.007.

Bronte, V., Brandau, S., Chen, S.-H., Colombo, M.P., Frey, A.B., Greten, T.F., Mandruzzato, S., Murray, P.J., Ochoa, A., Ostrand-Rosenberg, S., et al. (2016). Recommendations for myeloid-derived suppressor cell nomenclature and characterization standards. Nature communications *7*, 12150. 10.1038/ncomms12150.

Brosens, L.A.A., Hackeng, W.M., Offerhaus, G.J., Hruban, R.H., and Wood, L.D. (2015). Pancreatic adenocarcinoma pathology: changing “landscape”. Journal of Gastrointestinal Oncology *6*, 358-374.

Brown, C.Y., Lagnado, C.A., and Goodall, G.J. (1996). A cytokine mRNA-destabilizing element that is structurally and functionally distinct from A+U-rich elements. Proceedings of the National Academy of Sciences of the United States of America *93*, 13721-13725. 10.1073/pnas.93.24.13721.

Buchan , J.R., Muhlrad , D., and Parker , R. (2008). P bodies promote stress granule assembly in Saccharomyces cerevisiae. Journal of Cell Biology *183*, 441-455. 10.1083/jcb.200807043.

Buchan, J.R., Yoon, J.-H., and Parker, R. (2011). Stress-specific composition, assembly and kinetics of stress granules in Saccharomyces cerevisiae. Journal of Cell Science *124*, 228-239. 10.1242/jcs.078444.

Cai, X.Y., Gommoll, C.P., Jr., Justice, L., Narula, S.K., and Fine, J.S. (1998). Regulation of granulocyte colony-stimulating factor gene expression by interleukin-17. Immunology letters *62*, 51-58. 10.1016/s0165-2478(98)00027-3.

Cannons, J.L., Qi, H., Lu, K.T., Dutta, M., Gomez-Rodriguez, J., Cheng, J., Wakeland, E.K., Germain, R.N., and Schwartzberg, P.L. (2010). Optimal germinal center responses require a multistage T cell:B cell adhesion process involving integrins, SLAM-associated protein, and CD84. Immunity *32*, 253-265. 10.1016/j.immuni.2010.01.010.

Cannons, J.L., Tangye, S.G., and Schwartzberg, P.L. (2011). SLAM family receptors and SAP adaptors in immunity. Annu Rev Immunol *29*, 665-705. 10.1146/annurev-immunol-030409-101302.

Cantrell, D. (2015). Signaling in lymphocyte activation. Cold Spring Harbor perspectives in biology *7*. 10.1101/cshperspect.a018788.

Caput, D., Beutler, B., Hartog, K., Thayer, R., Brown-Shimer, S., and Cerami, A. (1986). Identification of a common nucleotide sequence in the 3'-untranslated region of mRNA molecules specifying inflammatory mediators. Proceedings of the National Academy of Sciences of the United States of America *83*, 1670-1674. 10.1073/pnas.83.6.1670.

Carballo, E., Lai, W.S., and Blackshear, P.J. (2000). Evidence that tristetraprolin is a physiological regulator of granulocyte-macrophage colony-stimulating factor messenger RNA deadenylation and stability. Blood *95*, 1891-1899.

References

Celli, S., Lemaître, F., and Bousso, P. (2007). Real-time manipulation of T cell-dendritic cell interactions in vivo reveals the importance of prolonged contacts for CD4+ T cell activation. Immunity *27*, 625-634. 10.1016/j.immuni.2007.08.018.

Charenton, C., Gaudon-Plesse, C., Fourati, Z., Taverniti, V., Back, R., Kolesnikova, O., Séraphin, B., and Graille, M. (2017). A unique surface on Pat1 C-terminal domain directly interacts with Dcp2 decapping enzyme and Xrn1 5'-3' mRNA exonuclease in yeast. Proceedings of the National Academy of Sciences of the United States of America *114*, E9493-e9501. 10.1073/pnas.1711680114.

Charles A. Janeway, J., and Medzhitov, R. (2002). Innate Immune Recognition. Annual Review of Immunology *20*, 197-216. 10.1146/annurev.immunol.20.083001.084359.

Cheadle, C., Fan, J., Cho-Chung, Y.S., Werner, T., Ray, J., Do, L., Gorospe, M., and Becker, K.G. (2005). Control of gene expression during T cell activation: alternate regulation of mRNA transcription and mRNA stability. BMC Genomics *6*, 75. 10.1186/1471-2164-6-75.

Chen, L., and Flies, D.B. (2013). Molecular mechanisms of T cell co-stimulation and co-inhibition. Nature Reviews Immunology *13*, 227-242. 10.1038/nri3405.

Chen, W., Jin, W., Hardegen, N., Lei, K.J., Li, L., Marinos, N., McGrady, G., and Wahl, S.M. (2003). Conversion of peripheral CD4+CD25- naive T cells to CD4+CD25+ regulatory T cells by TGF-beta induction of transcription factor Foxp3. The Journal of experimental medicine *198*, 1875-1886. 10.1084/jem.20030152.

Choi, J., Lee, K., Ingvarsdottir, K., Bonasio, R., Saraf, A., Florens, L., Washburn, M.P., Tadros, S., Green, M.R., and Busino, L. (2018a). Loss of KLHL6 promotes diffuse large B-cell lymphoma growth and survival by stabilizing the mRNA decay factor roquin2. Nature cell biology *20*, 586-596. 10.1038/s41556-018-0084-5.

Choi, J., Saraf, A., Florens, L., Washburn, M.P., and Busino, L. (2018b). PTPN14 regulates Roquin2 stability by tyrosine dephosphorylation. Cell Cycle *17*, 2243-2255. 10.1080/15384101.2018.1522912.

Choi, S.S., Jang, E., Oh, Y.K., Jang, K., Cho, M.L., Park, S.H., and Youn, J. (2019). Aged Sanroque Mice Spontaneously Develop Sjögren's Syndrome-like Disease. Immune Netw *19*, e7. 10.4110/in.2019.19.e7.

Choi, Y.S., Eto, D., Yang, J.A., Lao, C., and Crotty, S. (2013a). Cutting edge: STAT1 is required for IL-6-mediated Bcl6 induction for early follicular helper cell differentiation. Journal of immunology (Baltimore, Md. : 1950) *190*, 3049-3053. 10.4049/jimmunol.1203032.

Choi, Y.S., Kageyama, R., Eto, D., Escobar, T.C., Johnston, R.J., Monticelli, L., Lao, C., and Crotty, S. (2011). ICOS receptor instructs T follicular helper cell versus effector cell differentiation via induction of the transcriptional repressor Bcl6. Immunity *34*, 932-946. 10.1016/j.immuni.2011.03.023.

Choi, Y.S., Yang, J.A., Yusuf, I., Johnston, R.J., Greenbaum, J., Peters, B., and Crotty, S. (2013b). Bcl6 expressing follicular helper CD4 T cells are fate committed early and have the capacity to form memory. Journal of immunology (Baltimore, Md. : 1950) *190*, 4014-4026. 10.4049/jimmunol.1202963.

Chowdhury, A., Mukhopadhyay, J., and Tharun, S. (2007). The decapping activator Lsm1p-7p-Pat1p complex has the intrinsic ability to distinguish between oligoadenylated and polyadenylated RNAs. Rna *13*, 998-1016. 10.1261/rna.502507.

References

Cobo, I., Martinelli, P., Flández, M., Bakiri, L., Zhang, M., Carrillo-de-Santa-Pau, E., Jia, J., Sánchez-Arévalo Lobo, V.J., Megías, D., Felipe, I., et al. (2018). Transcriptional regulation by NR5A2 links differentiation and inflammation in the pancreas. Nature *554*, 533-537. 10.1038/nature25751.

Codutti, L., Leppek, K., Zálešák, J., Windeisen, V., Masiewicz, P., Stoecklin, G., and Carlomagno, T. (2015). A Distinct, Sequence-Induced Conformation Is Required for Recognition of the Constitutive Decay Element RNA by Roquin. Structure *23*, 1437-1447. 10.1016/j.str.2015.06.001.

Coffelt, S.B., Kersten, K., Doornebal, C.W., Weiden, J., Vrijland, K., Hau, C.S., Verstegen, N.J.M., Ciampricotti, M., Hawinkels, L., Jonkers, J., and de Visser, K.E. (2015). IL-17-producing γδ T cells and neutrophils conspire to promote breast cancer metastasis. Nature *522*, 345-348. 10.1038/nature14282.

Collart, M.A. (2016). The Ccr4-Not complex is a key regulator of eukaryotic gene expression. Wiley Interdiscip Rev RNA *7*, 438-454. 10.1002/wrna.1332.

Crotty, S. (2011). Follicular Helper CD4 T Cells (TFH). Annual Review of Immunology *29*, 621-663. 10.1146/annurev-immunol-031210-101400.

Crotty, S. (2014). T follicular helper cell differentiation, function, and roles in disease. Immunity *41*, 529-542. 10.1016/j.immuni.2014.10.004.

Crotty, S. (2019). T Follicular Helper Cell Biology: A Decade of Discovery and Diseases. Immunity *50*, 1132-1148. 10.1016/j.immuni.2019.04.011.

Czar, M.J., Kersh, E.N., Mijares, L.A., Lanier, G., Lewis, J., Yap, G., Chen, A., Sher, A., Duckett, C.S., Ahmed, R., and Schwartzberg, P.L. (2001). Altered lymphocyte responses and cytokine production in mice deficient in the X-linked lymphoproliferative disease gene SH2D1A/DSHP/SAP. Proceedings of the National Academy of Sciences of the United States of America *98*, 7449-7454. 10.1073/pnas.131193098.

Decker, C.J., and Parker, R. (2012). P-bodies and stress granules: possible roles in the control of translation and mRNA degradation. Cold Spring Harbor perspectives in biology *4*, a012286. 10.1101/cshperspect.a012286.

Del Poggetto, E., Ho, I.L., Balestrieri, C., Yen, E.Y., Zhang, S., Citron, F., Shah, R., Corti, D., Diaferia, G.R., Li, C.Y., et al. (2021). Epithelial memory of inflammation limits tissue damage while promoting pancreatic tumorigenesis. Science (New York, N.Y.) *373*, eabj0486. 10.1126/science.abj0486.

Dennaoui, R., Shrestha, H., and Wagner, K.U. (2021). Models of pancreatic ductal adenocarcinoma. Cancer Metastasis Rev *40*, 803-818. 10.1007/s10555-021-09989-9.

DiToro, D., Winstead, C.J., Pham, D., Witte, S., Andargachew, R., Singer, J.R., Wilson, C.G., Zindl, C.L., Luther, R.J., Silberger, D.J., et al. (2018). Differential IL-2 expression defines developmental fates of follicular versus nonfollicular helper T cells. Science (New York, N.Y.) *361*. 10.1126/science.aao2933.

Dominguez-Villar, M., and Hafler, D.A. (2018). Regulatory T cells in autoimmune disease. Nature immunology *19*, 665-673. 10.1038/s41590-018-0120-4.

Dougan, S.K. (2017). The Pancreatic Cancer Microenvironment. Cancer J *23*, 321-325. 10.1097/ppo.0000000000000288.

References

Drees, C., Vahl, J.C., Bortoluzzi, S., Heger, K.D., Fischer, J.C., Wunderlich, F.T., Peschel, C., and Schmidt-Supprian, M. (2017). Roquin Paralogs Differentially Regulate Functional NKT Cell Subsets. The Journal of Immunology *198*, 2747-2759. 10.4049/jimmunol.1601732.

Drosten, M., Guerra, C., and Barbacid, M. (2018). Genetically Engineered Mouse Models of K-Ras-Driven Lung and Pancreatic Tumors: Validation of Therapeutic Targets. Cold Spring Harb Perspect Med *8*. 10.1101/cshperspect.a031542.

Ellyard, J.I., Chia, T., Rodriguez-Pinilla, S.M., Martin, J.L., Hu, X., Navarro-Gonzalez, M., Garcia, J.F., Delfau-Larue, M.H., Montes-Moreno, S., Gaulard, P., et al. (2012). Heterozygosity for Roquinsan leads to angioimmunoblastic T-cell lymphoma-like tumors in mice. Blood *120*, 812-821. 10.1182/blood-2011-07-365130.

Ene-Obong, A., Clear, A.J., Watt, J., Wang, J., Fatah, R., Riches, J.C., Marshall, J.F., Chin-Aleong, J., Chelala, C., Gribben, J.G., et al. (2013). Activated pancreatic stellate cells sequester CD8+ T cells to reduce their infiltration of the juxtatumoral compartment of pancreatic ductal adenocarcinoma. Gastroenterology *145*, 1121-1132. 10.1053/j.gastro.2013.07.025.

Essig, K., Hu, D., Guimaraes, J.C., Alterauge, D., Edelmann, S., Raj, T., Kranich, J., Behrens, G., Heiseke, A., Floess, S., et al. (2017). Roquin Suppresses the PI3K-mTOR Signaling Pathway to Inhibit T Helper Cell Differentiation and Conversion of Treg to Tfr Cells. Immunity *47*, 1067-1082.e1012. 10.1016/j.immuni.2017.11.008.

Essig, K., Kronbeck, N., Guimaraes, J.C., Lohs, C., Schlundt, A., Hoffmann, A., Behrens, G., Brenner, S., Kowalska, J., Lopez-Rodriguez, C., et al. (2018). Roquin targets mRNAs in a 3'-UTR-specific manner by different modes of regulation. Nature communications *9*, 3810. 10.1038/s41467-018-06184-3.

Eto, D., Lao, C., DiToro, D., Barnett, B., Escobar, T.C., Kageyama, R., Yusuf, I., and Crotty, S. (2011). IL-21 and IL-6 are critical for different aspects of B cell immunity and redundantly induce optimal follicular helper CD4 T cell (Tfh) differentiation. PloS one *6*, e17739. 10.1371/journal.pone.0017739.

Fabian, M.R., Frank, F., Rouya, C., Siddiqui, N., Lai, W.S., Karetnikov, A., Blackshear, P.J., Nagar, B., and Sonenberg, N. (2013). Structural basis for the recruitment of the human CCR4-NOT deadenylase complex by tristetraprolin. Nat Struct Mol Biol *20*, 735-739. 10.1038/nsmb.2572.

Fan, J., Yang, X., Wang, W., Wood, W.H., 3rd, Becker, K.G., and Gorospe, M. (2002). Global analysis of stress-regulated mRNA turnover by using cDNA arrays. Proceedings of the National Academy of Sciences of the United States of America *99*, 10611-10616. 10.1073/pnas.162212399.

Fazilleau, N., McHeyzer-Williams, L.J., Rosen, H., and McHeyzer-Williams, M.G. (2009). The function of follicular helper T cells is regulated by the strength of T cell antigen receptor binding. Nature immunology *10*, 375-384. 10.1038/ni.1704.

Fontenot, J.D., Gavin, M.A., and Rudensky, A.Y. (2003). Foxp3 programs the development and function of CD4+CD25+ regulatory T cells. Nature immunology *4*, 330-336. 10.1038/ni904.

Fontenot, J.D., Rasmussen, J.P., Gavin, M.A., and Rudensky, A.Y. (2005). A function for interleukin 2 in Foxp3-expressing regulatory T cells. Nature immunology *6*, 1142-1151. 10.1038/ni1263.

Fossum, S., and Rolstad, B. (1986). The roles of interdigitating cells and natural killer cells in the rapid rejection of allogeneic lymphocytes. European journal of immunology *16*, 440-450. 10.1002/eji.1830160422.

References

Fröland, S., Natvig, J.B., and Berdal, P. (1971). Surface-bound immunoglobulin as a marker of B lymphocytes in man. Nat New Biol *234*, 251-252. 10.1038/newbio234251a0.

Fromm, S.A., Truffault, V., Kamenz, J., Braun, J.E., Hoffmann, N.A., Izaurralde, E., and Sprangers, R. (2012). The structural basis of Edc3- and Scd6-mediated activation of the Dcp1:Dcp2 mRNA decapping complex. Embo j *31*, 279-290. 10.1038/emboj.2011.408.

Fu, M., and Blackshear, P.J. (2017). RNA-binding proteins in immune regulation: a focus on CCCH zinc finger proteins. Nature reviews. Immunology *17*, 130-143. 10.1038/nri.2016.129.

Garneau, N.L., Wilusz, J., and Wilusz, C.J. (2007). The highways and byways of mRNA decay. Nat Rev Mol Cell Biol *8*, 113-126. 10.1038/nrm2104.

Garside, P., Ingulli, E., Merica, R.R., Johnson, J.G., Noelle, R.J., and Jenkins, M.K. (1998). Visualization of specific B and T lymphocyte interactions in the lymph node. Science (New York, N.Y.) *281*, 96-99. 10.1126/science.281.5373.96.

Gewies, A., Gorka, O., Bergmann, H., Pechloff, K., Petermann, F., Jeltsch, Katharina M., Rudelius, M., Kriegsmann, M., Weichert, W., Horsch, M., et al. (2014). Uncoupling Malt1 Threshold Function from Paracaspase Activity Results in Destructive Autoimmune Inflammation. Cell Reports *9*, 1292-1305. https://doi.org/10.1016/j.celrep.2014.10.044.

Ghoreschi, K., Laurence, A., Yang, X.P., Tato, C.M., McGeachy, M.J., Konkel, J.E., Ramos, H.L., Wei, L., Davidson, T.S., Bouladoux, N., et al. (2010). Generation of pathogenic T(H)17 cells in the absence of TGF-β signalling. Nature *467*, 967-971. 10.1038/nature09447.

Gigoux, M., Shang, J., Pak, Y., Xu, M., Choe, J., Mak, T.W., and Suh, W.K. (2009). Inducible costimulator promotes helper T-cell differentiation through phosphoinositide 3-kinase. Proceedings of the National Academy of Sciences of the United States of America *106*, 20371-20376. 10.1073/pnas.0911573106.

Gitlin, A.D., Shulman, Z., and Nussenzweig, M.C. (2014). Clonal selection in the germinal centre by regulated proliferation and hypermutation. Nature *509*, 637-640. 10.1038/nature13300.

Glasmacher, E., Hoefig, K.P., Vogel, K.U., Rath, N., Du, L., Wolf, C., Kremmer, E., Wang, X., and Heissmeyer, V. (2010). Roquin binds inducible costimulator mRNA and effectors of mRNA decay to induce microRNA-independent post-transcriptional repression. Nature immunology *11*, 725-733. 10.1038/ni.1902.

Goenka, R., Barnett, L.G., Silver, J.S., O'Neill, P.J., Hunter, C.A., Cancro, M.P., and Laufer, T.M. (2011). Cutting edge: dendritic cell-restricted antigen presentation initiates the follicular helper T cell program but cannot complete ultimate effector differentiation. Journal of immunology (Baltimore, Md. : 1950) *187*, 1091-1095. 10.4049/jimmunol.1100853.

Greten, F.R., and Grivennikov, S.I. (2019). Inflammation and Cancer: Triggers, Mechanisms, and Consequences. Immunity *51*, 27-41. https://doi.org/10.1016/j.immuni.2019.06.025.

Grivennikov, S., Karin, E., Terzic, J., Mucida, D., Yu, G.Y., Vallabhapurapu, S., Scheller, J., Rose-John, S., Cheroutre, H., Eckmann, L., and Karin, M. (2009). IL-6 and Stat3 are required for survival of intestinal epithelial cells and development of colitis-associated cancer. Cancer cell *15*, 103-113. 10.1016/j.ccr.2009.01.001.

References

Gruber, A.R., Bernhart, S.H., and Lorenz, R. (2015). The ViennaRNA web services. Methods in molecular biology (Clifton, N.J.) *1269*, 307-326. 10.1007/978-1-4939-2291-8_19.

Grujic, M., Bartholdy, C., Remy, M., Pinschewer, D.D., Christensen, J.P., and Thomsen, A.R. (2010). The Role of CD80/CD86 in Generation and Maintenance of Functional Virus-Specific CD8⁺ T Cells in Mice Infected with Lymphocytic Choriomeningitis Virus. The Journal of Immunology *185*, 1730-1743. 10.4049/jimmunol.0903894.

Guerra, C., Collado, M., Navas, C., Schuhmacher, A.J., Hernandez-Porras, I., Canamero, M., Rodriguez-Justo, M., Serrano, M., and Barbacid, M. (2011). Pancreatitis-induced inflammation contributes to pancreatic cancer by inhibiting oncogene-induced senescence. Cancer cell *19*, 728-739. 10.1016/j.ccr.2011.05.011.

Guerra, C., Schuhmacher, A.J., Canamero, M., Grippo, P.J., Verdaguer, L., Perez-Gallego, L., Dubus, P., Sandgren, E.P., and Barbacid, M. (2007). Chronic pancreatitis is essential for induction of pancreatic ductal adenocarcinoma by K-Ras oncogenes in adult mice. Cancer cell *11*, 291-302. 10.1016/j.ccr.2007.01.012.

Hall, A.O., Silver, J.S., and Hunter, C.A. (2012). The immunobiology of IL-27. Adv Immunol *115*, 1-44. 10.1016/b978-0-12-394299-9.00001-1.

Hamada, S., Masamune, A., Takikawa, T., Suzuki, N., Kikuta, K., Hirota, M., Hamada, H., Kobune, M., Satoh, K., and Shimosegawa, T. (2012). Pancreatic stellate cells enhance stem cell-like phenotypes in pancreatic cancer cells. Biochem Biophys Res Commun *421*, 349-354. 10.1016/j.bbrc.2012.04.014.

Hanahan, D., and Weinberg, R.A. (2011). Hallmarks of cancer: the next generation. Cell *144*, 646-674. 10.1016/j.cell.2011.02.013.

Hao, S., and Baltimore, D. (2009). The stability of mRNA influences the temporal order of the induction of genes encoding inflammatory molecules. Nature immunology *10*, 281-288. 10.1038/ni.1699.

Harada, T., Chelala, C., Bhakta, V., Chaplin, T., Caulee, K., Baril, P., Young, B.D., and Lemoine, N.R. (2008). Genome-wide DNA copy number analysis in pancreatic cancer using high-density single nucleotide polymorphism arrays. Oncogene *27*, 1951-1960. 10.1038/sj.onc.1210832.

Hardtke, S., Ohl, L., and Förster, R. (2005). Balanced expression of CXCR5 and CCR7 on follicular T helper cells determines their transient positioning to lymph node follicles and is essential for efficient B-cell help. Blood *106*, 1924-1931. 10.1182/blood-2004-11-4494.

Harker, J.A., Dolgoter, A., and Zuniga, E.I. (2013). Cell-intrinsic IL-27 and gp130 cytokine receptor signaling regulates virus-specific $CD4^+$ T cell responses and viral control during chronic infection. Immunity *39*, 548-559. 10.1016/j.immuni.2013.08.010.

Hata, T., Suenaga, M., Marchionni, L., Macgregor-Das, A., Yu, J., Shindo, K., Tamura, K., Hruban, R.H., and Goggins, M. (2018). Genome-Wide Somatic Copy Number Alterations and Mutations in High-Grade Pancreatic Intraepithelial Neoplasia. Am J Pathol *188*, 1723-1733. 10.1016/j.ajpath.2018.03.012.

Hathcock, K.S., Laszlo, G., Pucillo, C., Linsley, P., and Hodes, R.J. (1994). Comparative analysis of B7-1 and B7-2 costimulatory ligands: expression and function. The Journal of experimental medicine *180*, 631-640. 10.1084/jem.180.2.631.

References

Haynes, N.M., Allen, C.D.C., Lesley, R., Ansel, K.M., Killeen, N., and Cyster, J.G. (2007). Role of CXCR5 and CCR7 in Follicular Th Cell Positioning and Appearance of a Programmed Cell Death Gene-1^{High} Germinal Center-Associated Subpopulation. The Journal of Immunology *179*, 5099-5108. 10.4049/jimmunol.179.8.5099.

Heissmeyer, V., and Vogel, K.U. (2013). Molecular control of Tfh-cell differentiation by Roquin family proteins. Immunological reviews *253*, 273-289. 10.1111/imr.12056.

Hennecke, J., and Wiley, D.C. (2001). T Cell Receptor–MHC Interactions up Close. Cell *104*, 1-4. 10.1016/S0092-8674(01)00185-4.

Hezel, A.F., Kimmelman, A.C., Stanger, B.Z., Bardeesy, N., and Depinho, R.A. (2006). Genetics and biology of pancreatic ductal adenocarcinoma. Genes & development *20*, 1218-1249. 10.1101/gad.1415606.

Hingorani, S.R., Petricoin, E.F., Maitra, A., Rajapakse, V., King, C., Jacobetz, M.A., Ross, S., Conrads, T.P., Veenstra, T.D., Hitt, B.A., et al. (2003). Preinvasive and invasive ductal pancreatic cancer and its early detection in the mouse. Cancer cell *4*, 437-450.

Hingorani, S.R., Wang, L., Multani, A.S., Combs, C., Deramaudt, T.B., Hruban, R.H., Rustgi, A.K., Chang, S., and Tuveson, D.A. (2005). Trp53R172H and KrasG12D cooperate to promote chromosomal instability and widely metastatic pancreatic ductal adenocarcinoma in mice. Cancer cell *7*, 469-483. 10.1016/j.ccr.2005.04.023.

Hirahara, K., Onodera, A., Villarino, A.V., Bonelli, M., Sciumè, G., Laurence, A., Sun, H.W., Brooks, S.R., Vahedi, G., Shih, H.Y., et al. (2015). Asymmetric Action of STAT Transcription Factors Drives Transcriptional Outputs and Cytokine Specificity. Immunity *42*, 877-889. 10.1016/j.immuni.2015.04.014.

Hiramatsu, Y., Suto, A., Kashiwakuma, D., Kanari, H., Kagami, S., Ikeda, K., Hirose, K., Watanabe, N., Grusby, M.J., Iwamoto, I., and Nakajima, H. (2010). c-Maf activates the promoter and enhancer of the IL-21 gene, and TGF-beta inhibits c-Maf-induced IL-21 production in CD4+ T cells. J Leukoc Biol *87*, 703-712. 10.1189/jlb.0909639.

Hirano, T., Nakajima, K., and Hibi, M. (1997). Signaling mechanisms through gp130: a model of the cytokine system. Cytokine & growth factor reviews *8*, 241-252. 10.1016/s1359-6101(98)80005-1.

Hofacker, I.L., Fontana, W., Stadler, P.F., Bonhoeffer, L.S., Tacker, M., and Schuster, P. (1994). Fast folding and comparison of RNA secondary structures. Monatshefte für Chemie / Chemical Monthly *125*, 167-188. 10.1007/BF00818163.

Hofstetter, H.H., Ibrahim, S.M., Koczan, D., Kruse, N., Weishaupt, A., Toyka, K.V., and Gold, R. (2005). Therapeutic efficacy of IL-17 neutralization in murine experimental autoimmune encephalomyelitis. Cell Immunol *237*, 123-130. 10.1016/j.cellimm.2005.11.002.

Hosein, A.N., Brekken, R.A., and Maitra, A. (2020). Pancreatic cancer stroma: an update on therapeutic targeting strategies. Nat Rev Gastroenterol Hepatol *17*, 487-505. 10.1038/s41575-020-0300-1.

Houseley, J., LaCava, J., and Tollervey, D. (2006). RNA-quality control by the exosome. Nat Rev Mol Cell Biol *7*, 529-539. 10.1038/nrm1964.

References

Hruban, R.H., Goggins, M., Parsons, J., and Kern, S.E. (2000). Progression model for pancreatic cancer. Clinical cancer research : an official journal of the American Association for Cancer Research *6*, 2969-2972.

Hu, J., Havenar-Daughton, C., and Crotty, S. (2013). Modulation of SAP dependent T:B cell interactions as a strategy to improve vaccination. Curr Opin Virol *3*, 363-370. 10.1016/j.coviro.2013.05.015.

Hu, W., Sweet, T.J., Chamnongpol, S., Baker, K.E., and Coller, J. (2009). Co-translational mRNA decay in Saccharomyces cerevisiae. Nature *461*, 225-229. 10.1038/nature08265.

Huang, S., Hendriks, W., Althage, A., Hemmi, S., Bluethmann, H., Kamijo, R., Vilcek, J., Zinkernagel, R.M., and Aguet, M. (1993). Immune response in mice that lack the interferon-gamma receptor. Science (New York, N.Y.) *259*, 1742-1745. 10.1126/science.8456301.

Huber, M., Brehm, C.U., Gress, T.M., Buchholz, M., Alashkar Alhamwe, B., von Strandmann, E.P., Slater, E.P., Bartsch, J.W., Bauer, C., and Lauth, M. (2020). The Immune Microenvironment in Pancreatic Cancer. Int J Mol Sci *21*. 10.3390/ijms21197307.

Ijichi, H., Chytil, A., Gorska, A.E., Aakre, M.E., Fujitani, Y., Fujitani, S., Wright, C.V., and Moses, H.L. (2006). Aggressive pancreatic ductal adenocarcinoma in mice caused by pancreas-specific blockade of transforming growth factor-beta signaling in cooperation with active Kras expression. Genes & development *20*, 3147-3160. 10.1101/gad.1475506.

Ivanov, II, McKenzie, B.S., Zhou, L., Tadokoro, C.E., Lepelley, A., Lafaille, J.J., Cua, D.J., and Littman, D.R. (2006). The orphan nuclear receptor RORgammat directs the differentiation program of proinflammatory IL-17+ T helper cells. Cell *126*, 1121-1133. 10.1016/j.cell.2006.07.035.

Iwasaki, A., and Medzhitov, R. (2004). Toll-like receptor control of the adaptive immune responses. Nature immunology *5*, 987-995. 10.1038/ni1112.

Jackson, E.L., Willis, N., Mercer, K., Bronson, R.T., Crowley, D., Montoya, R., Jacks, T., and Tuveson, D.A. (2001). Analysis of lung tumor initiation and progression using conditional expression of oncogenic K-ras. Genes & development *15*, 3243-3248. 10.1101/gad.943001.

Jacob, J., Kelsoe, G., Rajewsky, K., and Weiss, U. (1991). Intraclonal generation of antibody mutants in germinal centres. Nature *354*, 389-392. 10.1038/354389a0.

Janeway, C.A., Jr., and Bottomly, K. (1994). Signals and signs for lymphocyte responses. Cell *76*, 275-285. 10.1016/0092-8674(94)90335-2.

Janeway, C.A., Jr., and Medzhitov, R. (2002). Innate immune recognition. Annu Rev Immunol *20*, 197-216. 10.1146/annurev.immunol.20.083001.084359.

Janowski, R., Heinz, G.A., Schlundt, A., Wommelsdorf, N., Brenner, S., Gruber, A.R., Blank, M., Buch, T., Buhmann, R., Zavolan, M., et al. (2016). Roquin recognizes a non-canonical hexaloop structure in the 3'-UTR of Ox40. Nature communications *7*, 11032. 10.1038/ncomms11032.

Jeltsch, K.M., and Heissmeyer, V. (2016). Regulation of T cell signaling and autoimmunity by RNA-binding proteins. Current opinion in immunology *39*, 127-135. 10.1016/j.coi.2016.01.011.

Jeltsch, K.M., Hu, D., Brenner, S., Zoller, J., Heinz, G.A., Nagel, D., Vogel, K.U., Rehage, N., Warth, S.C., Edelmann, S.L., et al. (2014). Cleavage of roquin and regnase-1 by the paracaspase MALT1

releases their cooperatively repressed targets to promote T(H)17 differentiation. Nature immunology *15*, 1079-1089. 10.1038/ni.3008.

Jenkins, M.K., Ashwell, J.D., and Schwartz, R.H. (1988). Allogeneic non-T spleen cells restore the responsiveness of normal T cell clones stimulated with antigen and chemically modified antigen-presenting cells. Journal of immunology (Baltimore, Md. : 1950) *140*, 3324-3330.

Ji, B., Tsou, L., Wang, H., Gaiser, S., Chang, D.Z., Daniluk, J., Bi, Y., Grote, T., Longnecker, D.S., and Logsdon, C.D. (2009). Ras activity levels control the development of pancreatic diseases. Gastroenterology *137*, 1072-1082, 1082.e1071-1076. 10.1053/j.gastro.2009.05.052.

Jin, C., Lagoudas, G.K., Zhao, C., Bullman, S., Bhutkar, A., Hu, B., Ameh, S., Sandel, D., Liang, X.S., Mazzilli, S., et al. (2019). Commensal Microbiota Promote Lung Cancer Development via γδ T Cells. Cell *176*, 998-1013.e1016. 10.1016/j.cell.2018.12.040.

Jing, Q., Huang, S., Guth, S., Zarubin, T., Motoyama, A., Chen, J., Di Padova, F., Lin, S.C., Gram, H., and Han, J. (2005). Involvement of microRNA in AU-rich element-mediated mRNA instability. Cell *120*, 623-634. 10.1016/j.cell.2004.12.038.

Johnson, B.L., d'Alincourt Salazar, M., Mackenzie-Dyck, S., D'Apuzzo, M., Shih, H.P., Manuel, E.R., and Diamond, D.J. (2019). Desmoplasia and oncogene driven acinar-to-ductal metaplasia are concurrent events during acinar cell-derived pancreatic cancer initiation in young adult mice. PloS one *14*, e0221810. 10.1371/journal.pone.0221810.

Johnston, R.J., Choi, Y.S., Diamond, J.A., Yang, J.A., and Crotty, S. (2012). STAT5 is a potent negative regulator of TFH cell differentiation. The Journal of experimental medicine *209*, 243-250. 10.1084/jem.20111174.

Johnston, R.J., Poholek, A.C., DiToro, D., Yusuf, I., Eto, D., Barnett, B., Dent, A.L., Craft, J., and Crotty, S. (2009). Bcl6 and Blimp-1 are reciprocal and antagonistic regulators of T follicular helper cell differentiation. Science (New York, N.Y.) *325*, 1006-1010. 10.1126/science.1175870.

Jonas, S., Christie, M., Peter, D., Bhandari, D., Loh, B., Huntzinger, E., Weichenrieder, O., and Izaurralde, E. (2014). An asymmetric PAN3 dimer recruits a single PAN2 exonuclease to mediate mRNA deadenylation and decay. Nat Struct Mol Biol *21*, 599-608. 10.1038/nsmb.2837.

Jones, S., Zhang, X., Parsons, D.W., Lin, J.C., Leary, R.J., Angenendt, P., Mankoo, P., Carter, H., Kamiyama, H., Jimeno, A., et al. (2008). Core signaling pathways in human pancreatic cancers revealed by global genomic analyses. Science (New York, N.Y.) *321*, 1801-1806. 10.1126/science.1164368.

Kabelitz, D., and Janssen, O. (1997). Antigen-induced death of T-lymphocytes. Front Biosci *2*, d61-77. 10.2741/a175.

Kamperschroer, C., Roberts, D.M., Zhang, Y., Weng, N.P., and Swain, S.L. (2008). SAP enables T cells to help B cells by a mechanism distinct from Th cell programming or CD40 ligand regulation. Journal of immunology (Baltimore, Md. : 1950) *181*, 3994-4003. 10.4049/jimmunol.181.6.3994.

Kanda, M., Matthaei, H., Wu, J., Hong, S.M., Yu, J., Borges, M., Hruban, R.H., Maitra, A., Kinzler, K., Vogelstein, B., and Goggins, M. (2012). Presence of somatic mutations in most early-stage pancreatic intraepithelial neoplasia. Gastroenterology *142*, 730-733.e739. 10.1053/j.gastro.2011.12.042.

References

Kaplan, M.H., Schindler, U., Smiley, S.T., and Grusby, M.J. (1996). Stat6 is required for mediating responses to IL-4 and for development of Th2 cells. Immunity *4*, 313-319. 10.1016/s1074-7613(00)80439-2.

Karagiannidis, I., Jerman, S.J., Jacenik, D., Phinney, B.B., Yao, R., Prossnitz, E.R., and Beswick, E.J. (2020). G-CSF and G-CSFR Modulate CD4 and CD8 T Cell Responses to Promote Colon Tumor Growth and Are Potential Therapeutic Targets. Front Immunol *11*, 1885. 10.3389/fimmu.2020.01885.

Karanjawala, Z.E., Illei, P.B., Ashfaq, R., Infante, J.R., Murphy, K., Pandey, A., Schulick, R., Winter, J., Sharma, R., Maitra, A., et al. (2008). New markers of pancreatic cancer identified through differential gene expression analyses: claudin 18 and annexin A8. Am J Surg Pathol *32*, 188-196. 10.1097/PAS.0b013e31815701f3.

Kay, J., Thadhani, E., Samson, L., and Engelward, B. (2019). Inflammation-induced DNA damage, mutations and cancer. DNA Repair (Amst) *83*, 102673. 10.1016/j.dnarep.2019.102673.

Kedersha , N., Stoecklin , G., Ayodele , M., Yacono , P., Lykke-Andersen , J., Fritzler , M.J., Scheuner , D., Kaufman , R.J., Golan , D.E., and Anderson , P. (2005). Stress granules and processing bodies are dynamically linked sites of mRNP remodeling. Journal of Cell Biology *169*, 871-884. 10.1083/jcb.200502088.

Khabar, K.S. (2005). The AU-rich transcriptome: more than interferons and cytokines, and its role in disease. J Interferon Cytokine Res *25*, 1-10. 10.1089/jir.2005.25.1.

Kiraly, O., Gong, G., Olipitz, W., Muthupalani, S., and Engelward, B.P. (2015). Inflammation-induced cell proliferation potentiates DNA damage-induced mutations in vivo. PLoS Genet *11*, e1004901. 10.1371/journal.pgen.1004901.

Kirkegård, J., Mortensen, F.V., and Cronin-Fenton, D. (2017). Chronic Pancreatitis and Pancreatic Cancer Risk: A Systematic Review and Meta-analysis. Am J Gastroenterol *112*, 1366-1372. 10.1038/ajg.2017.218.

Kitamura, D., Roes, J., Kuhn, R., and Rajewsky, K. (1991). A B cell-deficient mouse by targeted disruption of the membrane exon of the immunoglobulin mu chain gene. Nature *350*, 423-426. 10.1038/350423a0.

Kleeff, J., Korc, M., Apte, M., La Vecchia, C., Johnson, C.D., Biankin, A.V., Neale, R.E., Tempero, M., Tuveson, D.A., Hruban, R.H., and Neoptolemos, J.P. (2016). Pancreatic cancer. Nature Reviews Disease Primers *2*, 16022. 10.1038/nrdp.2016.22.

Klein, A.P. (2021). Pancreatic cancer epidemiology: understanding the role of lifestyle and inherited risk factors. Nature Reviews Gastroenterology & Hepatology *18*, 493-502. 10.1038/s41575-021-00457-x.

Kong, K., Guo, M., Liu, Y., and Zheng, J. (2020). Progress in Animal Models of Pancreatic Ductal Adenocarcinoma. J Cancer *11*, 1555-1567. 10.7150/jca.37529.

Kopp, J.L., von Figura, G., Mayes, E., Liu, F.F., Dubois, C.L., Morris, J.P.t., Pan, F.C., Akiyama, H., Wright, C.V., Jensen, K., et al. (2012). Identification of Sox9-dependent acinar-to-ductal reprogramming as the principal mechanism for initiation of pancreatic ductal adenocarcinoma. Cancer cell *22*, 737-750. 10.1016/j.ccr.2012.10.025.

Kou, F., Wu, L., Ren, X., and Yang, L. (2020). Chromosome Abnormalities: New Insights into Their Clinical Significance in Cancer. Mol Ther Oncolytics *17*, 562-570. 10.1016/j.omto.2020.05.010.

References

Kuilman, T., Velds, A., Kemper, K., Ranzani, M., Bombardelli, L., Hoogstraat, M., Nevedomskaya, E., Xu, G., de Ruiter, J., Lolkema, M.P., et al. (2015). CopywriteR: DNA copy number detection from off-target sequence data. Genome Biol *16*, 49. 10.1186/s13059-015-0617-1.

Kumar, J., Fraser, F.W., Riley, C., Ahmed, N., McCulloch, D.R., and Ward, A.C. (2014). Granulocyte colony-stimulating factor receptor signalling via Janus kinase 2/signal transducer and activator of transcription 3 in ovarian cancer. Br J Cancer *110*, 133-145. 10.1038/bjc.2013.673.

Lai, W.S., Carballo, E., Strum, J.R., Kennington, E.A., Phillips, R.S., and Blackshear, P.J. (1999). Evidence that tristetraprolin binds to AU-rich elements and promotes the deadenylation and destabilization of tumor necrosis factor alpha mRNA. Mol Cell Biol *19*, 4311-4323. 10.1128/mcb.19.6.4311.

Lai, W.S., Carballo, E., Thorn, J.M., Kennington, E.A., and Blackshear, P.J. (2000). Interactions of CCCH zinc finger proteins with mRNA. Binding of tristetraprolin-related zinc finger proteins to Au-rich elements and destabilization of mRNA. J Biol Chem *275*, 17827-17837. 10.1074/jbc.M001696200.

Lampel, M., and Kern, H.F. (1977). Acute interstitial pancreatitis in the rat induced by excessive doses of a pancreatic secretagogue. Virchows Arch A Pathol Anat Histol *373*, 97-117. 10.1007/bf00432156.

Langowski, J.L., Zhang, X., Wu, L., Mattson, J.D., Chen, T., Smith, K., Basham, B., McClanahan, T., Kastelein, R.A., and Oft, M. (2006). IL-23 promotes tumour incidence and growth. Nature *442*, 461-465. 10.1038/nature04808.

Lanier, L.L., O'Fallon, S., Somoza, C., Phillips, J.H., Linsley, P.S., Okumura, K., Ito, D., and Azuma, M. (1995). CD80 (B7) and CD86 (B70) provide similar costimulatory signals for T cell proliferation, cytokine production, and generation of CTL. Journal of immunology (Baltimore, Md. : 1950) *154*, 97-105.

LeBien, T.W., and Tedder, T.F. (2008). B lymphocytes: how they develop and function. Blood *112*, 1570-1580. 10.1182/blood-2008-02-078071.

Lee, A.Y.L., Dubois, C.L., Sarai, K., Zarei, S., Schaeffer, D.F., Sander, M., and Kopp, J.L. (2019). Cell of origin affects tumour development and phenotype in pancreatic ductal adenocarcinoma. Gut *68*, 487-498. 10.1136/gutjnl-2017-314426.

Lee, P.P., Fitzpatrick, D.R., Beard, C., Jessup, H.K., Lehar, S., Makar, K.W., Perez-Melgosa, M., Sweetser, M.T., Schlissel, M.S., Nguyen, S., et al. (2001). A critical role for Dnmt1 and DNA methylation in T cell development, function, and survival. Immunity *15*, 763-774.

Lee, S.K., Rigby, R.J., Zotos, D., Tsai, L.M., Kawamoto, S., Marshall, J.L., Ramiscal, R.R., Chan, T.D., Gatto, D., Brink, R., et al. (2011). B cell priming for extrafollicular antibody responses requires Bcl-6 expression by T cells. The Journal of experimental medicine *208*, 1377-1388. 10.1084/jem.20102065.

Lee, S.K., Silva, D.G., Martin, J.L., Pratama, A., Hu, X., Chang, P.P., Walters, G., and Vinuesa, C.G. (2012). Interferon-γ excess leads to pathogenic accumulation of follicular helper T cells and germinal centers. Immunity *37*, 880-892. 10.1016/j.immuni.2012.10.010.

Leppek, K., Schott, J., Reitter, S., Poetz, F., Hammond, M.C., and Stoecklin, G. (2013). Roquin promotes constitutive mRNA decay via a conserved class of stem-loop recognition motifs. Cell *153*, 869-881. 10.1016/j.cell.2013.04.016.

Lesina, M., Kurkowski, M.U., Ludes, K., Rose-John, S., Treiber, M., Kloppel, G., Yoshimura, A., Reindl, W., Sipos, B., Akira, S., et al. (2011). Stat3/Socs3 activation by IL-6 transsignaling promotes

progression of pancreatic intraepithelial neoplasia and development of pancreatic cancer. Cancer cell *19*, 456-469. 10.1016/j.ccr.2011.03.009.

Li, W., Gao, B., Lee, S.M., Bennett, K., and Fang, D. (2007). RLE-1, an E3 ubiquitin ligase, regulates C. elegans aging by catalyzing DAF-16 polyubiquitination. Dev Cell *12*, 235-246. 10.1016/j.devcel.2006.12.002.

Li, Y., Dai, J., Song, M., Fitzgerald-Bocarsly, P., and Kiledjian, M. (2012). Dcp2 decapping protein modulates mRNA stability of the critical interferon regulatory factor (IRF) IRF-7. Mol Cell Biol *32*, 1164-1172. 10.1128/mcb.06328-11.

Liang, J., Saad, Y., Lei, T., Wang, J., Qi, D., Yang, Q., Kolattukudy, P.E., and Fu, M. (2010). MCP-induced protein 1 deubiquitinates TRAF proteins and negatively regulates JNK and NF-kappaB signaling. The Journal of experimental medicine *207*, 2959-2973. 10.1084/jem.20092641.

Liggitt, D., and Dintzis, S.M. (2018). 14 - Pancreas. In Comparative Anatomy and Histology (Second Edition), P.M. Treuting, S.M. Dintzis, and K.S. Montine, eds. (Academic Press), pp. 241-250. https://doi.org/10.1016/B978-0-12-802900-8.00014-2.

Linterman, M.A., Rigby, R.J., Wong, R., Silva, D., Withers, D., Anderson, G., Verma, N.K., Brink, R., Hutloff, A., Goodnow, C.C., and Vinuesa, C.G. (2009a). Roquin differentiates the specialized functions of duplicated T cell costimulatory receptor genes CD28 and ICOS. Immunity *30*, 228-241. 10.1016/j.immuni.2008.12.015.

Linterman, M.A., Rigby, R.J., Wong, R.K., Yu, D., Brink, R., Cannons, J.L., Schwartzberg, P.L., Cook, M.C., Walters, G.D., and Vinuesa, C.G. (2009b). Follicular helper T cells are required for systemic autoimmunity. The Journal of experimental medicine *206*, 561-576. 10.1084/jem.20081886.

Liot, S., Balas, J., Aubert, A., Prigent, L., Mercier-Gouy, P., Verrier, B., Bertolino, P., Hennino, A., Valcourt, U., and Lambert, E. (2021). Stroma Involvement in Pancreatic Ductal Adenocarcinoma: An Overview Focusing on Extracellular Matrix Proteins. Front Immunol *12*, 612271. 10.3389/fimmu.2021.612271.

Liou, G.Y., Döppler, H., Necela, B., Krishna, M., Crawford, H.C., Raimondo, M., and Storz, P. (2013). Macrophage-secreted cytokines drive pancreatic acinar-to-ductal metaplasia through NF-κB and MMPs. J Cell Biol *202*, 563-577. 10.1083/jcb.201301001.

Liu, H., Rodgers, N.D., Jiao, X., and Kiledjian, M. (2002). The scavenger mRNA decapping enzyme DcpS is a member of the HIT family of pyrophosphatases. Embo j *21*, 4699-4708. 10.1093/emboj/cdf448.

Liu, X., Chen, X., Zhong, B., Wang, A., Wang, X., Chu, F., Nurieva, R.I., Yan, X., Chen, P., van der Flier, L.G., et al. (2014). Transcription factor achaete-scute homologue 2 initiates follicular T-helper-cell development. Nature *507*, 513-518. 10.1038/nature12910.

Liu, Z., Liu, J.Q., Talebian, F., Wu, L.C., Li, S., and Bai, X.F. (2013). IL-27 enhances the survival of tumor antigen-specific CD8+ T cells and programs them into IL-10-producing, memory precursor-like effector cells. European journal of immunology *43*, 468-479. 10.1002/eji.201242930.

Longnecker, D.S. (2021). Anatomy and Histology of the Pancreas. https://pancreapedia.org/reviews/anatomy-and-histology-of-pancreas.

References

Lu, W., Zhou, M., Wang, B., Liu, X., and Li, B. (2020). Roquin1 inhibits the proliferation of breast cancer cells by inducing G1/S cell cycle arrest via selectively destabilizing the mRNAs of cell cycle-promoting genes. Journal of experimental & clinical cancer research : CR *39*, 255. 10.1186/s13046-020-01766-w.

Lykke-Andersen, J., and Wagner, E. (2005). Recruitment and activation of mRNA decay enzymes by two ARE-mediated decay activation domains in the proteins TTP and BRF-1. Genes & development *19*, 351-361. 10.1101/gad.1282305.

Ma, Y., Hwang, R.F., Logsdon, C.D., and Ullrich, S.E. (2013). Dynamic mast cell-stromal cell interactions promote growth of pancreatic cancer. Cancer research *73*, 3927-3937. 10.1158/0008-5472.Can-12-4479.

Mace, T.A., Ameen, Z., Collins, A., Wojcik, S., Mair, M., Young, G.S., Fuchs, J.R., Eubank, T.D., Frankel, W.L., Bekaii-Saab, T., et al. (2013a). Pancreatic cancer-associated stellate cells promote differentiation of myeloid-derived suppressor cells in a STAT3-dependent manner. Cancer research *73*, 3007-3018. 10.1158/0008-5472.Can-12-4601.

Mace, T.A., Bloomston, M., and Lesinski, G.B. (2013b). Pancreatic cancer-associated stellate cells: A viable target for reducing immunosuppression in the tumor microenvironment. Oncoimmunology *2*, e24891. 10.4161/onci.24891.

MacLennan, I.C. (1994). Germinal centers. Annu Rev Immunol *12*, 117-139. 10.1146/annurev.iy.12.040194.001001.

Martin, T.D., Patel, R.S., Cook, D.R., Choi, M.Y., Patil, A., Liang, A.C., Li, M.Z., Haigis, K.M., and Elledge, S.J. (2021). The adaptive immune system is a major driver of selection for tumor suppressor gene inactivation. Science (New York, N.Y.) *373*, 1327-1335. 10.1126/science.abg5784.

Maruyama, T., Araki, T., Kawarazaki, Y., Naguro, I., Heynen, S., Aza-Blanc, P., Ronai, Z., Matsuzawa, A., and Ichijo, H. (2014). Roquin-2 promotes ubiquitin-mediated degradation of ASK1 to regulate stress responses. Sci Signal *7*, ra8. 10.1126/scisignal.2004822.

Matsushita, K., Takeuchi, O., Standley, D.M., Kumagai, Y., Kawagoe, T., Miyake, T., Satoh, T., Kato, H., Tsujimura, T., Nakamura, H., and Akira, S. (2009). Zc3h12a is an RNase essential for controlling immune responses by regulating mRNA decay. Nature *458*, 1185-1190. 10.1038/nature07924.

McAdam, A.J., Greenwald, R.J., Levin, M.A., Chernova, T., Malenkovich, N., Ling, V., Freeman, G.J., and Sharpe, A.H. (2001). ICOS is critical for CD40-mediated antibody class switching. Nature *409*, 102-105. 10.1038/35051107.

McAllister, F., Bailey, J.M., Alsina, J., Nirschl, C.J., Sharma, R., Fan, H., Rattigan, Y., Roeser, J.C., Lankapalli, R.H., Zhang, H., et al. (2014). Oncogenic Kras activates a hematopoietic-to-epithelial IL-17 signaling axis in preinvasive pancreatic neoplasia. Cancer cell *25*, 621-637. 10.1016/j.ccr.2014.03.014.

McFarland-Mancini, M.M., Funk, H.M., Paluch, A.M., Zhou, M., Giridhar, P.V., Mercer, C.A., Kozma, S.C., and Drew, A.F. (2010). Differences in wound healing in mice with deficiency of IL-6 versus IL-6 receptor. Journal of immunology (Baltimore, Md. : 1950) *184*, 7219-7228. 10.4049/jimmunol.0901929.

Medzhitov, R. (2008). Origin and physiological roles of inflammation. Nature *454*, 428-435. 10.1038/nature07201.

Medzhitov, R., and Janeway, C., Jr. (2000). Innate immunity. The New England journal of medicine *343*, 338-344. 10.1056/nejm200008033430506.

References

Mescher, M.F., Curtsinger, J.M., Agarwal, P., Casey, K.A., Gerner, M., Hammerbeck, C.D., Popescu, F., and Xiao, Z. (2006). Signals required for programming effector and memory development by CD8+ T cells. Immunological reviews *211*, 81-92. 10.1111/j.0105-2896.2006.00382.x.

Miao, R., Huang, S., Zhou, Z., Quinn, T., Van Treeck, B., Nayyar, T., Dim, D., Jiang, Z., Papasian, C.J., Eugene Chen, Y., et al. (2013). Targeted disruption of MCPIP1/Zc3h12a results in fatal inflammatory disease. Immunol Cell Biol *91*, 368-376. 10.1038/icb.2013.11.

Mino, T., Murakawa, Y., Fukao, A., Vandenbon, A., Wessels, H.H., Ori, D., Uehata, T., Tartey, S., Akira, S., Suzuki, Y., et al. (2015). Regnase-1 and Roquin Regulate a Common Element in Inflammatory mRNAs by Spatiotemporally Distinct Mechanisms. Cell *161*, 1058-1073. 10.1016/j.cell.2015.04.029.

Mino, T., and Takeuchi, O. (2015). Regnase-1 and Roquin regulate inflammatory mRNAs. Oncotarget *6*, 17869-17870. 10.18632/oncotarget.4891.

Mitchell, P., Petfalski, E., Shevchenko, A., Mann, M., and Tollervey, D. (1997). The exosome: a conserved eukaryotic RNA processing complex containing multiple 3'-->5' exoribonucleases. Cell *91*, 457-466. 10.1016/s0092-8674(00)80432-8.

Morishima, N., Owaki, T., Asakawa, M., Kamiya, S., Mizuguchi, J., and Yoshimoto, T. (2005). Augmentation of effector CD8+ T cell generation with enhanced granzyme B expression by IL-27. Journal of immunology (Baltimore, Md. : 1950) *175*, 1686-1693. 10.4049/jimmunol.175.3.1686.

Mucciolo, G., Curcio, C., Roux, C., Li, W.Y., Capello, M., Curto, R., Chiarle, R., Giordano, D., Satolli, M.A., Lawlor, R., et al. (2021). IL17A critically shapes the transcriptional program of fibroblasts in pancreatic cancer and switches on their protumorigenic functions. Proceedings of the National Academy of Sciences of the United States of America *118*. 10.1073/pnas.2020395118.

Mueller, S., Engleitner, T., Maresch, R., Zukowska, M., Lange, S., Kaltenbacher, T., Konukiewitz, B., Öllinger, R., Zwiebel, M., Strong, A., et al. (2018). Evolutionary routes and KRAS dosage define pancreatic cancer phenotypes. Nature *554*, 62-68. 10.1038/nature25459.

Mugridge, J.S., Coller, J., and Gross, J.D. (2018). Structural and molecular mechanisms for the control of eukaryotic 5′–3′ mRNA decay. Nature Structural & Molecular Biology *25*, 1077-1085. 10.1038/s41594-018-0164-z.

Mullen, A.C., High, F.A., Hutchins, A.S., Lee, H.W., Villarino, A.V., Livingston, D.M., Kung, A.L., Cereb, N., Yao, T.P., Yang, S.Y., and Reiner, S.L. (2001). Role of T-bet in commitment of TH1 cells before IL-12-dependent selection. Science (New York, N.Y.) *292*, 1907-1910. 10.1126/science.1059835.

Multhoff, G., and Radons, J. (2012). Radiation, Inflammation, and Immune Responses in Cancer. Frontiers in Oncology *2*. 10.3389/fonc.2012.00058.

Murakawa, Y., Hinz, M., Mothes, J., Schuetz, A., Uhl, M., Wyler, E., Yasuda, T., Mastrobuoni, G., Friedel, C.C., Dolken, L., et al. (2015). RC3H1 post-transcriptionally regulates A20 mRNA and modulates the activity of the IKK/NF-kappaB pathway. Nature communications *6*, 7367. 10.1038/ncomms8367.

Murphy, K.M., and Reiner, S.L. (2002). The lineage decisions of helper T cells. Nature reviews. Immunology *2*, 933-944. 10.1038/nri954.

Murphy, K.W., C. (2017). Janeway's Immunebiology, 9th Edition (Garland Science, Taylor & Francis Group, LLC).

References

Nagarajan, V.K., Jones, C.I., Newbury, S.F., and Green, P.J. (2013). XRN 5'→3' exoribonucleases: structure, mechanisms and functions. Biochim Biophys Acta *1829*, 590-603. 10.1016/j.bbagrm.2013.03.005.

Nish, S.A., Schenten, D., Wunderlich, F.T., Pope, S.D., Gao, Y., Hoshi, N., Yu, S., Yan, X., Lee, H.K., Pasman, L., et al. (2014). T cell-intrinsic role of IL-6 signaling in primary and memory responses. Elife *3*, e01949. 10.7554/eLife.01949.

Nurieva, R.I., Chung, Y., Hwang, D., Yang, X.O., Kang, H.S., Ma, L., Wang, Y.H., Watowich, S.S., Jetten, A.M., Tian, Q., and Dong, C. (2008). Generation of T follicular helper cells is mediated by interleukin-21 but independent of T helper 1, 2, or 17 cell lineages. Immunity *29*, 138-149. 10.1016/j.immuni.2008.05.009.

Nurieva, R.I., Chung, Y., Martinez, G.J., Yang, X.O., Tanaka, S., Matskevitch, T.D., Wang, Y.H., and Dong, C. (2009). Bcl6 mediates the development of T follicular helper cells. Science (New York, N.Y.) *325*, 1001-1005. 10.1126/science.1176676.

Nurieva, R.I., Podd, A., Chen, Y., Alekseev, A.M., Yu, M., Qi, X., Huang, H., Wen, R., Wang, J., Li, H.S., et al. (2012). STAT5 protein negatively regulates T follicular helper (Tfh) cell generation and function. J Biol Chem *287*, 11234-11239. 10.1074/jbc.M111.324046.

O'Shea, J.J., and Paul, W.E. (2010). Mechanisms underlying lineage commitment and plasticity of helper CD4+ T cells. Science (New York, N.Y.) *327*, 1098-1102. 10.1126/science.1178334.

Oestreich, K.J., Mohn, S.E., and Weinmann, A.S. (2012). Molecular mechanisms that control the expression and activity of Bcl-6 in TH1 cells to regulate flexibility with a TFH-like gene profile. Nature immunology *13*, 405-411. 10.1038/ni.2242.

Öhlund, D., Handly-Santana, A., Biffi, G., Elyada, E., Almeida, A.S., Ponz-Sarvise, M., Corbo, V., Oni, T.E., Hearn, S.A., Lee, E.J., et al. (2017). Distinct populations of inflammatory fibroblasts and myofibroblasts in pancreatic cancer. The Journal of experimental medicine *214*, 579-596. 10.1084/jem.20162024.

Orth, M., Metzger, P., Gerum, S., Mayerle, J., Schneider, G., Belka, C., Schnurr, M., and Lauber, K. (2019). Pancreatic ductal adenocarcinoma: biological hallmarks, current status, and future perspectives of combined modality treatment approaches. Radiation Oncology *14*, 141. 10.1186/s13014-019-1345-6.

Özdemir, B.C., Pentcheva-Hoang, T., Carstens, J.L., Zheng, X., Wu, C.C., Simpson, T.R., Laklai, H., Sugimoto, H., Kahlert, C., Novitskiy, S.V., et al. (2014). Depletion of carcinoma-associated fibroblasts and fibrosis induces immunosuppression and accelerates pancreas cancer with reduced survival. Cancer cell *25*, 719-734. 10.1016/j.ccr.2014.04.005.

Park, H., Li, Z., Yang, X.O., Chang, S.H., Nurieva, R., Wang, Y.H., Wang, Y., Hood, L., Zhu, Z., Tian, Q., and Dong, C. (2005). A distinct lineage of CD4 T cells regulates tissue inflammation by producing interleukin 17. Nature immunology *6*, 1133-1141. 10.1038/ni1261.

Patel, M.B., Pothula, S.P., Xu, Z., Lee, A.K., Goldstein, D., Pirola, R.C., Apte, M.V., and Wilson, J.S. (2014). The role of the hepatocyte growth factor/c-MET pathway in pancreatic stellate cell-endothelial cell interactions: antiangiogenic implications in pancreatic cancer. Carcinogenesis *35*, 1891-1900. 10.1093/carcin/bgu122.

References

Pedros, C., Zhang, Y., Hu, J.K., Choi, Y.S., Canonigo-Balancio, A.J., Yates, J.R., 3rd, Altman, A., Crotty, S., and Kong, K.F. (2016). A TRAF-like motif of the inducible costimulator ICOS controls development of germinal center TFH cells via the kinase TBK1. Nature immunology *17*, 825-833. 10.1038/ni.3463.

Pennock, N.D., Gapin, L., and Kedl, R.M. (2014). IL-27 is required for shaping the magnitude, affinity distribution, and memory of T cells responding to subunit immunization. Proceedings of the National Academy of Sciences *111*, 16472-16477. 10.1073/pnas.1407393111.

Pergolini, I., Crippa, S., Pagnanelli, M., Belfiori, G., Pucci, A., Partelli, S., Rubini, C., Castelli, P., Zamboni, G., and Falconi, M. (2019). Prognostic impact of Ki-67 proliferative index in resectable pancreatic ductal adenocarcinoma. BJS Open *3*, 646-655. 10.1002/bjs5.50175.

Perusina Lanfranca, M., Zhang, Y., Girgis, A., Kasselman, S., Lazarus, J., Kryczek, I., Delrosario, L., Rhim, A., Koneva, L., Sartor, M., et al. (2020). Interleukin 22 Signaling Regulates Acinar Cell Plasticity to Promote Pancreatic Tumor Development in Mice. Gastroenterology *158*, 1417-1432.e1411. 10.1053/j.gastro.2019.12.010.

Pinho, A.V., Rooman, I., Reichert, M., De Medts, N., Bouwens, L., Rustgi, A.K., and Real, F.X. (2011). Adult pancreatic acinar cells dedifferentiate to an embryonic progenitor phenotype with concomitant activation of a senescence programme that is present in chronic pancreatitis. Gut *60*, 958-966. 10.1136/gut.2010.225920.

Pratama, A., Ramiscal, R.R., Silva, D.G., Das, S.K., Athanasopoulos, V., Fitch, J., Botelho, N.K., Chang, P.P., Hu, X., Hogan, J.J., et al. (2013). Roquin-2 shares functions with its paralog Roquin-1 in the repression of mRNAs controlling T follicular helper cells and systemic inflammation. Immunity *38*, 669-680. 10.1016/j.immuni.2013.01.011.

Putland, R.A., Sassinis, T.A., Harvey, J.S., Diamond, P., Coles, L.S., Brown, C.Y., and Goodall, G.J. (2002). RNA destabilization by the granulocyte colony-stimulating factor stem-loop destabilizing element involves a single stem-loop that promotes deadenylation. Mol Cell Biol *22*, 1664-1673. 10.1128/mcb.22.6.1664-1673.2002.

Qi, H., Cannons, J.L., Klauschen, F., Schwartzberg, P.L., and Germain, R.N. (2008). SAP-controlled T-B cell interactions underlie germinal centre formation. Nature *455*, 764-769. 10.1038/nature07345.

Qureshi, O.S., Zheng, Y., Nakamura, K., Attridge, K., Manzotti, C., Schmidt, E.M., Baker, J., Jeffery, L.E., Kaur, S., Briggs, Z., et al. (2011). Trans-endocytosis of CD80 and CD86: a molecular basis for the cell-extrinsic function of CTLA-4. Science (New York, N.Y.) *332*, 600-603. 10.1126/science.1202947.

Rahib, L., Smith, B.D., Aizenberg, R., Rosenzweig, A.B., Fleshman, J.M., and Matrisian, L.M. (2014). Projecting cancer incidence and deaths to 2030: the unexpected burden of thyroid, liver, and pancreas cancers in the United States. Cancer research *74*, 2913-2921. 10.1158/0008-5472.Can-14-0155.

Ramiscal, R.R., Parish, I.A., Lee-Young, R.S., Babon, J.J., Blagih, J., Pratama, A., Martin, J., Hawley, N., Cappello, J.Y., Nieto, P.F., et al. (2015). Attenuation of AMPK signaling by ROQUIN promotes T follicular helper cell formation. Elife *4*. 10.7554/eLife.08698.

Rehage, N., Davydova, E., Conrad, C., Behrens, G., Maiser, A., Stehklein, J.E., Brenner, S., Klein, J., Jeridi, A., Hoffmann, A., et al. (2018). Binding of NUFIP2 to Roquin promotes recognition and regulation of ICOS mRNA. Nature communications *9*, 299. 10.1038/s41467-017-02582-1.

References

Rhim, A.D., Mirek, E.T., Aiello, N.M., Maitra, A., Bailey, J.M., McAllister, F., Reichert, M., Beatty, G.L., Rustgi, A.K., Vonderheide, R.H., et al. (2012). EMT and dissemination precede pancreatic tumor formation. Cell *148*, 349-361. 10.1016/j.cell.2011.11.025.

Rhim, A.D., Oberstein, P.E., Thomas, D.H., Mirek, E.T., Palermo, C.F., Sastra, S.A., Dekleva, E.N., Saunders, T., Becerra, C.P., Tattersall, I.W., et al. (2014). Stromal elements act to restrain, rather than support, pancreatic ductal adenocarcinoma. Cancer cell *25*, 735-747. 10.1016/j.ccr.2014.04.021.

Ridker, P.M., MacFadyen, J.G., Thuren, T., Everett, B.M., Libby, P., and Glynn, R.J. (2017). Effect of interleukin-1β inhibition with canakinumab on incident lung cancer in patients with atherosclerosis: exploratory results from a randomised, double-blind, placebo-controlled trial. Lancet *390*, 1833-1842. 10.1016/s0140-6736(17)32247-x.

Rissland, O.S. (2017). The organization and regulation of mRNA-protein complexes. Wiley Interdiscip Rev RNA *8*. 10.1002/wrna.1369.

Rock, K.L., and Kono, H. (2008). The inflammatory response to cell death. Annu Rev Pathol *3*, 99-126. 10.1146/annurev.pathmechdis.3.121806.151456.

Rothwell, P.M., Fowkes, F.G., Belch, J.F., Ogawa, H., Warlow, C.P., and Meade, T.W. (2011). Effect of daily aspirin on long-term risk of death due to cancer: analysis of individual patient data from randomised trials. Lancet *377*, 31-41. 10.1016/s0140-6736(10)62110-1.

Rothwell, P.M., Wilson, M., Price, J.F., Belch, J.F., Meade, T.W., and Mehta, Z. (2012). Effect of daily aspirin on risk of cancer metastasis: a study of incident cancers during randomised controlled trials. Lancet *379*, 1591-1601. 10.1016/s0140-6736(12)60209-8.

Ruterbusch, M., Pruner, K.B., Shehata, L., and Pepper, M. (2020). In Vivo CD4(+) T Cell Differentiation and Function: Revisiting the Th1/Th2 Paradigm. Annu Rev Immunol *38*, 705-725. 10.1146/annurev-immunol-103019-085803.

Sakaguchi, S., Sakaguchi, N., Asano, M., Itoh, M., and Toda, M. (1995). Immunologic self-tolerance maintained by activated T cells expressing IL-2 receptor alpha-chains (CD25). Breakdown of a single mechanism of self-tolerance causes various autoimmune diseases. Journal of immunology (Baltimore, Md. : 1950) *155*, 1151-1164.

Sakaguchi, S., Yamaguchi, T., Nomura, T., and Ono, M. (2008). Regulatory T cells and immune tolerance. Cell *133*, 775-787. 10.1016/j.cell.2008.05.009.

Sakurai, S., Ohto, U., and Shimizu, T. (2015). Structure of human Roquin-2 and its complex with constitutive-decay element RNA. Acta Crystallogr F Struct Biol Commun *71*, 1048-1054. 10.1107/s2053230x15011887.

Saraiva, M., and O'Garra, A. (2010). The regulation of IL-10 production by immune cells. Nature Reviews Immunology *10*, 170-181. 10.1038/nri2711.

Sawada, S., Scarborough, J.D., Killeen, N., and Littman, D.R. (1994). A lineage-specific transcriptional silencer regulates CD4 gene expression during T lymphocyte development. Cell *77*, 917-929. 10.1016/0092-8674(94)90140-6.

Schäfer, I.B., Rode, M., Bonneau, F., Schüssler, S., and Conti, E. (2014). The structure of the Pan2-Pan3 core complex reveals cross-talk between deadenylase and pseudokinase. Nat Struct Mol Biol *21*, 591-598. 10.1038/nsmb.2834.

References

Schlundt, A., Heinz, G.A., Janowski, R., Geerlof, A., Stehle, R., Heissmeyer, V., Niessing, D., and Sattler, M. (2014). Structural basis for RNA recognition in roquin-mediated post-transcriptional gene regulation. Nat Struct Mol Biol *21*, 671-678. 10.1038/nsmb.2855.

Scholzen, T., and Gerdes, J. (2000). The Ki-67 protein: from the known and the unknown. J Cell Physiol *182*, 311-322. 10.1002/(sici)1097-4652(200003)182:3<311::Aid-jcp1>3.0.Co;2-9.

Schuetz, A., Murakawa, Y., Rosenbaum, E., Landthaler, M., and Heinemann, U. (2014). Roquin binding to target mRNAs involves a winged helix-turn-helix motif. Nature communications *5*, 5701. 10.1038/ncomms6701.

Schutte, M., Hruban, R.H., Geradts, J., Maynard, R., Hilgers, W., Rabindran, S.K., Moskaluk, C.A., Hahn, S.A., Schwarte-Waldhoff, I., Schmiegel, W., et al. (1997). Abrogation of the Rb/p16 tumor-suppressive pathway in virtually all pancreatic carcinomas. Cancer research *57*, 3126-3130.

Schwickert, T.A., Victora, G.D., Fooksman, D.R., Kamphorst, A.O., Mugnier, M.R., Gitlin, A.D., Dustin, M.L., and Nussenzweig, M.C. (2011). A dynamic T cell-limited checkpoint regulates affinity-dependent B cell entry into the germinal center. The Journal of experimental medicine *208*, 1243-1252. 10.1084/jem.20102477.

Sharif, H., Ozgur, S., Sharma, K., Basquin, C., Urlaub, H., and Conti, E. (2013). Structural analysis of the yeast Dhh1-Pat1 complex reveals how Dhh1 engages Pat1, Edc3 and RNA in mutually exclusive interactions. Nucleic Acids Res *41*, 8377-8390. 10.1093/nar/gkt600.

Shi, C., Washington, M.K., Chaturvedi, R., Drosos, Y., Revetta, F.L., Weaver, C.J., Buzhardt, E., Yull, F.E., Blackwell, T.S., Sosa-Pineda, B., et al. (2014). Fibrogenesis in pancreatic cancer is a dynamic process regulated by macrophage-stellate cell interaction. Lab Invest *94*, 409-421. 10.1038/labinvest.2014.10.

Siegel, R.L., Miller, K.D., Fuchs, H.E., and Jemal, A. (2021). Cancer Statistics, 2021. CA: a cancer journal for clinicians *71*, 7-33. 10.3322/caac.21654.

Siess, D.C., Vedder, C.T., Merkens, L.S., Tanaka, T., Freed, A.C., McCoy, S.L., Heinrich, M.C., Deffebach, M.E., Bennett, R.M., and Hefeneider, S.H. (2000). A human gene coding for a membrane-associated nucleic acid-binding protein. J Biol Chem *275*, 33655-33662. 10.1074/jbc.M004461200.

Singh, S.K., Mishra, M.K., Eltoum, I.-E.A., Bae, S., Lillard, J.W., and Singh, R. (2018). CCR5/CCL5 axis interaction promotes migratory and invasiveness of pancreatic cancer cells. Scientific Reports *8*, 1323. 10.1038/s41598-018-19643-0.

Sledzinska, A., Hemmers, S., Mair, F., Gorka, O., Ruland, J., Fairbairn, L., Nissler, A., Muller, W., Waisman, A., Becher, B., and Buch, T. (2013). TGF-beta signalling is required for CD4(+) T cell homeostasis but dispensable for regulatory T cell function. PLoS biology *11*, e1001674. 10.1371/journal.pbio.1001674.

Srivastava, M., Duan, G., Kershaw, N.J., Athanasopoulos, V., Yeo, J.H., Ose, T., Hu, D., Brown, S.H., Jergic, S., Patel, H.R., et al. (2015). Roquin binds microRNA-146a and Argonaute2 to regulate microRNA homeostasis. Nature communications *6*, 6253. 10.1038/ncomms7253.

Stoecklin, G., Lu, M., Rattenbacher, B., and Moroni, C. (2003). A constitutive decay element promotes tumor necrosis factor alpha mRNA degradation via an AU-rich element-independent pathway. Mol Cell Biol *23*, 3506-3515. 10.1128/mcb.23.10.3506-3515.2003.

References

Storz, P. (2017). Acinar cell plasticity and development of pancreatic ductal adenocarcinoma. Nat Rev Gastroenterol Hepatol *14*, 296-304. 10.1038/nrgastro.2017.12.

Sun, M., Schwalb, B., Pirkl, N., Maier, K.C., Schenk, A., Failmezger, H., Tresch, A., and Cramer, P. (2013). Global analysis of eukaryotic mRNA degradation reveals Xrn1-dependent buffering of transcript levels. Mol Cell *52*, 52-62. 10.1016/j.molcel.2013.09.010.

Swain, S.L., Weinberg, A.D., English, M., and Huston, G. (1990). IL-4 directs the development of Th2-like helper effectors. Journal of immunology (Baltimore, Md. : 1950) *145*, 3796-3806.

Szabo, S.J., Kim, S.T., Costa, G.L., Zhang, X., Fathman, C.G., and Glimcher, L.H. (2000). A novel transcription factor, T-bet, directs Th1 lineage commitment. Cell *100*, 655-669. 10.1016/s0092-8674(00)80702-3.

Takeda, K., Tanaka, T., Shi, W., Matsumoto, M., Minami, M., Kashiwamura, S., Nakanishi, K., Yoshida, N., Kishimoto, T., and Akira, S. (1996). Essential role of Stat6 in IL-4 signalling. Nature *380*, 627-630. 10.1038/380627a0.

Tam, H.H., Melo, M.B., Kang, M., Pelet, J.M., Ruda, V.M., Foley, M.H., Hu, J.K., Kumari, S., Crampton, J., Baldeon, A.D., et al. (2016). Sustained antigen availability during germinal center initiation enhances antibody responses to vaccination. Proceedings of the National Academy of Sciences of the United States of America *113*, E6639-e6648. 10.1073/pnas.1606050113.

Tan, D., Zhou, M., Kiledjian, M., and Tong, L. (2014). The ROQ domain of Roquin recognizes mRNA constitutive-decay element and double-stranded RNA. Nat Struct Mol Biol *21*, 679-685. 10.1038/nsmb.2857.

Tanaka, M., Shibahara, J., Fukushima, N., Shinozaki, A., Umeda, M., Ishikawa, S., Kokudo, N., and Fukayama, M. (2011). Claudin-18 is an early-stage marker of pancreatic carcinogenesis. J Histochem Cytochem *59*, 942-952. 10.1369/0022155411420569.

Tang, D., Yuan, Z., Xue, X., Lu, Z., Zhang, Y., Wang, H., Chen, M., An, Y., Wei, J., Zhu, Y., et al. (2012). High expression of Galectin-1 in pancreatic stellate cells plays a role in the development and maintenance of an immunosuppressive microenvironment in pancreatic cancer. International journal of cancer *130*, 2337-2348. 10.1002/ijc.26290.

Teixeira, D., and Parker, R. (2007). Analysis of P-body assembly in Saccharomyces cerevisiae. Mol Biol Cell *18*, 2274-2287. 10.1091/mbc.e07-03-0199.

Tsukita, S., and Furuse, M. (2000). Pores in the wall: claudins constitute tight junction strands containing aqueous pores. J Cell Biol *149*, 13-16. 10.1083/jcb.149.1.13.

Uehata, T., Iwasaki, H., Vandenbon, A., Matsushita, K., Hernandez-Cuellar, E., Kuniyoshi, K., Satoh, T., Mino, T., Suzuki, Y., Standley, D.M., et al. (2013). Malt1-induced cleavage of regnase-1 in CD4(+) helper T cells regulates immune activation. Cell *153*, 1036-1049. 10.1016/j.cell.2013.04.034.

Uhlén, M., Fagerberg, L., Hallström, B.M., Lindskog, C., Oksvold, P., Mardinoglu, A., Sivertsson, Å., Kampf, C., Sjöstedt, E., Asplund, A., et al. (2015). Proteomics. Tissue-based map of the human proteome. Science (New York, N.Y.) *347*, 1260419. 10.1126/science.1260419.

Ukleja, M., Cuellar, J., Siwaszek, A., Kasprzak, J.M., Czarnocki-Cieciura, M., Bujnicki, J.M., Dziembowski, A., and Valpuesta, J.M. (2016). The architecture of the Schizosaccharomyces pombe CCR4-NOT complex. Nature communications *7*, 10433. 10.1038/ncomms10433.

References

Vijayan, D., Mohd Redzwan, N., Avery, D.T., Wirasinha, R.C., Brink, R., Walters, G., Adelstein, S., Kobayashi, M., Gray, P., Elliott, M., et al. (2016). IL-27 Directly Enhances Germinal Center B Cell Activity and Potentiates Lupus in Sanroque Mice. Journal of immunology (Baltimore, Md. : 1950) *197*, 3008-3017. 10.4049/jimmunol.1600652.

Vinuesa, C.G., Cook, M.C., Angelucci, C., Athanasopoulos, V., Rui, L., Hill, K.M., Yu, D., Domaschenz, H., Whittle, B., Lambe, T., et al. (2005). A RING-type ubiquitin ligase family member required to repress follicular helper T cells and autoimmunity. Nature *435*, 452-458. 10.1038/nature03555.

Vinuesa, C.G., Linterman, M.A., Yu, D., and MacLennan, I.C.M. (2016). Follicular Helper T Cells. Annual Review of Immunology *34*, 335-368. 10.1146/annurev-immunol-041015-055605.

Vogel, K.U., Edelmann, S.L., Jeltsch, K.M., Bertossi, A., Heger, K., Heinz, G.A., Zoller, J., Warth, S.C., Hoefig, K.P., Lohs, C., et al. (2013). Roquin paralogs 1 and 2 redundantly repress the Icos and Ox40 costimulator mRNAs and control follicular helper T cell differentiation. Immunity *38*, 655-668. 10.1016/j.immuni.2012.12.004.

Walker, L.S., Gulbranson-Judge, A., Flynn, S., Brocker, T., Raykundalia, C., Goodall, M., Förster, R., Lipp, M., and Lane, P. (1999). Compromised OX40 function in CD28-deficient mice is linked with failure to develop CXC chemokine receptor 5-positive CD4 cells and germinal centers. The Journal of experimental medicine *190*, 1115-1122. 10.1084/jem.190.8.1115.

Walker, L.S., and Sansom, D.M. (2011). The emerging role of CTLA4 as a cell-extrinsic regulator of T cell responses. Nature reviews. Immunology *11*, 852-863. 10.1038/nri3108.

Walker, S.R., Nelson, E.A., Yeh, J.E., Pinello, L., Yuan, G.C., and Frank, D.A. (2013). STAT5 outcompetes STAT3 to regulate the expression of the oncogenic transcriptional modulator BCL6. Mol Cell Biol *33*, 2879-2890. 10.1128/mcb.01620-12.

Watanabe, M., Fujihara, C., Radtke, A.J., Chiang, Y.J., Bhatia, S., Germain, R.N., and Hodes, R.J. (2017). Co-stimulatory function in primary germinal center responses: CD40 and B7 are required on distinct antigen-presenting cells. The Journal of experimental medicine *214*, 2795-2810. 10.1084/jem.20161955.

Weaver, C.T., Hatton, R.D., Mangan, P.R., and Harrington, L.E. (2007). IL-17 family cytokines and the expanding diversity of effector T cell lineages. Annu Rev Immunol *25*, 821-852. 10.1146/annurev.immunol.25.022106.141557.

Webb, S., Morris, C., and Sprent, J. (1990). Extrathymic tolerance of mature T cells: clonal elimination as a consequence of immunity. Cell *63*, 1249-1256. 10.1016/0092-8674(90)90420-j.

Webster, M.W., Chen, Y.H., Stowell, J.A.W., Alhusaini, N., Sweet, T., Graveley, B.R., Coller, J., and Passmore, L.A. (2018). mRNA Deadenylation Is Coupled to Translation Rates by the Differential Activities of Ccr4-Not Nucleases. Mol Cell *70*, 1089-1100.e1088. 10.1016/j.molcel.2018.05.033.

Weinstein, J.S., Herman, E.I., Lainez, B., Licona-Limón, P., Esplugues, E., Flavell, R., and Craft, J. (2016). TFH cells progressively differentiate to regulate the germinal center response. Nature immunology *17*, 1197-1205. 10.1038/ni.3554.

Wing, J.B., Ise, W., Kurosaki, T., and Sakaguchi, S. (2014). Regulatory T cells control antigen-specific expansion of Tfh cell number and humoral immune responses via the coreceptor CTLA-4. Immunity *41*, 1013-1025. 10.1016/j.immuni.2014.12.006.

References

Wolf, J., and Passmore, L.A. (2014). mRNA deadenylation by Pan2-Pan3. Biochem Soc Trans *42*, 184-187. 10.1042/bst20130211.

Wu, D., Muhlrad, D., Bowler, M.W., Jiang, S., Liu, Z., Parker, R., and Song, H. (2014). Lsm2 and Lsm3 bridge the interaction of the Lsm1-7 complex with Pat1 for decapping activation. Cell Res *24*, 233-246. 10.1038/cr.2013.152.

Xu, H., Li, X., Liu, D., Li, J., Zhang, X., Chen, X., Hou, S., Peng, L., Xu, C., Liu, W., et al. (2013). Follicular T-helper cell recruitment governed by bystander B cells and ICOS-driven motility. Nature *496*, 523-527. 10.1038/nature12058.

Yachida, S., White, C.M., Naito, Y., Zhong, Y., Brosnan, J.A., Macgregor-Das, A.M., Morgan, R.A., Saunders, T., Laheru, D.A., Herman, J.M., et al. (2012). Clinical significance of the genetic landscape of pancreatic cancer and implications for identification of potential long-term survivors. Clinical cancer research : an official journal of the American Association for Cancer Research *18*, 6339-6347. 10.1158/1078-0432.Ccr-12-1215.

Yamaguchi, T., Kishi, A., Osaki, M., Morikawa, H., Prieto-Martin, P., Wing, K., Saito, T., and Sakaguchi, S. (2013). Construction of self-recognizing regulatory T cells from conventional T cells by controlling CTLA-4 and IL-2 expression. Proceedings of the National Academy of Sciences of the United States of America *110*, E2116-2125. 10.1073/pnas.1307185110.

Yang, B., Kang, H., Fung, A., Zhao, H., Wang, T., and Ma, D. (2014). The role of interleukin 17 in tumour proliferation, angiogenesis, and metastasis. Mediators Inflamm *2014*, 623759. 10.1155/2014/623759.

Yang, X.O., Panopoulos, A.D., Nurieva, R., Chang, S.H., Wang, D., Watowich, S.S., and Dong, C. (2007). STAT3 regulates cytokine-mediated generation of inflammatory helper T cells. J Biol Chem *282*, 9358-9363. 10.1074/jbc.C600321200.

Yoshida, H., and Hunter, C.A. (2015). The immunobiology of interleukin-27. Annu Rev Immunol *33*, 417-443. 10.1146/annurev-immunol-032414-112134.

Yu, D., Rao, S., Tsai, L.M., Lee, S.K., He, Y., Sutcliffe, E.L., Srivastava, M., Linterman, M., Zheng, L., Simpson, N., et al. (2009). The Transcriptional Repressor Bcl-6 Directs T Follicular Helper Cell Lineage Commitment. Immunity *31*, 457-468. https://doi.org/10.1016/j.immuni.2009.07.002.

Yu, D., Tan, A.H., Hu, X., Athanasopoulos, V., Simpson, N., Silva, D.G., Hutloff, A., Giles, K.M., Leedman, P.J., Lam, K.P., et al. (2007). Roquin represses autoimmunity by limiting inducible T-cell co-stimulator messenger RNA. Nature *450*, 299-303. 10.1038/nature06253.

Yusuf, I., Kageyama, R., Monticelli, L., Johnston, R.J., Ditoro, D., Hansen, K., Barnett, B., and Crotty, S. (2010). Germinal center T follicular helper cell IL-4 production is dependent on signaling lymphocytic activation molecule receptor (CD150). Journal of immunology (Baltimore, Md. : 1950) *185*, 190-202. 10.4049/jimmunol.0903505.

Zhang, Y., Yan, W., Collins, M.A., Bednar, F., Rakshit, S., Zetter, B.R., Stanger, B.Z., Chung, I., Rhim, A.D., and di Magliano, M.P. (2013). Interleukin-6 is required for pancreatic cancer progression by promoting MAPK signaling activation and oxidative stress resistance. Cancer research *73*, 6359-6374. 10.1158/0008-5472.Can-13-1558-t.

Zhao, J., Chen, X., Herjan, T., and Li, X. (2019). The role of interleukin-17 in tumor development and progression. Journal of Experimental Medicine *217*. 10.1084/jem.20190297.

References

Zhou, G., and Ono, S.J. (2005). Induction of BCL-6 gene expression by interferon-gamma and identification of an IRE in exon I. Exp Mol Pathol *78*, 25-35. 10.1016/j.yexmp.2004.08.008.

Zhou, M., Lu, W., Li, B., Yuan, X., Liu, M., Han, J., Liu, X., and Li, A. (2021). Roquin2 suppresses breast cancer progression by inhibiting tumor angiogenesis via selectively destabilizing proangiogenic factors mRNA. Int J Biol Sci *17*, 2884-2898. 10.7150/ijbs.59891.

Appendices

Appendix 1: Significantly deregulated genes in WT vs. DKO^{T} T_H1 cells.

Gene.name	pval	log2fc	Diff.expressed
Pdzk1ip1	0.019	5	UP
Sema3b	0.027	5.345	UP
Gm15987	0.032	3.642	UP
Ermn	0.025	4.319	UP
Zcchc18	0.002	3.279	UP
Tlr9	0.026	4.409	UP
Gm14718	0.033	3.22	UP
RP24-312B12.1	0.013	2.653	UP
Kit	0.025	3.02	UP
Prickle1	0.039	1.173	UP
Gpld1	0.024	2.661	UP
Maf	0.029	2.104	UP
Bmf	0.005	3.352	UP
Pou2f2	4.03E-04	1.911	UP
Ppic	0.029	1.634	UP
Icos	2.45E-05	2.703	UP
Zbtb32	0.004	3.757	UP
Zbtb18	0.044	1.372	UP
Sdc4	0.047	2.277	UP
Ikzf2	0.02	1.689	UP
Furin	0.043	1.568	UP
Ncf1	3.33E-06	2.145	UP
Pipox	0.024	2.169	UP
Rilpl2	0.003	1.519	UP
Clip3	0.048	2.098	UP
Pim2	1.00E-04	2.419	UP
Ebi3	0.001	4.358	UP
Alcam	0.033	1.542	UP
Cd40lg	0.002	1.935	UP
Smox	0.037	1.643	UP
Sp6	0.027	2.067	UP
Fes	0.031	1.902	UP
Cd81	0.041	1.84	UP
Zfp827	0.004	2.095	UP
Gbp11	0.024	1.239	UP
Fam46a	0.018	1.411	UP
Gbp11	0.028	1.224	UP
Tns1	0.014	1.115	UP
Rims3	0.022	1.261	UP
Ell2	0.031	1.466	UP
Slfn5	0.044	1.686	UP
Tnfsf14	0.009	2.926	UP
Rgs1	0.035	1.697	UP
Pnpla3	0.048	2.996	UP
St6galnac2	0.029	2.033	UP
Cd86	0.001	2.154	UP
Ctla4	0.005	2.799	UP
Batf	8.95E-06	1.395	UP
Ntng2	0.001	1.197	UP
Il9r	0.021	4.877	UP
Ctla2a	0.005	1.407	UP
Sh2d1a	0.006	1.556	UP
Slamf6	0.001	2.17	UP
Cpd	0.002	1.988	UP
Neurl3	1.35E-07	1.908	UP
Slc25a53	0.029	1.174	UP
Gimap7	0.005	1.117	UP
Pkhd1l1	0.009	2.742	UP
Ms4a4c	4.20E-06	2.201	UP
Abhd17c	0.014	1.065	UP
Cd200	0.041	1.188	UP
Gbp5	0.004	1.3	UP
Adap1	3.77E-06	1.721	UP
Tnip3	0.02	1.701	UP
Bcl2l1	1.35E-07	1.524	UP

Tnfsf13b	0.031	2.188	UP
Hip1r	0.026	1.096	UP
Rasgrp4	0.002	1.715	UP
Ctla2b	0.009	1.857	UP
Usp6nl	0.018	1.043	UP
Bcl3	0.004	1.847	UP
Dclk2	0.002	1.226	UP
Zc3h12d	3.88E-04	1.588	UP
Dpp4	0.008	1.19	UP
Ccr4	0.044	1.113	UP
Tmem154	4.28E-05	1.235	UP
Jdp2	0.033	1.699	UP
Pik3c2b	0.034	1.744	UP
Gpr179	0.044	2.335	UP
Casp4	4.99E-04	1.566	UP
Bcam	0.043	2.739	UP
Glrx	0.03	1.047	UP
Plxnb2	0.049	2.219	UP
Vill	0.025	1.63	UP
Otud5	1.44E-08	1.666	UP
P2ry14	0.003	1.752	UP
6430571L13Rik	0.008	2.557	UP
Hemk1	0.016	1.399	UP
Tnfrsf8	0.004	3.74	UP
Ptger2	0.022	1.382	UP
Nr4a3	0.039	1.68	UP
Gpr125	0.035	1.678	UP
H2-Oa	0.016	2.419	UP
Lpxn	0.02	1.094	UP
Tbkbp1	0.038	1.168	UP
Tnfrsf13b	0.01	1.063	UP
Ramp1	0.047	1.071	UP
Ssh1	0.001	1.064	UP
Tnfrsf25	0.017	1.274	UP
Aim2	0.002	1.374	UP
Fam213a	0.03	1.781	UP
Gm15558	0.038	1.046	UP
Dynlt3	0.044	1.209	UP
Sdcbp2	0.046	1.148	UP
Plcl1	0.015	1.537	UP
Slc22a15	0.028	1.187	UP
Stx11	0.048	1.203	UP
Casp1	0.029	1.257	UP
Tox2	0.038	2.158	UP
Myb	0.005	1.521	UP
Ankrd37	0.017	2.459	UP
AA467197	0.025	-1.403	DOWN
Plscr1	0.043	1.693	UP
Dlg3	0.038	1.347	UP
H2-Q6	3.58E-07	1.414	UP
Dock6	0.012	1.667	UP
H2-Q5	0.01	1.159	UP
S100a11	0.019	1.145	UP
Irf4	0.016	1.13	UP
Trerf1	0.011	1.132	UP
Ccr7	0.012	1.053	UP
Rmdn1	0.032	1.002	UP
Unc93b1	0.006	1.751	UP
Ica1	0.041	1.338	UP
Cpm	0.014	1.114	UP
Pcyt1b	0.04	1.421	UP
Dhdh	0.047	1.741	UP
Ksr1	2.14E-04	1.12	UP
Gm20645	0.008	1.074	UP
Zfpm1	0.001	1.188	UP
Ldhb	0.047	1.076	UP
Sv2a	0.047	1.052	UP
Ccdc40	0.039	1.587	UP
Unc119b	0.022	1.11	UP
Unc119	4.80E-04	1.702	UP
Hrsp12	0.018	1.613	UP

Mrpl45	0.005	1.134	UP
Dennd3	0.048	1.339	UP
Tnfsf11	0.042	1.31	UP
Lmna	0.005	1.739	UP
St3gal1	0.017	1.169	UP
Ccdc136	0.013	1.782	UP
Tbc1d4	0.022	1.172	UP
Lbp	0.012	2.754	UP
Unc5b	0.004	2.447	UP
Capn3	2.09E-04	2.39	UP
Slc15a2	0.035	2.018	UP
Tnfrsf4	0.008	2.006	UP
Baiap3	0.033	1.976	UP
Zc3h12a	9.22E-05	1.727	UP
Nfkbid	0.015	1.716	UP
Gfi1	0.006	1.629	UP
Serpinb6b	0.02	1.607	UP
Pilrb1	0.045	1.588	UP
Itpr1	3.50E-05	1.507	UP
Trib1	0.033	1.466	UP
Polr1c	1.45E-04	1.43	UP
Zfp446	0.049	1.406	UP
Cep290	0.017	1.384	UP
Ccl5	0.049	1.347	UP
Tm2d3	0.007	1.298	UP
Irf5	0.031	1.278	UP
Lfng	0.007	1.27	UP
Mxd4	0.04	1.25	UP
Fchsd2	0.002	1.204	UP
Ndst2	0.006	1.189	UP
Ptpn21	0.032	1.183	UP
Cyp4f16	0.025	1.165	UP
Atp13a2	0.027	1.158	UP
Bcr	0.003	1.153	UP
Slfn10-ps	0.022	1.092	UP
Mea1	0.012	1.089	UP
Fuca2	0.038	1.014	UP
Cep85l	0.025	1.011	UP
9130208D14Rik	0.034	-1.195	DOWN
Lilrb4	0.026	-1.134	DOWN
Gm14085	0.044	-1.119	DOWN
Nrp1	0.024	1.454	UP
Drc1	0.031	-1.544	DOWN
Map6	0.012	-1.216	DOWN
Ppm1l	0.029	-1.033	DOWN
Setbp1	0.043	-1.084	DOWN
Dock4	0.013	-1.716	DOWN
Nacc2	0.031	-1.77	DOWN
38960	0.029	-1.007	DOWN
Ifitm1	0.028	-2.498	DOWN
Aven	0.021	-1.131	DOWN
D8Ertd82e	0.034	-1.186	DOWN
Plxdc2	0.004	-1.301	DOWN
Pydc3	0.034	-1.934	DOWN
Paqr4	0.02	-1.256	DOWN
Zdhhc14	0.022	-1.169	DOWN
Plxdc1	0.029	-1.228	DOWN
Arsb	0.034	-1.06	DOWN
Nav1	0.035	-1.671	DOWN
Klf3	0.037	-1.064	DOWN
Ggt1	0.004	-1.962	DOWN
Fbln1	0.029	-1.066	DOWN
B630019A10Rik	0.044	-1.032	DOWN
Ifitm2	0.024	-1.586	DOWN
Mcoln2	0.037	-1.269	DOWN
Sytl2	0.017	-1.204	DOWN
Rap1gap2	0.001	-1.37	DOWN
Nkg7	0.05	-1.469	DOWN
Rtn4rl1	0.019	-1.338	DOWN
Ccr2	0.017	-2.199	DOWN
Mb21d1	0.021	-1.175	DOWN

Pdlim4	0.032	-2.25	DOWN
Ifitm3	0.001	-2.805	DOWN

Appendix 2: Significantly deregulated genes in primary tumors from $Kras^{G12D}$ mice reconstituted with WT or DKO^{T} bone marrow.

GeneName	log2FoldChange	pvalue	padj
Prr9	4.651977184	0.00059315	0.02617622
Cstdc4	3.537662071	5.27E-05	0.003998395
Stfa1	3.337004747	0.00101966	0.03861737
Cyp21a1	2.950414593	0.00141614	0.048855345
Chil3	2.84092372	0.00048143	0.022736058
Car4	2.833258185	0.00095861	0.037199399
Csta2	2.823456315	6.27E-05	0.00457848
Wfdc21	2.691784688	0.00015102	0.009210095
Cxcl5	2.551450513	7.86E-06	0.000870351
En1	2.313937602	9.61E-08	2.06E-05
Fabp7	2.292224294	0.00095085	0.037119627
H2-Q10	2.247210886	0.00010312	0.006855571
Clec1b	2.242714095	7.51E-09	2.37E-06
Cyp26a1	2.200702029	9.51E-05	0.006379817
Igfbp2	2.17887871	3.31E-06	0.000436607
Col11a1	2.120550389	8.63E-08	1.91E-05
Cxcr2	2.01235842	2.48E-05	0.002205638
Mmp8	2.003463113	2.71E-06	0.000378589
Cd177	1.981440539	0.00133114	0.046544805
Mmp13	1.964542785	1.83E-10	1.09E-07
Il1r2	1.960426426	0.00013272	0.00846052
Rab15	1.945017474	0.00016082	0.009640359
2310057J18Rik	1.889616914	7.80E-07	0.000125827
Mmp9	1.862963571	6.27E-06	0.000735616
Il1a	1.785124235	5.87E-05	0.004367449
Fpr2	1.765913344	0.00054248	0.024866526
Nnat	1.713949846	0.00014947	0.009210095
Ffar2	1.643124566	0.00083683	0.033844825
Gnaz	1.633987484	0.00091077	0.036173898
Cxcl2	1.621019624	5.01E-05	0.003883473
Gm19951	1.598743211	0.00054348	0.024866526
Sox11	1.581790155	4.08E-06	0.000517771
Mcpt8	1.545801377	0.00010942	0.007212611
Hoga1	1.530818857	0.00017017	0.010043577
G430095P16Rik	1.523240244	0.00021671	0.011988541
AU022793	1.49008917	0.00094936	0.037119627
Fpr1	1.429827538	0.00101345	0.038476499
Gm8797	1.408481984	0.00116593	0.042695584
Il1b	1.401908889	8.47E-05	0.005883917
Mmp7	1.387074306	2.36E-06	0.000342269
Cdh6	1.376356838	1.60E-07	3.14E-05
Cdkn2a	1.367008277	0.00050649	0.023591259
Col12a1	1.36655718	8.48E-07	0.000135404
Uts2	1.363159471	0.00046071	0.021890667
Mcemp1	1.325719371	0.00067112	0.028876676
Tnfrsf11b	1.321533649	1.66E-05	0.001588953
Thbs2	1.292495534	1.58E-08	4.40E-06
Trim15	1.288572755	0.00124448	0.044416895
Acsbg1	1.277132095	0.0002107	0.01181959
AA467197	1.248211575	1.03E-05	0.001085544
Inhba	1.247241108	0.00068442	0.029286272
Nt5e	1.239711655	0.00023227	0.012668606
Prss22	1.19373779	0.00018352	0.010567677
Anxa8	1.170324504	4.51E-07	7.67E-05
Cpxm2	1.144083554	0.00130809	0.0461556
Dkk2	1.143773885	0.00082953	0.033698449
Cldn6	1.139774608	0.00126059	0.044888489
Cd300lf	1.130367214	3.03E-05	0.002553992
Fbn2	1.124808164	7.87E-06	0.000870351
Fndc10	1.095381182	0.00050716	0.023591259

Igfbp3	1.086860075	8.05E-06	0.000873338
Atp10b	1.082045992	0.00120683	0.043677071
Cirbp	1.063091768	3.20E-12	3.31E-09
Dusp28	1.059256882	0.00069584	0.029693073
Clec5a	1.024982316	0.0001296	0.008295247
Egln3	1.018331693	0.00107776	0.040227698
Tmeff1	1.006066321	0.00100718	0.0383321
Nkd2	0.995848466	2.84E-07	5.23E-05
Acp5	0.992451336	5.47E-05	0.004130088
Zfp618	0.99078032	2.15E-06	0.000319916
Prxl2a	0.976143583	2.36E-05	0.002174908
Rgs4	0.976054208	0.00046467	0.02201128
Ncmap	0.968615523	1.54E-05	0.001482003
Mir22hg	0.958674329	8.07E-06	0.000873338
Tnfrsf22	0.936380476	0.001326	0.046469915
Sirpb1c	0.934933572	0.0005571	0.025158927
Cdh17	0.925874354	0.00041594	0.020265676
Ccdc125	0.925452849	0.0007651	0.031944558
Efna4	0.899013298	8.75E-05	0.006022395
Pmaip1	0.866359234	0.0013613	0.047385457
Gadd45a	0.860645298	0.00012687	0.008154274
Cxcl14	0.851680681	0.00014987	0.009210095
Ecm1	0.84864817	0.00025151	0.013527411
Serpinb5	0.842126427	7.30E-05	0.005207366
Cd14	0.841555569	5.65E-05	0.004251398
Mmp14	0.821099628	2.39E-05	0.002179737
Mex3a	0.808458854	0.00024028	0.01305919
Mpzl1	0.806290167	9.47E-05	0.006379817
Slc7a2	0.800055478	0.00022441	0.012363448
Fkbp10	0.795002501	0.0003192	0.016481154
Tnfaip2	0.793877411	3.52E-06	0.000458158
Sdc1	0.778445023	0.00015093	0.009210095
Mal	0.776723233	3.24E-05	0.002701443
Cdkn2b	0.768279402	0.00096301	0.037199399
S100a14	0.767451534	1.16E-05	0.001177935
Nbl1	0.765374991	0.0001557	0.009384502
Postn	0.750545914	0.0001435	0.008997449
Slc39a4	0.744075586	0.00120052	0.043550438
Ctse	0.743952669	0.00086887	0.034957968
Col5a2	0.743119957	0.00016642	0.009877056
Msr1	0.739436164	0.00039894	0.019679999
Gnpda2	0.736893119	1.11E-05	0.001141955
Lamb3	0.733763873	0.0009951	0.037965708
Haghl	0.733160533	1.78E-05	0.001690355
Lmcd1	0.724926485	0.0006325	0.027598456
Serpinf1	0.700895143	3.28E-05	0.002719923
Ptk7	0.699769023	0.00054421	0.024866526
Morrbid	0.695814362	0.00140606	0.048615883
Endod1	0.665696887	0.00108156	0.04027235
Aplp2	0.664322108	0.00082091	0.033640112
Lratd1	0.660519183	0.00134319	0.04686049
Rnf128	0.650306783	0.00041735	0.020265676
Cpxm1	0.639664588	0.0002628	0.013957271
Prdx5	0.635580666	0.00034688	0.017688724
Emp2	0.634429409	0.00093094	0.036721079
Pgd	0.630083413	0.00123673	0.044242311
St3gal4	0.629319358	0.00096765	0.03728573
Tmem9	0.619588308	0.00049391	0.023254283
Epcam	0.614357235	0.00093403	0.036721079
Krtcap3	0.612021295	0.00104976	0.039467857
Cttn	0.607079232	9.31E-05	0.006352335
Ift43	0.599550876	0.00054945	0.024959099
Cd44	0.597152993	0.00074981	0.031390794
Frrs1	0.589989159	0.00040668	0.019998259
Ptgs1	0.587560637	0.00118709	0.043217299
Serinc2	0.587436112	0.0003423	0.017556968
Pafah1b3	0.561112895	5.23E-05	0.003987728
Sat1	0.54705564	0.0004416	0.021177473
Ctnnb1	0.522554623	0.00020295	0.011513417
Cadm1	0.505065367	0.00126921	0.044988748
Svbp	0.498097148	0.00082488	0.033698449

Mrps9	0.484455618	0.00102681	0.038793483
2200002D01Rik	0.48155793	0.00138926	0.048142482
Mkrn1	0.470547233	0.0003209	0.01651428
Rflnb	0.456485065	0.00098836	0.037801671
Cd81	0.426823664	0.00058751	0.026001432
Leprot	0.407805417	0.0005459	0.024870767
Spp1	0.401291344	0.00037499	0.018798267
Emp1	0.352629214	0.00131591	0.046314659
Serp1	-0.542352938	0.00086568	0.034920359
Eif4a2	-0.572739893	6.20E-05	0.004552016
Ifitm3	-0.644526001	0.00056807	0.025440195
Trabd	-0.657853636	0.00137979	0.047921293
Ankrd12	-0.661019682	0.00026211	0.013957271
Manf	-0.671423679	0.00017558	0.010224582
Snd1	-0.672090537	0.00087711	0.035198063
Hspa5	-0.699649129	0.00014951	0.009210095
Mlxip	-0.7107082	0.00107079	0.040064188
Il6st	-0.722123447	0.00098459	0.037750805
Irak1	-0.737727781	0.00021211	0.01181959
Fam129a	-0.76622843	5.11E-05	0.003940961
Man1a	-0.792079404	0.00055351	0.025069741
Ndrg1	-0.793009561	0.00145398	0.049934428
Ddx58	-0.794549427	0.00036599	0.018466184
Nr1d2	-0.801005195	0.00014189	0.008934437
Flrt2	-0.801214582	0.00036541	0.018466184
Tram1	-0.801414124	0.00022508	0.012363448
Mndal	-0.808106095	0.00037888	0.018931789
4930503L19Rik	-0.839378315	0.00095136	0.037119627
Deptor	-0.850399689	0.00126899	0.044988748
Tnfrsf18	-0.894307661	0.00067596	0.029004415
Azin1	-0.90485242	0.00057806	0.025803738
Scd1	-0.916793595	0.00050698	0.023591259
Nrp1	-0.917665538	2.72E-05	0.002356397
Irf7	-0.929516574	0.00081254	0.033385394
Edem3	-0.930507062	0.00011043	0.00724846
Cpox	-0.932802403	0.00109286	0.040498502
C4b	-0.938146507	0.00052875	0.024448996
Dbp	-0.939848998	0.00052021	0.024126049
Magt1	-0.954811751	5.82E-07	9.70E-05
Rhou	-0.971198499	8.01E-05	0.005621942
Ghr	-0.976105036	0.00043724	0.021033835
Fgl2	-0.97673828	0.00083104	0.033698449
Snora57	-0.996968109	0.00077798	0.032120086
Trac	-1.007126222	0.00143186	0.049287906
Hsph1	-1.014795325	3.65E-05	0.002961006
Creld2	-1.016778216	1.27E-08	3.72E-06
Lrmp	-1.021509692	8.02E-05	0.005621942
Enpp2	-1.021732274	0.00123435	0.044242311
Slfn8	-1.022169101	0.00070742	0.030104228
Traf1	-1.032124255	3.77E-05	0.003025482
Gm22748	-1.040465726	0.00024298	0.013159842
Fabp4	-1.049727212	8.85E-08	1.93E-05
Cyfip2	-1.051334745	0.00042006	0.020333466
Rsad2	-1.065023343	0.0005612	0.025270153
Nfatc2	-1.065980116	0.00035032	0.017791489
Trim30a	-1.071566317	2.47E-05	0.002205638
Scarna2	-1.071927631	0.0009027	0.03594574
Gm26917	-1.084063137	0.00066543	0.028711892
Edem2	-1.0905933	0.00077221	0.032068291
Ifi209	-1.10345609	4.05E-08	1.06E-05
Ifit3	-1.104078516	0.00041305	0.020247204
Ptger3	-1.106081878	0.00115731	0.042480381
Plcb4	-1.11533609	0.00016119	0.009640359
Lyrm9	-1.115668401	0.00071875	0.030336243
Ccl12	-1.119092115	0.0008267	0.033698449
Gm37194	-1.125805118	0.00093326	0.036721079
Dhx34	-1.136452464	0.00073861	0.0310899
Abca9	-1.1389905	0.00128651	0.045497732
Slfn5	-1.139243515	1.18E-05	0.001189621
Fbxo31	-1.140985633	0.00026311	0.013957271
Ifit2	-1.143723203	0.00042221	0.020374006

Pltp	-1.169171424	0.00014631	0.009102023
Ptger4	-1.181418657	7.10E-05	0.005093758
Bcl11a	-1.183456961	0.00109041	0.040498502
Gstm1	-1.184521846	2.26E-07	4.28E-05
BE692007	-1.185164448	0.00145709	0.049934428
Aldh6a1	-1.191099031	0.00012648	0.008154274
Grem1	-1.204008005	0.00065057	0.028149085
Ifrd2	-1.208745301	3.01E-06	0.000405799
Mthfd2	-1.217551972	3.75E-05	0.003025482
Gm8995	-1.221937015	0.00039111	0.019479972
Lars2	-1.226137873	0.0003104	0.016082749
Ifi27l2a	-1.238601356	4.34E-05	0.003416411
Cxcl10	-1.265763063	0.0006128	0.02689038
Igf1	-1.278907558	4.84E-05	0.003766965
Tgfbr3	-1.286076118	7.78E-05	0.005503464
Slc41a1	-1.288476025	0.00050458	0.023591259
Il33	-1.294004116	0.00022906	0.012537425
Il7r	-1.298253829	0.00105744	0.039660408
Lgals2	-1.300152601	9.26E-05	0.006347667
Homer2	-1.304917157	0.00121539	0.043884498
Ifi213	-1.305562731	0.00054092	0.024866526
Clec10a	-1.308399314	0.00146057	0.049943237
Herpud1	-1.31433511	1.26E-06	0.000192703
Mx1	-1.339550798	0.00041678	0.020265676
Cfd	-1.342065228	0.00045141	0.021514696
Ly6c2	-1.342311787	0.00064813	0.028121865
Ahcy	-1.368143499	0.00020366	0.011513417
Lifr	-1.375662083	1.68E-06	0.000254864
Kctd14	-1.377810966	0.00087995	0.035220549
Slc6a9	-1.380478516	0.00123531	0.044242311
Gprin3	-1.39618174	0.00020744	0.011684441
Pex11a	-1.40069637	0.00013903	0.008789863
Gm24949	-1.403360919	0.00062938	0.027539929
Apoc1	-1.412506499	5.33E-06	0.000660041
Naaladl2	-1.412716985	0.00015449	0.009347878
Nupr1	-1.427715394	2.92E-06	0.000397268
Tle6	-1.441768659	0.00097594	0.037511847
Nfasc	-1.44577649	8.11E-05	0.005660881
Itprid2	-1.448137369	3.79E-07	6.67E-05
Ivd	-1.468231488	1.35E-05	0.001333687
Tent5c	-1.470182773	1.14E-06	0.000176028
Ifit1bl1	-1.497963878	0.00114776	0.042330573
Ifi27l2b	-1.500281875	5.71E-05	0.004270618
Ang	-1.511251272	0.00044506	0.021277618
Clec4a1	-1.522422996	0.00028848	0.015147825
Oas2	-1.529885905	0.00037438	0.018798267
Slc16a7	-1.55329347	6.93E-06	0.000796176
Tmeff2	-1.5585206	0.00056826	0.025440195
Ifi205	-1.568840459	2.92E-06	0.000397268
Igdcc4	-1.588835811	0.00017429	0.010215344
Cxcl13	-1.602026935	2.48E-05	0.002205638
Chl1	-1.638489729	0.00011679	0.007633134
Ighm	-1.639206766	9.42E-07	0.000148901
Rbp4	-1.647136532	5.74E-06	0.000695131
Trim30c	-1.655985094	0.00089812	0.035855537
Cd28	-1.666813815	0.0009625	0.037199399
E230001N04Rik	-1.672135152	0.00077967	0.032120086
Fmo1	-1.680915071	0.00074168	0.031134386
Tmem97	-1.693219466	2.14E-05	0.002001081
Il4i1	-1.697588442	0.00016241	0.0096759
Gm49839	-1.702017672	0.00096027	0.037199399
Cmah	-1.702516971	1.49E-05	0.001438286
Anpep	-1.71744439	4.92E-06	0.00061438
Vegfd	-1.722955629	8.75E-05	0.006022395
Rgs18	-1.739382882	0.00021483	0.011927317
Tnfrsf4	-1.75460746	2.98E-05	0.002519217
Cd79b	-1.770945405	0.00031044	0.016082749
Casp9	-1.771041526	3.56E-07	6.43E-05
Sox6	-1.775549833	0.00060536	0.026639205
Gamt	-1.776015814	2.81E-05	0.002417151
Nr5a2	-1.77808549	0.00012525	0.008117897

Fmo2	-1.783789896	9.48E-05	0.006379817
Ogn	-1.79876894	4.08E-07	7.03E-05
Cbs	-1.802302502	0.00077587	0.032120086
Ifi206	-1.817580382	1.21E-05	0.001204968
Il2ra	-1.847704949	0.00021213	0.01181959
Map2	-1.855592601	0.00012431	0.008090553
Kmo	-1.858645035	2.56E-05	0.002256211
Arfgef3	-1.885648117	6.47E-07	0.000105446
Wnk2	-1.886197146	6.73E-05	0.004850153
Foxp2	-1.903932523	0.0007709	0.032068291
Chst2	-1.909719207	0.00057971	0.025803738
Car3	-1.910601746	5.24E-07	8.83E-05
Cd5	-1.972412769	0.00071635	0.030317699
Habp2	-1.972800157	3.80E-05	0.003032327
Cd6	-1.999667692	9.45E-05	0.006379817
Gm4759	-2.017248706	0.00039786	0.019679999
H2-T24	-2.046779709	0.00109905	0.040630844
Dym	-2.048981051	0.00030659	0.015990216
Serpini1	-2.051400047	6.17E-06	0.00073504
Gm22003	-2.060563654	1.02E-05	0.001083828
Neb	-2.090113254	5.16E-05	0.003957703
Pcp4l1	-2.090712921	2.43E-05	0.002197025
Matn4	-2.09836348	0.00029157	0.015258385
Ms4a4c	-2.106325118	4.52E-08	1.15E-05
Arhgef26	-2.131020136	7.56E-08	1.70E-05
Arhgdig	-2.131595472	1.13E-07	2.32E-05
Gjb2	-2.146059434	0.00017053	0.010043577
Cth	-2.149440954	3.70E-06	0.00047779
Col28a1	-2.15161867	3.36E-05	0.002771432
Ccdc141	-2.186062245	0.00093365	0.036721079
Synm	-2.213042865	7.84E-06	0.000870351
Pik3c2g	-2.243539211	2.58E-05	0.002256211
Sel1l	-2.262785488	3.99E-07	6.95E-05
5330417C22Rik	-2.264677253	0.00025701	0.013775426
Ces1d	-2.265697768	2.90E-05	0.002472097
Aldh1l2	-2.284295531	1.42E-05	0.001390775
Myo15b	-2.297745006	0.00017476	0.010215344
Aldh1a7	-2.325521678	5.52E-06	0.0006738
Noxa1	-2.330491168	6.12E-08	1.41E-05
Dpt	-2.343705856	9.98E-11	6.42E-08
Cpn1	-2.360994411	1.96E-06	0.00029543
Ighg2c	-2.383923539	6.92E-06	0.000796176
Ero1lb	-2.448646336	1.20E-09	5.32E-07
Synpo2	-2.47054784	2.75E-06	0.000379855
Abca8b	-2.481244963	0.00058233	0.025846026
Hmgcs2	-2.496766654	1.59E-08	4.40E-06
Ccr6	-2.504608626	0.00017815	0.010297037
Egf	-2.513766029	6.68E-05	0.00483875
Ttn	-2.549901619	5.26E-08	1.27E-05
Retnla	-2.568398476	7.87E-06	0.000870351
Sec14l4	-2.606042101	0.00034715	0.017688724
Foxp3	-2.617036549	0.00039501	0.019611395
Gm6545	-2.621578226	2.39E-05	0.002179737
Gm20275	-2.638799931	8.12E-06	0.000873338
Gpt	-2.649957419	6.68E-09	2.23E-06
Tnxb	-2.660724422	7.59E-05	0.005394958
Gls2	-2.699711934	5.92E-05	0.004367449
Ighg1	-2.702520142	0.00104672	0.039449283
Zbtb16	-2.745541234	1.47E-05	0.001436634
Acacb	-2.74789733	0.00131858	0.046314659
Dmbt1	-2.773694108	1.19E-05	0.001194901
Abca8a	-2.783528277	1.81E-08	4.92E-06
BC147527	-2.803442005	2.64E-07	4.93E-05
Mmrn1	-2.817299398	4.05E-05	0.003202612
Reg1	-2.836288894	3.94E-06	0.000504974
Nr0b2	-2.85591846	8.97E-06	0.000958556
P2rx1	-2.889509737	1.11E-07	2.32E-05
Serpina10	-2.894338395	1.54E-07	3.06E-05
Slc25a35	-2.904303128	5.12E-08	1.26E-05
Alb	-2.908474033	0.00019368	0.011070225
Pah	-2.940918323	0.00013444	0.008534976

Iglc2	-2.959024109	3.24E-05	0.002701443
Ighg2b	-2.98100844	1.28E-07	2.57E-05
Sntb1	-2.992146819	3.57E-07	6.43E-05
Gm44441	-2.998498765	0.00118855	0.043217299
Eci3	-3.016278328	4.83E-05	0.003766965
Ms4a1	-3.078680176	3.82E-05	0.003032327
Gm49016	-3.085700962	0.00015185	0.00922393
Fetub	-3.099327089	6.94E-06	0.000796176
Gm2663	-3.116377487	0.00010167	0.006788464
Reg3b	-3.130032475	5.52E-06	0.0006738
Gm13381	-3.154002178	0.00118414	0.043217299
Ggt1	-3.158889735	8.52E-10	4.00E-07
Aass	-3.190771233	6.65E-05	0.004833419
Azgp1	-3.239034469	0.00017718	0.010279131
Klf15	-3.260064443	7.90E-12	6.80E-09
Ighd	-3.313327008	2.89E-05	0.002469825
Iglc3	-3.351673726	0.00027941	0.014771484
Reg3g	-3.364888975	1.05E-05	0.001090694
Ttpa	-3.392948768	0.00014405	0.008997449
Gnmt	-3.421573946	0.00019975	0.011375363
Clec3b	-3.490857465	2.12E-09	7.81E-07
Slc38a3	-3.504433534	3.33E-06	0.000436607
Bex2	-3.534306578	2.26E-06	0.000333809
Cckar	-3.613229355	1.04E-05	0.001090187
Gabra4	-3.639467052	5.03E-08	1.26E-05
Mia	-3.649153778	2.29E-05	0.002121163
Sostdc1	-3.679991992	0.00071346	0.030278049
Slc38a5	-3.701736849	5.92E-05	0.004367449
Fgl1	-3.703371075	1.26E-07	2.57E-05
Cabp2	-3.717502895	2.03E-05	0.001906904
Fam13a	-3.749615935	1.65E-07	3.19E-05
Gm13010	-3.835761682	0.00115479	0.042480381
Cd209a	-3.838447126	4.82E-12	4.67E-09
Ctrb1	-3.849843433	3.67E-09	1.32E-06
Dusp26	-3.900461416	2.57E-05	0.002256211
Prss2	-3.908798485	6.62E-08	1.51E-05
Try5	-3.916100944	3.64E-07	6.49E-05
Prss3	-3.947580529	2.58E-06	0.000362649
Reg2	-3.958352648	1.93E-07	3.69E-05
Rims1	-4.004202515	1.32E-05	0.001314157
Rnu12	-4.006443425	0.00028445	0.014986634
Rbpjl	-4.054192999	9.72E-08	2.06E-05
Derl3	-4.091600998	1.25E-09	5.33E-07
1810009J06Rik	-4.145988649	1.34E-09	5.48E-07
Bhlha15	-4.150579292	1.77E-11	1.44E-08
Klk1b11	-4.162781243	4.24E-06	0.000533954
Itih4	-4.167277087	5.57E-09	1.96E-06
Gm4744	-4.191536842	3.46E-05	0.002823933
Hsd17b13	-4.248746706	1.07E-05	0.001102654
Gm13017	-4.407836917	0.00122477	0.044120142
1810053B23Rik	-4.432625101	3.14E-06	0.000418834
1810044K17Rik	-4.453596354	0.00025143	0.013527411
Kirrel2	-4.46395976	0.00063872	0.027791286
Pnliprp2	-4.480460779	2.10E-09	7.81E-07
Cela1	-4.48889262	7.39E-10	3.58E-07
Gm5771	-4.499451055	6.76E-09	2.23E-06
Chrdl2	-4.562853175	0.00010915	0.007212611
Cpa1	-4.566000026	1.70E-09	6.73E-07
Spink1	-4.583593557	6.93E-09	2.24E-06
Gp2	-4.588621354	1.08E-09	4.94E-07
Gm20629	-4.598564102	0.00019213	0.011022579
Tmed6	-4.600055049	5.73E-09	1.97E-06
Cela2a	-4.635997349	3.29E-10	1.82E-07
Pnliprp1	-4.656528719	3.04E-11	2.14E-08
Cuzd1	-4.708453575	1.84E-08	4.92E-06
1810010K12Rik	-4.709306912	2.36E-06	0.000342269
Amy2b	-4.724245193	2.89E-10	1.66E-07
Erp27	-4.730742628	1.88E-11	1.45E-08
Gm10334	-4.74380504	6.27E-06	0.000735616
Cel	-4.791183475	7.25E-10	3.58E-07
Amy1	-4.839875336	5.99E-10	3.09E-07

Vip	-4.861702896	2.64E-05	0.002296285
1810028F09Rik	-4.888947617	3.56E-13	7.87E-10
Aqp12	-4.891718495	1.48E-08	4.24E-06
Klk1b4	-4.89518782	8.79E-09	2.67E-06
Vtn	-4.895829957	1.27E-09	5.33E-07
Klk1	-4.9094973	2.28E-13	5.89E-10
Reg3a	-4.914395423	1.77E-09	6.84E-07
Try10	-4.917415314	8.55E-09	2.65E-06
Zg16	-4.997951338	1.63E-12	2.19E-09
Sycn	-5.006369282	5.55E-11	3.74E-08
Slc39a5	-5.007205863	4.18E-08	1.08E-05
Cela3b	-5.007512952	6.23E-12	5.68E-09
Cpa2	-5.096640049	2.96E-11	2.14E-08
Cpb1	-5.104885804	6.99E-13	1.35E-09
Clps	-5.173274813	3.03E-12	3.31E-09
Grpr	-5.1972648	3.40E-05	0.002788591
Rnase1	-5.215623793	1.69E-12	2.19E-09
Ctrl	-5.277024918	9.90E-14	3.07E-10
Try4	-5.294597909	5.99E-16	9.29E-12
Pdia2	-5.307162407	2.61E-14	1.28E-10
Tsga10ip	-5.339320398	2.42E-06	0.000347285
Reg3d	-5.353080803	1.18E-12	2.03E-09
Pla2g1b	-5.418184809	1.67E-12	2.19E-09
1810063I02Rik	-5.429745397	2.03E-05	0.001906904
Amy2a5	-5.448075942	5.64E-08	1.32E-05
Gm10417	-5.45730892	2.48E-06	0.000352956
2210010C04Rik	-5.47071481	1.81E-15	1.40E-11
Cblif	-5.578386543	6.14E-07	0.000101136
Klk1b5	-5.590155856	1.04E-10	6.42E-08
Hamp2	-5.675822718	7.98E-06	0.000873338
1810018F18Rik	-5.708860358	5.95E-06	0.000715031
Pnlip	-5.733223754	3.30E-14	1.28E-10
Smim38	-5.735696743	1.02E-06	0.000159509
Serpini2	-5.779857995	2.68E-12	3.19E-09
Prss1	-5.807799197	5.88E-10	3.09E-07
Gm5409	-5.866653371	7.18E-06	0.000817693
Ctrc	-5.983764381	5.63E-08	1.32E-05
Klk1b3	-6.281305894	1.19E-08	3.55E-06

Appendix 3: Overview over all copy number alterations in primary tumor cell lines.

Name	Chrom	Start	End	Mean (log2fc)	Gene	FC
D15_CL	19	31868764	31948995	1.2679	A1cf	2.408107839
D13-A_CL	12	112653821	112674884	0.9567	Akt1	1.940865306
D16_CL	12	112653821	112674884	-1.0225	Akt1	0.492262587
W12_CL	12	112653821	112674884	-1.0768	Akt1	0.474079199
D15_CL	19	20492715	20643465	1.2679	Aldh1a1	2.408107839
D15_CL	12	52503972	52571975	-1.262	Arhgap5	0.416965522
D16_CL	12	52503972	52571975	-1.0225	Arhgap5	0.492262587
W12_CL	12	52503972	52571975	-1.0768	Arhgap5	0.474079199
D16_CL	4	133679008	133756769	-0.8195	Arid1a	0.56663829
W12_CL	4	133679008	133756769	-1.0822	Arid1a	0.47230804
D16_CL	4	117926162	117929763	-1.1134	Artn	0.462203471
W12_CL	4	117926162	117929763	-1.0822	Artn	0.47230804
D16_CL	12	3426857	3506852	-1.0225	Asxl2	0.492262587
W12_CL	12	3426857	3506852	-1.0768	Asxl2	0.474079199
W12_CL	14	31251450	31259944	-1.112	Bap1	0.462652214
D13-A_CL	12	107910403	108003602	-0.8839	Bcl11b	0.541900544
D16_CL	12	107910403	108003602	-1.0225	Bcl11b	0.492262587
W12_CL	12	107910403	108003602	-1.0768	Bcl11b	0.474079199
D15_CL	7	19808462	19822770	-1.1274	Bcl3	0.457739913
W12_CL	14	34410734	34503341	-1.112	Bmpr1a	0.462652214
W12_CL	14	30039939	30491455	-1.112	Cacna1d	0.462652214
D16_CL	4	150917322	151861876	-0.8195	Camta1	0.56663829
W12_CL	4	150917322	151861876	-1.0822	Camta1	0.47230804

D15_CL	7	19778881	19796809	-1.1274	Cblc	0.457739913
W12_CL	14	50789248	50807732	-1.112	Ccnb1ip1	0.462652214
D16_CL	4	21727701	21759922	-1.1134	Ccnc	0.462203471
D15_CL	19	29367455	29388095	1.2679	Cd274	2.408107839
D17_CL	1	143598800	143702893	-0.7848	Cdc73	0.580432417
D17_CL	15	18818947	19014236	-0.8847	Cdh10	0.541600134
D17_CL	8	102632095	102785642	-1.0437	Cdh11	0.485081815
D13-B_CL	4	11758147	11817895	0.8603	Cdh17	1.815415776
D16_CL	4	11758147	11817895	-1.1134	Cdh17	0.462203471
D13-A_CL	4	89274471	89294653	-3.3355	Cdkn2a	0.099063678
D16_CL	4	89274471	89294653	-1.1134	Cdkn2a	0.462203471
D17_CL	4	89274471	89294653	-0.9519	Cdkn2a	0.516951199
W12_CL	4	89274471	89294653	-1.0822	Cdkn2a	0.47230804
D13-B_CL	4	109660876	109667189	0.7993	Cdkn2c	1.740256544
D16_CL	4	109660876	109667189	-1.1134	Cdkn2c	0.462203471
W12_CL	4	109660876	109667189	-1.0822	Cdkn2c	0.47230804
D16_CL	4	3938888	3951046	-1.1134	Chchd7	0.462203471
D17_CL	5	74997988	75044774	-0.798	Chic2	0.575145947
D16_CL	4	18860454	19122526	-1.1134	Cnbd1	0.462203471
D16_CL	4	126024550	126044440	-0.8195	Csf3r	0.56663829
W12_CL	4	126024550	126044440	-1.0822	Csf3r	0.47230804
D17_CL	15	47580637	48792063	-0.9733	Csmd3	0.509339673
D15_CL	19	39269405	39330713	1.2679	Cyp2c29	2.408107839
D15_CL	19	39389556	39463075	1.2679	Cyp2c38	2.408107839
D15_CL	19	39510862	39568529	1.2679	Cyp2c39	2.408107839
W12_CL	14	73025603	73049114	-1.112	Cysltr2	0.462652214
D13-A_CL	12	104687742	104751952	-0.8839	Dicer1	0.541900544
D16_CL	12	104687742	104751952	-1.0225	Dicer1	0.492262587
W12_CL	12	104687742	104751952	-1.0768	Dicer1	0.474079199
D16_CL	12	3806007	3914443	-1.0225	Dnmt3a	0.492262587
W12_CL	12	3806007	3914443	-1.0768	Dnmt3a	0.474079199
D16_CL	4	28813131	28967499	-1.1134	Epha7	0.462203471
W12_CL	14	66084374	66124500	-1.112	Ephx2	0.462652214
D13-B_CL	4	109280268	109387817	0.7993	Eps15	1.740256544
D16_CL	4	109280268	109387817	-1.1134	Eps15	0.462203471
W12_CL	4	109280268	109387817	-1.0822	Eps15	0.47230804
D15_CL	7	19382010	19395694	-1.1274	Ercc2	0.457739913
D15_CL	12	38779380	38870484	-1.262	Etv1	0.416965522
D16_CL	12	38779380	38870484	-1.0225	Etv1	0.492262587
W12_CL	12	38779380	38870484	-1.0768	Etv1	0.474079199
D16_CL	4	43002343	43010506	-1.1134	Fancg	0.462203471
D15_CL	19	34290666	34327772	1.2679	Fas	2.408107839
D15_CL	19	10199132	10204169	1.2679	Fen1	2.408107839
W12_CL	14	9550092	11162035	-1.112	Fhit	0.462652214
D17_CL	5	74535449	74598800	-0.798	Fip1l1	0.575145947
D15_CL	12	57540628	57546916	-1.262	Foxa1	0.416965522
D16_CL	12	57540628	57546916	-1.0225	Foxa1	0.492262587
W12_CL	12	57540628	57546916	-1.0768	Foxa1	0.474079199
W12_CL	10	42181841	42276755	-1.0454	Foxo3	0.484510555
D13-A_CL	4	94599385	94599795	-3.6833	Gm12657	0.0778424
D13-B_CL	4	94599385	94599795	0.7993	Gm12657	1.740256544
D16_CL	4	94599385	94599795	-1.1134	Gm12657	0.462203471
D17_CL	4	94599385	94599795	-0.9519	Gm12657	0.516951199
W12_CL	4	94599385	94599795	-1.0822	Gm12657	0.47230804
D15_CL	19	16132831	16387463	1.2679	Gnaq	2.408107839
D13-A_CL	12	102469135	102497907	-0.8839	Golga5	0.541900544
D16_CL	12	102469135	102497907	-1.0225	Golga5	0.492262587
W12_CL	12	102469135	102497907	-1.0768	Golga5	0.474079199
D15_CL	12	78226379	78684772	-1.262	Gphn	0.416965522
D16_CL	12	78226379	78684772	-1.0225	Gphn	0.492262587
W12_CL	12	78226379	78684772	-1.0768	Gphn	0.474079199
D15_CL	12	73901375	73947530	-1.262	Hif1a	0.416965522
D16_CL	12	73901375	73947530	-1.0225	Hif1a	0.492262587
W12_CL	12	73901375	73947530	-1.0768	Hif1a	0.474079199
D16_CL	12	110690605	110702728	-1.0225	Hsp90aa1	0.492262587
W12_CL	12	110690605	110702728	-1.0768	Hsp90aa1	0.474079199
D16_CL	4	136143497	136145755	-0.8195	Id3	0.56663829
W12_CL	4	136143497	136145755	-1.0822	Id3	0.47230804
D16_CL	12	113418558	113422730	-1.0225	Ighm	0.492262587
W12_CL	12	113418558	113422730	-1.0768	Ighm	0.474079199
D17_CL	11	11685003	11772926	-0.8806	Ikzf1	0.543141498

D13-A_CL	4	101152367	101265282	2.2669	Jak1	4.812878489
D13-B_CL	4	101152367	101265282	0.7993	Jak1	1.740256544
D16_CL	4	101152367	101265282	-1.1134	Jak1	0.462203471
D17_CL	4	101152367	101265282	-0.9519	Jak1	0.516951199
W12_CL	4	101152367	101265282	-1.0822	Jak1	0.47230804
D15_CL	19	29251828	29313080	1.2679	Jak2	2.408107839
D13-A_CL	4	95049034	95052222	-0.9904	Jun	0.503338201
D13-B_CL	4	95049034	95052222	0.7993	Jun	1.740256544
D16_CL	4	95049034	95052222	-1.1134	Jun	0.462203471
D17_CL	4	95049034	95052222	-0.9519	Jun	0.516951199
W12_CL	4	95049034	95052222	-1.0822	Jun	0.47230804
W12_CL	14	21481434	21672478	-1.112	Kat6b	0.462652214
D17_CL	5	75932827	75978458	-0.798	Kdr	0.575145947
D17_CL	5	75574916	75656722	-0.798	Kit	0.575145947
D16_CL	4	55527143	55532466	-1.1134	Klf4	0.462203471
W12_CL	14	47648448	47739894	-1.112	Ktn1	0.462652214
D16_CL	4	129548344	129573641	-0.8195	Lck	0.56663829
W12_CL	4	129548344	129573641	-1.0822	Lck	0.47230804
W12_CL	14	75131101	75230842	-1.112	Lcp1	0.462652214
D15_CL	19	5795690	5802672	1.2679	Malat1	2.408107839
D15_CL	12	76937269	76962201	-1.262	Max	0.416965522
D16_CL	12	76937269	76962201	-1.0225	Max	0.492262587
W12_CL	12	76937269	76962201	-1.0768	Max	0.474079199
D15_CL	19	6334979	6340891	1.2679	Men1	2.408107839
D16_CL	4	87769925	88033364	-1.1134	Mllt3	0.462203471
D13-B_CL	4	116702279	116708406	0.7993	Mmachc	1.740256544
D16_CL	4	116702279	116708406	-1.1134	Mmachc	0.462203471
W12_CL	4	116702279	116708406	-1.0822	Mmachc	0.47230804
D16_CL	4	154869585	154895528	-0.8195	Mmel1	0.56663829
W12_CL	4	154869585	154895528	-1.0822	Mmel1	0.47230804
D16_CL	4	118442415	118457513	-1.1134	Mpl	0.462203471
W12_CL	4	118442415	118457513	-1.0822	Mpl	0.47230804
D17_CL	13	73328513	73332178	-0.7951	Mrpl36	0.576303226
D16_CL	4	148448611	148557683	-0.8195	Mtor	0.56663829
W12_CL	4	148448611	148557683	-1.0822	Mtor	0.47230804
D13-B_CL	4	116807723	116819440	0.7993	Mutyh	1.740256544
D16_CL	4	116807723	116819440	-1.1134	Mutyh	0.462203471
W12_CL	4	116807723	116819440	-1.0822	Mutyh	0.47230804
D16_CL	4	122995652	123002485	-0.8195	Mycl	0.56663829
W12_CL	4	122995652	123002485	-1.0822	Mycl	0.47230804
D16_CL	12	12936093	12941914	-1.0225	Mycn	0.492262587
W12_CL	12	12936093	12941914	-1.0768	Mycn	0.474079199
D16_CL	4	15957925	15992589	-1.1134	Nbn	0.462203471
D16_CL	12	4247362	4477182	-1.0225	Ncoa1	0.492262587
W12_CL	12	4247362	4477182	-1.0768	Ncoa1	0.474079199
W12_CL	14	32159865	32179855	-1.112	Ncoa4	0.462652214
D16_CL	4	82290173	82705750	-1.1134	Nfib	0.462203471
D15_CL	19	46304320	46312385	1.2679	Nfkb2	2.408107839
D15_CL	12	70011435	70113717	-1.262	Nin	0.416965522
D16_CL	12	70011435	70113717	-1.0225	Nin	0.492262587
W12_CL	12	70011435	70113717	-1.0768	Nin	0.474079199
D15_CL	12	56531958	56536908	-1.262	Nkx2-1	0.416965522
D16_CL	12	56531958	56536908	-1.0225	Nkx2-1	0.492262587
W12_CL	12	56531958	56536908	-1.0768	Nkx2-1	0.474079199
D16_CL	4	48045153	48086447	-1.1134	Nr4a3	0.462203471
D15_CL	19	46883317	47015153	1.2679	Nt5c2	2.408107839
D16_CL	4	44524757	44710487	-1.1134	Pax5	0.462203471
D16_CL	4	139737062	139833528	-0.8195	Pax7	0.56663829
W12_CL	4	139737062	139833528	-1.0822	Pax7	0.47230804
W12_CL	14	31019138	31121592	-1.112	Pbrm1	0.462652214
D15_CL	19	29410919	29471161	1.2679	Pdcd1lg2	2.408107839
D17_CL	5	75152292	75198215	-0.798	Pdgfra	0.575145947
D17_CL	5	67094399	67099301	-0.798	Phox2b	0.575145947
D16_CL	4	3900996	3938423	-1.1134	Plag1	0.462203471
D13-A_CL	17	20945311	20965916	0.8156	Ppp2r1a	1.760029976
W12_CL	10	44437177	44528501	-1.0454	Prdm1	0.484510555
D16_CL	4	154316125	154636873	-0.8195	Prdm16	0.56663829
W12_CL	4	154316125	154636873	-1.0822	Prdm16	0.47230804
D16_CL	4	143107391	143212995	-0.8195	Prdm2	0.56663829
W12_CL	4	143107391	143212995	-1.0822	Prdm2	0.47230804
D16_CL	4	83455680	83486459	-1.1134	Psip1	0.462203471

D15_CL	19	32757497	32826160	1.2679	Pten	2.408107839
D15_CL	12	79297282	79814690	-1.262	Rad51b	0.416965522
D16_CL	12	79297282	79814690	-1.0225	Rad51b	0.492262587
W12_CL	12	79297282	79814690	-1.0768	Rad51b	0.474079199
W12_CL	14	73183673	73325822	-1.112	Rb1	0.462652214
D17_CL	5	65861213	65896700	-0.798	Rhoh	0.575145947
W12_CL	14	51144998	51146785	-1.112	Rnase1	0.462652214
W12_CL	14	18267823	18271391	-1.112	Rpl15	0.462652214
D16_CL	4	152325742	152334071	-0.8195	Rpl22	0.56663829
W12_CL	4	152325742	152334071	-1.0822	Rpl22	0.47230804
D13-B_CL	4	13743436	13893649	0.8603	Runx1t1	1.815415776
D16_CL	4	13743436	13893649	-1.1134	Runx1t1	0.462203471
D17_CL	13	74322254	74350280	-0.7951	Sdha	0.576303226
D15_CL	19	10500534	10526142	1.2679	Sdhaf2	2.408107839
D16_CL	4	140961203	140979193	-0.8195	Sdhb	0.56663829
W12_CL	4	140961203	140979193	-1.0822	Sdhb	0.47230804
D15_CL	19	5273932	5295455	1.2679	Sf3b2	2.408107839
D16_CL	4	127021324	127037013	-0.8195	Sfpq	0.56663829
W12_CL	4	127021324	127037013	-1.0822	Sfpq	0.47230804
D15_CL	19	58973356	59076100	1.2679	Shtn1	2.408107839
D16_CL	4	155154075	155222592	-0.8195	Ski	0.56663829
W12_CL	4	155154075	155222592	-1.0822	Ski	0.47230804
D17_CL	5	53038081	53071664	-0.798	Slc34a2	0.575145947
D16_CL	4	141467890	141538597	-0.8195	Spen	0.56663829
W12_CL	4	141467890	141538597	-1.0822	Spen	0.47230804
D13-B_CL	4	115000159	115043196	0.7993	Stil	1.740256544
D16_CL	4	115000159	115043196	-1.1134	Stil	0.462203471
W12_CL	4	115000159	115043196	-1.0822	Stil	0.47230804
D15_CL	19	46396896	46488804	1.2679	Sufu	2.408107839
D13-B_CL	4	115056426	115071755	0.7993	Tal1	1.740256544
D16_CL	4	115056426	115071755	-1.1134	Tal1	0.462203471
W12_CL	4	115056426	115071755	-1.0822	Tal1	0.47230804
D16_CL	4	53779705	53788712	-1.1134	Tal2	0.462203471
D15_CL	19	55741820	55933654	1.2679	Tcf7l2	2.408107839
D13-A_CL	12	105216750	105222793	-0.8839	Tcl1	0.541900544
D16_CL	12	105216750	105222793	-1.0225	Tcl1	0.492262587
W12_CL	12	105216750	105222793	-1.0768	Tcl1	0.474079199
D17_CL	5	72755716	72868483	-0.798	Tec	0.575145947
D17_CL	13	73626911	73649843	-0.7951	Tert	0.576303226
D16_CL	4	126164082	126202760	-0.8195	Thrap3	0.56663829
W12_CL	4	126164082	126202760	-1.0822	Thrap3	0.47230804
D15_CL	19	45150680	45156943	1.2679	Tlx1	2.408107839
D16_CL	4	63959785	64047015	-1.1134	Tnc	0.462203471
D16_CL	4	154921933	154928563	-0.8195	Tnfrsf14	0.56663829
W12_CL	4	154921933	154928563	-1.0822	Tnfrsf14	0.47230804
W12_CL	14	31208312	31211729	-1.112	Tnnc1	0.462652214
W12_CL	14	52279146	52296401	-1.112	Tox4	0.462652214
D13-A_CL	12	101834043	101913267	-0.8839	Trip11	0.541900544
D16_CL	12	101834043	101913267	-1.0225	Trip11	0.492262587
W12_CL	12	101834043	101913267	-1.0768	Trip11	0.474079199
D15_CL	12	91384563	91549808	-1.262	Tshr	0.416965522
D16_CL	12	91384563	91549808	-1.0225	Tshr	0.492262587
W12_CL	12	91384563	91549808	-1.0768	Tshr	0.474079199
D15_CL	19	55316295	55627309	1.2679	Vti1a	2.408107839
D16_CL	12	4843303	4860043	-1.0225	Wdcp	0.492262587
W12_CL	12	4843303	4860043	-1.0768	Wdcp	0.474079199
D16_CL	4	46155347	46196311	-1.1134	Xpa	0.462203471
W12_CL	14	65358389	65398930	-1.112	Zfp395	0.462652214
W12_CL	14	56886653	56962701	-1.112	Zmym2	0.462652214

Appendix 4: R-Script used to generate volcano plots.

```
RNASeq_all <- read.csv(file= '/Users/temssyraj/Desktop/Arbeit/Doktorarbeit/Ninas\ mRNA\ Seq\
Data_R\ Analysis/Differentially\ expressed\ genes_without\ Roquin\ exclusive\ filter.csv')
head(RNASeq_all)

WTvsDKOall <- ggplot(data=RNASeq_all, aes(x=fc, y=-log10(pval))) + geom_point() +
theme_minimal()
WTvsDKOall

RNASeq_all$diffexpressed <- "NO"
RNASeq_all$diffexpressed[RNASeq_all$fc >= 1 & RNASeq_all$pval <= 0.05] <- "UP"
RNASeq_all$diffexpressed[RNASeq_all$fc <= -1 & RNASeq_all$pval <= 0.05] <- "DOWN"

head(RNASeq_all)

DKOcolours <- c("lightskyblue2", "red3", "grey")
names(DKOcolours) <- c("DOWN", "UP", "NO")

RNASeq_all$delable <- NA
RNASeq_all$delable[RNASeq_all$diffexpressed !="NO"] <-
RNASeq_all$Gene.name[RNASeq_all$diffexpressed !="NO"]

WTvsDKOall2 <- ggplot(data=RNASeq_all, aes(x=fc, y=-log10(pval), col=diffexpressed,
label=delable)) +
  geom_point(aes(size=0.1, alpha=0.4)) + #change point size
  labs(y=expression('-Log'[10]*'Pval'), x=expression('Log'[2]*'fold change')) +
  xlim(-4, 6) +
  ylim(0,100) +
  theme_minimal() +
  geom_text_repel(aes(size=0.1)) + #change font size
  geom_vline(xintercept=c(-1,1), col="black", linetype="dotted") +
  geom_hline(yintercept=-log10(0.05), col="black", linetype="dotted") +
  scale_colour_manual(values = DKOcolours)


WTvsDKOall2
head(RNASeq_all)
```

Publications

First author publication:

Behrens*, G., Edelmann*, S.L., **Raj*, T**., Kronbeck, N., Monecke, T., Davydova, E., Wong, E.H., Kifinger, L., Giesert, F., Kirmaier, M.E., et al. (2021). Disrupting Roquin-1 interaction with Regnase-1 induces autoimmunity and enhances antitumor responses. Nature immunology. 10.1038/s41590-021-01064-3.

* authors contributed equally

Co-author publication:

Essig, K., Hu, D., Guimaraes, J.C., Alterauge, D., Edelmann, S., **Raj, T**., Kranich, J., Behrens, G., Heiseke, A., Floess, S., et al. (2017). Roquin Suppresses the PI3K-mTOR Signaling Pathway to Inhibit T Helper Cell Differentiation and Conversion of Treg to Tfr Cells. Immunity 47, 1067-1082.e1012. 10.1016/j.immuni.2017.11.008.

Acknowledgments

I would like to take this opportunity to thank everyone who has helped and supported me throughout the last five years. This thesis would not have been possible without the support of these people.

First and foremost, I would like to thank my supervisor Prof. Dr. Vigo Heissmeyer for giving me the opportunity to work on this exciting project, for his great mentorship and open-door policy. His great and critical input has greatly contributed towards the progress and the quality of this work.

I would like to thank Prof. Dr. Anne Krug and Prof. Dr. Dirk Baumjohann as members of my thesis advisory committee for critical discussions and suggestions.

I would like to thank Prof. Dr. Desheng Hu for his initial analysis of the pancreas phenotype which has led to the establishment of the second part of this project. Dr. Desheng Hu contributed data presented in Figures 28, 29, 33, 34 and 44.

I would like to express my gratitude to all my collaborators who have strongly contributed to the work presented in this thesis:
Prof. Dr. Mathias Heikenwälder from the German Cancer Research Center, Heidelberg and his former and current lab members Dr. Jessica Zoeller, Dr. Gaia Bianco, Jenifer Hetzer and Danijela Heide for strong input into the pancreas aspect of this project (sections 4.2 and 4.3) through critical discussions and by performing all the immunehistological stainings and initial analyses.
Prof. Dr. Roland Rad from the TU Munich and Dr. Sebastian Mueller for library preparation and bioinformatical analysis of the whole exome and RNA sequencing of the pancreas tumor cell lines and primary tumors (section. 4.2).
PD Dr. med. vet. Katja Steiger from the TU Munich for analysis of the pancreas tumor sections and for teaching me how to analyze histological samples.

I would like to express my deepest gratitude to all current and former members of the AG Heissmeyer, both at the Biomedical Center and the Helmholtz Center, for their great mental and experimental support, and fantastic working atmosphere.

Acknowledgments

I would like to acknowledge people that have provided me with figures, technical support and advice throughout this project.

In particular, I would like to thank Claudia Lohs for her excellent technical support and great organization skills. Without her help and knowledge of mouse genetics this project would not have progressed as smoothly.

Dr. Stephanie Edelmann for teaching me how to perform *i.v.* injections, for her great advice throughout this work and experimental contributions. She has contributed Figure 22.

Dr. Nina Kronbeck who has generated mRNA Seq data shown in Figure 25.

Dr. Gesine Behrens for always having an open ear and being the best lab-neighbor one could wish for.

Elaine Wong, who has always jumped in to help during large experiments.

Furthermore, I would like to thank Dr. Lisa Richter and Pardis Khosravani from the Core Facility Flow Cytometry at the BMC, the staff from the animal facility, both at the Helmholtz Center and the BMC. In particular, I want to thank Michael Hagemann and Franziska Liebl, for taking such great care of my mice.

My deepest gratitude goes to my family, who have always believed in me and supported me in every step I have taken. Thank you for always being there for me.